NUREG/CR-3262
PNL-5515
Vol. 7

COBRA-NC:A Thermal Hydraulics Code for Transient Analysis of Nuclear Reactor Components

Vol. 7: Assessment Manual for Containment Applications

Prepared by C. L. Wheeler, M. J. Thurgood, T. E. Guidotti, D. E. DeBellis

Pacific Northwest Laboratory
Operated by
Battelle Memorial Institute

Prepared for
U.S. Nuclear Regulatory Commission

NUREG/CR-3262
PNL-5515
Vol. 7
R4

COBRA-NC:A Thermal Hydraulics Code for Transient Analysis of Nuclear Reactor Components

Vol. 7: Assessment Manual for Containment Applications

Manuscript Completed: March 1986
Date Published: April 1986

Prepared by
C. L. Wheeler, M. J. Thurgood, T. E. Guidotti, D. E. DeBellis

Pacific Northwest Laboratory
Richland, WA 99352

Prepared for
Division of Accident Evaluation
Office of Nuclear Regulatory Research
U.S. Nuclear Regulatory Commission
Washington, D.C. 20555
NRC FIN B2466

ABSTRACT

COBRA-NC is a digital computer program written in FORTRAN IV that simulates the response of nuclear reactor components and systems to thermal-hydraulic transients. The code solves the multicomponent compressible, three-dimensional, two-fluid, three-field equations for two-phase flow. The three fields are the vapor/gas field, the continuous liquid field, and the liquid drop field. This volume of the manual provides the user with the results of comparisons between COBRA-NC predictions and data obtained from containment systems experiments. These data comparisons provide an indication of the code's ability to predict the response of multicompartment nuclear containment systems to postulated loss-of-coolant accidents that result in the release of steam, water, and/or noncondensable gases into nuclear containments.

CONTENTS

FIGURES

TABLES

ACKNOWLEDGEMENTS

COBRA-NC is the result of the efforts of a number of people. We wish to acknowledge the main contributors and to express our appreciation to those who have offered their advice and suggestions.

The main contributors to the program are listed below.

Fluid Dynamics:	M. J. Thurgood, T. L. George, and T. E. Guidotti
Heat Transfer:	J. M. Kelly and R. J. Kohrt
Turbulence Model:	K. R. Crowell
Graphics and Programming:	A. S. Koontz
Simulations:	D. E. DeBellis

We wish to thank Dr. T. Lee of the U.S. Nuclear Regulatory Commission for his patience, support, and suggestions during this large undertaking. We also wish to thank Drs. Tong, Shotkin, Lee, Han, and Zuber of the U.S. Nuclear Regulatory Commission and members of the Advanced Code Review Group for their many helpful suggestions. We also express our gratitude to our manager, Dr. D. S. Trent, for his support, and Cathy Darby for typing this report.

SUMMARY

COBRA-NC is a digital thermal-hydraulic computer program that simulates the response of nuclear reactor components and systems to loss-of-coolant accidents. It utilizes a multicomponent, two-fluid, three-field representation of two-phase flow. Conservation equations are solved for water and its vapor, and for a noncondensable gas mixture comprised of n species. The flow field may be modeled using a lumped parameter approach or a multidimensional finite-difference approach. The code has been designed to predict two-phase jet impingement loads, room pressurization, and the migration of hydrogen and other noncondensable gases within the containment. This volume of the code documentation describes the major containment data comparisons made with COBRA-NC during the process of code development. The code was assessed against steam-water blowdown data and hydrogen distribution data. Several of these calculations were performed in a blind pretest prediction mode as a stringent test of the predictive capability of the code. The overall comparison of the code with data is very good, although it must be recognized that further study of some phenomena, such as steam condensation, warrant further study.

COBRA-NC: A THERMAL-HYDRAULICS CODE FOR TRANSIENT ANALYSIS OF NUCLEAR REACTOR COMPONENTS

VOLUME 7: ASSESSMENT MANUAL FOR CONTAINMENT APPLICATIONS

1.0 INTRODUCTION

The COBRA-NC computer code was developed by the Pacific Northwest Laboratory for the United States Nuclear Regulatory Commission. The Pacific Northwest Laboratory is operated for the Department of Energy by Battelle Memorial Institute.

COBRA-NC was developed to perform analyses of thermal-hydraulic transients in various components of light-water reactors including the reactor core, reactor vessel, steam generators, and the reactor containment building. It was merged with a system code to provide a primary coolant-system analysis capability (Ref. 10). The documentation for the code is broken up into several volumes because of its wide range of application. Volume 1, Equations and Constitutive Models, contains a description of the basic conservation equations and constitutive models used in the code. Volume 2 contains the finite-difference equations and a description of the procedures used for their numerical solution. Volumes 3 through 5 are the Users' Manuals. They contain line-by-line input instructions for COBRA-NC and user guidance for application of the code. Volume 3, the Users' Manual for General Two-Phase Thermal Hydraulics, contains an explanation for all of the input data required for general application of the code. Volume 4 is the Users' Manual for Containment Analysis and contains an explanation of the input data required for containment analysis only. It also provides examples of containment modeling procedures. Volume 5 is the Users' Manual for Flow Blockage and Hot Bundle Analysis and describes the input required for performing such analysis.

Volumes 6, 7, and 8 are the Assessment Manuals. They contain the results of simulations run to assess the performance of the code in each of the areas discussed above. Volume 9 is the Programmers' Manual. It explains the details of COBRA-NC's working parts from a programmers' viewpoint. The structure of the code is described along with a verbal description of the major variables and subroutines used in the code.

This volume, the Assessment Manual for Containment Applications, presents comparisons of COBRA-NC predictions with experimental data taken from scaled containment test facilities. COBRA-NC is designed to predict room pressurization, pressure differentials between rooms, jet impingement forces, and asymmetric loads during a loss-of-coolant accident. It is also designed to predict the distribution of hydrogen and noncondensable gases within the containment building, both during and following a loss-of-coolant accident where hydrogen may be generated by metal-water reactions or by radiolysis. The COBRA-NC code provides a two-component, two-fluid, three-field representation of two-phase flow. It is a two-component model to allow the

modeling of water and its vapor as well as a noncondensable gas mixture. The gas mixture may consist of any number of gas species. The properties of eight gases are currently coded.

The two-fluid capability is used to predict the two-phase flows associated with steam-water blowdown into the containment, condensation of steam in the containment atmosphere and on containment structural surfaces, flow through pressure suppression pools, containment sprays, etc. The three fields are 1) the vapor-gas mixture, 2) the continuous-liquid phase, and 3) the liquid-drop phase. The continuous-liquid phase is used to model liquid films on containment structures, pools on containment floors, and pressure suppression pools. The liquid-drop phase is used to model the two-phase jet, containment sprays, and drop entrainment between containment rooms.

Three momentum, four mass, and two energy equations are solved for the fluid. Momentum equations are solved for the vapor-gas mixture, the continuous liquid and the liquid-drop fields. Thus, each of these may travel at different velocities. A liquid film flowing down walls with vapor flowing across it can be modeled. The vapor may also contain drops that travel at a still different velocity than the vapor.

Mass equations are solved for the noncondensable gas, the vapor, the continuous liquid, and the liquid drops. Thus, the mass of each phase can be accounted for. In addition, a mass-transport equation is solved for each species of the noncondensable gas mixture, so that the concentration of each species can be determined. Energy equations are solved for the vapor-gas mixture and for the continuous liquid-drop mixture. It is therefore assumed that both the vapor and gas in a given computational cell will have the same temperature, and that the liquid film and liquid drops within a given mesh cell will be at the same temperature. These two mixtures, however, can have different temperatures. This model permits the modeling of nonsaturated air (air with a relative humidity of less than 100%) and superheated vapor in the presence of subcooled liquid.

The code is a three-dimensional, compressible-flow, finite-difference code formulated in Cartesian coordinates. However, it features an extremely flexible noding scheme that allows it to be run in a lumped parameter, one-dimensional, two-dimensional, or three-dimensional mode. It has a finite-difference slab conduction model for structural heat transfer. Any number of materials may be used in each slab, and the number of heat transfer nodes through the thickness of the slab may be specified by the user.

A mixing-length turbulence model has also been included to allow the user to model turbulent shear flows and the turbulent diffusion of gas species due to concentration gradients.

A general set of boundary conditions has been included to facilitate the modeling of containment sprays, blowers, blowdown flows, etc. The code does

not contain specific models for hydrogen source terms. These must be specified as a boundary condition for the calculation.

This volume documents the major containment data comparisons made with COBRA-NC during the process of code development. The purpose of these data comparisons was to verify the correctness of the coding and to assess the ability of the code to predict the major phenomena governing the thermal-hydraulic response of the containment during a loss-of-coolant accident. The code was assessed against two major types of data: 1) steam-water blowdown data, and 2) hydrogen distribution data. These tests were conducted in several containment facilities including the German HDR and Battelle-Frankfurt facilities, and the Hanford Engineering Development Laboratory's Containment Systems Test Facility. Several calculations were performed in a blind pretest prediction mode as a stringent test of the predictive capability as opposed to post-test calculations that can be used to adjust the model in the code to give improved comparisons with the data.

Comparisons with various experimental data are provided in Sections 2 through 9 of this manual. A brief description of the experiment is given for each case to familiarize the reader with the experiment. The code input model is described, and the results of the code prediction are presented. Some general conclusions about the code's current capabilities are made in Section 10.0.

2.0 CSNI NUMERICAL BENCHMARK PROBLEM

The Committee on the Safety of Nuclear Installations (CSNI) of the Organization for Economic Cooperation and Development (OECD) devised a test problem to test the numerical accuracy and convergence errors of containment computer codes in the computation of mass and energy conservation for the fluid and in the computation of heat conduction into solid walls (Ref. 1). The problem consists of a single fluid volume into which steam and water are injected and from which heat is transferred to a single concrete wall. The variation of the wall surface temperature with time was chosen to allow an analytical solution of the heat conduction into a semi-infinite solid slab. The problem time scale and wall thickness were chosen to meet the boundary conditions. The required inflow of mass and energy was then evaluated, and became the standard input data required by COBRA-NC.

The limiting assumptions in this numerical benchmark problem are:

- homogeneous equilibrium mixing of liquid, vapor, and air
- the thermal properties of water are taken from standard steam tables
- constant specific heat for air
- constant thermal properties for the concrete wall
- constant heat transfer coefficient between containment atmosphere and wall surface.

The temperature wave will penetrate only a few millimeters into the concrete wall in the short time scale of this numerical test problem. This will make the test a stringent test of convergence.

2.1 Description of Problem

Dimensions of the assumed containment volume were based on one of the compartments of the Battelle-Frankfurt Containment Experiment used in CSNI containment standard problem #2. The problem was developed by specifying the wall surface temperature (T_s) as a function of time given by

$$T_s = T_o + a(1-e^{-\lambda t}) \qquad (1)$$

For this problem the parameters a and λ are a = 120K and λ = 0.5. For the above wall surface temperature, the solution for the wall temperature (T_w) at a distance x from the wall surface at time t is given by

$$T_w = T_o + \operatorname{erfc}\left(\frac{x}{2\sqrt{\alpha t}}\right) - \frac{a e^{-\lambda t}}{2}\left\{e^{ix\sqrt{\frac{\bar{\lambda}}{\alpha}}}\operatorname{erfc}\left(\frac{x}{2\sqrt{\alpha t}} + i\sqrt{\lambda t}\right)\right.$$

$$\left. + e^{-ix\sqrt{\frac{\bar{\lambda}}{a}}}\operatorname{erfc}\left(\frac{\lambda}{2\sqrt{\alpha t}} - i\sqrt{\lambda t}\right)\right\} \qquad (2)$$

From this, the total heat transferred through the surface between time t = o and time t is obtained:

$$Q \cdot \text{Area} = \frac{4\ ak}{\sqrt{\lambda \alpha \pi}}\ \text{Area}\ (\lambda t)^{3/2} \sum_{p=o}^{\infty} a_p\ (\lambda t)^p \qquad (3)$$

where $a_o = 1/3$

$$a_p = \frac{-2}{2p+3}\ a_{p-1}$$

The heat flux passing through the wall surface at time t is given by

$$\text{Flux}(t) = \frac{dQ}{dt} \cdot \text{Area} = \text{Area} \cdot \frac{4\,ak}{\sqrt{\lambda\alpha\pi}} \left\{\frac{3}{2}\,\frac{(\lambda t)^{3/2}}{t}\right.$$

$$\left. \sum_{p=o}^{\infty} a_p\,(\lambda t)^p + (\lambda t)^{3/2} \sum_{p=o}^{\infty} a_p p\,\frac{(\lambda t)^p}{t}\right\} \qquad (4)$$

The containment temperature (T_c) at time t was found using:

$$T_c = T_s + \frac{\text{Flux}(t)}{\text{Area} \cdot h} \qquad (5)$$

where h is a constant heat transfer coefficient. The mass of water/steam in the containment (M_{in}) at time t was then found as follows:

Energy of input water = (energy required to heat air) + (internal energy of steam in containment) + (internal energy of water in containment)

+ (Energy flowing into wall)

$$= C_v M_{air} + \int P_{air}\,dV + (h_g M_g - P_s V_g) + (h_f M_f - P_s V_f) + QA \qquad (6)$$

The integral, $\int P_{air}\,dV$, was approximated as $-P_{air}\,(V - V_f)$ to simplify the calculation, as it has an insignificant effect on the results. Also, the hydrostatic pressure in the containment was taken as zero so

$$P = P_s + P_{air}$$

which becomes

$$P = \{P_o \frac{T_c}{T_o} \frac{V}{V - V_f}\} + P_s \tag{8}$$

assuming air is an ideal gas.

Replacing the masses of steam and water by their specific volumes and approximate volume terms, the enthalpy equation becomes

$$H_{in}M_{in} = C_v M_{air} T - P_s V + M_{in} [h_g (\frac{V - V_f}{V_g - V_f}) + h_f - h_f (\frac{V - V_f}{V_g - V_f})]$$

$$- P_o \frac{T_c}{T_o} \frac{V}{} + Q \bullet \text{Area} \tag{9}$$

This equation was rearranged as a quadratic equation and was solved for M_{in}. The steam pressure, P_s, was found from the saturated steam tables using the temperature, T_c, as were values for V_f, V_g, h_f, and h_g. Values for M_{in} at various times was calculated from Equation (9) using these values, a constant input enthalpy, and Q•Area for time t from Equation (3).

The containment pressures at various times were calculated from Equation (8). The mass flow rates at time t were chosen to give the necessary M_{in} values for a linear interpolation method.

The geometry parameters and thermal properties for the concrete wall and containment volume are given in Table 1.

Table 1 Problem parameters

Thermal conductivity of wall	$K = 1.5$ W/mK
Heat transfer coefficient between atmosphere and wall surface	$h = 2000$ W/m^{2}K
Thermal diffusivity of wall	$\alpha = 7.33 \times 10^{-7}$ m^2/sec
Wall surface area	Area = 90 m^2
Wall thickness	= 0.1 m
Initial wall temperature	$T_s = 25^\circ$C
Initial containment temperature	$T_c = 25^\circ$C
Initial containment pressure	$P_o = 1$ bar
Containment volume	$V = 40$ m^3
Mass of air in containment	$M = 51.67$ kg
Specific heat capacity of air in containment	$C_v = 718$ J/kg K
Enthalpy of input water	$H_{in} = 1400 \times 10^3$ J/kg

The input mass flow rate as a function of time is given in Table 2.

Table 2 Input water flow rate

Time (sec)	Input Water Flow Rate (kg/sec)
0.0	26.14
0.2	57.46
0.3	69.62
0.4	82.42
0.5	94.12
0.6	105.42
0.7	115.60
0.8	124.52
0.9	132.92
1.0	139.40
1.2	149.28
1.4	155.70
1.6	155.82
1.8	154.70
2.0	148.86
2.2	142.06
2.4	133.04
2.6	123.46
2.8	112.98
3.0	102.60
3.2	92.44
3.4	82.30
3.6	72.10
3.8	63.00
4.0	55.00
4.2	47.60
4.4	40.80
4.6	34.0
4.8	28.5
5.0	23.0
5.2	18.8
5.4	14.9
5.6	11.2
5.8	8.2
6.0	5.8

2.2 COBRA-NC Model Description

A schematic of the COBRA-NC model is shown in Figure 1, which shows a single computational cell that is initially filled with air. This computational cell is thermally connected to a thermal conductor that models the concrete wall to which heat is transferred. The initial condition and properties of the air and concrete wall are as specified in Table 1. A steam/water flow boundary condition was specified into the computational cell at the rate specified in Table 2 and with the constant enthalpy specified in Table 1.

The objective of the calculation was to obtain the same wall temperature, steam temperature (or partial pressure), and room pressure as was used in the analytical solution. If the code predicts the same wall temperature as was used to develop the analytical solution, then one can have confidence that the code is correctly conserving mass and energy in the fluid volume, and that energy is conserved in the conduction solution. One of the key factors in obtaining the correct result with the computer code is the discretization of the thermal conductor. A fine nodalization must be used near the wall surface to correctly resolve the steep temperature gradient near the surface. The predicted wall surface temperatures will be too low if the node size is too large near the wall surface. This will result in larger heat transfer rates from the fluid and an underprediction of fluid temperature and pressure. The wall was modeled with five equally spaced nodes in the first 0.0025 m of the wall thickness, five equally spaced nodes in the next 0.0213 m, five equally spaced nodes in the next 0.0254 m, and five nodes in the last 0.0508 m.

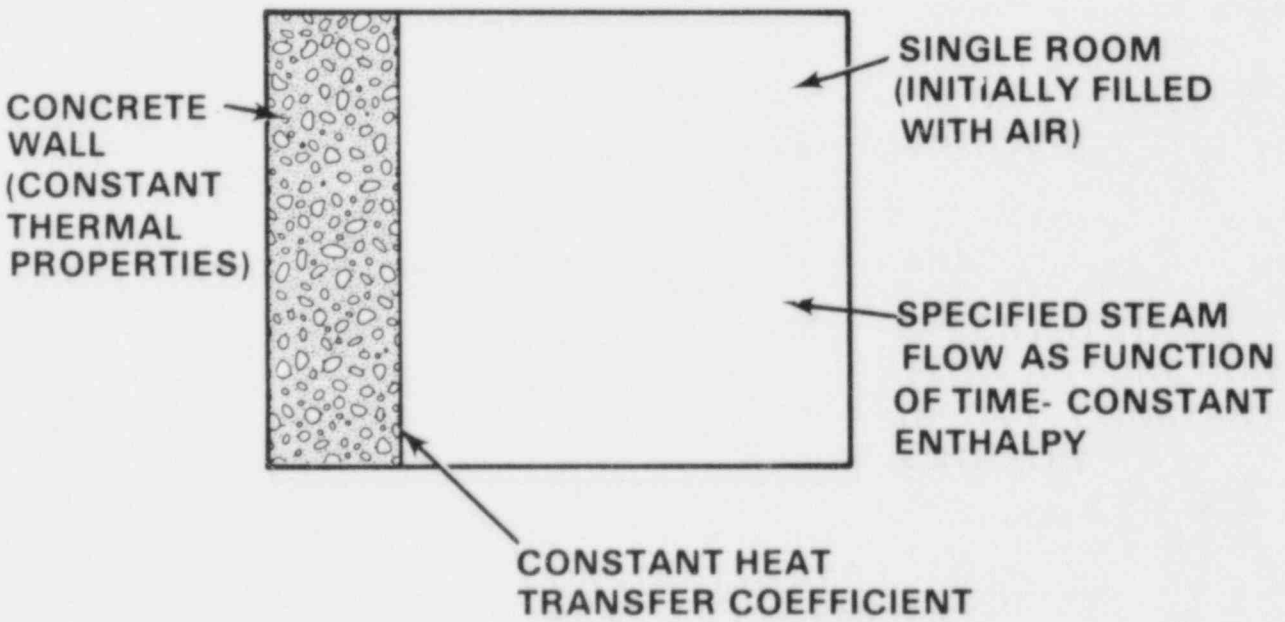

Figure 1 Benchmark problem model

2.3 Discussion of Results

Comparisons between COBRA-NC predictions and the analytical solution for the benchmark problem are shown in Figures 2 through 4. The total pressure in the containment volume is shown in Figure 2, the partial pressure of the steam in Figure 3, and the wall surface temperature in Figure 4. All three parameters are in nearly perfect agreement with the analytical solution. This indicates that, for a single-volume problem, COBRA-NC conserves mass and energy in the fluid and energy in the solid wall. The good prediction with the steam partial pressure means that the fluid temperature was correctly calculated, since the fluid temperature is equal to the steam saturation temperature. The good prediction of wall surface temperature means that the wall temperature was adequately modeled.

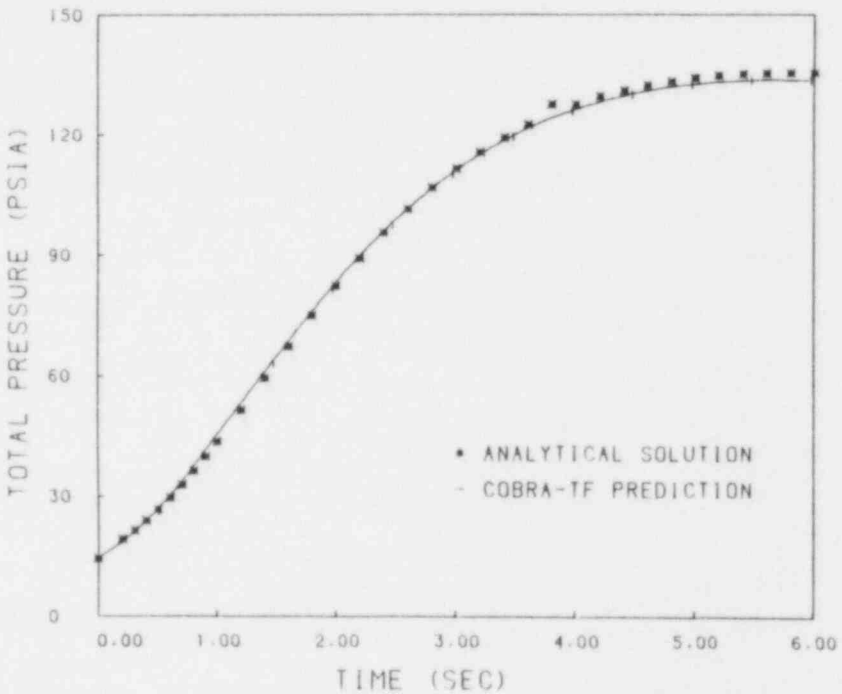

Figure 2 Total pressure in containment

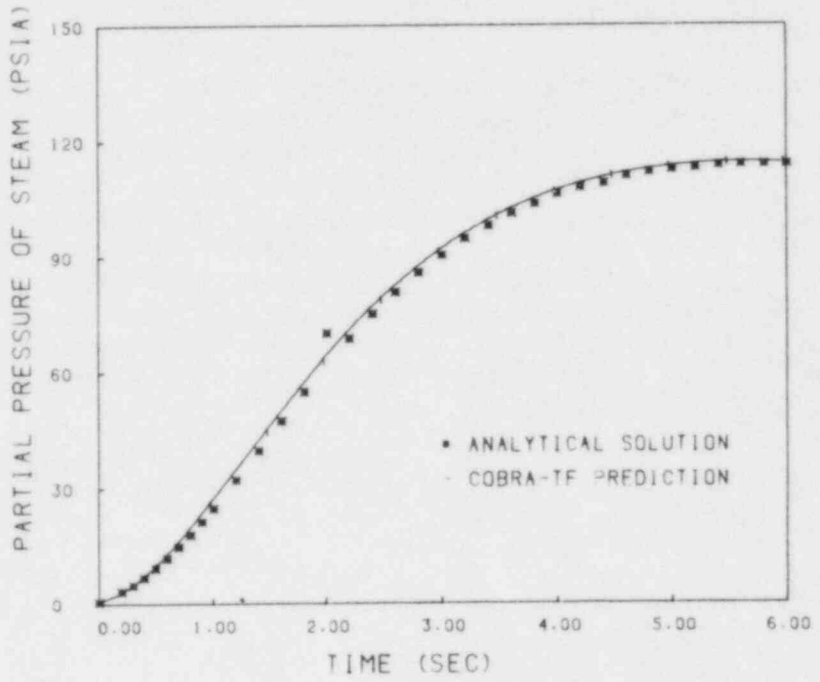

Figure 3 Partial pressure of steam in containment

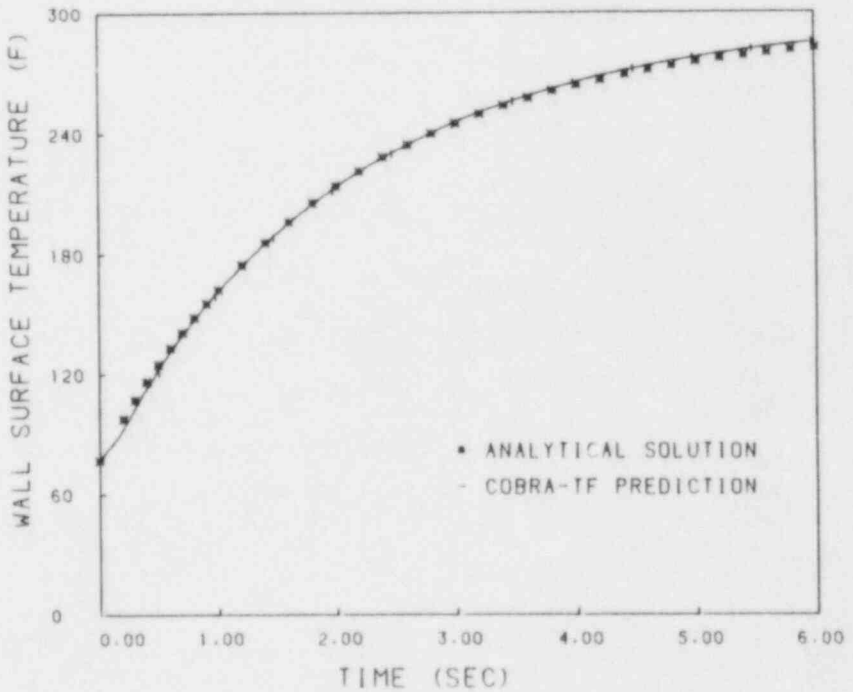

Figure 4 Wall surface temperature

3.0 CSNI STANDARD PROBLEM NO. 2

Standard Problem No. 2 of the Committee on the Safety of Nuclear Installations (CSNI) (Ref. 2) was performed in the model containment of Battelle Institut, Frankfurt, FRG, and sponsored by the Federal Ministry for Research and Technology within the framework of the German Reactor Safety Research Program. Standard Problem No. 2 is based on a pressurized water-blowdown experiment D-16 to approximate the accident condition assumed for design of full-pressure containments. This problem was modeled with COBRA-NC to assess the code's ability to predict the pressure history of a multicompartment containment to a water blowdown transient.

3.1 Description of Experiment

The facility consists of a high-pressure blowdown system and a model containment. The high-pressure system is installed mainly outside the containment and consists of a pressure vessel, a pipeline with a length approximately 26 m, and a recirculation system. The pipeline is connected to the pressure vessel and leads through the containment to the break compartment.

The heated water in the pressure vessel and in the piping is kept at an approximately homogeneous temperature by the recirculating system prior to rupture. The model containment consists of six compartments arranged according to Figures 5 and 6. The rupture occurs approximately in the middle of the smallest compartment R4. The fluid branches at the upper part of compartment R4. One portion flows into compartment R5 via vent (orifice) and from there, over a short flow path, through the ceiling of the compartment (vent orifice) into the dome of the big compartment R9. The other portion flows through vent (orifice) into compartment R7 and from there, after flowing longitudinally through R7, via vent (orifice) at the floor into compartment R8. Compartment R8 as well as compartment R6, which is symmetrical to it, are open to compartment R9 by several holes into the walls. During the experiment a small additional gap formed between rupture compartment R4 and dome compartment R9.

The most important containment dimensions are given in Table 3, which lists the subcompartment volumes, concrete surface areas, metal surface areas, and vent flow areas. The steel surfaces are not coated; the concrete surfaces are provided with coating. The initial conditions for the containment are given in Table 4. The boundary conditions for the containment are the measured mass flow rates at a distance of about 2.7 m upstream from the rupture with the associated specific enthalpy as a function of time (Table 5). These mass flow values are determined from the signals of a gamma-densitometer and from the mean value of the measured curves of two drag bodies.

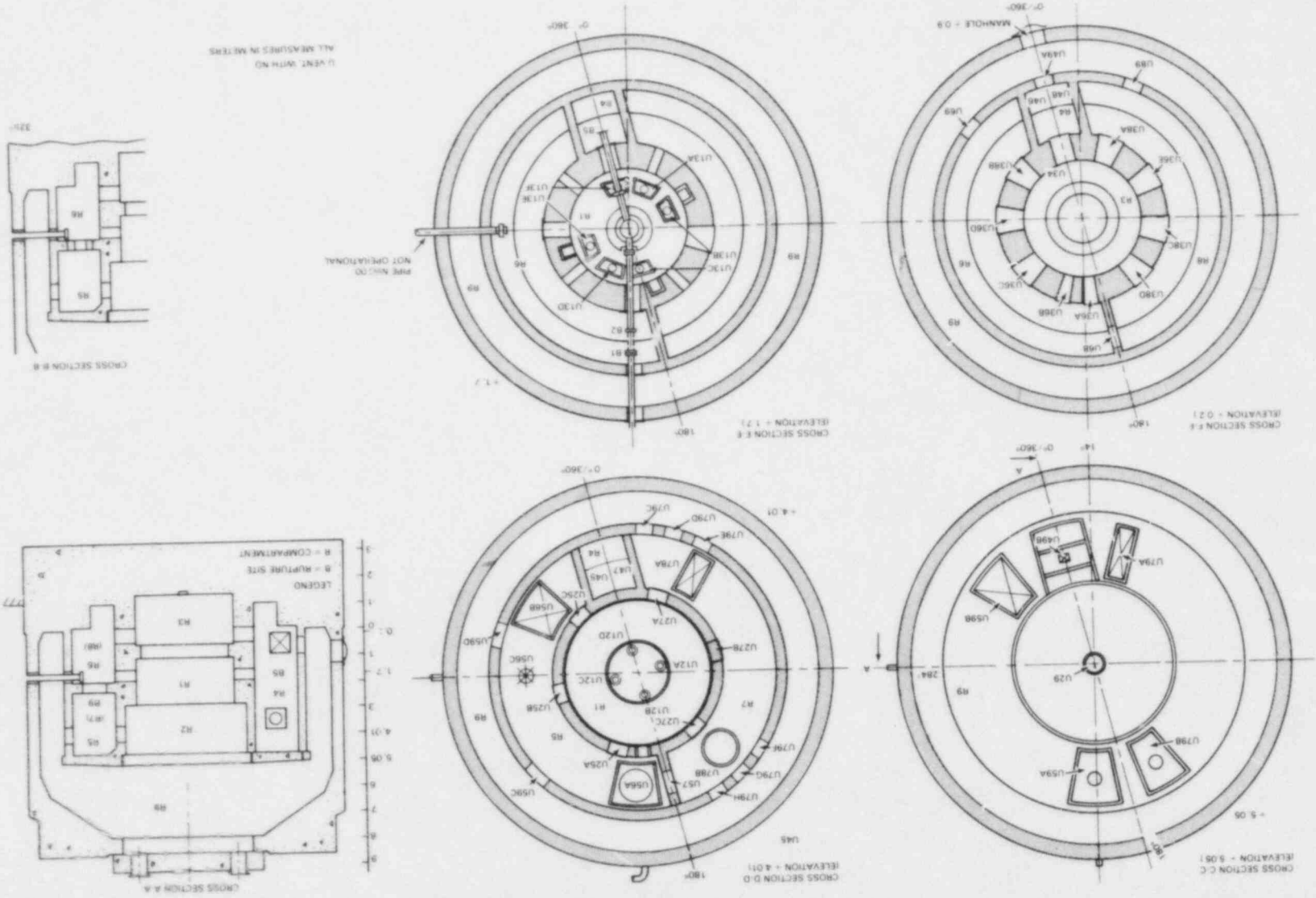

Figure 5 Battelle-Frankfurt model containment

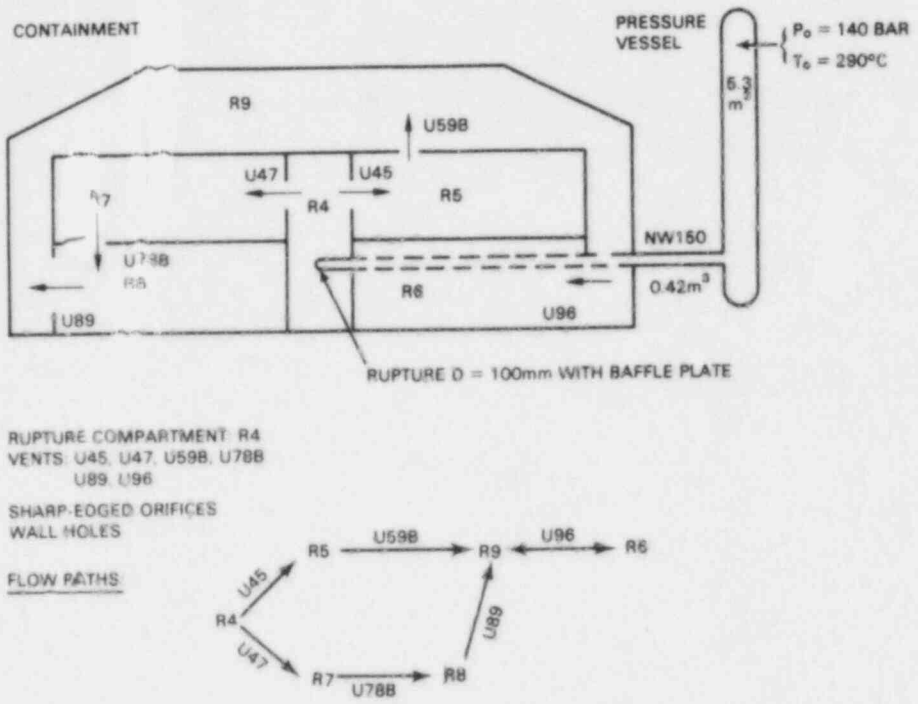

Figure 6 Scheme of the containment and flow paths for test D16/CASP2

Table 3 Dimensions of containment compartments and vents in experiment CASP2

Compartment Number	Volume (m^3)	Surface Area Concrete (m^2)	Surface Area Metal (m^2)
R4 (rupture)	13.66	38.63	8.83
R5	41.05	76.08	17.23
R6	41.26	90.12	9.58
R7	40.40	76.63	15.41
R8	40.53	92.00	6.17
R9	465.00	645.82	57.30
Sum of all compartments	641.90	1019.28	114.52

Vent No.	Compartments Connected	Vent Shape	Vent Diameter (mm)	Vent Area (geometrical) (m_2)
U 45	R4/R5	sharp-edged orifice	750	0.442
U 47	R4/R7	sharp-edged orifice	750	0.442
U 59B	R5/R9	sharp-edged orifice	550	0.238
U 78B	R7/R8	sharp-edged orifice	550	0.238
U 89	R8/R9	several holes in	-	1.933
U 96	R9/R6	the walls	-	2.109
	R4/R9	gap	-	0.0292

Table 4 Containment initial conditions

P_{Co} = 1.0 bar
T_{R4} = 23.5°C
T_{R5} = 23.0°C
T_{R6} = 26.0°C
T_{R7} = 24.0°C
T_{R8} = 24.5°C
T_{R9} = 30.5°C (center and dome)
T_{R9a} = 25.0°C (annulus)
Φ_r = 100% (relative atmospheric humidity)

mean values of compartments R4 to R9, volumetric average for whole containment: T_{Co} = 27.6°C

Table 5 Break mass flow and specific enthalpy

D16/CASP2

Time (s)	Mass Flow (kg/s)	Mass Flow (lbm/sec)	Temperature (°C)	Density (kg/m^3)	Spec. enthalpy (kj/kg)	Spec. enthalpy (Btu/lbm)
0	0	(0.0)	260	795	1134	(489.0)
0.004	52	(114.4)	260	784	1135	(489.4)
0.005	145	(319.0)	260	784	1135	(489.4)
0.028	200	(440.0)	260	784	1135	(489.4)
0.056	200	(440.0)	260	784	1135	(489.4)
0.067	340	(748.0)	260	784	1135	(489.4)
0.086	335	(737.0	260	784	1135	(489.4)
0.105	405	(891.0)	260	784	1135	(489.4)
0.200	368	(809.0)	260	784	1135	(489.4)
0.350	270	(594.0)	283	715	1255	(541.0)
0.400	210	(462.0)	282	640	1260	(543.0)
0.500	205	(451.0)	281	600	1260	(543.0)
0.750	300	(660.0)	272	764	1195	(515.0)
0.850	324	(713.0)	272	764	1195	(515.0)
0.920	374	(823.0)	273	763	1201	(518.0)
1.20	230	(506.0)	281	580	1263	(544.6)
2.00	200	(440.0)	280	530	1267	(546.3)
2.50	180	(396.0)	279	500	1267	(546.3)
4.00	165	(363.0)	275	430	1261	(543.7)
10.00	145	(319.0)	268.5	310	1266	(545.9)
16.33	130	(286.0)	261	300	1225	(528.2)
23.50	115	(253.0)	252.5	255	1195	(515.3)
24.30	78	(171.6)	250	125	1323	(570.5)
30.00	25	(55.0)	207	20	1737	(748.9)
40.00	3	(6.6)	156	3	2752	(1186.0)
50.00	0	(0.0)	152	2.7	2748	(1184.0)

The mass flow values measured for the short-term period up to 1.2 s have been taken without any correction. The measured mass flow values for the long-term period above 4 s have been corrected by a factor of about 1.2, so that the time integral for mass flow rate up to 50 s is equal to the discharged mass predicted from an integral mass balance. For the intermediate period from 1.2 to 4 s an interpolation is done.

The specific enthalpy of the fluid is determined from the measurement for density and temperature for single-phase flow and from density and pressure for two-phase flow.

3.2 COBRA-NC Model Description

Standard Problem No. 2 was modeled using the lumped parameter option. The nodalization used is shown in Figure 7. The containment was modeled with twenty-one channels, each one node high. Channels 1 through 4 model room 6; channels 5 through 8 model room 5. Channels 9 and 15 represent room 4 whose vertical height extends through the lower two levels of the containment. The large room 9 is modeled with channels 10, 16, and 21. The containment was divided into three sections. The height of each section was chosen to reflect the average height of rooms modeled in the section. Section 1 contains channel 1 through 10. Section 2 contains channels 11 through 20. Section 3 contains channel 21. The area for each channel was obtained by dividing the room volume (Table 3) by the section height and by the number of channels used to model the room. The channel input data is given in Table 6.

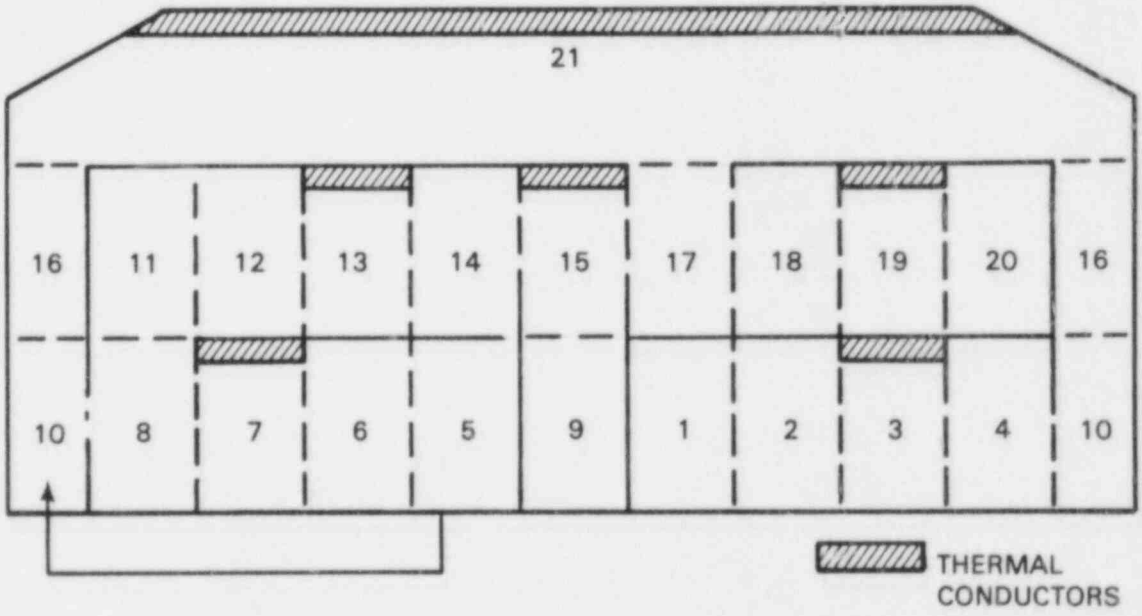

Figure 7 COBRA-NC mesh for CSNI-2

Table 6 Channel input data

Channel Channel	Room Number	Area ($in.^2$)	Wetted Perimeter	Bottom Connection Area ($in.^2$)	Top Connection Area ($in.^2$)	Height	Vent Modeled by Connection
1	6	6323.0	194.6			99.4	
2	6	6323.0	194.6			99.4	
3	6	6323.0	194.6			99.4	
4	6	6323.0	194.6			99.4	
5	8	6213.0	191.2			99.4	
6	8	6213.0	191.2			99.4	
7	8	6213.0	191.2			99.4	
8	8	6213.0	191.2		368.7	99.4	U 78B
9	4	4257.0	245.2			99.4	
10	9	52000.0	2515.0			99.4	
10	7	6393.0	196.8	368.7		96.35	
12	7	6393.0	196.8			96.35	
13	7	6393.0	196.8			96.35	
14	7	6393.0	196.8			96.35	
15	4	4257.0	245.2			96.35	
16	9	52000.0	2515.0			96.35	
17	5	6495.0	199.9		368.7		U 59B
18	5	6495.0	199.9			96.35	
19	5	6495.0	199.9			96.35	
20	5	6495.0	199.9			96.35	
21	9	52000.0	988.4	368.7		352.08	

The long annular rooms (5, 6, 7, and 8) were divided into four cells to model the propagation of the steam front through the room.

The area of vertical flow openings between rooms are provided in Table 6. Horizontal flow openings between rooms are modeled as gaps between the connecting channels. In addition, the connections between channels used to model a single room (e.g., channels 1, 2, 3, and 4) are also modeled as gaps. The input data for each of the gaps are given in Table 7. The gap width was obtained by dividing the flow area by the height of the section containing the gap. The centroid distances were obtained from the physical dimension of the containment provided in Figure 5.

Heat transfer surfaces were modeled using 12 thermal conductors, two for each room. The first conductor in each room was used to model the concrete structures, and the second was used to model metal structures. The channels that transfer heat to the thermal conductors are illustrated in Figure 7 with a cross-hatched box at the top of the channel. The input data for the thermal conductors are given in Table 8.

Table 7 Gap input data

Gap No.	Channels Connected by Gap	Gap Width (in.)	Area ($in.^2$)	Centroid Distance (in.)	Velocity Head Loss Coefficient	Opening Number Modeled by Gap
1	1&2	64.96	6460.0	97.34		
2	2&3	64.96	6460.0	97.34		
3	3&4	64.96	6460.0	97.34		
4	4&10	32.85	3266.0	64.9	2.91	U 96
5	5&10	30.11	2994.0	64.9	2.77	U 89
6	5&6	64.96	6460.0	95.64		
7	6&7	64.96	6460.0	95.64		
8	7&8	64.96	6460.0	95.64		
9	11&12	64.96	6259.0	98.4		
10	12&13	64.96	6259.0	98.4		
11	13&14	64.96	6259.0	98.4		
12	14&15	6.78	653.0	86.6	2.85	U 47
13	15&17	6.78	653.0	87.39	2.85	U 45
14	17&18	64.96	6259.0	99.99		
15	18&19	64.96	6259.0	99.99		
16	19&20	64.96	6259.0	99.99		

Table 8 Thermal conductor input data

Room Number	Conductor Number	Channel Number	Surface Area ($in.^2$)	Material Thickness (in.)	Wetted Perimeter (in.)	Material
6	1	3	139,613.0	4.92	1404.0	Concrete
8	2	7	142,597.0	4.92	1434.0	Concrete
7	3	13	118,800.0	4.92	1233.0	Concrete
4	4	15	59,833.0	4.92	621.0	Concrete
5	5	19	118,029.0	4.92	1225.0	Concrete
9	6	21	1,000,963.0	4.92	2843.0	Steel
6	7	3	14,846.0	0.5	149.3	Steel
8	8	7	9,563.0	0.5	96.17	Steel
7	9	13	23,885.0	0.5	247.9	Steel
4	10	15	13,691.0	0.5	142.1	Steel
5	11	19	24,309.0	0.5	277.2	Steel
9	12	21	88,830.0	0.5	25[illegible].3	Steel

Conductors were chosen so that the wetted perimeter times the node height would equal the surface areas for solid structures provided in Table 3. The material properties used for the thermal conductors are provided in Table 9. The material properties were assumed to be independent of temperature.

Table 9 Material properties

Material Type	Material	Density (lbm/ft^3)	Specific Heat (Btu/lbm°F)	Thermal Conductivity (Btu/hr-ft°F)
1	Concrete	138.79	0.220	0.8673
2	Steel	487.32	0.113	30.0000

The containment structures and atmosphere were initialized to a temperature of 26.5°C; the volumetric average temperature for the whole containment as given in Table 4. The air in the containment atmosphere was assumed to have a relative humidity of 100% and a pressure of one bar.

The break mass flow and enthalpy were modeled as a type 2 (flow and enthalpy) boundary condition at the bottom of channel 9 using the values specified in Table 5 as a function of time.

3.3 Discussion of Results

Code predictions of room pressures and differential pressures between rooms were made for the short time range (0.0 to 2.5 s), and predictions of room pressures were made for the intermediate time range (0.0 to 50.0 s).

Three sets of data comparisons were made. The first set was made using the Uchida correlation with an maximum value of 1590.0 W/m^2k (280 $Btu/m\text{-}ft^2\text{-}°F$) for the heat transfer coefficient between the containment atmosphere and solid structure. This correlation can be expected to overpredict the room pressure, since it does not model the enhanced heat transfer due to the highly turbulent flow that exists during blowdown. Predictions for the pressure in rooms 4, 5, and 9 for the short time range are shown in Figures 8, 9, and 10. The measured data is shown in the figures with asterisks and the code prediction as a solid line. The pressures are overpredicted by about 20% in each of the rooms as was expected because of the heat transfer coefficient used. These results are not unreasonable and represent a reasonably conservative prediction of the measured data. The differential pressure between rooms 4 and 9, 5 and 9, and 4 and 5 are shown in Figures 11, 12, and 13, respectively. Again, the code predictions, shown in these figures as solid circles, are slightly higher than the measured data, shown as a solid line. The comparison is quite reasonable, indicating that the loss coefficients used for the openings are about right.

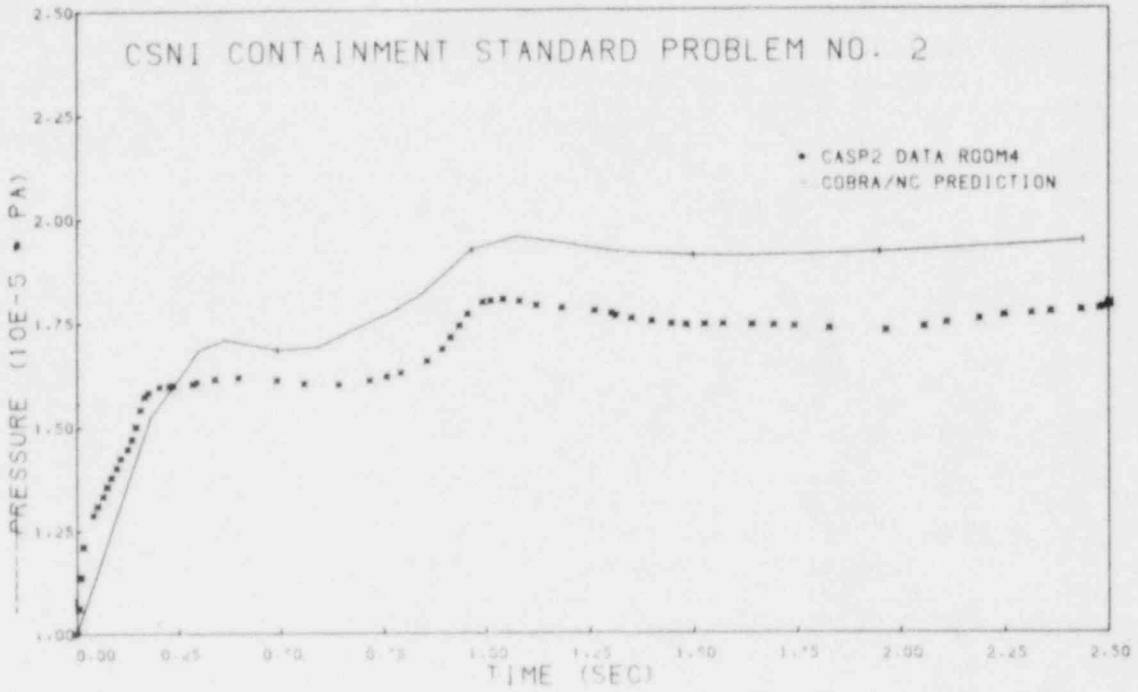

Figure 8 Absolute pressure in room 4 for the short time range

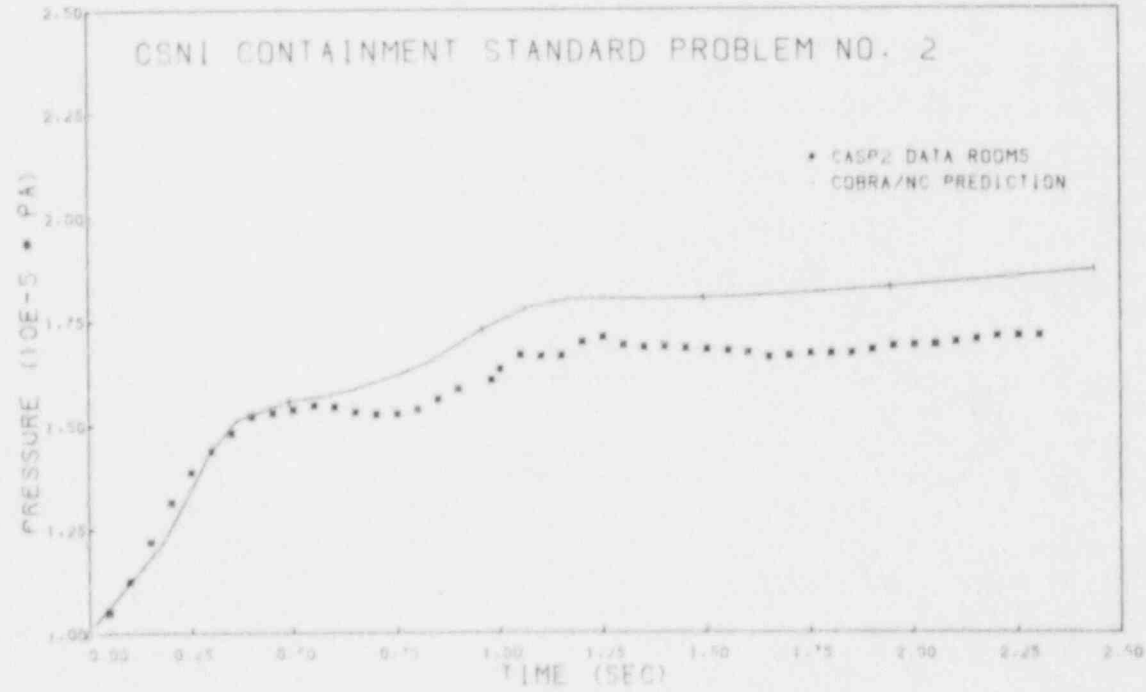

Figure 9 Absolute pressure in room 5 for the short time range

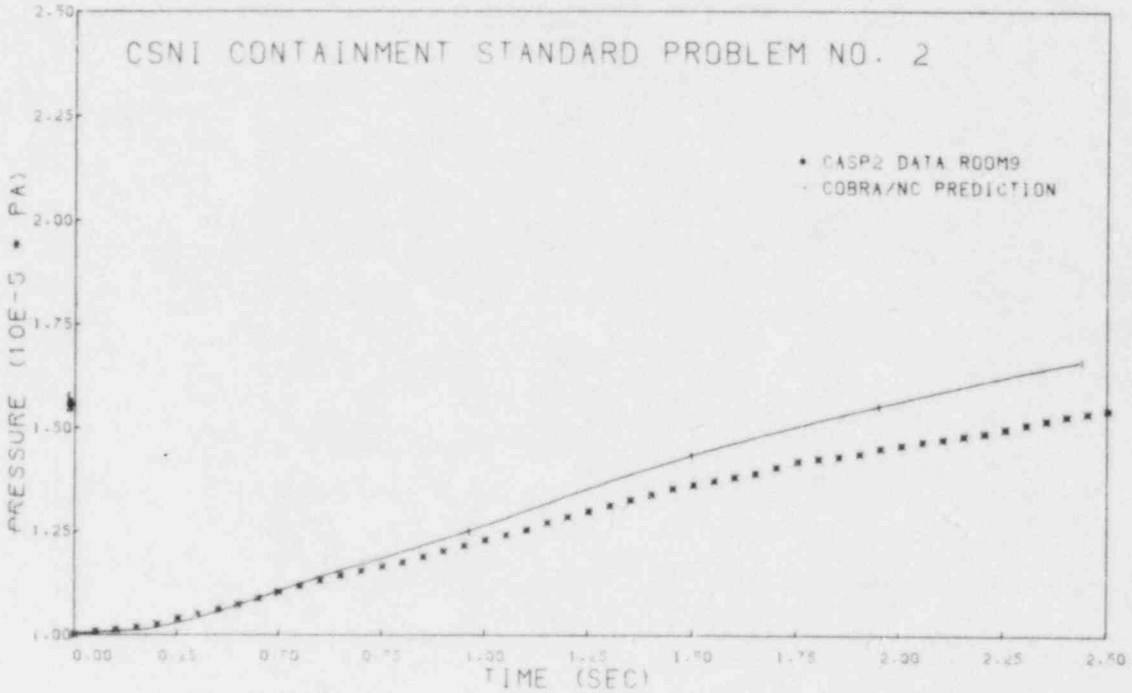

Figure 10 Absolute pressure in room 9 for the short time range

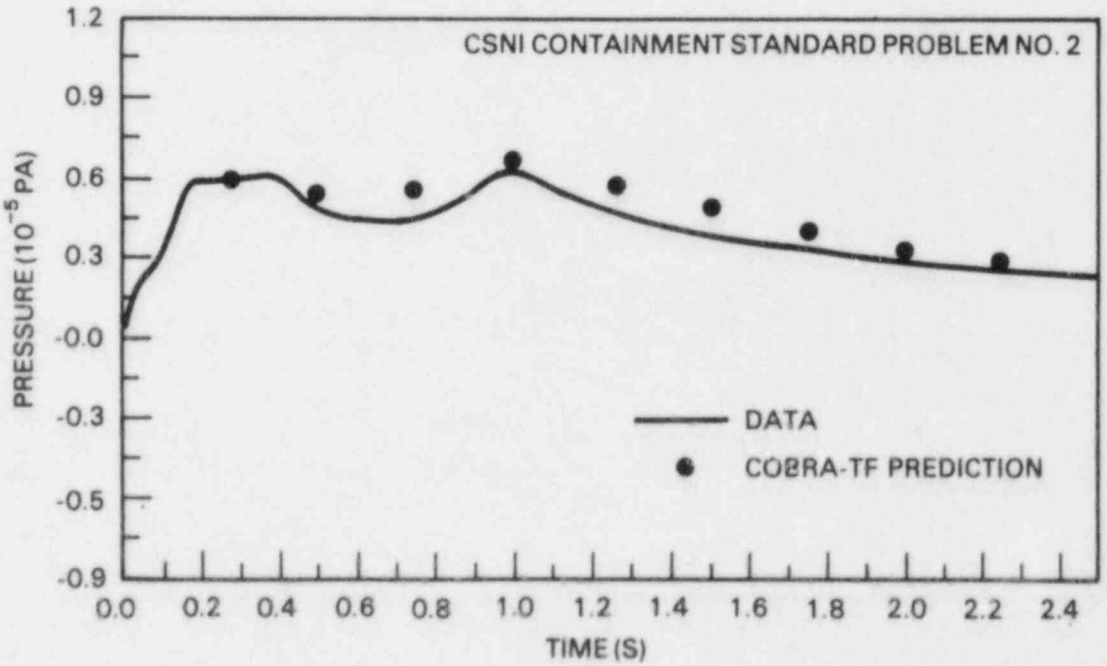

Figure 11 Differential pressure between rooms 4 and 9

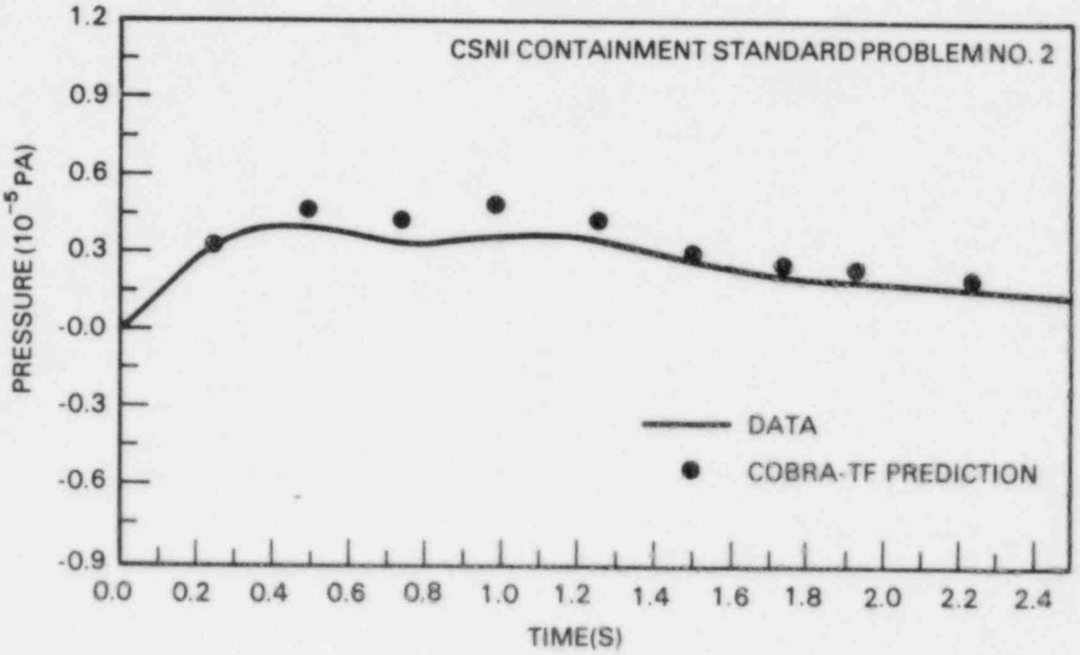

Figure 12 Differential pressure between rooms 5 and 7

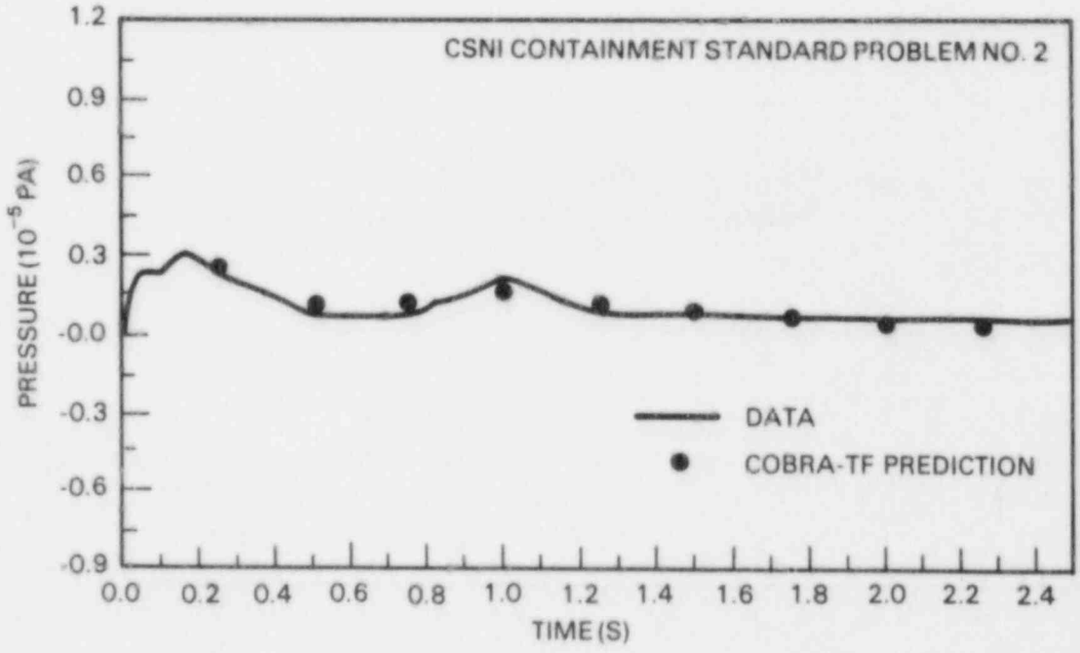

Figure 13 Differential pressure between rooms 4 and 5

The pressure histories for rooms 4, 5, and 9 for the medium time range are shown in Figures 14, 15, and 16. As expected, the predicted pressures, shown as solid lines, are about 10% higher than the measured pressures, shown as asterisks, at the peak. Again, this is a reasonably conservative prediction based on use of the Uchida correlation for the condensation heat transfer coefficient.

The second set of comparisons consists of code predictions made using the Uchida correlation with an upper limit of 4,291 W/m^2K (757.0 $Btu/m\text{-}ft^2\text{-}°F$). This is the peak value of heat transfer coefficient given by the Tagami correlation for this test based on the volume of rooms 4, 5, 7, and 8. Predictions for the short time duration are shown in Figures 17, 18, and 19. Predictions for the long time duration are shown in Figures 20, 21, and 22. There is a slight decrease in the predicted pressures but not as large as one would expect from the large increase in the upper limit on the heat transfer coefficient. This indicated that the peak value of heat transfer coefficient was not reached for most or all of the heat transfer surfaces. Again, the predictions are reasonably conservative.

The third set of comparisons is based on the use of the Tagami correlation to predict the condensation heat transfer coefficient in rooms 4, 5, 7, and 8 for the first 23.5 s, and the Uchida correlation was used in all rooms after 23.5 s. The Tagami correlation is

$$h_T = 411. \left(\frac{t}{t_p}\right) \left(\frac{Q}{Vt_p}\right)^{0.62}$$

where Q = total blowdown energy = 5.2213E9 J
V = volume of rooms 4, 5, 7, and 8 = 135.7 m^3
t_p = time to end of water blowdown = 23.5 s
t = transient time.

Predictions based on this model for the condensation heat transfer coefficient are given in Figures 23, 24, and 25. The predictions are very close to the data using this model. However, this model has the disadvantage of requiring the code user to guess which room volumes to include in the volume used to calculate the heat transfer coefficient from the Tagami correlation. This simulation required 50 s of computer time on a CDC 7600 computer for the intermediate time range calculation.

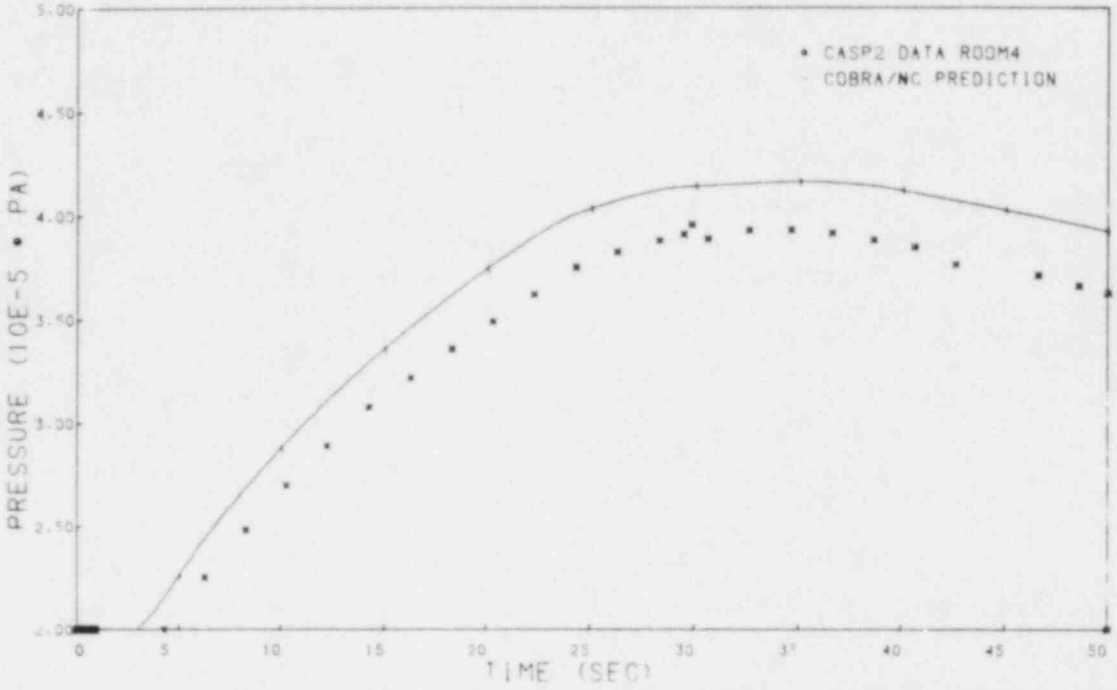

Figure 14 Absolute pressure in room 4 for the intermediate time range

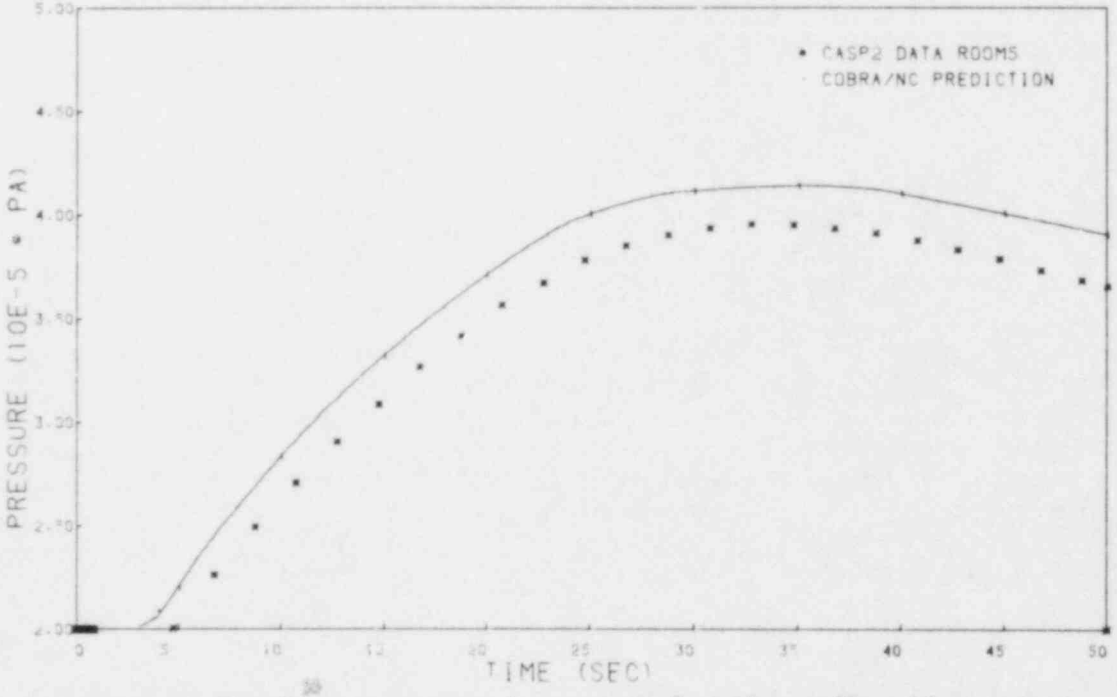

Figure 15 Absolute pressure in room 5 for the medium time range

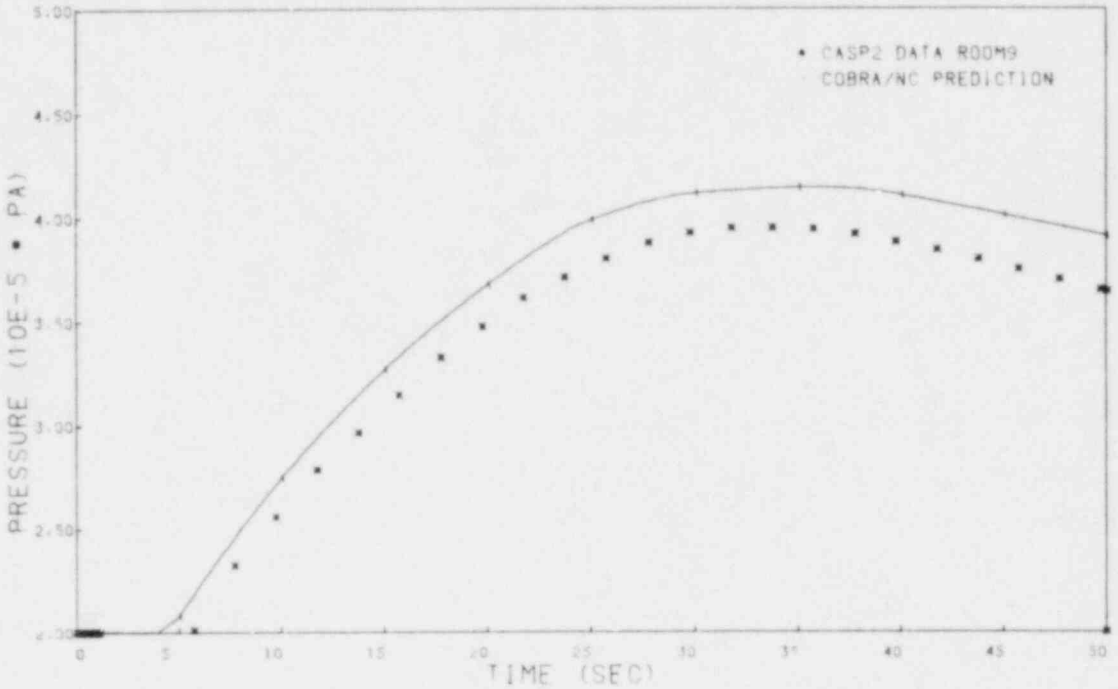

Figure 16 Absolute pressure in room 9 for the intermediate time range

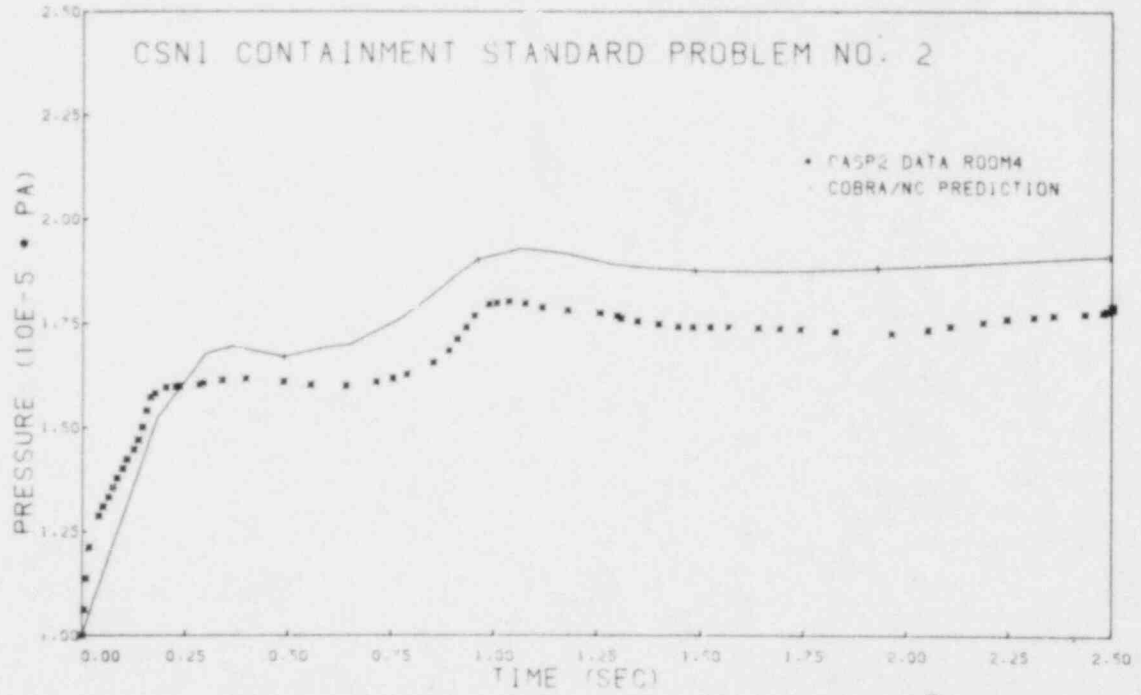

Figure 17 Pressure in room 4, h_{max} = 4,291 $W/m^{2o}K$

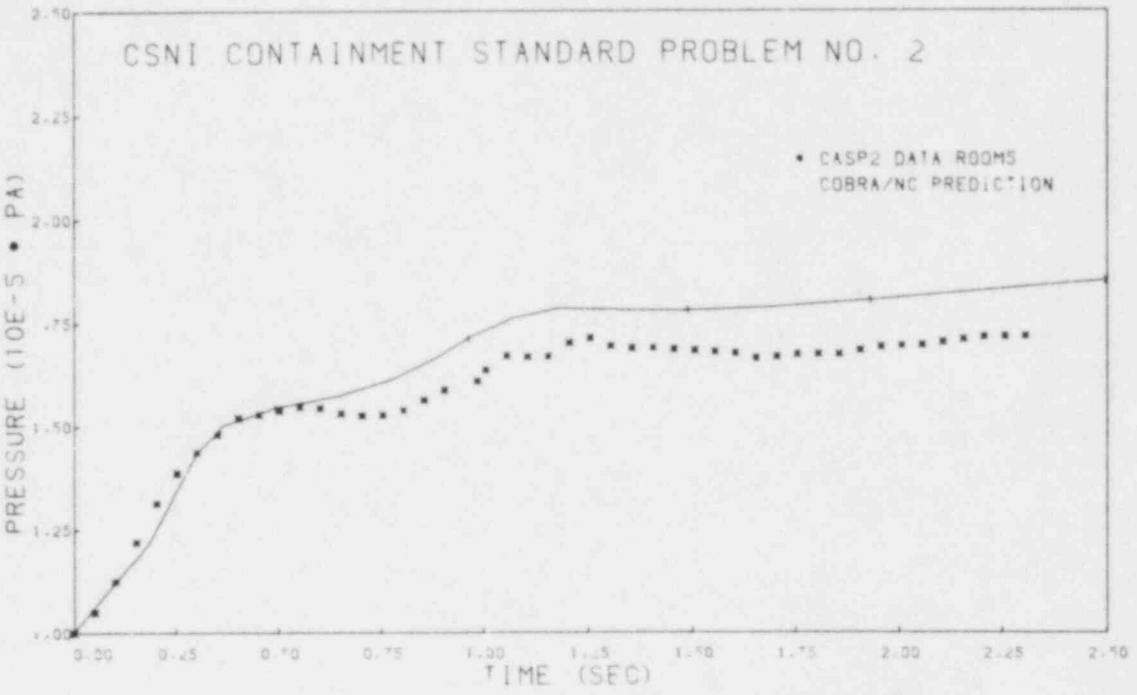

Figure 18 Pressure in room 5, h_{max} = 4,291 W/m^2°K

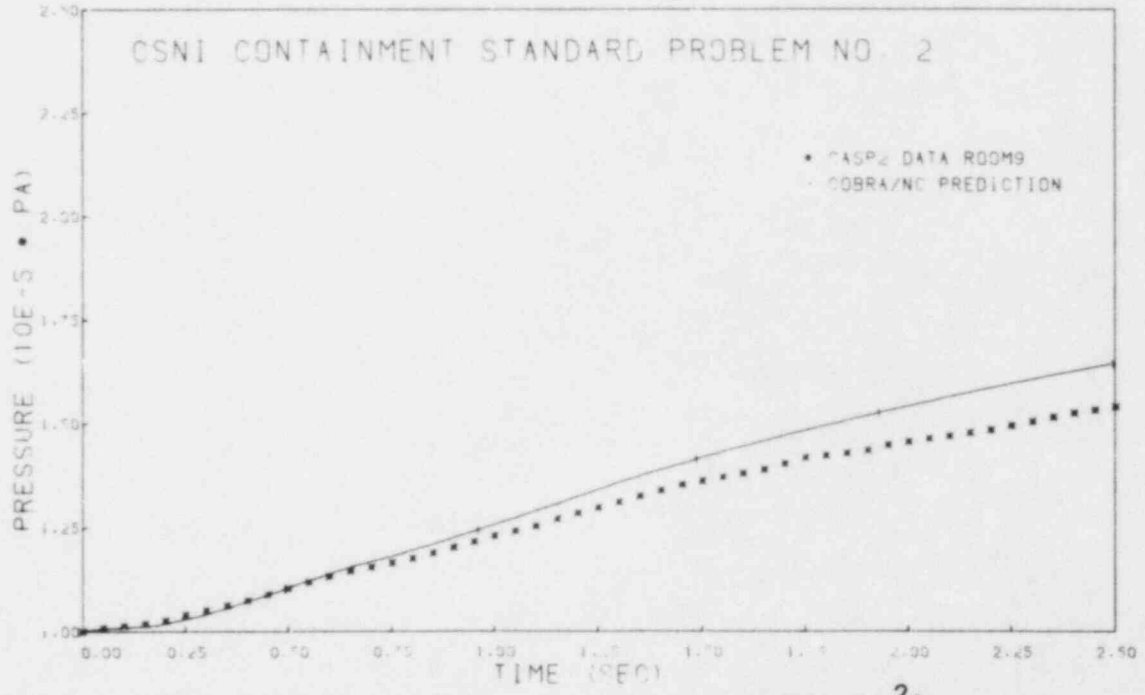

Figure 19 Pressure in room 9, h_{max} = 4,291 W/m^2°K

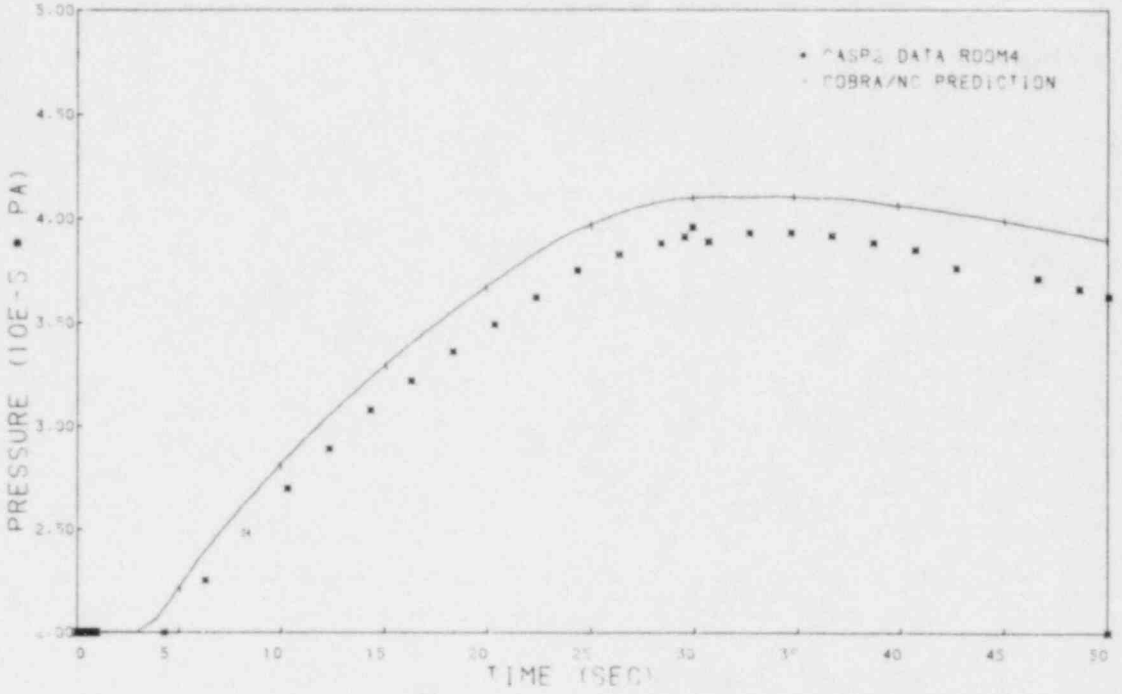

Figure 20 Pressure in room 4, h_{max} = 4,291 W/m^2°K

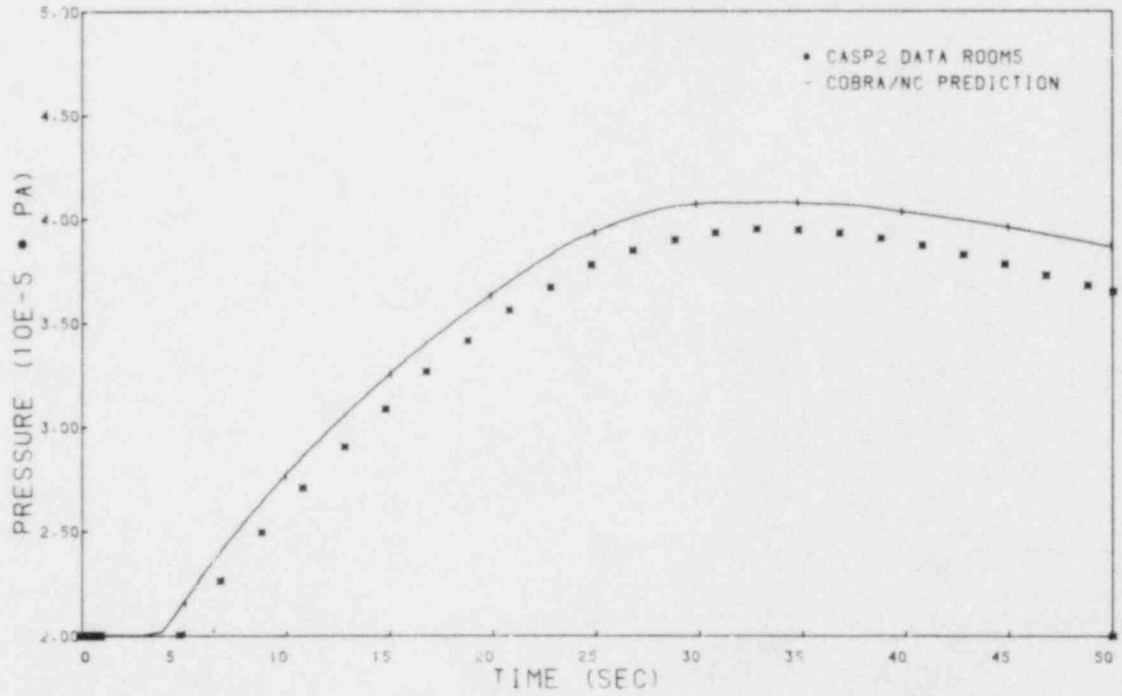

Figure 21 Pressure in room 5, h_{max} = 4,291 W/m^2°K

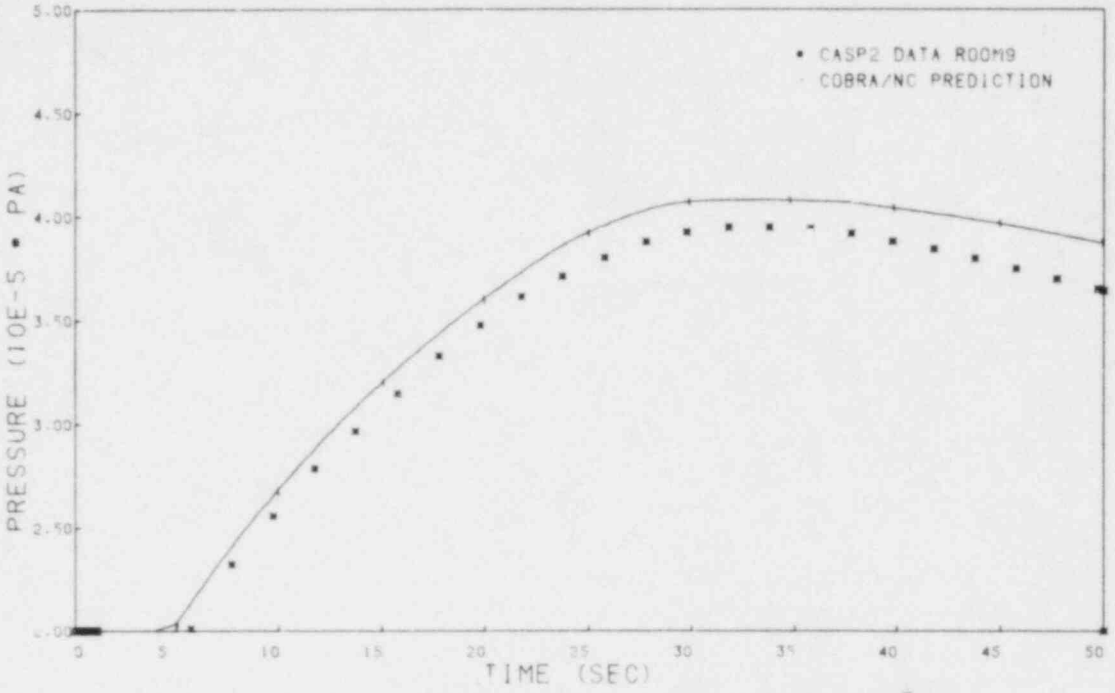

Figure 22 Pressure in room 9, h_{max} = 4,291 W/m^2°K

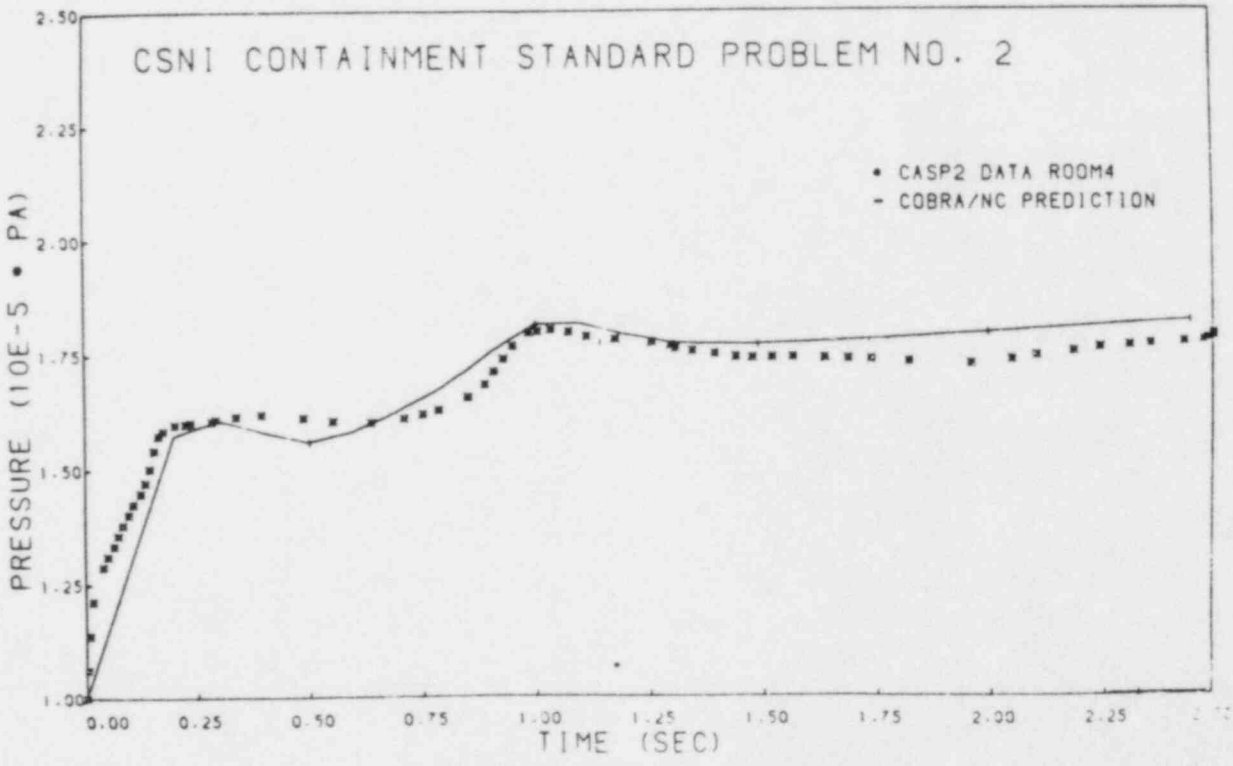

Figure 23 Pressure in room 4 using the Tagami-Uchida correlation

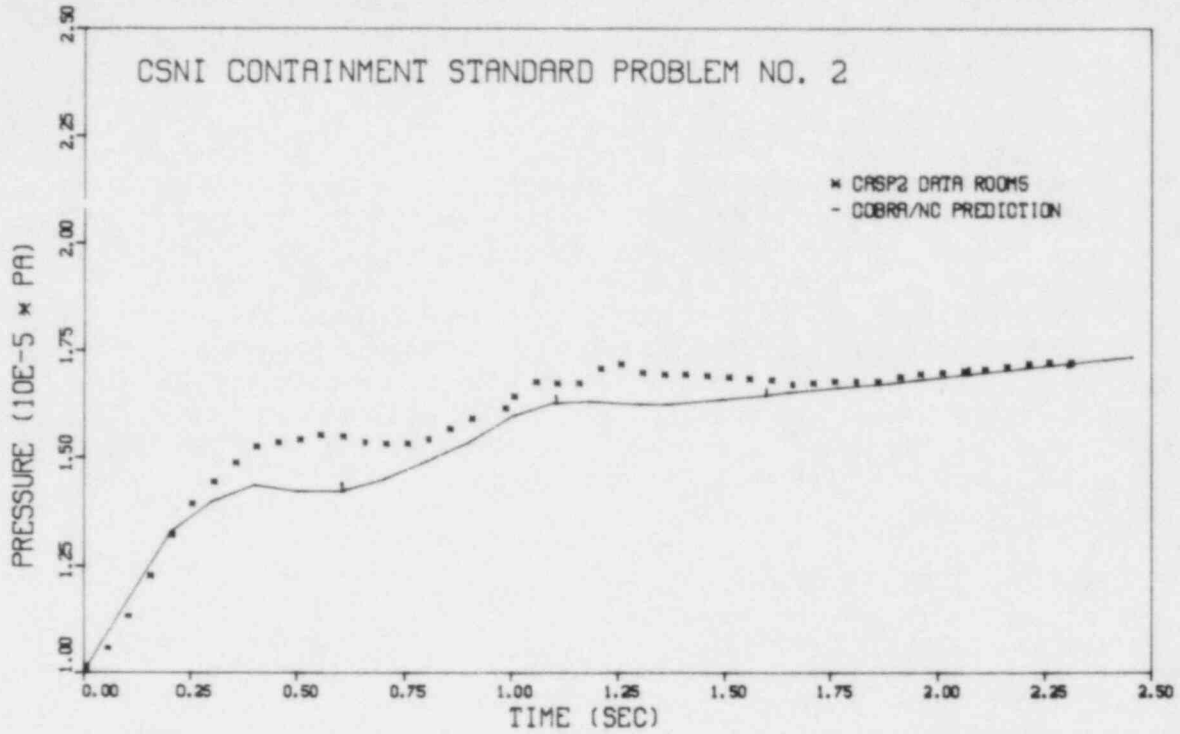

Figure 24 Pressure in room 5 using the Tagami-Uchida correlation

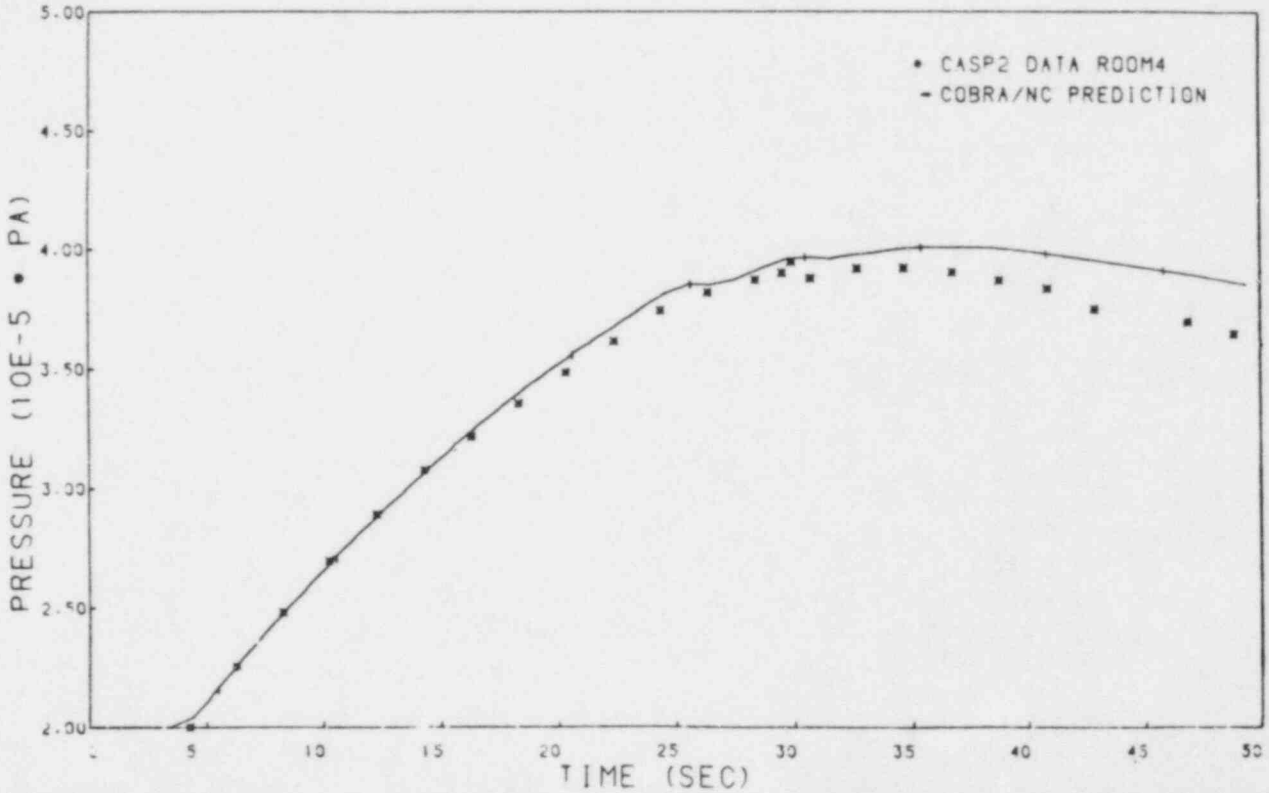

Figure 25 Pressure in room 4 for the medium time range using the Tagami-Uchida correlation

4.0 CSNI STANDARD PROBLEM NO. 3 (CASP3)

The CSNI Containment Analysis Standard Problem No. 3 is based on a steam/water blowdown into a two-compartment simulated containment (Ref. 3). The experiment was conducted in the Lucas Heights Research Laboratory Blowdown/Containment Rig for the Australian Atomic Energy Commission. This experiment was significantly different than CSNI Standard Problem No. 2 in that it was performed in a containment that was much smaller and that had steel rather than concrete walls. It is a simpler system, but, it makes severe demands on some aspects of the analytical modeling techniques and scaling laws. COBRA-NC was used to predict the response of the containment to the blowdown transient. This was a post-test calculation to assess the models for condensation heat transfer coefficients.

4.1 Description of Experiment

The experimental apparatus consisted of a high-pressure blowdown vessel connected to a two-compartment steel containment vessel by a blowdown pipe. The containment vessel is shown in Figure 26. The vessel is uninsulated and freestanding within a large building. The two containment compartments are interconnected via a square-edge orifice plate and a flow tube. There is a circular deflector plate at 45° to the incoming blowdown flow in the upper compartment to disperse the influx around the chamber and prevent large crossflows at the intercompartment orifice. The containment is arranged so that water condensed on the surface of the top chamber will be collected on the partition plate and not flow through the orifice. The geometrical dimensions, materials, and material properties of the test containment are given in Tables 10 and 11. The initial conditions for the test are given in Table 12. The blowdown mass flow rate and enthalpy were determined from drag-disc flowmeter, fluid temperature, density, and pressure measurements, and are given in Table 13.

4.2 COBRA-NC Model Description

Standard Problem No. 3 was modeled using the lumped parameter option. The nodalization used is shown in Figure 27. The containment was modeled with four lumped parameter nodes. The first (channel 1) modeled the lower part of compartment B beneath the flow tube. The second channel modeled the flow tube. The third modeled the upper region of compartment B that surrounds the flow tube. The fourth channel was used to model compartment A. The channel input data was calculated from information provided in Figure 26 and Table 10 and are listed in Table 14.

The vessel walls and internal structures were modeled with nine thermal conductors to model heat transfer from the containment atmosphere to solid surfaces. The logic in COBRA-NC does not allow a thermal conductor to connect to two channels in two different sections. Therefore, the partition wall

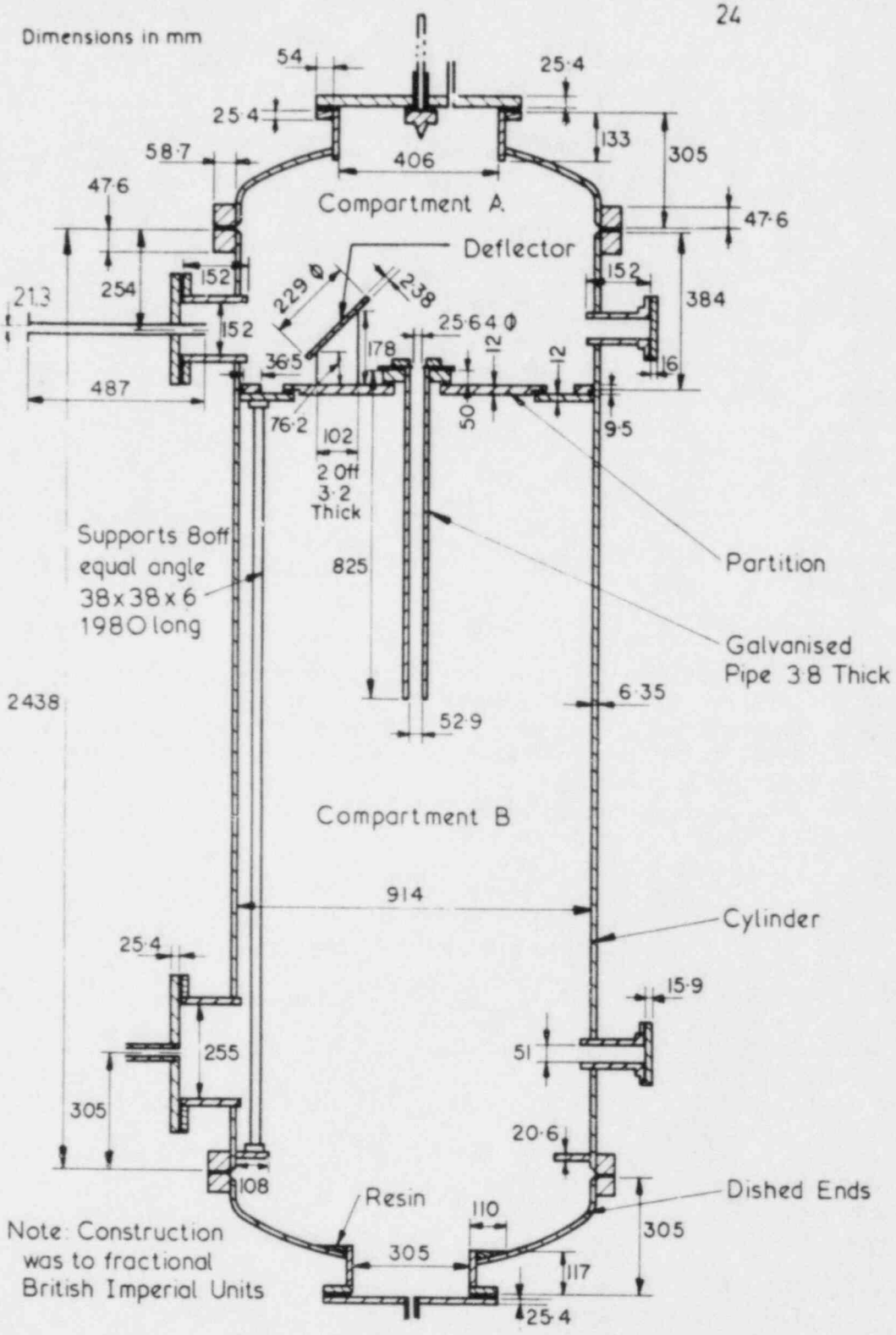

Figure 26 Containment vessel

Table 10 Containment geometrical data

Item	Enclosed Volume m^3	Surface Area m^2	Thickness[1] mm	Material[2]
COMPARTMENT A[3]				
Dished end	0.112	1.10	6.4	CS
Cylinder (inc. ports)	0.257	1.24	6.4	CS
Partition wall[4,5]	-	0.77	12.0	MS
Deflector (front only)	-	0.041	2.4	MS
COMPARTMENT B[3]				
Partition wall	-	0.66	12.0	MS
Cylinder (inc. ports)	1.33	5.97	6.4	CS
Dished end	0.108	1.07	6.4	CS
Supports[4]	-	2.47	6.0	MS
Support shelf	-	0.57	21.0	CS
Flow pipe internal	0.00055	0.137	3.8	Galv'd MS
external	-	0.147		

Notes: 1. Thickness of region with most surface area (rounded off).
2. Carbon steel AS.B58 (CS) mild steel (MS).
3. Unless otherwise stated, all internal surfaces covered with zinc-rich paint British Paints Zincanode 304 at nominal thickness 75.10^{-6} m.
4. Zinc plated, not painted.
5. Includes flow pipe mount.

Table 11 Material Properties

Material	Density $kg\ m^{-3}$	Specific Heat $J\ kg^{-1}\ K^{-1}$	Thermal Conductivity $W\ m^{-1}\ K^{-1}$	Temperature °C
Carbon steel[1]	7860	486	51	100
Mild steel[1]	7860	486	51	100
Zinc paint[2]	3260	430	11	-

Notes: 1. Data taken from "Metals Reference Book", C. J. Smithells (Fifth Edition) for materials of nearest specification.
2. Data estimated

Table 12 Initial conditions

Item	Value
Pressure vessel	
Pressure	10.4 MPa
Temperature in vessel	587°K
Water Mass (total	8.5 kg
Containment (both compartments)	
Pressure	100 kPa
Wall temperature	16.3°C
Humidity	100%
Ambient conditions	
Pressure	99.3 kPa
Temperature	16.5°C

Table 13 Blowdown flow rate and enthalpy

Time s	Mass Flow rate kg s^{-1}	Enthalpy kJ.kg^{-1}
0.	0.	94.5
0.048	0.875	322
0.15	0.96	1000
0.55	0.833	1125
0.65	0.834	1134
0.82	0.895	1091
1.0	0.817	1169
1.3	0.829	1283
2.0	0.784	1351
3.0	0.747	1379
4.0	0.707	1373
6.0	0.638	1351
8.0	0.578	1334
10.0	0.520	1306
10.9	0.503	1290
11.7	0.488	1274
11.8	0.093	2170
12.5	0.104	2161
13.0	0.106	2153
18.0	0.040	2810
30.0	0.008	2913
43.0	0.0	2900

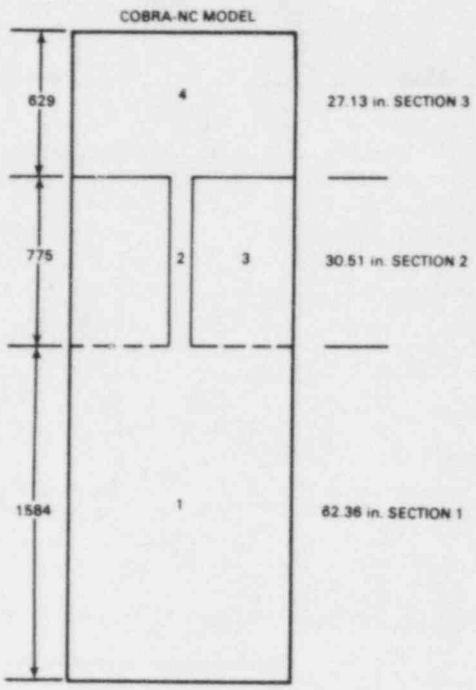

Figure 27 COBRA-NC mesh for CSNI-3

Table 14 Channel input data

Channel Number	Area ($in.^2$)	Height (in.)	Wetted Perimeter (in.)
1	914.4	62.36	160.9
2	3.407	30.51	6.542
3	1007.0	30.51	167.5
4	828.4	27.13	113.0

between the upper and lower compartment, was split at the center line. Half of the mass was modeled in the upper compartment and half of the mass was modeled in the lower compartment. Thus, no heat transfer from the atmosphere in compartment A through the partition to the atmosphere in compartment B was calculated. The input data for the nine thermal conductors is given in Table 15. The outside surface of the vessel wall was set to the measured temperatures for the upper compartment and to the ambient temperature for the

Table 15 Conduction model input

Conductor Number (TYPE)	Channel Number	Surface Area ($in.^2$)	Material Volume ($in.^3$)	Material Thickness (in.)	Wetted Perimeter (in.)	Surface Modeled by Conductor
1(WALL)	3	1,022.9	241.6	0.2362	33.5	Partition wall on compartment B side
2 (TUBE)	1	7,327.3	1846.4	0.2520	117.5	Vessel wall in compartment B - lower section
3 (TUBE)	3	3584.9	903.4	0.2520	117.5	Vessel wall in compartment B - upper section
4 (WALL)	1	883.6	365.3	0.4134	14.1	Support shelf in compartment B
5 (TUBE)	2	212.3	31.77	0.1496	6.9	Inside of flow pipe
5 (TUBE)	3	227.8	34.08	0.1496	7.4	Outside of flow pipe
6 (WALL)	4	1193.7	281.9	0.2362	44.0	Partition wall on compartment A side
7 (TUBE)	4	3827.6	913.8	0.2519	133.7	Vessel wall in compartment A
8 (WALL)	1	2570.7	303.6	0.1181	41.2	Supports in compartment B - lower section
9 (WALL)	3	2570.7	303.6	0.1181	41.2	Supports in compartment B - upper section

lower compartment to account for heat loss to the surroundings. The material properties given in Table 11 were used for the appropriate conductors. The initial conditions for the containment were set to those specified in Table 12. A flow and a pressure boundary condition were specified at the top of channel 4 using the flow rate and enthalpies provided in Table 13.

4.3 Discussion of Results

This experiment differs from other water blowdown containment experiments in that it consisted of a high energy blowdown rate into a small steel compartment rather than a larger concrete compartment. The effects of turbulence can be expected to dominate the heat transfer during such an experiment. This test was first simulated using the Tagami correlation for the condensation heat transfer coefficient in the upper compartment during the water blowdown period and the Uchida correlation thereafter. The Uchida correlation was used in the lower compartment. The upper compartment pressure prediction for this case is shown in Figure 28. As can be seen from the figures, the compartment pressure is greatly overpredicted, indicating that the Tagami model does not adequately model the condensation heat transfer processes for this experiment.

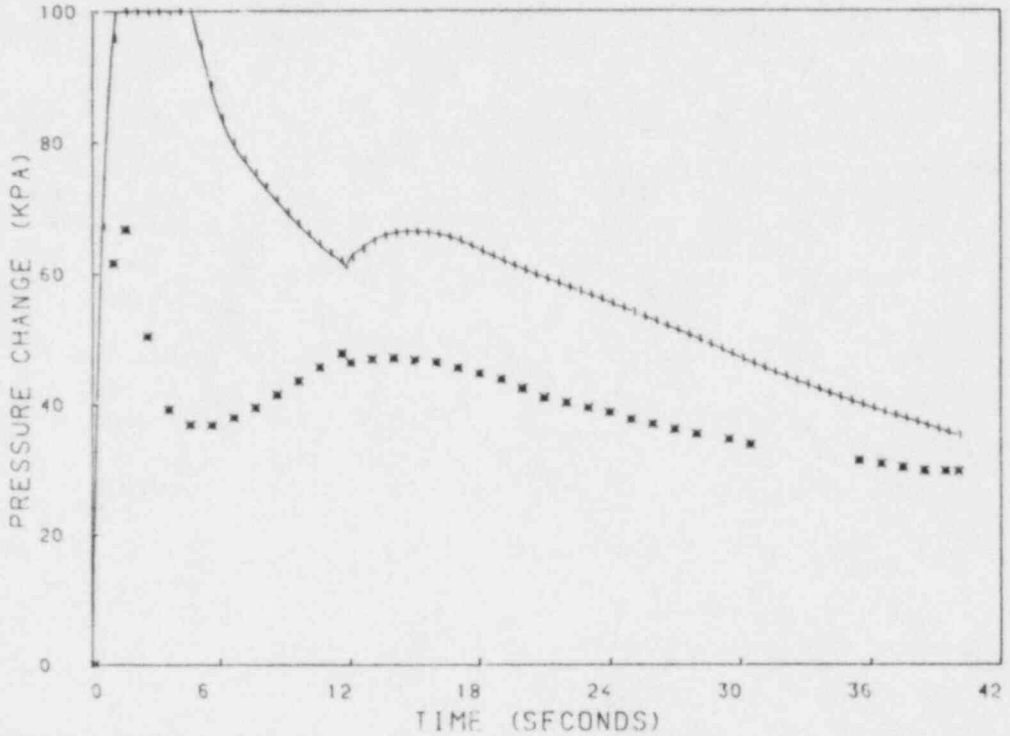

Figure 28 Prediction for the pressure in the upper compartment based on the Tagami-Uchida heat transfer coefficient model

The Uchida correlation also underpredicts the heat transfer during the post-blowdown interval.

The model was then run using a "best-fit" heat transfer coefficient. This model was developed by assuming a rapid increase to the maximum value predicted by the Tagami correlation. The value was held constant till the end of blowdown, at which time the heat transfer coefficient was reduced to a value of 3.0 $kW/m^{2o}K$ and held constant for the remainder of the test. The Uchida correlation was used in the lower compartment. The values used for heat transfer coefficients during the transient are compared to measured values and values used by other standard problem participants in Figure 29. The COBRA-NC values are designated USA in this and all of the remaining figures. The measured data is shown with an asterisk and the COBRA-NC values with a triangle. All measured values are taken at a single point in the compartment. Considerable spatial variation in each of the quantities (other than pressure) was measured in each compartment, so the code values should be thought of as average values for the entire compartment. Heat transfer coefficients for the lower compartment are shown in Figure 30. Pressure predictions for the upper and lower compartment are shown in Figure 31. There is reasonable agreement between the COBRA-NC prediction and the data, indicating that the code can predict the shape and magnitude of the pressure in each compartment

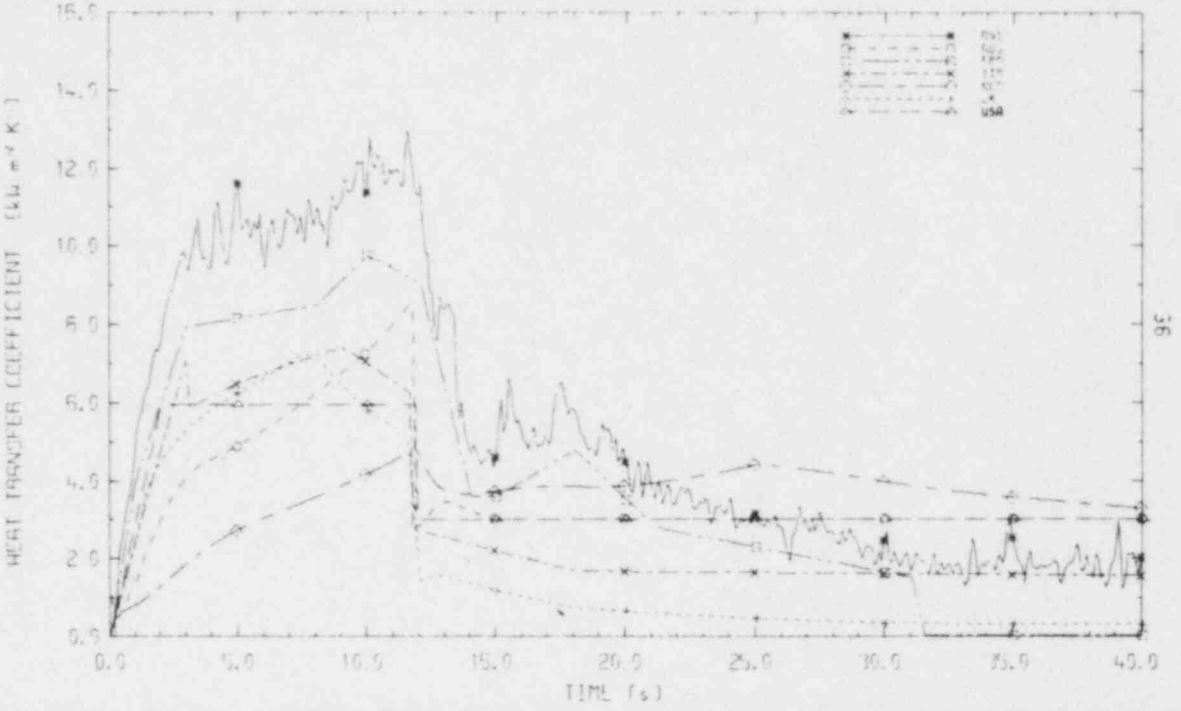

Figure 29 CASP3: average heat transfer coefficient comparison compartment A

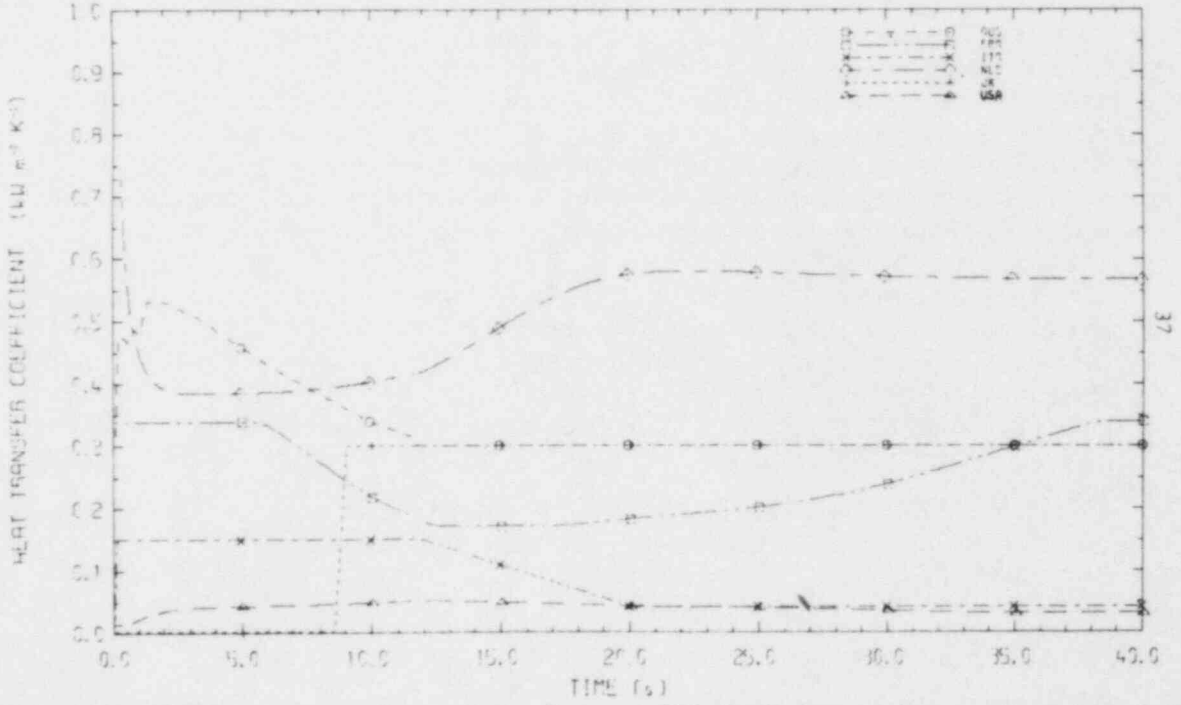

Figure 30 CASP3: average heat transfer coefficient comparison compartment B

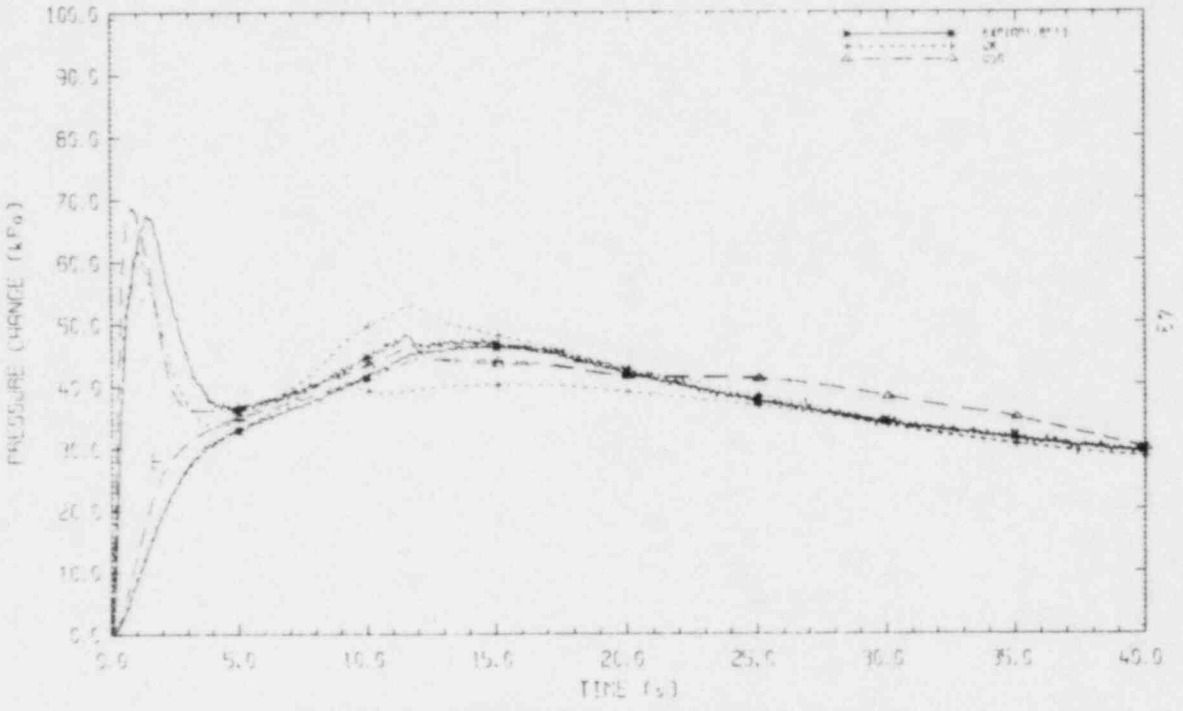

Figure 31 CASP3: pressure comparison

provided that a good value for the heat transfer coefficient is available. Comparison with the measured fluid temperatures and the wall temperature in compartment A are shown in Figures 32 and 33. Again, these should be regarded as compartment average values. The predictions certainly fall within the range of measurements taken at different locations in the compartment. Gas temperature measurements at three locations are given in Figure 34. The differential pressure between compartments is shown in Figure 35.

It may be that the vast disparity in scale between this test and a reactor containment makes the behavior so different as to nullify the value of the test. However, the test does point out that the simple correlations now used for condensation heat transfer are limited in their range of applicability, and that more sophisticated models for condensation heat transfer processes are required before the code can be applied to new situations with greater confidence.

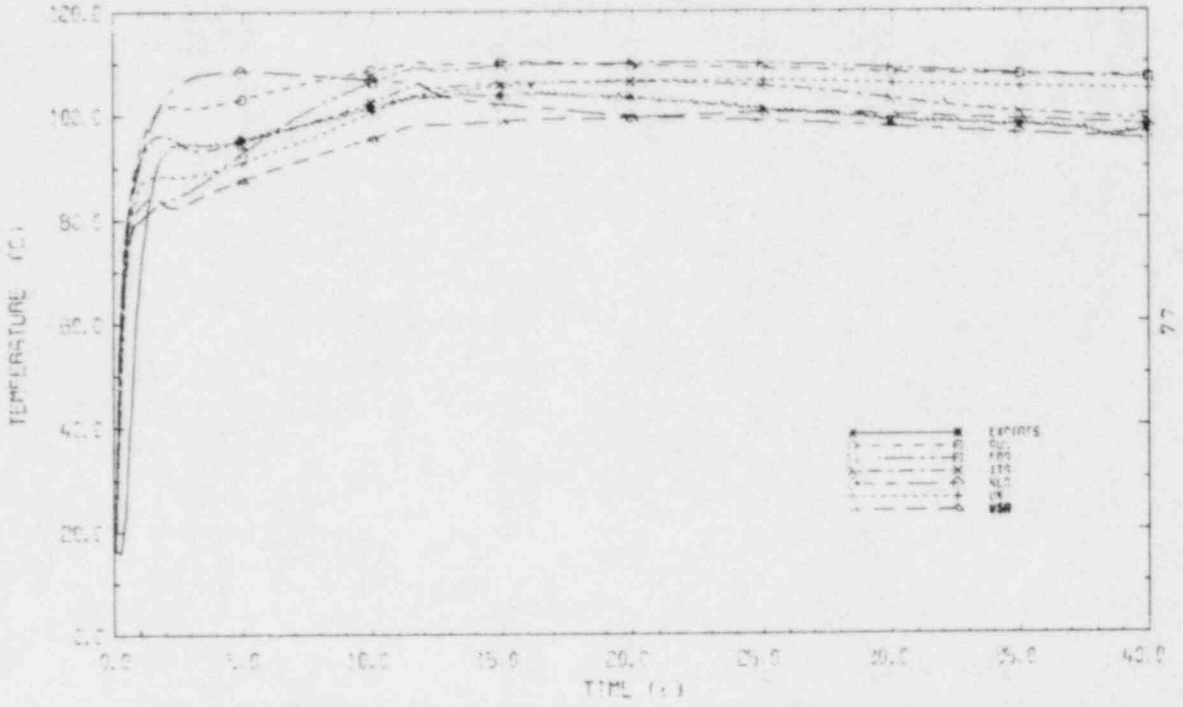

Figure 32 CASP3: fluid temperature comparison compartment A

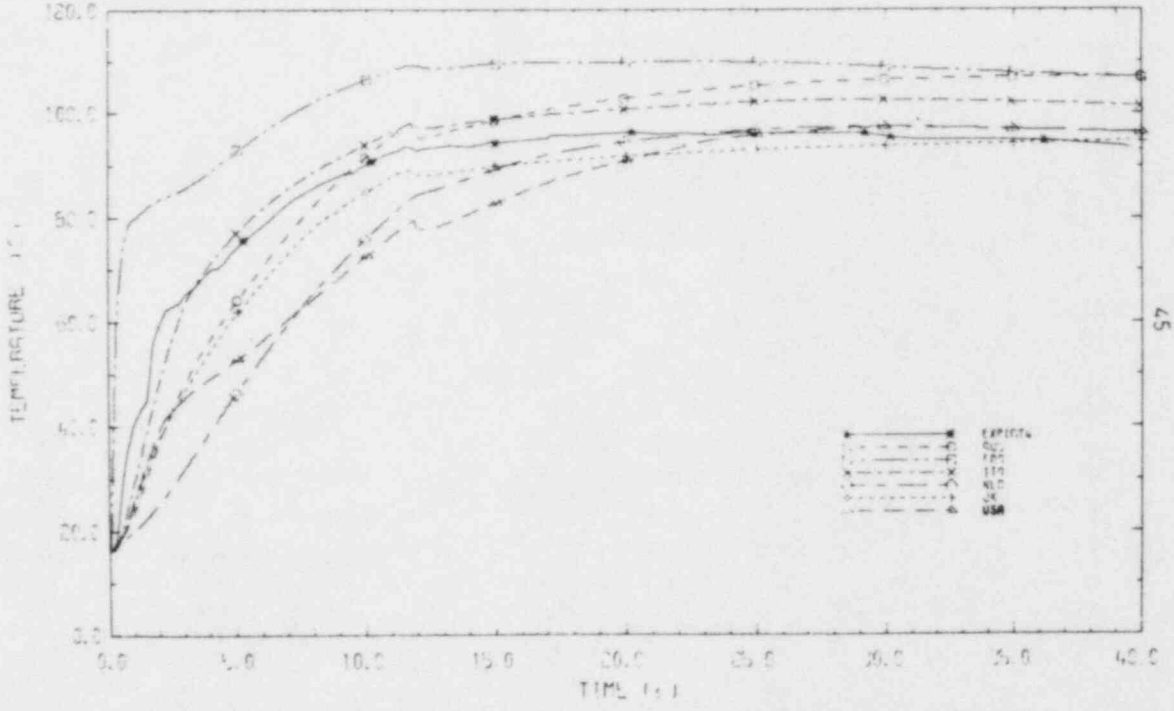

Figure 33 CASP3: wall temperature comparison compartment A

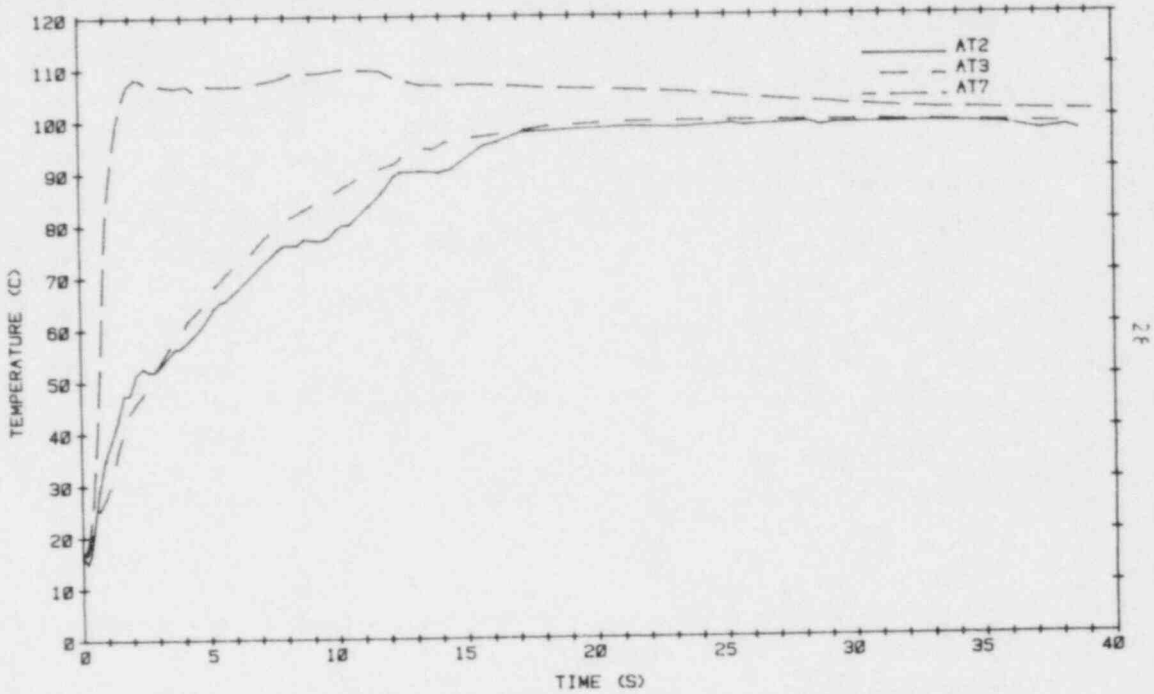

Figure 34 CASP3: gas temperatures in compartment A

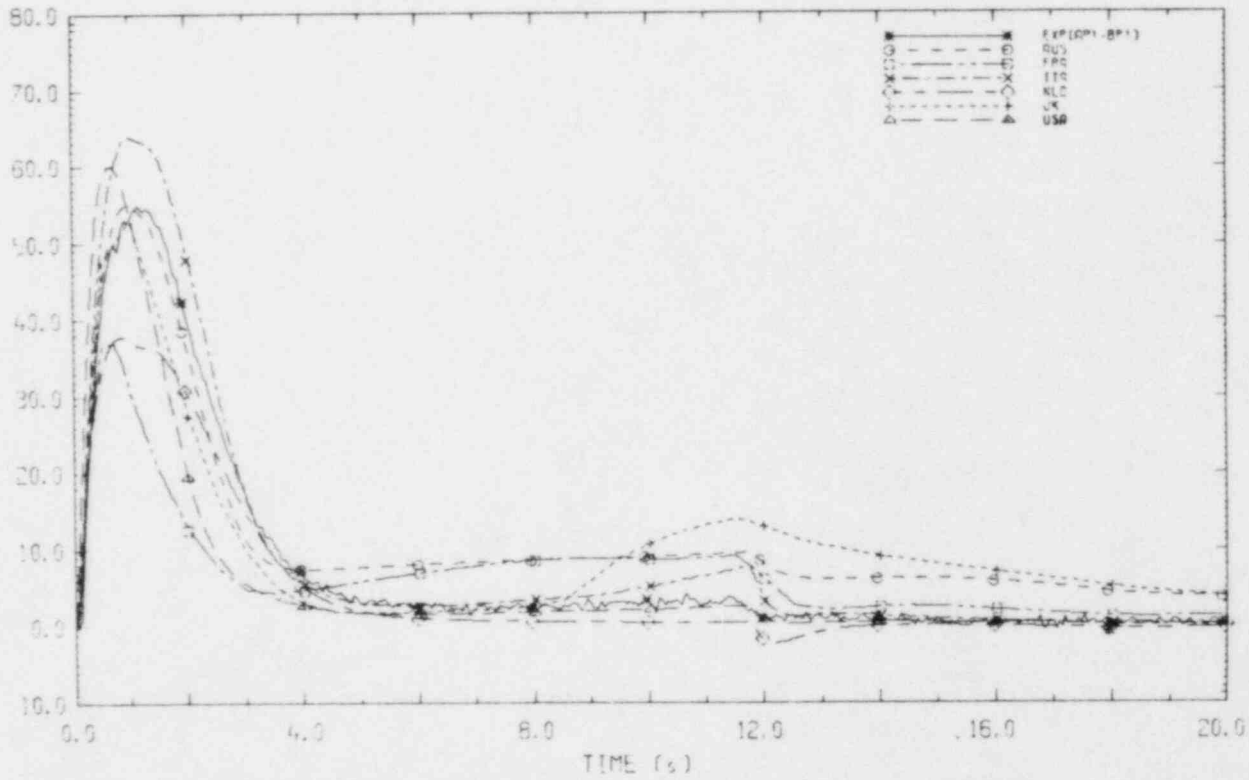

Figure 35 CASP3: differential pressure across partition

5.0 BATTELLE-FRANKFURT STEAM BLOWDOWN TESTS D1 AND D15

Several steam blowdown experiments were conducted in the Battelle-Frankfurt model containment (Ref. 4). The purpose of these tests, referred to as the D series, was to measure the response of containment systems to high-energy steam blowdown flows for the purpose of providing experimental data under idealized, simplified conditions for the assessment of computer codes to be used for the analysis of full-scale containments. COBRA-NC was used to simulate the tests in order to evaluate the condensation heat transfer coefficients to be used in the code. Two D series tests were simulated, test D1 and test D15.

5.1 Description of the Experiment

The experimental facility is described in Section 3.1. A drawing of the model containment is given in Figure 5. The high-pressure system initially contained a steam/water mixture at the saturation conditions for 69.5 bar for test D1 and 69.8 bar for test D15. The duration of the steam blowdown was 3.0 s for test D1 and 2.92 s for test D15.

The compartmental arrangement for test D1 is shown in Figure 36. The blowdown is located in room 6. Room 6 is connected to room 4 via a horizontal flow path. Room 4, in turn, connects to room 9 via a vertical flow path. The volumes of each of the rooms and surface areas of solid structure are given in Table 16. The area of openings between each room was 0.2827 m^2. The initial room pressure was 1.0 bar, and the initial temperature was 13.2°C. The blowdown consisted of saturated steam with an average enthalpy of 1192.7 Btu/lbm. The mass flow rate for test D1 is given in Table 17.

The compartment arrangement for test D15 is shown in Figure 37.

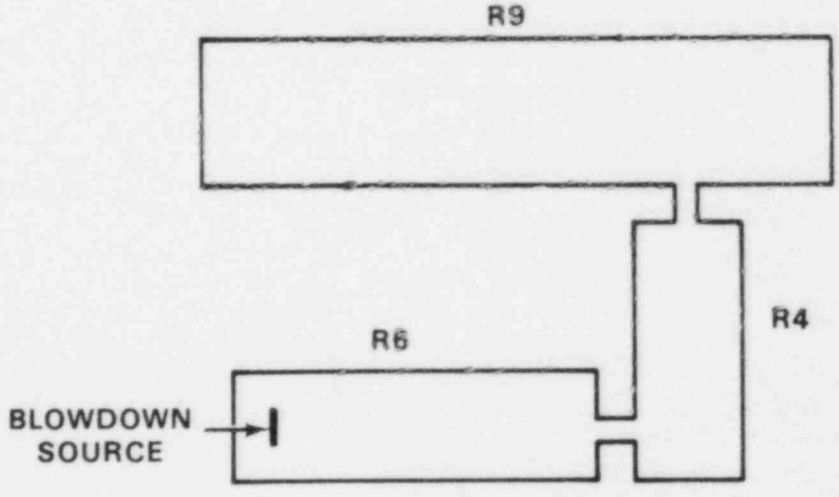

Figure 36 Compartment configuration for test D1

Table 16 Geometrical data for test D1

Room Number	Volume (m^3)	Surface Area (m^2)
6	41.26	118.0
4	12.00	55.0
9	550.00	896.0

Table 17 Blowdown mass flow rate for test D1

Time (s)	Mass Flow (kg/s)	(lbm/sec)
7.00	0.0	0.0
0.02	72.4	159.6
0.05	84.6	186.5
0.075	86.6	190.9
0.1	82.4	181.6
0.2	71.4	157.4
0.3	57.8	127.4
0.5	49.9	110.0
1.0	45.3	99.8
1.5	43.1	95.0
2.0	41.4	91.3
3.0	36.8	81.1

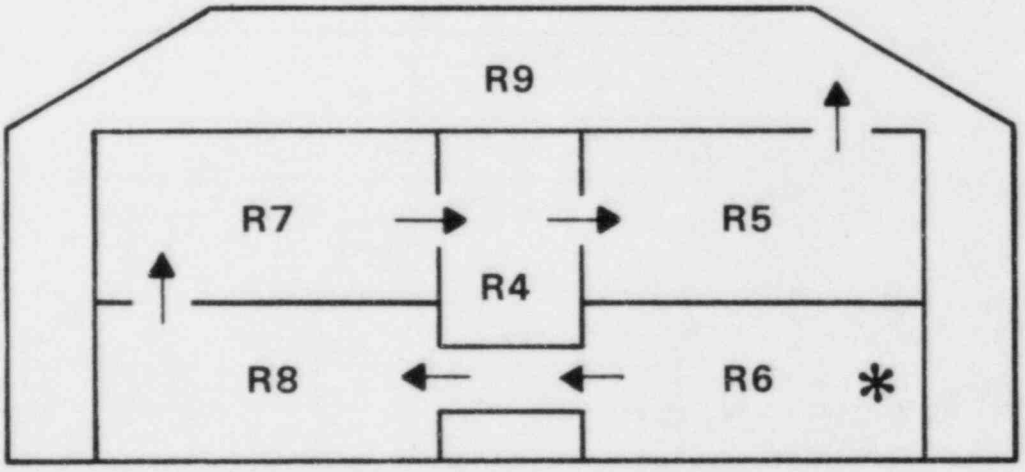

Figure 37 Compartment arrangement for test D15

The blowdown nozzle is located in room 6. Room 6 connects with room 8 through a 0.430 m^2 horizontal duct. Room 8 connects vertically to room 7 through a 0.442 m^2 orifice. Room 7, 4, and 5 then connect in a horizontal chain through two 0.442 m^2 orifices. Room 5 connects to room 9 through a vertical 0.442 m^2 orifice. The room volumes and structural surface area for test D15 are given in Table 18. The initial atmosphere conditions for test D15 were 100% humidity, 1 bar, and 19.9°C. The blowdown consisted of saturated steam at the mass flow rates and enthalpies given in Table 19.

Table 18 Geometrical data for test D15

Room Number	Volume (m^3)	Structural Surface Area Concrete (m^2)	Steel (m^2)
6	41.26	90.12	25.7
8	40.53	92.0	18.3
7	40.40	76.6	16.0
4	12.20	38.6	16.4
5	41.05	76.1	27.4
9	450.00	645.8	87.5

Table 19 Blowdown mass flow rate and enthalpy for test D15

Time (s)	Mass Flow (kg/s)	(lbm/sec)	(Btu/lbm)
0.000	0.0	0.0	1192.3
0.007	0.0	0.0	1192.3
0.015	70.0	154.3	1192.3
0.025	82.0	180.8	1192.1
0.060	88.0	194.0	1192.1
0.090	77.0	169.8	1189.5
0.150	74.0	163.1	1188.4
0.300	57.0	125.7	1184.6
0.550	47.0	103.6	1184.8
0.750	45.0	99.2	1183.8
2.800	38.0	83.8	1170.6
2.950	26.0	57.3	1171.1
3.000	60.0	132.3	635.4
4.000	73.0	160.9	639.1
6.000	57.0	125.7	689.9
10.000	40.0	88.2	824.2

5.2 COBRA-NC Model Description

Tests D1 and D15 were both modeled using the lumped parameter option. The nodalization used for test D1 is shown in Figure 38. The containment was modeled with four, single-celled channels. Channel 1 was used to model room 6. Channels 2 and 3 represent room 4 and channel 4 represents room 9. Thermal conductors were connected to each channel to model the heat transfer between the containment atmosphere and the containment solid structures. The channel input data for test D1 is given in Table 20. Horizontal connections between rooms were modeled with gaps. The gap input for test D1 are given in Table 21. Thermal conductor input data is given in Table 22. All structural surfaces were assumed to be constructed of concrete, 0.25 m thick. The flow rates given in Table 17 were specified as a flow boundary condition at the bottom of channel 1.

The nodalization used for test D15 is shown in Figure 39. Nineteen one node high channels were used to model the containment. Channels 1 through 4 modeled room 6. Channels 5 through 9 model room 8. Channels 9 and 14 represent room 4, channels 10 through 13 model room 7 and channels 15 through 18 represent room 5. The large room is modeled with channel 19. The crossover pipe, as well as the horizontal connection to room 4, are modeled as gaps. The vertical connections are modeled by specifying the correct flow area at the top of a channel.

The channel input data for test D15 is given in Table 23. The gap input data is given in Table 24. Input data for the thermal conductors are given in Table 25. The location of each of the thermal conductors is illustrated in Figure 39 as shaded boxes. The material properties used for the concrete and steel are given in Table 22. A flow boundary condition having the flow rate and enthalpy specified in Table 19 was specified at the bottom of channel 1.

5.3 Discussion of Results

Predictions were made for the pressure in several rooms of the containment for the duration of the steam blowdown transient (3.0 s). Two sets of data predictions were made for each test. The first set of predictions was made using the Uchida correlation with an upper limit of 1590 $w/m^{2o}K$. This upper limit only affected the last part of the transient (less than 0.5 s), since the value obtained from the Uchida correlation was below the upper limit during most of the transient based on the steam-to-air mass ratios computed by the code. The second set of comparisons was made using a constant value for the heat transfer coefficient equal to the peak value computed using the Tagami correlation. This set of comparisons was made to determine the sensitivity of the calculations to the value used for the heat transfer coefficient.

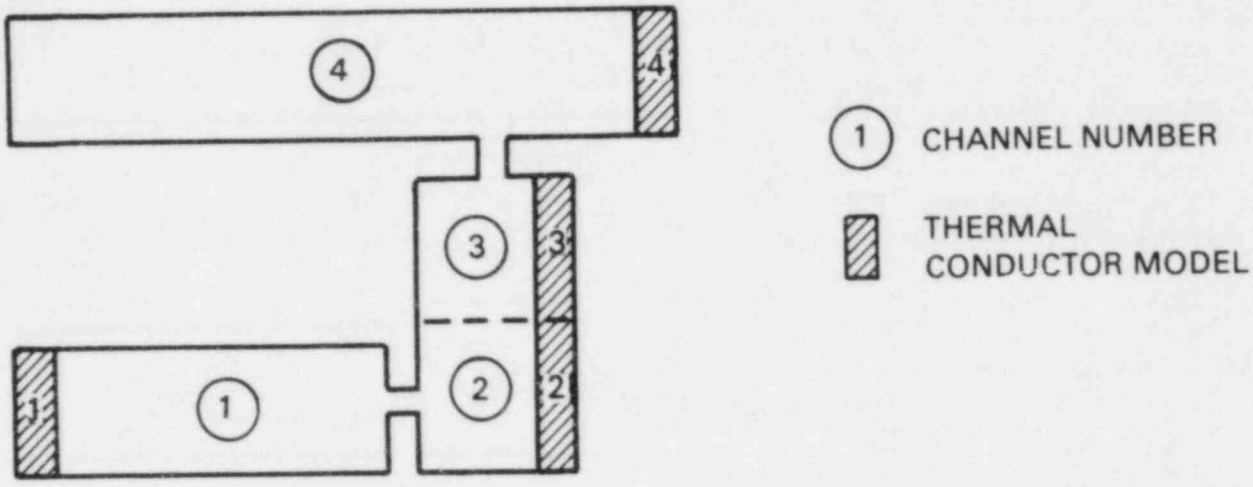

Figure 38 Nodalization for test D1

Table 20 Channel input data for test D1

Channel Number	Area ($in.^2$)	Wetted Perimeter (in.)	Area of Connection ($in.^2$)	Height (in.)
1	25,000	908.1		99.4
2	3,579	240.1		99.4
3	3,579	240.1	437.9	91.4
4	120,000	8,881.0		228.7

Table 21 Gap input data for test D1

Gap Number	Channels Connected by Gap	Gap Width (in.)	Area ($in.^2$)	Centroid Distance (in.)	Velocity Head Loss Coefficient
1	1 & 2	4.406	437.95	221.1	1.037

Table 22 Thermal conductor input data for test D1

Room Number	Conductor Number	Channel Number	Material Surface Area ($in.^2$)	Wetted Thickness (in.)	Perimeter (in.)
6	1	1	183,094	9.84	1842.0
4	2	2	25,257	9.84	254.1
4	3	3	23,224	9,84	254.1
9	4	4	1,383,589	9.84	4952.0

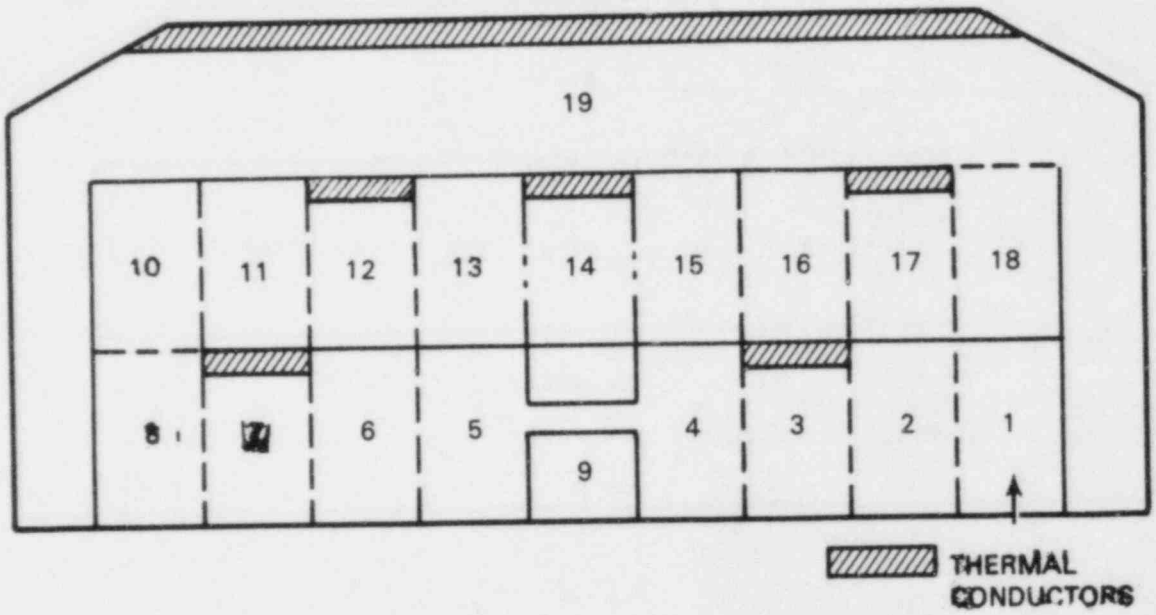

Figure 39 Nodalization for test D15

Table 23 Channel input data for test D15

Channel Number	Room Number	Area ($in.^2$)	Wetted Perimeter (in.)	Height (in.)	Connection Area ($in.^2$)	Vent Modeled by Connection
1	6	6323.0	194.6	99.45		
2	6	6323.0	194.6	99.45		
3	6	6323.0	194.6	99.45		
4	6	6323.0	194.6	99.45		
5	8	6213.0	191.6	99.45		
6	8	6213.0	191.2	99.45		
7	8	6213.0	191.2	99.45		
8	8	6213.0	191.2	99.45	685.2	U78B
9	4	3756.0	245.2	99.45		
10	7	6393.0	196.8	96.35		
11	7	6393.0	196.8	96.35		
12	7	6393.0	196.8	96.35		
13	7	6393.0	196.8	96.35		
14	4	3756.0	245.2	96.35		
15	5	6495.0	199.9	96.35		
16	5	6495.0	199.9	96.35		
17	5	6495.0	199.9	96.35		
18	5	6495.0	199.9	96.35	685.2	U59A
19	9	77904.0	988.8	352.08		

Table 24 Gap input data for test D15

Gap Number	Channels Connected by Gap	Gap Width (in.)	Area ($in.^2$)	Centroid Distance (in.)	Vent Modeled by Gap	Velocity Head Loss Coefficient
1	1 & 2	64.96	6460.0	97.34		
2	2 & 3	64.96	6460.0	97.34		
3	3 & 4	64.96	6460.0	97.34		
4	4 & 5	6.699	666.0	177.1	U46 & U48	1.52
5	5 & 6	64.96	6460.0	95.64		
6	6 & 7	64.96	6460.0	95.64		
7	7 & 8	64.96	6460.0	95.64		
8	10 & 11	64.96	6460.0	98.4		
9	11 & 12	64.96	6259.0	98.4		
10	12 & 13	64.96	6259.0	98.4		
11	13 & 14	7.110	685.0	86.6	U47	1.52
12	14 & 15	7.110	685.0	87.39	U45	1.52
13	15 & 16	64.96	6259.0	99.99		
14	16 & 17	64.96	6259.0	99.99		
15	17 & 18	64.96	2259.0	99.99		

Table 25 Thermal conductor input data

Room Number	Conductor Number	Channel Number	Surface Area ($in.^2$)	Material Thickness (in.)	Wetted Perimeter (in.)	Material
6	1	3	139,626.0	4.92	1404.0	Concrete
8	2	7	142,609.0	4.92	1434.0	Concrete
7	3	12	118,797.0	4.92	1233.0	Concrete
4	4	14	59,832.0	4.92	621.0	Concrete
5	5	17	118,026.0	4.92	1225.0	Concrete
9	6	19	742,536.0	4.92	2109.0	Concrete
6	7	3	39,838.0	0.5	401.0	Steel
8	8	7	23,342.0	0.5	285.0	Steel
7	9	12	18,402.0	0.5	191.0	Steel
4	10	14	25,435.0	0.5	264.0	Steel
5	11	17	31,506.0	0.5	327.0	Steel
9	12	19	100,695.0	0.5	286.0	Steel

Predictions for the pressure in rooms 6, 4, and 9 during test D1 using the Uchida correlation are shown in Figures 40, 41, and 42. The Uchida correlation apparently underpredicts the heat transfer during the first 3 s of the transient as the pressures in all three rooms are overpredicted. The overprediction is not unreasonable, however, and represents an acceptably conservative calculation. The prediction obtained using a constant heat transfer coefficient of 3773.0 $w/m^{2o}K$ is given in Figures 43, 44, and 45. These predictions compare fairly well with the data. More significantly, however, is the observation that a change of more than a factor of two in the heat transfer coefficient caused a 25% decrease in the peak pressure. This difference may not be important if the conservatively calculated pressure is well within the design limits of the containment.

Predictions for test D15 based on the Uchida correlation are given in Figures 46 through 50. Again, the pressures are overpredicted. Apparently the resistance to flow out of the intermediate rooms into the large room (room 7) is too restrictive in the calculation as the pressure in these rooms (4, 7, and 8) are overpredicted to a larger extent than the other rooms. It is possible that additional leakage paths occurred between room 4 and room 9 during the course of the experiment.

Results obtained using a constant heat transfer coefficient of 2413 $w/m^{2o}K$ are shown in Figures 51 through 55. The prediction is quite reasonable for all rooms. Again, the total change in peak pressure between the two calculations may not be significant when considering the containment design pressure.

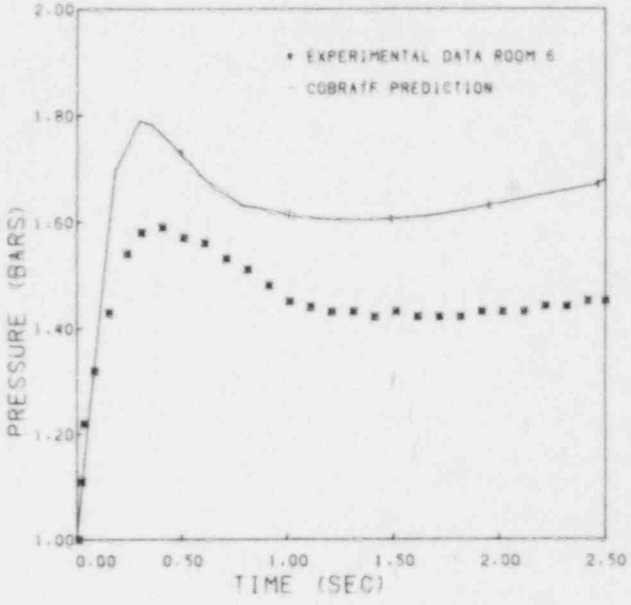

Figure 40 Pressure in room 6 for test D1-prediction based on the Uchida correlation

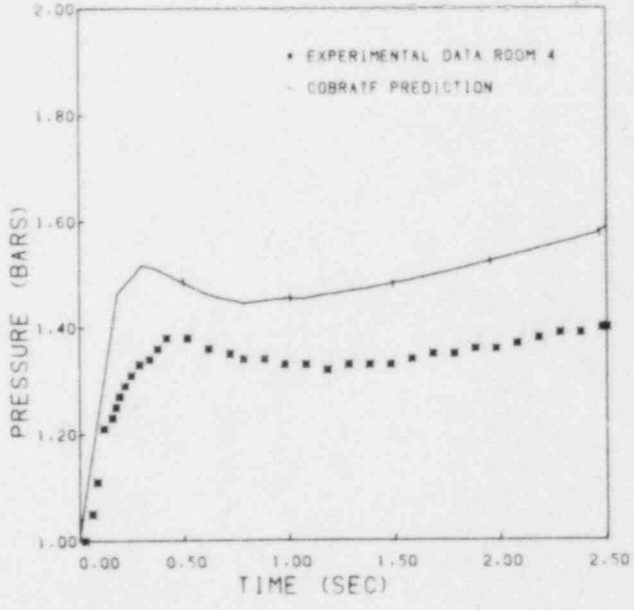

Figure 41 Pressure in room 4 for test D1-prediction based on the Uchida correlation

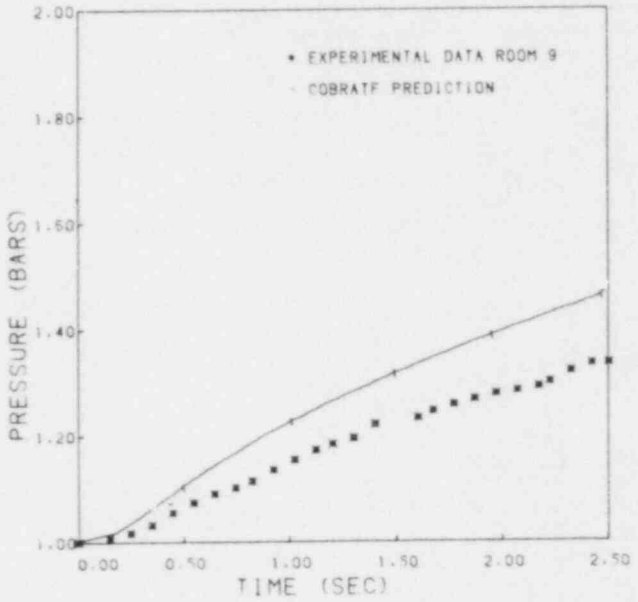

Figure 42 Pressure in room 9 for test D1-prediction based on the Uchida correlation

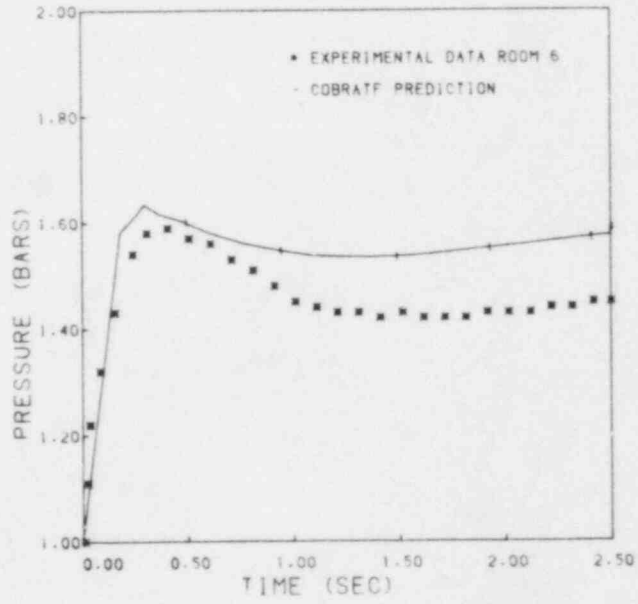

Figure 43 Pressure in room 6 for test D1-prediction using a constant heat-transfer coefficient

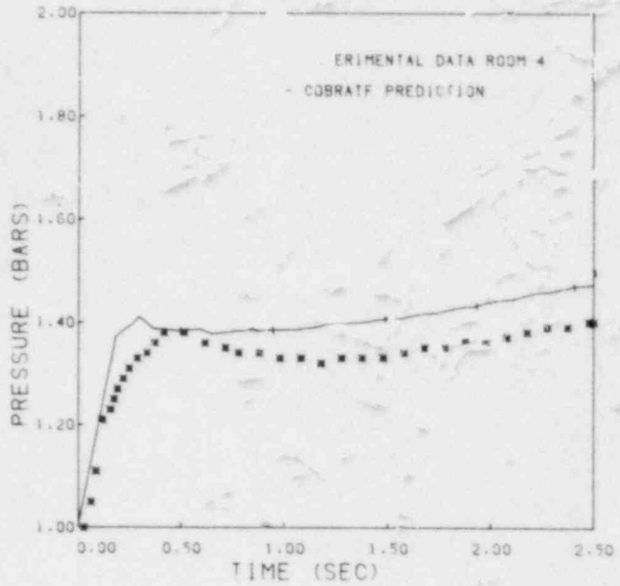

Figure 44 Pressure in room 4 for test D1-prediction using a constant heat-transfer coefficient

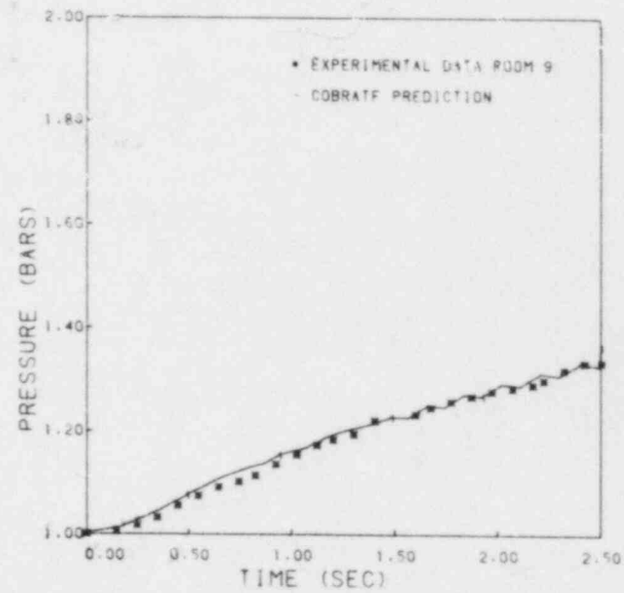

Figure 45 Pressure in room 9 for test D1-prediction using a constant heat-transfer coefficient

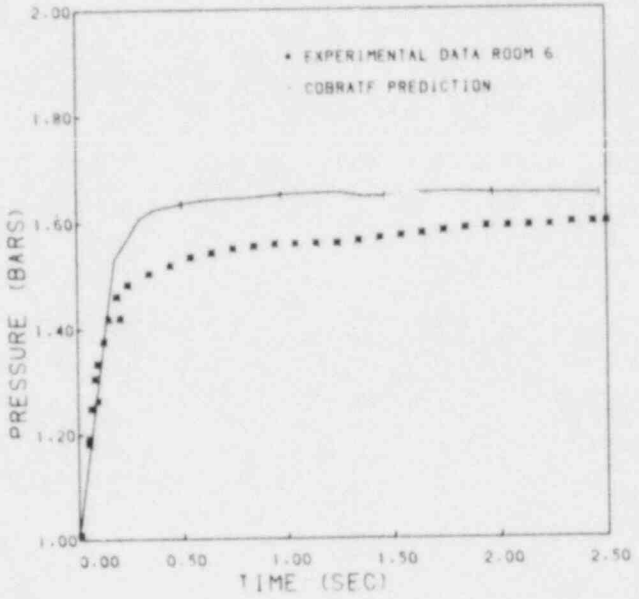

Figure 46 Pressure in room 6 for test D15-prediction based on the Uchida correlation

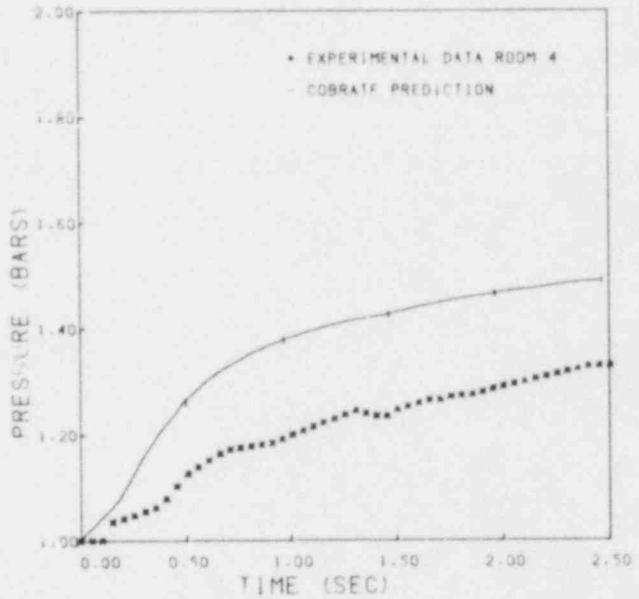

Figure 47 Pressure in room 4 for test D15-prediction based on the Uchida correlation

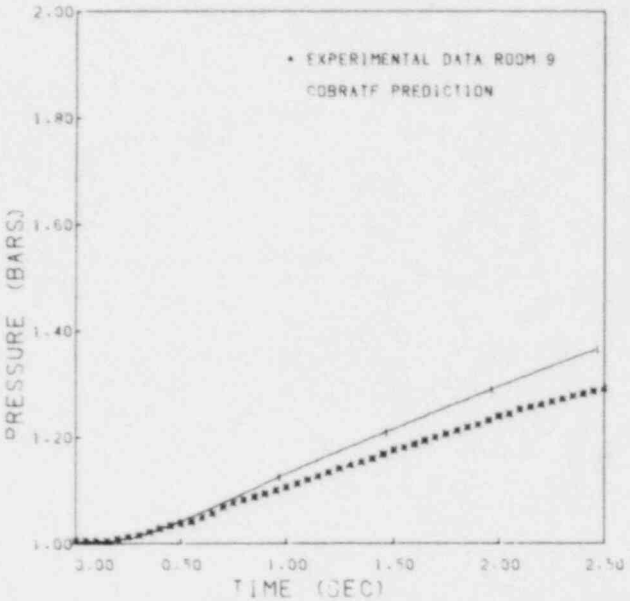

Figure 48 Pressure in room 9 for test D15-prediction based on the Uchida correlation

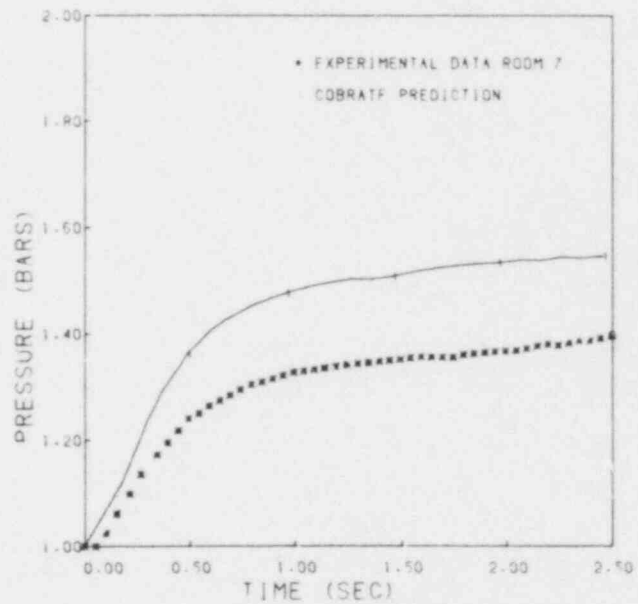

Figure 49 Pressure in room 7 for test D15-prediction based on the Uchida correlation

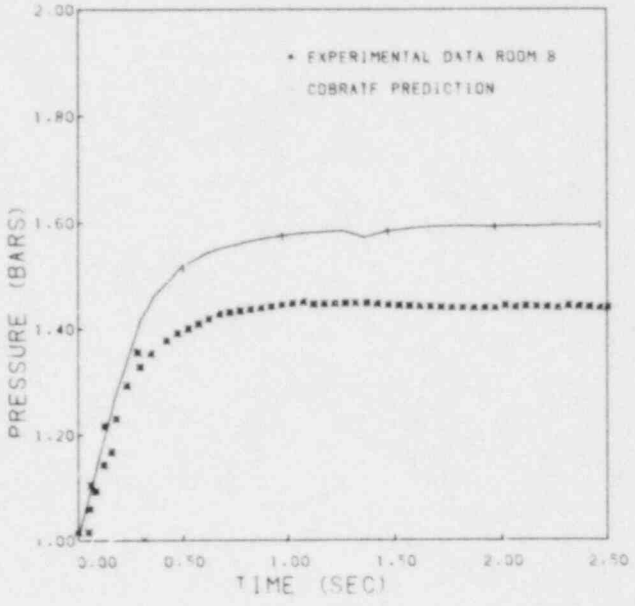

Figure 50 Pressure in room 8 for test D15-prediction based on the Uchida correlation

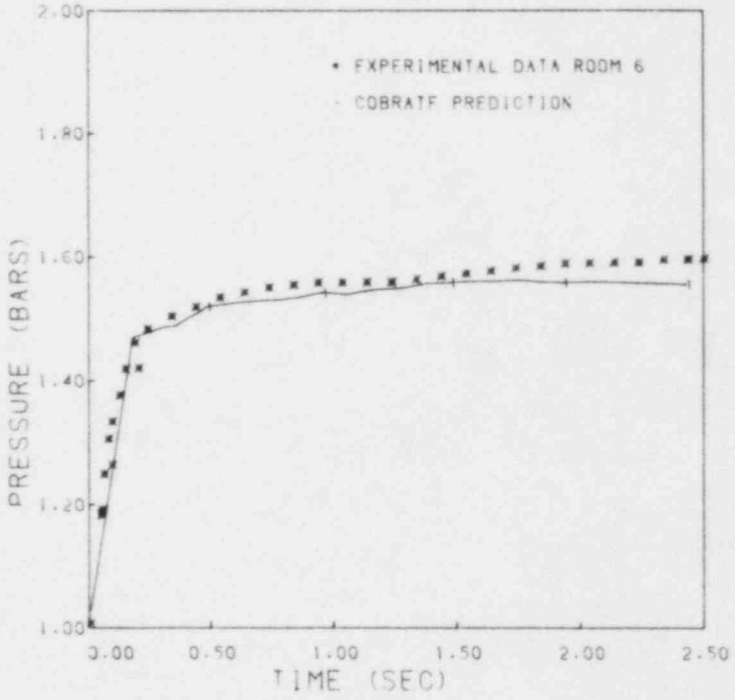

Figure 51 Pressure in room 6 for test D15-prediction using a constant heat-transfer coefficient

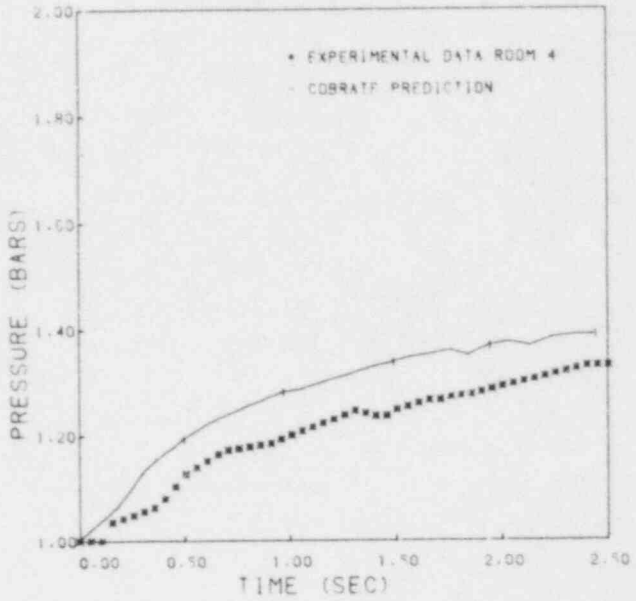

Figure 52 Pressure in room 4 for test D15-prediction using a constant heat-transfer coefficient

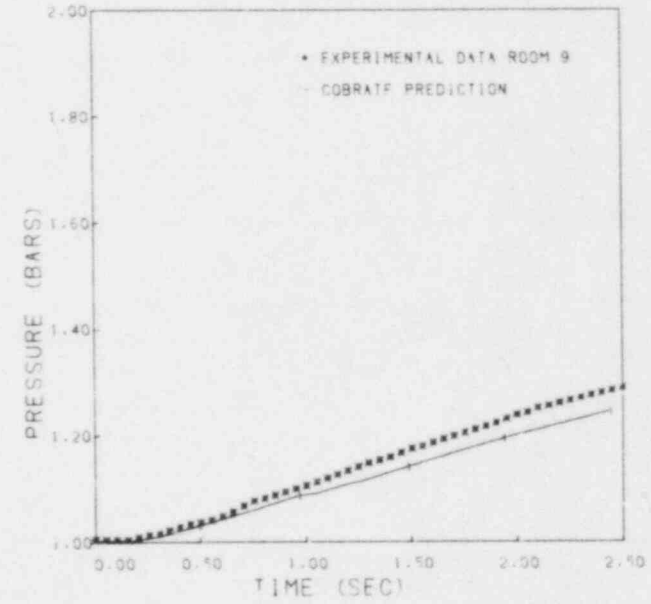

Figure 53 Pressure in room 9 for test D15-prediction using a constant heat-transfer coefficient

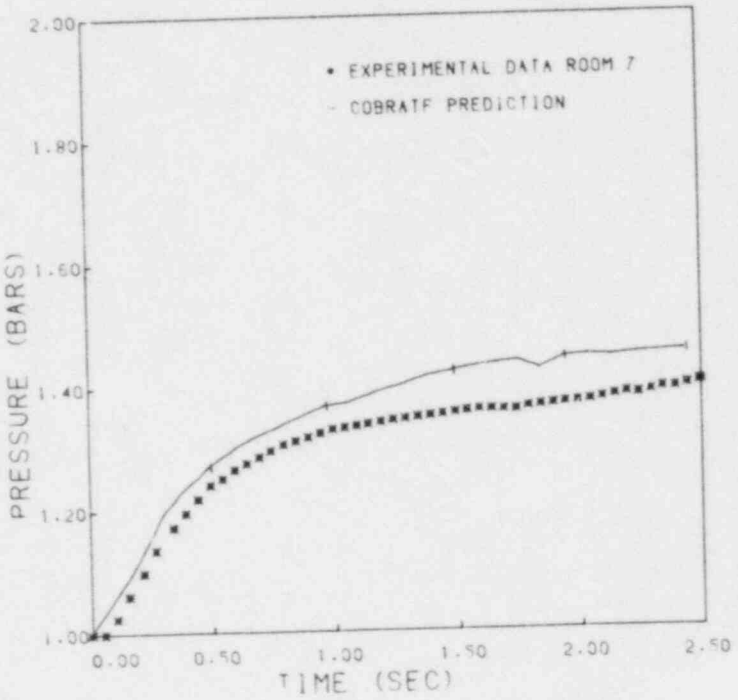

Figure 54 Pressure in room 7 for test D15-prediction using a constant heat-transfer coefficient

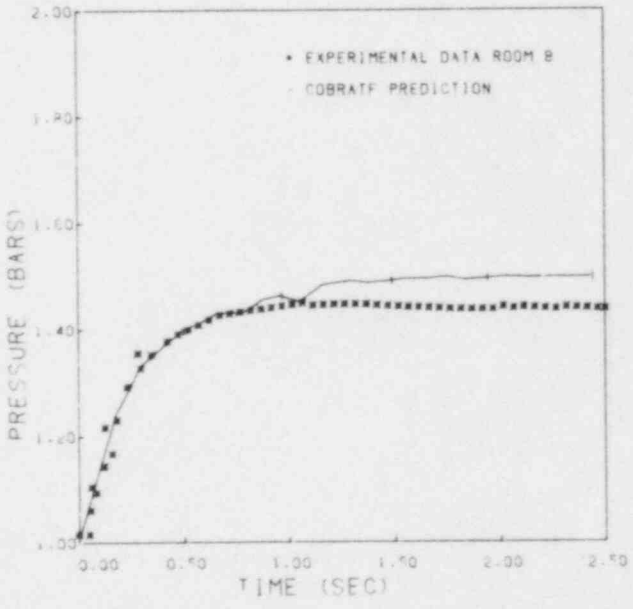

Figure 55 Pressure in room 8 for test D15-prediction using a constant heat-transfer coefficient

6.0 BATTELLE-FRANKFURT STEAM BLOWDOWN TESTS C13 AND C15

The Battelle-Frankfurt C series tests were run to model the response of nuclear reactor containments to high-energy steam/water blowdowns (Ref. 5). Two of these tests, tests C13 and C15, were selected for simulation by COBRA-NC to assess the code. These two tests have a different flow path geometry than the D series tests. They also differ from the D series test in that a steam/water mixture was used in the C series whereas a saturated steam blowdown was used in the D series.

6.1 Description of the Experiment

The experimental facility is described in Section 3.1 of this manual. A drawing of the model containment is given in Figure 5. The compartment arrangement for these two tests is shown in Figure 56. The blowdown was into room 1. All nine rooms of the containment were connected in these tests. Both tests C-13 and C-15 were designed to simulate PWR conditions prior to blowdown. The water in the pressure vessel was at 10 bar (2030 psia) and 295°C (563°F) for both tests. The only flow path from the blowdown room, room 1, was to room 3. From there the flow could enter each of the rooms via various flow paths. The primary difference between test C-13 and test C-15 was that the flow area between rooms 1 and 3 was halved in test C-15. The geometrical data for the containment rooms is given in Table 26.

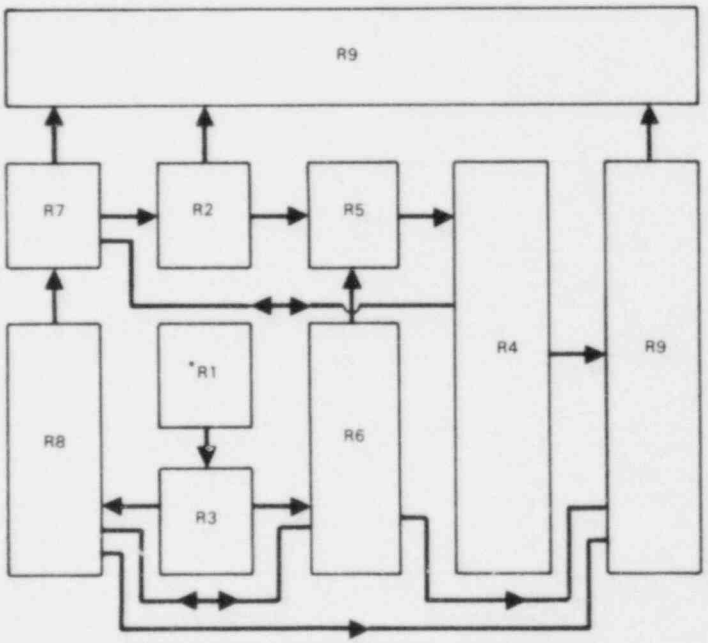

Figure 56 Compartment arrangement for tests C13 and C1

Table 26 Geometrical data for C series tests

Compartment Number	Volume (m^3)	Concrete (m^2)	Metal (m^2)
1	10.56	36.02	
2	17.70	5.98	
3	9.95	25.6	
4	13.02	38.65	8.8
5	1.05	76.10	17.2
6	1.26	90.18	9.59
7	0.0	76.68	15.2
8	0.53	92.05	6.17
9	367.36	65.82	57.3

Vent No.	Compartment Connected	Vent Area (m^2)
U3	R1/R3	0.3960
U25	R2/R5	0.0095
U27	R2/R7	0.053
U36	R3/R6	0.20
U38	R3/R8	0.20
U5	R/R5	0.276
U7	R/R7	0.276
U9	R/R9	0.059
U56	R5/R6	0.817
U59	R5/R9	0.238
U68	R6/R8	0.283
U69	R6/R9	0.118
U78	R7/R8	0.785
U79	R7/R9	0.238
U89	R8/R9	0.118

The blowdown mass flow rates and enthalpies for both tests are given in Table 27.

Table 27 Blowdown mass flow rate for tests C-13 and C-15

Time (s)	Mass Flow (kg/sec)	Enthalpy (kj/kg)
0.0	0.0	13.4
0.003	0.0	1314
0.007	537.	1314
0.036	230.2	1314
0.063	552.5	1314
0.105	665.9	1270
0.13	93.1	1274
0.199	22.5	1280
0.366	06.7	1298
0.766	33.2	1298
1.166	360.5	1296
1.567	390.7	1294
2.000	356.2	1294
4.007	317.2	1304
6.007	27.2	1318
8.007	225.9	1332
10.000	19.5	1327
18.208	73.2	1553
25.92	13.3	1255
33.198	9.6	967
40.000	2.0	988

6.2 COBRA-NC Model Description

Tests C-13 and C-15 were modeled using the lumped parameter option. The mesh used for the calculations is shown in Figure 57.

The large bold numbers in this figure represent the containment compartment number. The smaller number in the lower right hand corner of each box is the channel number used to model that portion of the compartment. The horizontal lines represent the gaps used to model horizontal connections between rooms. The gap number is indicated on each line. The containment was divided into four vertical sections to accommodate the room configuration. Sixteen channels were used to model the containment. Each channel was one node high.

The channel input data is given in Table 28. The gap input data is given in Table 29. The area of each channel was obtained by dividing the volume of the room by the height of the section containing the channel. The height of the section was chosen to be at the centerline of the floor separating the annular rooms. The gap width was obtained by dividing the flow area of the vent represented by the gap by the height of the connecting channels.

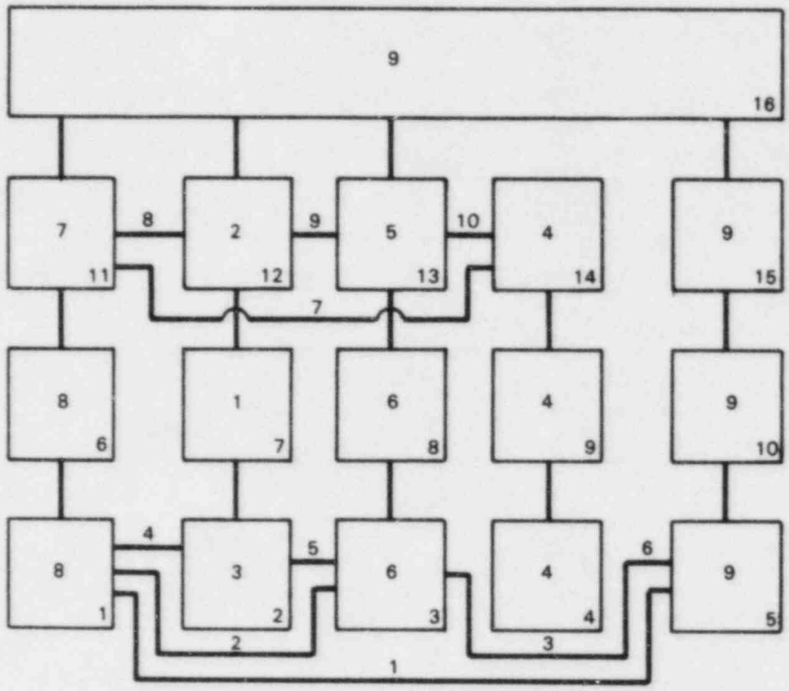

Figure 57 Nodalization for C series tests

Table 28 Channel input data for C series tests

Channel Number	Area ($in.^2$)	Wetted Perimeter (in.)	Area of Top Connection ($in.^2$)	Height (in.)	Loss Coefficient at Top Connection
1	21000	677.2		6.961	
2	31000	692.5	61.3	6.961	2.80
3	21000	677.2		6.961	
4	372	20.2		6.961	
5	50000	2523.0		6.961	
6	21000	677.2	1218.0	52.362	2.69
7	17000	637.0		52.362	
8	21000	677.0	1267.0	52.362	2.68
9	372	20.2		52.362	
10	50000	2523.0		52.362	
11	26000	677.2	368.3	96.57	2.89
12	27000	556.7	82.3	96.57	2.91
13	26000	677.2	368.3	96.57	2.89
14	372	20.2		96.57	
15	50000	2523.0		96.57	
16	150000	1385.0		135.827	

Table 29 Gap input data for C series tests

Gap Number	Channels Connected by Gap	Gap Width (in.)	Centroid Distance (in.)	Velocity Head Loss Coefficient
1	1&5	2.795	63.98	2.89
2	1&3	6.732	78.74	2.82
3	3&5	2.795	63.98	2.90
4	1&2	4.843	77.76	2.85
5	2&3	4.843	77.76	2.85
6	&5	1.417	77.76	2.84
7	11&1	4.449	78.74	2.68
8	11&12	0.157	76.77	2.91
9	12&13	0.157	76.77	2.91
10	13&1	4.449	78.74	2.68

The heat transfer surfaces within the test facility were modeled with 22 thermal conductors. The first sixteen conductors model the concrete walls within each of the sixteen channels. The remaining six conductors model the metal surfaces in rooms, 5, 6, 7, 8, and 9, respectively. The coating on the concrete walls was included in the thermal conductor model for these walls. The input data for the thermal conductors are given in Table 30.

The concrete walls were modeled with 20 nodes through the thickness of the wall. The metal walls were modeled with 15 nodes through the wall. The material properties used in the calculation are given in Table 31. A flow boundary condition having the flow rates and enthalpies specified in Table 27 was specified at the top of channel 7 using a type 3 and a type 1 boundary condition.

Table 30 Thermal conductor input data

Room Number	Conductor Number	Channel Number	Surface Area ($in.^2$)	Wetted Perimeter (in.)	Material Thickness (in.)	Material
8	1	1	78,960	1275.5	5.960	Concrete
3	2	2	39,451	607.3	5.960	Concrete
6	3	3	77,349	1190.7	5.960	Concrete
4	4	4	18,196	280.1	5.960	Concrete
9	5	5	168,600	2595.4	5.960	Concrete
8	6	6	63,646	1215.5	5.960	Concrete
1	7	7	55,802	1065.7	5.960	Concrete
6	8	8	62,347	1190.7	5.960	Concrete
4	9	9	14,667	280.1	5.960	Concrete
9	10	10	135,900	2595.4	5.960	Concrete
7	11	11	118,796	1231.6	5.960	Concrete
2	12	12	76,056	788.5	5.960	Concrete
5	13	13	117,899	1222.3	5.960	Concrete
4	14	14	27,018	280.1	5.960	Concrete
9	15	15	250,344	2595.5	5.960	Concrete
9	16	16	446,151	3284.7	5.960	Concrete
4	17	9	13,688	261.4	0.404	Carbon Steel
5	18	13	26,709	276.9	0.252	Carbon Steel
6	19	3	14,850	228.6	0.355	Carbon Steel
7	20	11	12,965	247.6	0.305	Carbon Steel
8	21	1	9,562	147.2	0.300	Carbon Steel
9	22	16	89,632	659.9	0.715	Carbon Steel

Table 31 Material properties of C series tests

Type Number	Material	Density (lbm/ft^3)	Specific Heat (Btu/lbm- °F)	Thermal Conductivity ($Btu/hr\text{-}ft^2\text{-}°F$)
1	Concrete coating	93.63	0.268	0.06
2	Concrete	183.79	0.220	0.8673
3	Steel	87.32	0.113	30.0

6.3 Discussion of Results

Both test C-13 and test C-15 were run using the Uchida condensation heat transfer coefficient model. An upper limit to the Uchida correlation of 381.0 Btu/hr-ft^2-°F was used for test C-13 and 419.0 Btu/hr-ft^2-°F for test C-15. COBRA-NC calculations of room pressures are compared with measured data in Figures 58 through 63 for test C-13, and Figures 64 through 69 for test C-15.

The figures show that agreement with the data is good for both tests in the two second simulation. Pressure in room 1, the break room, is shown in Figure 58 for test C-13 and Figure 64 for test C-15. COBRA-NC correctly predicts the increased pressure jump which occurs in room 1 during test C-15 due to the halving of the flow area between rooms 1 and 3 as compared to test C-13. Room 2 response, shown in Figures 59 and 65, is underpredicted by 21% for test C-13 and 24% for test C-15. The reason for this underprediction is not apparent. COBRA-NC shows a significant pressure drop between adjoining rooms (rooms 5, 7, and 9) and room 2, which would be expected given the small size of the connecting flow paths. However, the data indicates that little or no pressure differential exists.

Pressure responses for room 7 (test C-13) and room 5 (test C-15) are presented in Figures 60 and 66, respectively. Both exhibit the same type behavior, which is characteristic of rooms 4, 5, 6, 7, and 8 for both tests. Agreement with the data is excellent until approximately 0.25 sec, at which time the code begins to overpredict the pressure response. The maximum discrepancy is in the range of 20% to 25% for the five rooms. The onset of the overprediction corresponds to the end of the rapid initial pressurization in the break room and is caused by a sudden rise in the steam content of the room. Consequently, the inability of the code to follow the data could be the result of the lumped parameter model forcing steam into the rooms in a homogeneous manner.

The code does a better job of predicting pressure response in room 9 (Figures 61 and 67). This is most likely due to the large volume of this room that makes it less sensitive to dynamic pressurization effects. COBRA-NC calculates room 9 response to within 5% accuracy.

Data agreement for both tests is also very good in the 40 sec simulations. Pressure responses for both the break room (Figures 62 and 68) and adjoining rooms (Figures 63 and 56) are calculated well. The predicted response for room 1 is within 12% of the measured response for test C-13 and 8% for test C-15. The increased peak pressure in this room during test C-15 is evident. In the latter portion of the simulation, however, the break room responses are almost identical. This indicates that dynamic effects lose predominance as blowdown ends. During the latter portion of the simulation, the pressure decay rate calculated by COBRA-NC is less than that shown by the data. This is the result of not enough steam being condensed by the code. A possible reason for the low pressure decay rate could be either a deficiency in the wall heat-transfer modeling of the code or heat up of the heat slabs used for the wall

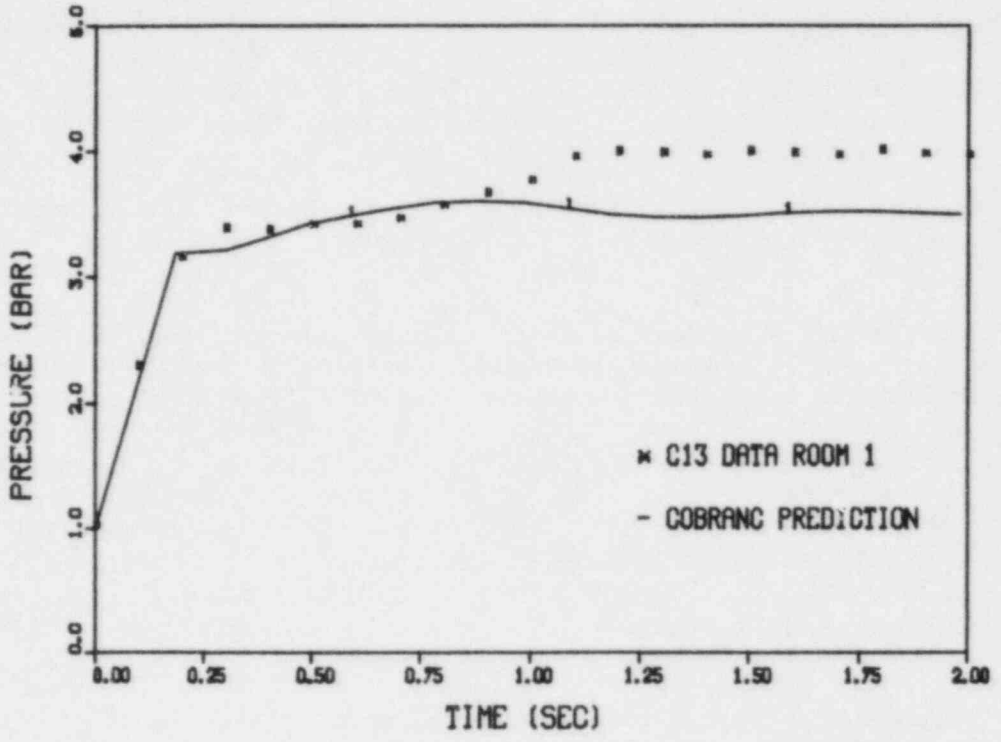

Figure 58 Test C13, room 1 short term response

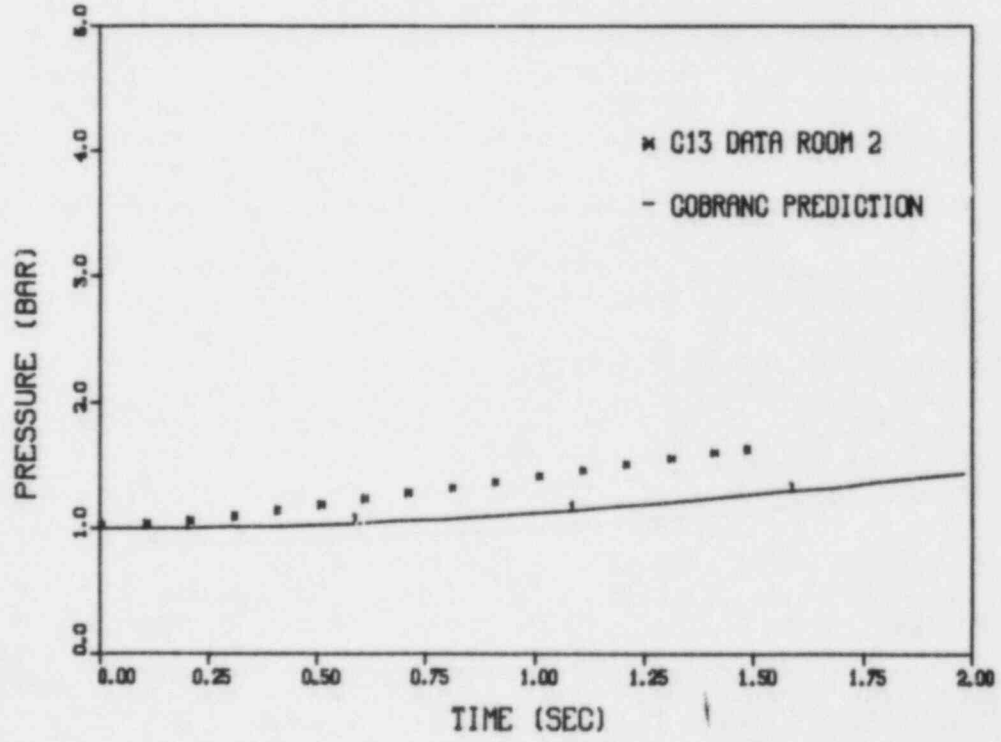

Figure 59 Test C13, room 2 short term response

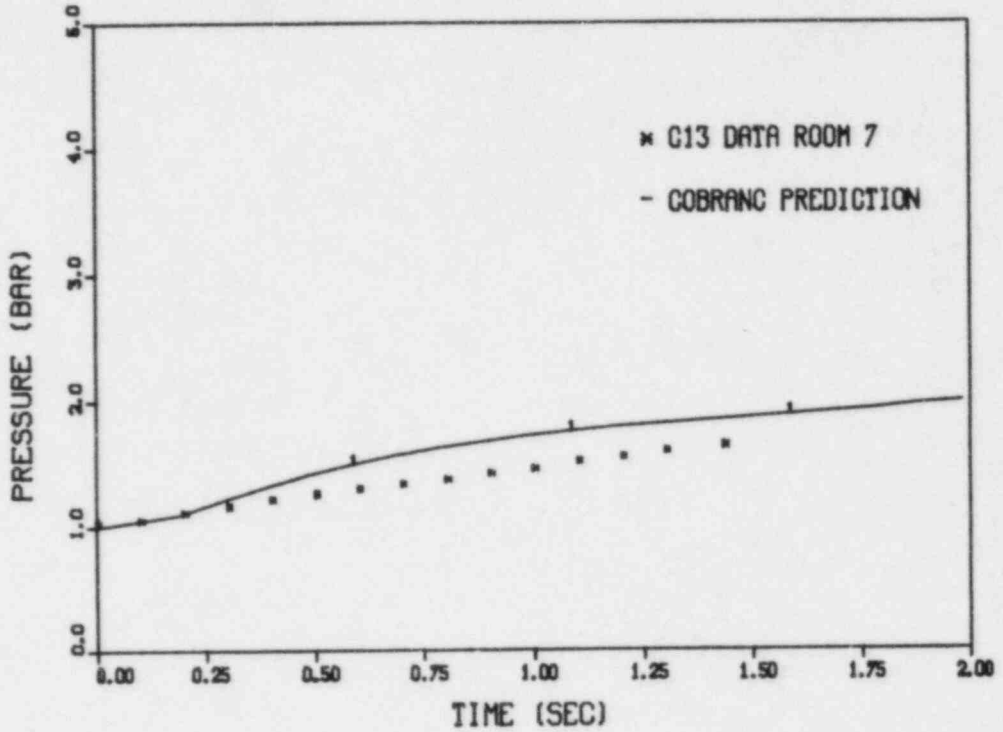

Figure 60 Test C13, room 7 short term response

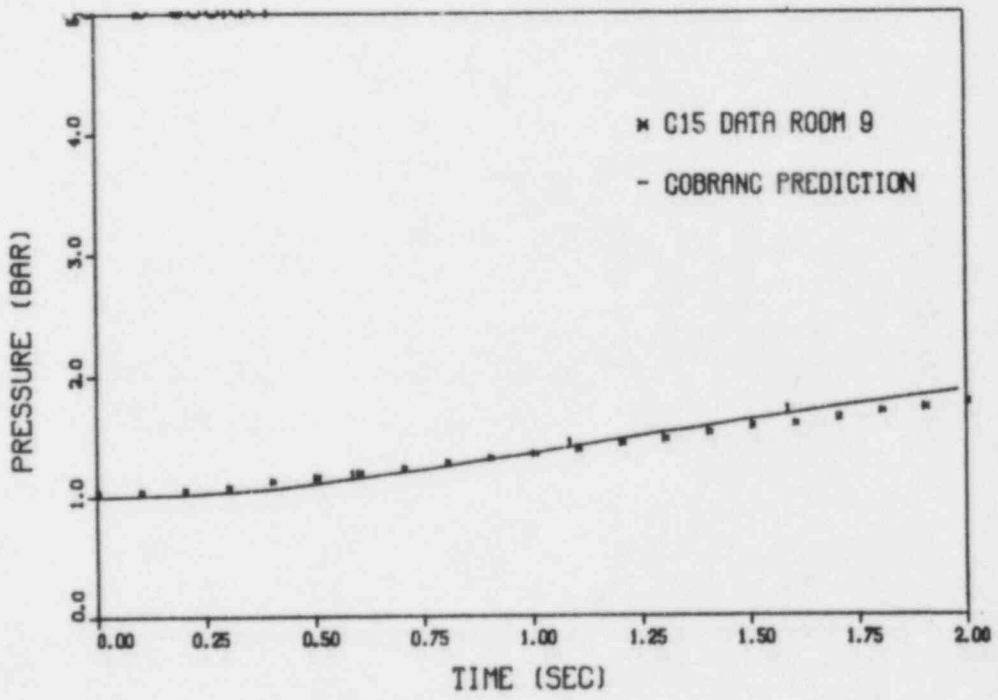

Figure 61 Test C13, room 9 short term response

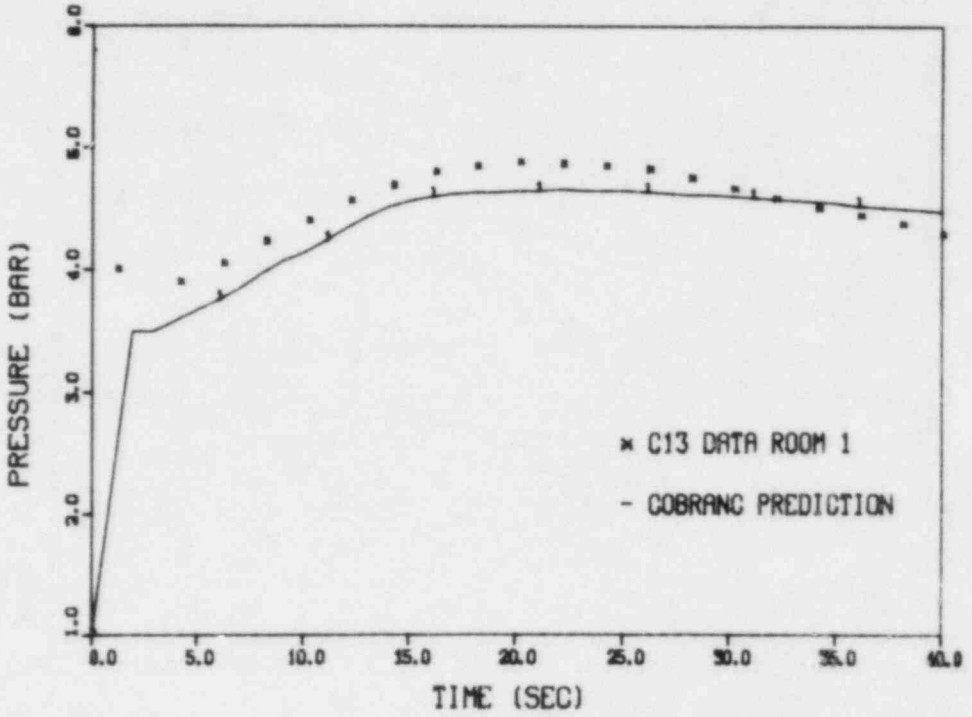

Figure 62 Test C13, room 1 medium term response

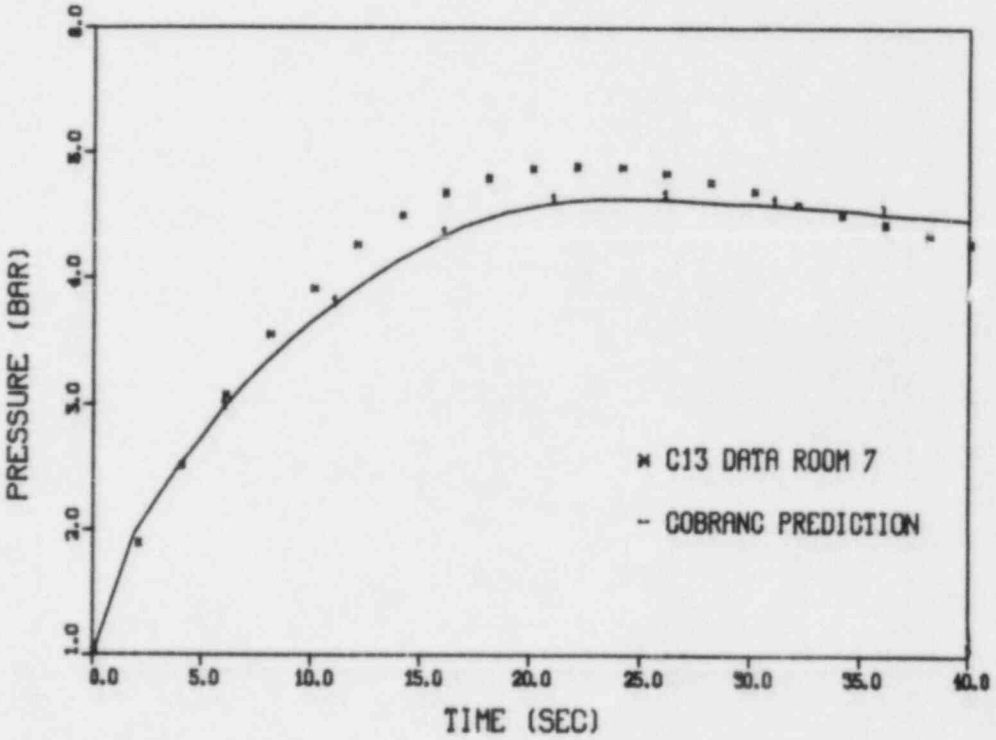

Figure 63 Test C13, room 7 medium term response

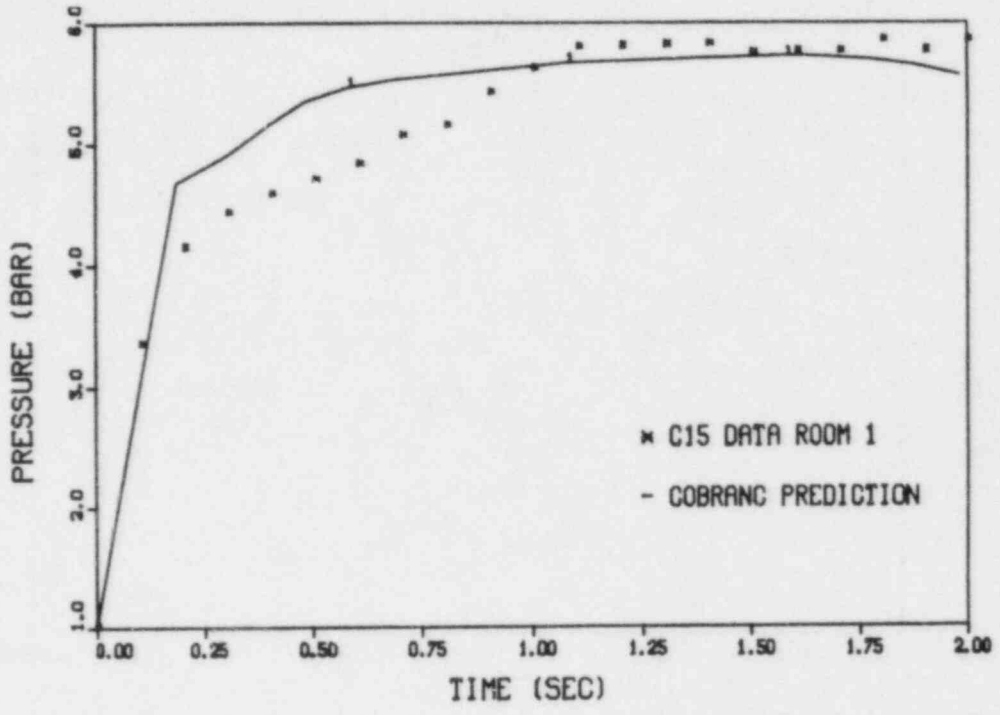

Figure 64 Test C15, room 1 short term response

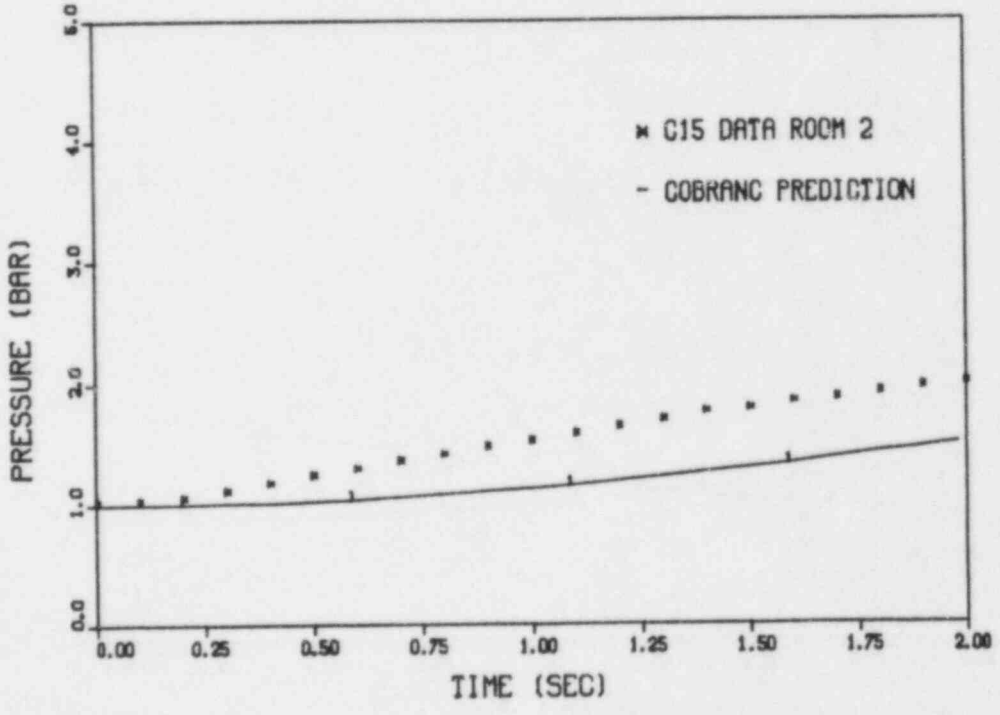

Figure 65 Test C15, room 2 short term response

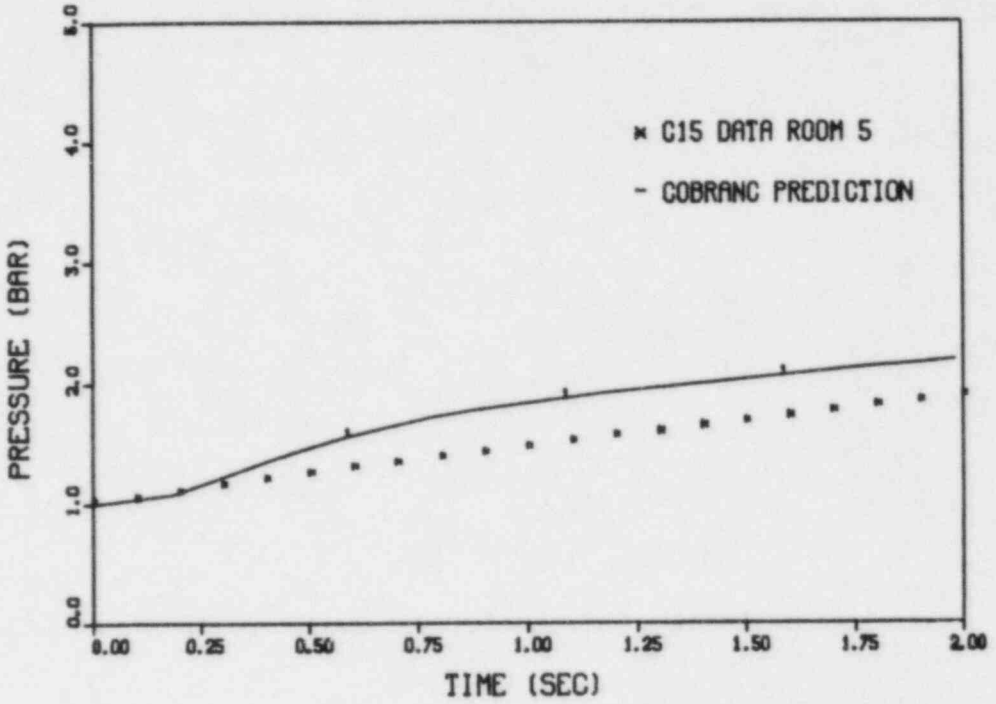

Figure 66 Test C15, room 5 short term response

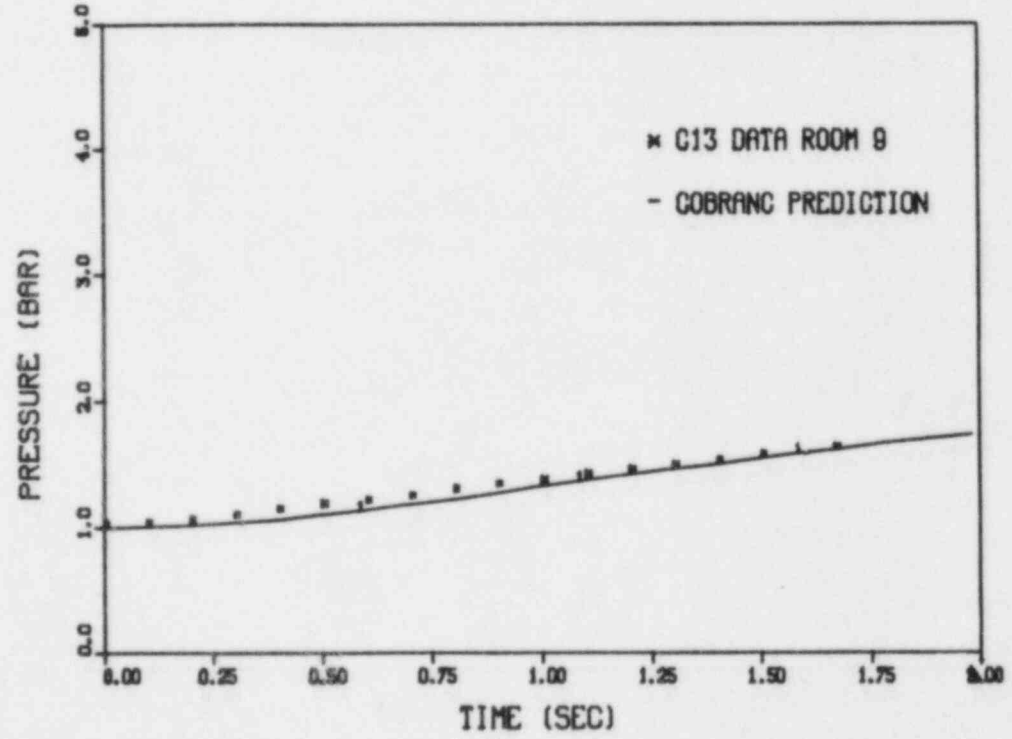

Figure 67 Test C15, room 9 short term response

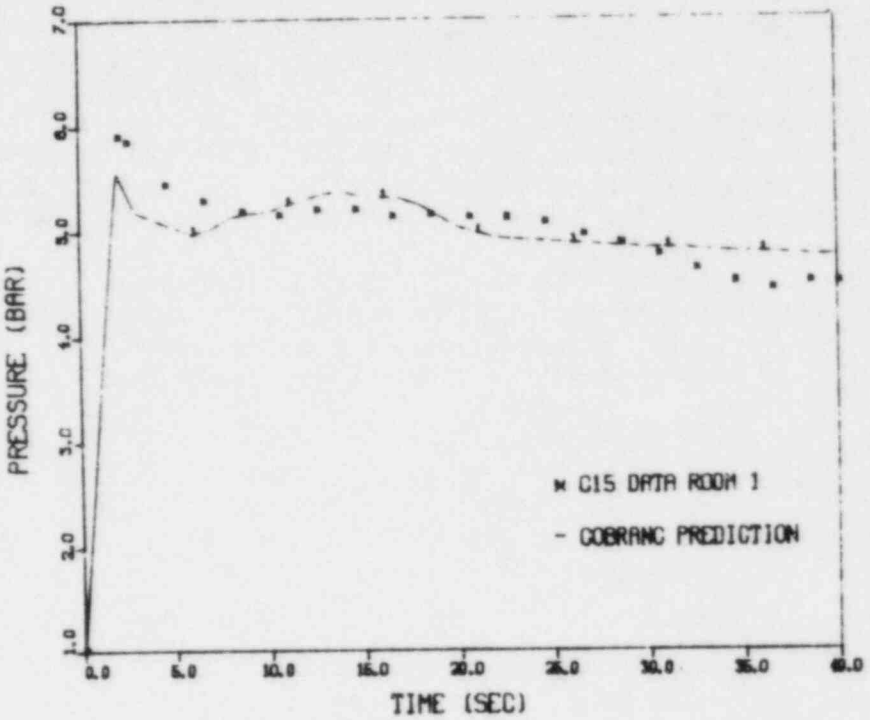

Figure 68 Test C15, room 1 medium term response

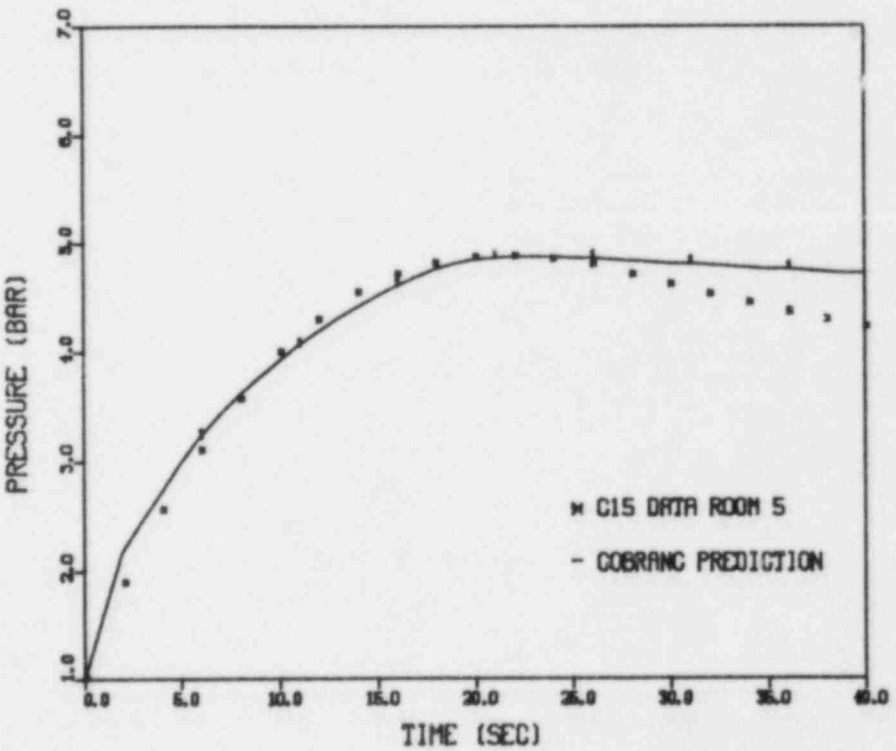

Figure 69 Test C15, room 5 medium term response

surfaces. An assumed average wall thickness was used, since this information was not available in the data reports. Consequently, some or all of the heat slabs used to model the wall surfaces could be insufficiently thick. It is very likely that the steam condensation in the large room (room 9) is underpredicted in the longer time periods, because the lumped parameter model used does not provide a sufficient number of flow paths between this and adjoining rooms to compute the natural convection currents that would exist following blowdown. These convection currents would mix the high steam content atmosphere of the inner rooms with the low steam content of the dome region and bring more steam into contact with the cooler structures in the dome region. This would increase the net condensation rate causing a more rapid depressurization of the containment in the longer time frames.

7.0 HDR CONTAINMENT STEAM BLOWDOWN TESTS V43 AND V44

The results of COBRA-NC predictions of the German Project HDR containment steam blowdown test V44 are presented in this section. This test was conducted in a large-scale containment.

The purpose of this simulation was to compare the experimental data with computer-code-calculated results. The calculations have been carried out as realistically as possible. These calculations are not "conservative" calculations as defined by the guidelines used in the licensing process. Rather, they are best-estimate predictions. A base-case calculation was run for four time periods. These were 0-5 sec, 0-50 sec, 0-200 sec, and 0-1500 sec. A series of calculations was then run to investigate the sensitivity of the short-time-period results to some of the main modeling assumptions. Results of the base case calculation as well as the sensitivity study are presented in this report.

A brief description of the experimental facility will be given followed by a description of the calculational model and input data. This will be followed by a discussion of the code predictions.

7.1 Description of the Experiment

The CONT-Steam-Tests are intended to simulate the rupture of a steam pipeline within a nuclear containment. The large mass flow following a loss-of-coolant accident leads to severe mechanical and thermodynamical stresses on the containment structures. The experiments carried out at the HDR facility measured these stresses for a large-scale plant. They are a good extension of the data base obtained from the small-scale facility at Battelle Institute's Frankfurt facility and throw more light on the quality of extrapolating results to a real plant.

The main components of the test facility are the reactor pressure vessel (RPV) with its associated flow circuit and break nozzle, the containment building, and the measurement facility. A drawing of the reactor pressure vessel is shown in Figure 70. It has a total volume of 75 m^3 and was filled with saturated water and steam at a pressure of 110 bar. The liquid level in the vessel was 9.2 m for test V44. The remainder of the vessel was filled with steam. In addition to the fluid volume contained within the vessel, there were several pipes hooked to the top and bottom of the vessel that were not isolated during blowdown and contributed significant volumes of steam and water to the blowdown.

Figures 71 and 72 show vertical cross sections of the containment building taken along the 90° to 270° diameter and the 0° to 180° diameter, respectively.

The smaller numbers shown in the figures are the numbers assigned to each room. Some individual rooms were lumped together by the experimenters to form 34 zones. These zones are designated by the larger bold numbers. Most

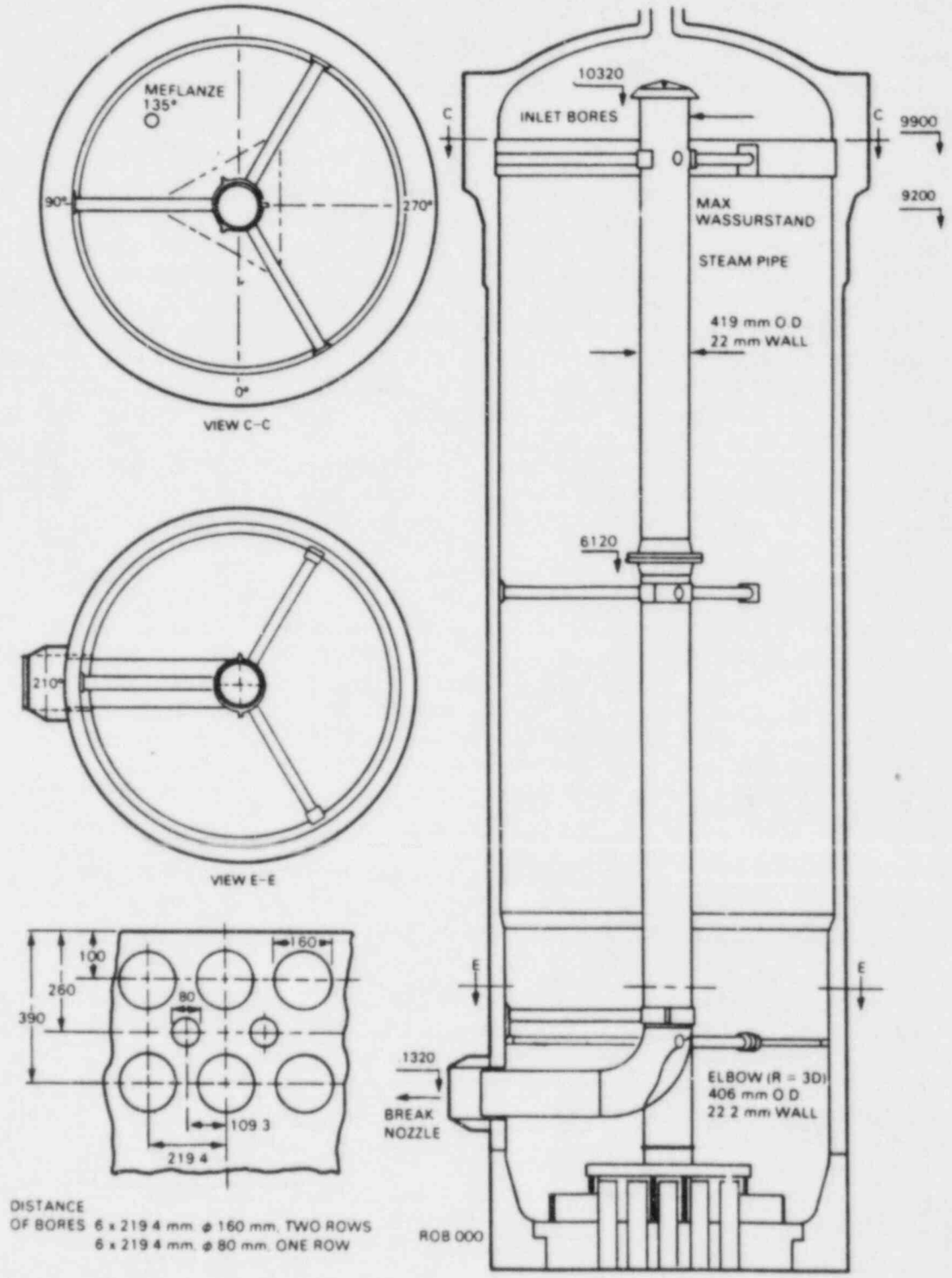

Figure 70 Reactor pressure vessel

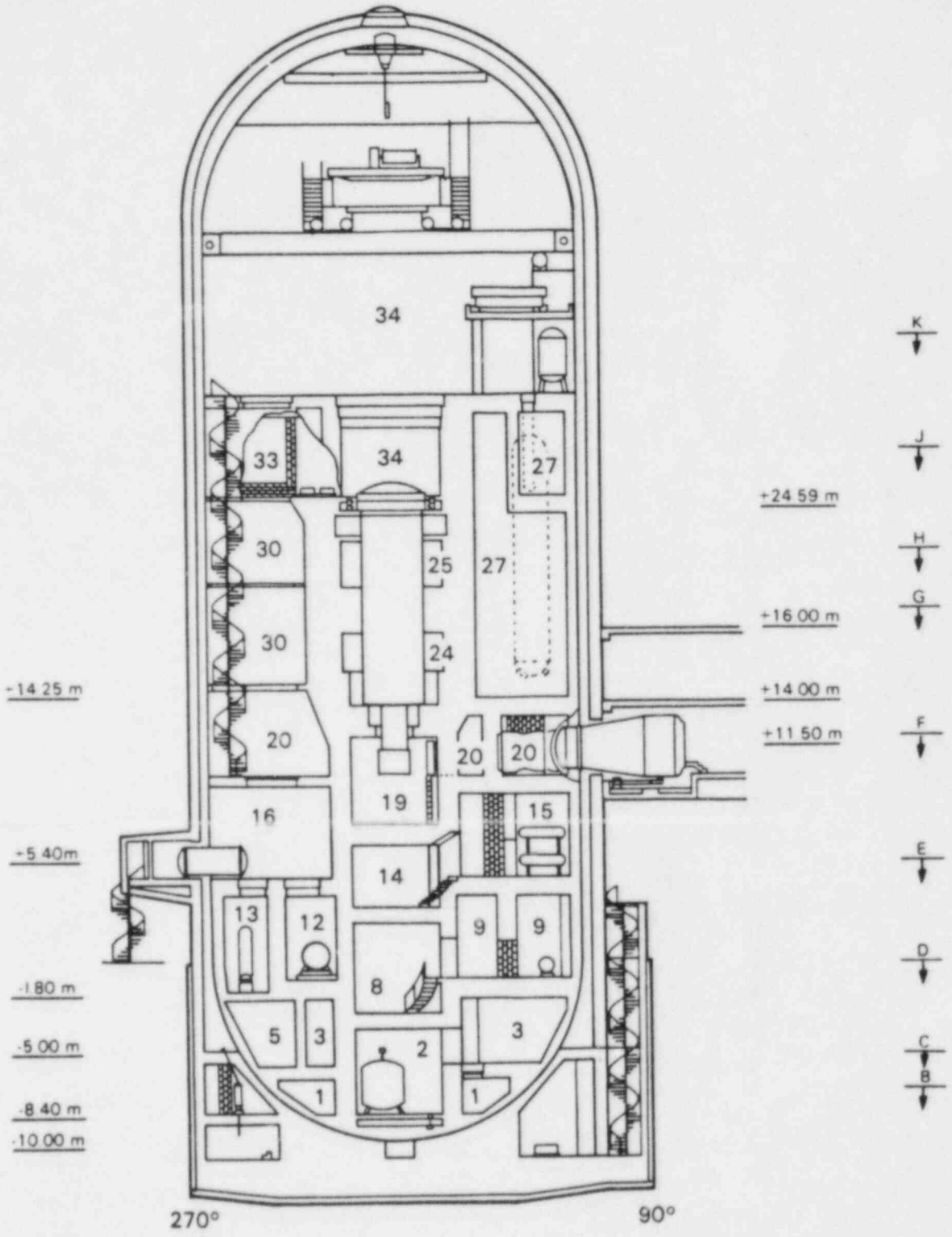

Figure 71 Vertical cross section of containment building along 90° to 270° diameter

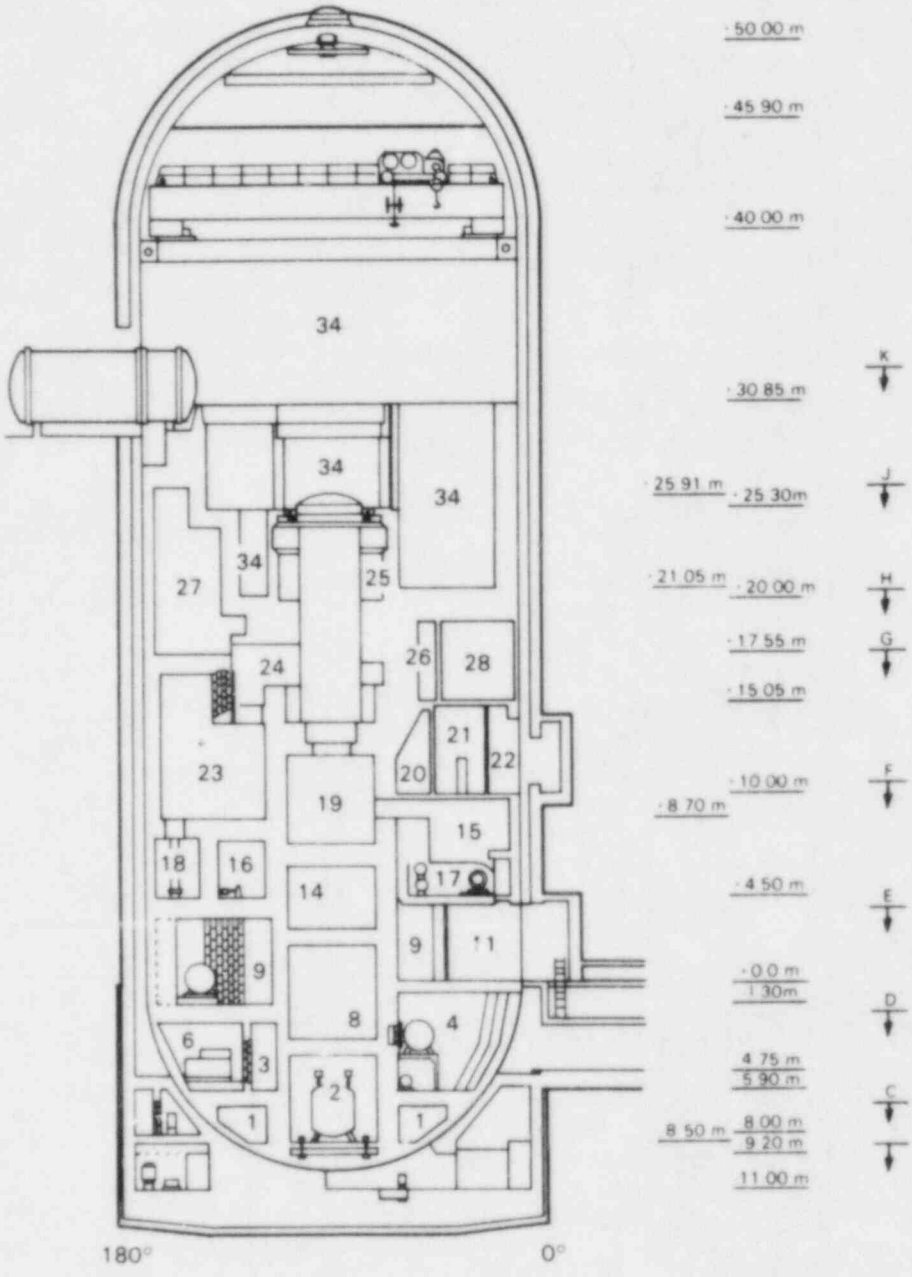

Figure 72 Vertical cross section of containment building along 0° to 180° diameter

of the facility data is presented in terms of these zones. Horizontal cross sections BB through kk of the containment are shown in Appendix A of this report. A brief description of each containment room and the 34 containment zones is provided in Tables A.1 and A.2. A schematic of the compartments and vent flow openings between each zone is shown in Figure 73. A compilation of the vent flow openings is given in Table A.3 of Appendix A.

The solid structures within each zone of the containment have been tabulated by the experimenters according to the material type and thickness. This compilation is given in Tables A.4 and A.5.

The blowdown nozzle was located in room 1603 (zone 23). The vent flow openings between room 1603 and other rooms are tabulated in Table A.6.

Instrumentation to measure the transient pressure, temperature, differential pressure, water carryover, steam/air composition, and heat transfer coefficients were located in several rooms in the containment. A more detailed description of the facility may be found in the experimenter's report (6,7).

7.2 COBRA-NC Model Description

To describe the COBRA-NC model for these experiments it is necessary to describe the computational model and the input model.

The input model for HDR steam blowdown test V44 is based on the 34-zone model developed by the HDR staff. A diagram of the COBRA-NC lumped-parameter nodalization is shown in Figure 74. Each box in this figure represents a computational node. The lines connecting the nodes represent flow paths between the nodes. The solid lines represent vertical flow paths and the dashed lines represent horizontal flow paths. The large number in the center of each box refers to the zone number that node represents. Some zones were divided up into two or more nodes to accommodate the node connection logic of the code. The number in the lower-right-hand corner of each box is the channel number. A channel is a vertical stack of computational cells one or more nodes high. The channels are arranged in nine rows or levels. These represent nine elevations into which the containment was divided. Gravity will cause water to flow downward from one elevation to another, provided that the vapor-gas updraft is not sufficient to prevent it. The horizontal connections between channels are referred to as gaps. The gaps are each numbered in the figure. All of the levels are composed of channels one node high except for the fifth level from the bottom. This level is three nodes high to accommodate the elevation of the vent holes in the blowdown compartment. The input data for each channel is given in Table 32. The height of each level of channels was estimated from the elevations given in Figures 70 and 71. The channel area was calculated by dividing the zone volume (given in Table A.1) by the estimated height of the level. The only change made in the input model between the pretest calculation and the post-test calculation was that zone 34 was divided into two nodes on the ninth level, and the node on the seventh level was eliminated. Also, the connections between zone 34 and rooms on the eighth

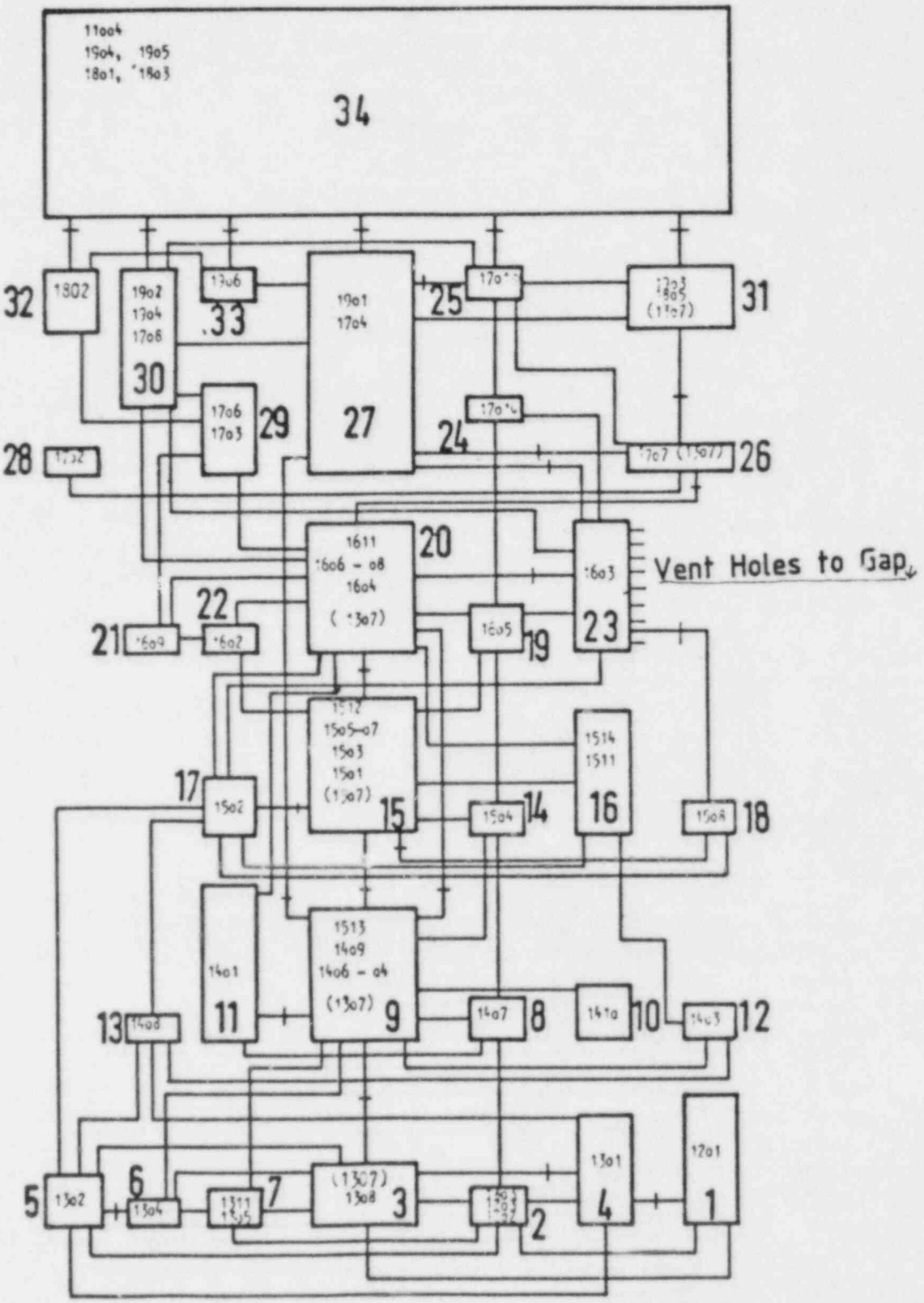

Figure 73 Schematic of compartments and vent flow openings

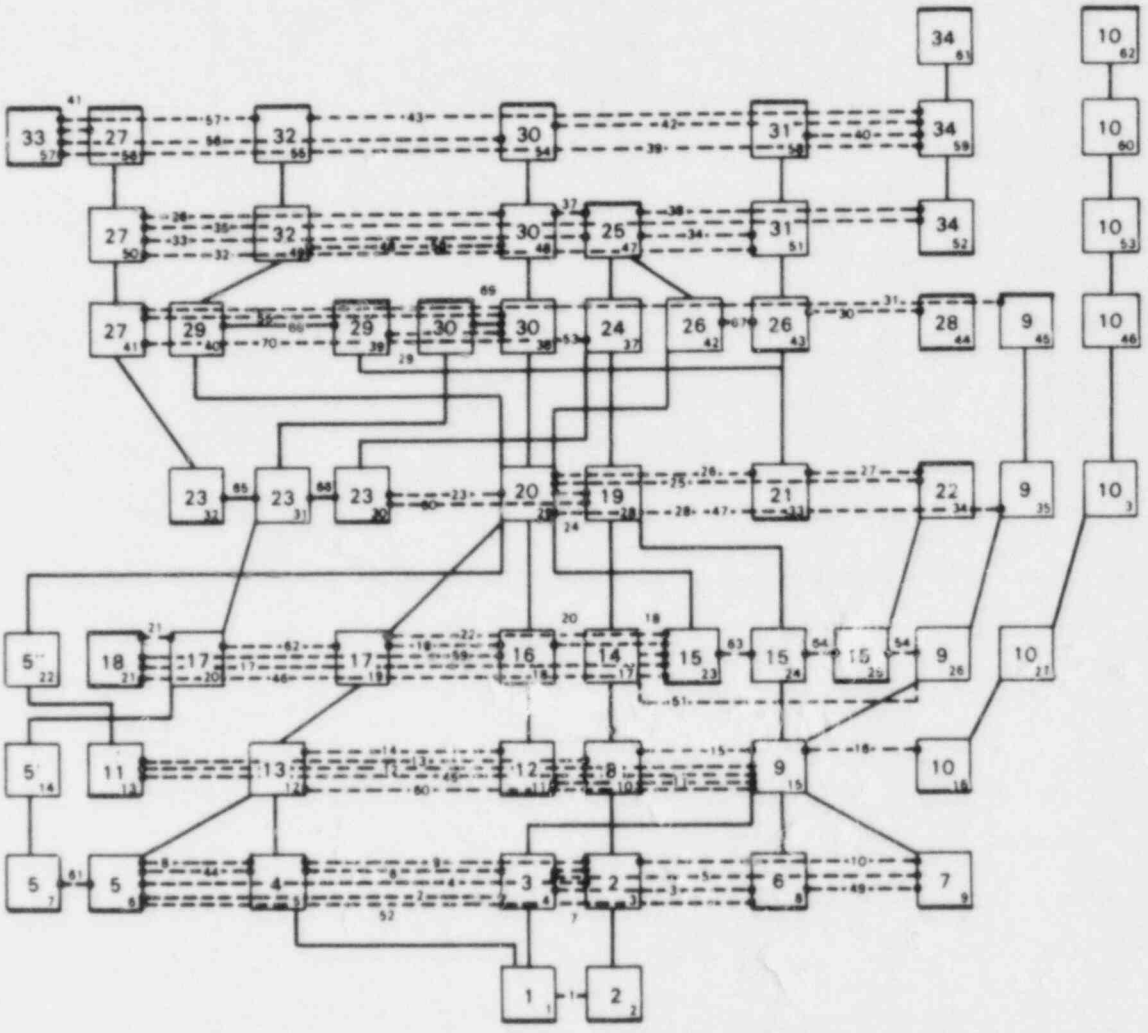

Figure 74 COBRA-NC nodalization of the HDR facility

Table 32 Channel Input Data

Channel Number	Zone Number	Volume (m^3)	Height (m)	Area (m^2)	Top Connection Area (m^2)	Top Connection CD	Bottom Connection Area (m^2)	Bottom Connection CD	Opening Numbers Modeled by Top Connection	Opening Numbers Modeled by Bottom Connection
1	1	152.000	2.7	56.300						
2	2	28.460	2.7	10.541						
3	2	49.540	4.7	10.541	0.337	0.621			9,10,11.1	
4	3	160.000	4.7	34.040	10.520	DP*	0.278	0.6	47,52,58.1,62.1,62.2,62.3,63.1	14,15
5	4	200.000	4.7	43.830	1.199	0.650	1.742	DP*	34	16,17,18,30.1,48,49,50,51
6	5	46.500	4.7	9.894	1.943	0.650			35,36,37,38	
7	5	46.500	4.7	9.894	0.930	0.700			151.1	
8	6	39.000	4.7	8.298	0.277	0.610			39,40.1,42,43	
9	7	63.000	4.7	13.404	1.645	0.610			40.2,41.1,44,45	
10	8	84.000	5.6	15.000	0.379	0.650			153.1,153.3	
11	12	76.000	5.6	13.570	3.500	0.800			148	
12	13	59.000	5.6	10.536	0.276	0.700			151.2	
13	11	296.000	5.6	52.860	0.220	0.600			84.1,84.2	
14	5'	5.200	5.6	0.930						
15	9	577.920	5.6	103.200						
16	10	1.390	5.6	2.749						
17	14	57.000	4.2	13.571	0.078	0.650			154.1	
18	16	235.000	4.2	55.950	0.330	0.700			152	
19	17	53.500	4.2	12.740	1.400	0.750			149	
20	17	53.500	4.2	12.740	0.280	0.550			150	
21	18	57.000	4.2	13.570						
22	5*	0.366	4.2	0.080						
23	15	181.000	4.2	43.090	6.613	0.786			159,120.1,120.2,155.1,155.2	
24	15	181.000	4.2	43.090	0.392	0.650	0.5	DP*	154.2,170	93.3
25	15	181.000	4.2	43.090	0.100	0.700			156	
26	9	1.848	4.2	0.440						
27	10	11.550	4.2	2.749						
28	19	93.000	6.35	14.650	1.374	0.600			138	
29	20	507.000	6.35	79.840						
30	23	93.300	6.35	14.690	3.190	0.350			143,145	
31	23	93.300	6.35	14.690	0.430	0.850			133	
32	23	93.300	6.35	14.690	2.593	0.350			110,176,180.2,183.1,183.2,183.3,140	
33	21	59.000	6.35	9.290	0.060	0.700			128.3	
34	22	61.000	6.35	9.610						
35	9	2.794	6.35	0.440						
36	10	17.460	6.35	2.749						

(Table 32, continued)

Channel Number	Zone Number	Volume (m^3)	Height (m)	Area (m^2)	Top Connection Area (m^2)	Top Connection CD	Bottom Connection Area (m^2)	Bottom Connection CD	Opening Numbers Modeled by Top Connection	Opening Numbers Modeled by Bottom Connection
37	24	44.000	5.55	7.930	1.700	0.700			134	
38	30	55.600	5.55	10.030			0.02	0.831		130,131.1,131.2,132
39	29	84.500	5.55	15.230						
40	29	84.500	5.55	15.230	0.072		0.304	0.7	175.1,175.2	174
41	27	297.900	5.55	53.670						
42	26	65.500	5.55	11.800	0.0327		0.650	6.97	0.85	136 119.1,119.2,173
43	26	65.500	5.55	11.800	7.97	0.85			118.1,118.2	
44	28	54.000	5.55	9.730						
45	9	2.442	5.55	0.440						
46	10	15.260	5.55	2.749						
47	25	64.000	4.7	13.620	3.00				182	
48	30	80.040	4.7	17.030						
49	32	57.340	4.7	12.200						
50	27	252.200	4.7	53.670						
51	31	127.900	4.7	27.220						
52	34	707.930	4.7	150.620						
53	10	12.920	4.7	2.749						
54	30	94.520	5.55	17.030	7.47				122.1,122.2,122.3	
55	32	67.719	5.55	12.200	0.060				157.1	
56	27	297.903	5.55	55.670						
57	33	62.000	5.55	11.170	0.075				157.2	
58	31	151.100	5.55	27.220	5.50				117.1,117.2,117.4,157.3	
59	34	1415.800	5.55	255.100						
60	10	15.260	5.55	2.749						
61	34	3196.000	9.15	346.400						
62	10	25.150	9.15	2.749						
63	30	39.020	5.55	7.030						

* Pressure dependent

level were changed from horizontal to vertical connections. These changes were made to permit the calculation of natural circulation between the upper and lower regions of the containment later in the transient.

The flow area for connections at the top and bottom of each channel were obtained from Table A.3 and are specified in Table 32.

The data for each horizontal flow connection are given in Table 33. The flow area is the sum of the flow paths between the two zones. The width of the vent opening is obtained by dividing the vent flow area by the height of the node.

The GRS estimates for the vent flow coefficients were used in these calculations except for vents U0143 and U0140 where a flow coefficient of 0.35 was assumed. This value was used to account for the additional flow resistance caused by the blowdown jet in front of these vents. When several vent holes were lumped together, an area-weighted average flow coefficient was used. The total flow area of pressure-dependent openings was used and the loss coefficient specified as a function of pressure drop across the opening to give the correct flow resistance.

At least one heat transfer slab was modeled for each of the 34 zones. All of the concrete surfaces in a zone were lumped together into a single slab for each zone. The surface area of this slab was set equal to the total concrete surface area for the zone, and the thickness of slab was calculated by dividing the total volume of concrete in the zone by the surface area for the zone. The metal surfaces were lumped into two slabs per zone. All of the metal was assumed to be steel. The slabs were divided into two groups, one for thicknesses less than 3 mm and the other for thicknesses greater than 3 mm but less than 20 mm. The material beyond 20 mm in depth was ignored. This corresponds to lumping all of the materials listed in Table A.5, class 2, 3 and 4 into a single slab of steel.

The data for the concrete slab conduction models are given in Table 34 and those for the steel slabs are given in Table 35. Each of the concrete slabs were divided into seven regions through their thickness. The region nearest the surface was 0.0051-m thick and was divided into four nodes, one on the surface. The second region was 0.0102-m thick and was divided into four nodes. The third region was 0.0152-m thick and was divided into three nodes, the fourth was 0.0203-m thick and divided into two nodes, the fifth 0.0407-m thick and divided into two nodes, the sixth 0.0407 m and one node thick, and the thickness of the seventh region varied depending on the slab and was divided in to from two to five nodes.

Table 33 Gap input data

Gap No.	Channels Connected by Gap	Area (m^2)	Flow Coefficient	Gap Width (m)	Opening Numbers Modeled by Gap
1	1 & 2	0.068	0.650	0.0257	1,2
2	4 & 6	1.551	0.784	0.3300	22,23,25,26.1
3	4 & 8	3.464	0.835	0.7370	27,31
4	3 & 6	0.120	0.600	0.0255	3
5	4 & 9	4.169	0.850	0.8870	32,33
6	4 & 5	2.251	0.706	0.4789	21,30.2,78
7	3 & 4	1.165	0.700	0.4819	5,6,12.1,13,26.2
8	5 & 6	0.298	0.522	0.0634	24,28,29
9	3 & 5	0.304	0.600	0.0647	7,8
10	3 & 9	0.149	0.600	0.317	4
11	11 & 15	3.042	0.747	0.5432	55,57,60,61.1,2,82.1,82.2
12	13 & 15	2.410	0.792	0.4304	11.3,,83.2,89
13	10 & 13	0.030	0.700	0.0054	11.2
14	11 & 12	0.099	0.700	0.0177	59
15	10 & 15	0.921	0.750	0.1645	54
16	15 & 16	1.360	0.800	0.2429	53
17	21 & 23	0.316	0.654	0.063	144.2,144.3,184.1,184.2
18	17 & 23	1.993	0.0796	0.4745	67,153.3
19	18 & 19	0.147	0.592	0.035	73,74,75,76
20	18 & 23	3.709	0.848	0.8831	63.1,64,77
21	20 & 21	0.180	0.700	0.0429	146.1
22	19 & 23	0.992	0.700	0.2362	68,69,70,71,72
23	29 & 30	2.372	0.752	0.2598	162,163,164.2,164.3,166.1
24	28 & 29	2.270	0.818	0.3575	167,168,169
25	29 & 34	1.430	0.800	0.2252	86
26	29 & 33	1.655	0.791	0.2602	80,81,87,88.2,172.1
27	33 & 34	0.104	0.721*	0.0164	88.1,172.2
28	29 & 35	0.500	0.650	0.0787	88.1,172.2
29	38 & 39	0.060	0.700	0.0108	128.1
30	43 & 44	1.440	0.800	0.2595	90
31	41 & 45	1.500	0.600	0.2703	93.1
32	50 & 51	0.438	0.680	0.0932	103,109,111
33	47 & 50	2.787	0.711	0.593	91,102,104,105,106.1,106.2.108,113.2
34	47 & 51	0.0806	0.650	0.0171	135
35	56 & 59	0.262	0.600	0.0472	100,101,107
36	48 & 50	0.450	0.887	0.0957	96,98
37	47 & 48	0.240	0.650	0.0511	126
38					
39	52 & 61	77.32	0.6	8.45	
40	58 & 59	5.500	0.792	0.9910	117.1,117.2,117.4,157.3

* Opening is pressure dependent

(Table 33, continued)

Gap No.	Channels Connected by Gap	Area (m^2)	Flow Coefficient	Gap Width (m)	Opening Numbers Modeled by Gap
41	56 & 57	0.396	0.674	0.0714	112,113.1
42	54 & 59	7.470	0.832	1.3459	122.1,122,2,122.3
43	55 & 59	0.060	0.6	0.0108	157.1
44	5 & 6	2.826	0.85[a]	0.6013	44
45	13 & 15	2.965	0.85[a]	0.5292	56
46	21 & 23	1.420	0.65[a]	0.3381	144.1
47	29 & 35	0.066	0.70	0.0104	171.2
48	25 & 27	0.300	0.55[a]	0.0638	139
49	8 & 9	5.924	0.846	1.2604	19,20
50	12 & 15	0.020	0.17	0.0036	58.2
51	17 & 26	0.088	0.7	0.021	65,66
52	6 & 8	3.068	0.85[a]	0.528	79
53	39 & 42	1.840	0.8	0.3315	91,175.3
54	25 & 26	7.980	0.832	1.9	63.2,121.1,121.2,142,158.1,158.2,160
55	38 & 41	0.296	0.61	0.0533	94,99,171.1
56	54 & 57	1.667	0.782	0.3004	123,123.1,124
57	55 & 57	0.064	0.7	0.0115	125
58	48 & 49	3.110	0.85	0.6617	137.1,137.2,141
59	18 & 21	1.242	0.79	0.2957	146.2,147,185
60	28 & 30	0.190	0.7	0.0449	165
61	6 & 7			9.32[a]	
62	19 & 20			5.71[a]	
63	23 & 24			10.23[a]	
64	24 & 25			10.23[a]	
65	31 & 32			6.94[a]	
66	30 & 31			6.94[a]	
67	42 & 43			4.11[a]	
68	39 & 40			5.48[a]	
69	38 & 63			3.00[a]	

(a) GAP used to model connection between two channels modeling the same zone. These gaps do not model flow openings between zones.

Table 34 Concrete conduction model input

Zone Number	Conductor Number	Channel Number	Surface Area (m^3)	Material Volume (m^3)	Material Thickness (m)	Wetted Perimeter (m)
1	1	1	221.60	126.30	0.5700	82.07
2	2	2	150.00	70.60	0.4710	20.28
3	3	4	418.40	155.50	0.3715	89.01
4	4	5	314.70	106.50	0.3383	66.96
5	5	6	140.10	52.91	0.3777	29.81
6	6	8	92.40	38.50	0.4167	19.66
7	7	9	135.55	59.18	0.4366	28.84
8	8	10	127.30	55.10	0.4328	22.73
9	9	15	834.86	313.20	0.3751	149.08
10	10	16	294.86	73.52	0.2493	52.65
11	11	13	258.98	89.34	0.3450	46.25
12	12	11	156.27	77.09	0.4933	27.91
13	13	12	140.08	53.03	0.3786	25.01
14	14	17	118.75	41.04	0.3456	28.27
15	15	23	676.20	202.28	0.2291	161.00
16	16	18	253.50	104.55	0.4124	60.36
17	17	19	193.25	53.55	0.2743	46.01
18	18	21	147.66	54.43	0.3686	35.16
19	19	28	132.05	59.74	0.4524	20.80
20	20	29	669.72	231.18	0.3452	105.47
21	21	33	96.06	14.33	0.1492	15.13
22	22	34	107.07	18.61	0.1738	16.86
23	23	30	330.39	161.57	0.4890	52.03
24	24	37	146.65	85.95	0.5861	26.42
25	25	47	111.34	99.63	0.8948	23.69
26	26	43	221.75	90.43	0.4078	39.95
27	27	41	896.77	477.65	0.5326	161.58
28	28	44	134.62	24.15	0.1794	24.26
29	29	39	216.05	71.39	0.3304	38.93
30	30	38	277.31	105.27	0.3796	49.97
31	31	51	349.22	125.71	0.5044	74.30
32	32	49	143.63	25.98	0.1809	30.56
33	33	57	93.09	42.88	0.4606	19.81
34	34	52	1212.72	566.64	0.4672	258.00

Table 35 Steel conduction model input

Zone Number	Thickness* Class	Conductor Number	Channel Number	Surface Area (m^2)	Material Volume (m^3)	Material Thickness (m)	Wetted Perimeter (m)
1	1	35	1	26.85	0.0166	0.0006	9.94
1	2	36	1	84.85	0.5099	0.0060	31.43
2	1	37	2	21.45	0.0225	0.0010	7.94
2	2	38	2	117.85	0.6143	0.0052	43.65
3	1	39	4	277.56	0.2552	0.0009	59.06
3	2	40	4	95.34	0.8492	0.0089	20.29
4	1	41	5	218.73	0.2182	0.0010	46.54
4	2	42	5	113.17	0.7275	0.0064	24.08
5	1	43	6	88.75	0.0774	0.0009	18.88
5	2	44	6	61.85	0.4108	0.0066	13.16
6	1	45	8	39.50	0.0459	0.0012	8.40
6	2	46	8	73.02	0.4572	0.0063	15.54
7	1	47	9	80.74	0.1041	0.0013	17.18
7	2	48	9	39.44	0.2507	0.0064	8.39
8	1	49	10	76.38	0.0652	0.0009	13.64
8	2	50	10	52.88	0.3088	0.0058	9.44
9	1	51	15	647.74	0.5928	0.0009	115.67
9	2	52	15	405.71	3.6234	0.0089	72.45
10	1	53	16	74.70	0.0703	0.0009	13.34
10	2	54	16	121.10	1.2367	0.0102	21.63
11	2	55	13	113.04	1.2259	0.0108	20.19
11	1	56	13	414.56	0.4462	0.0011	74.03
12	1	57	11	58.91	0.0458	0.0008	10.52
12	2	58	11	231.34	2.0759	0.0090	41.31
13	1	59	12	100.02	0.0744	0.0007	17.86
13	2	60	12	27.93	0.1531	0.0055	4.99
14	1	61	17	18.36	0.0149	0.0008	4.37
14	2	62	17	25.79	0.1762	0.0068	6.14
15	1	63	23	639.14	0.6087	0.0010	152.18
15	2	64	23	321.55	2.3421	0.0073	76.56
16	1	65	18	174.60	0.2063	0.0012	41.57
16	2	66	18	157.30	1.4336	0.0091	37.46
17	1	67	19	168.98	0.1547	0.0009	40.23
17	2	68	19	111.24	0.7795	0.0070	26.49
18	1	69	21	126.21	0.0982	0.0008	30.05
18	2	70	21	65.87	0.4347	0.0066	15.68
19	1	71	28	76.30	0.0709	0.0009	12.02
20	1	73	29	578.30	0.4636	0.0008	91.07
21	1	75	33	84.46	0.0742	0.0009	13.30
21	2	76	33	20.14	0.1098	0.0055	3.17
22	1	77	34	62.10	0.0583	0.0009	9.78
22	2	78	34	45.88	1.2057	0.0263	7.23
23	1	79	30	196.76	0.2658	0.0014	30.99

(Table 35, continued)

Zone Number	Thickness* Class	Conductor Number	Channel Number	Surface Area (m^2)	Material Volume (m^3)	Material Thickness (m)	Wetted Perimeter (m)
23	2	80	30	432.67	4.6672	0.0108	68.14
24	1	81	37	92.95	0.1358	0.0015	16.75
24	2	82	37	113.02	1.4140	0.0125	20.36
25	1	83	47	132.27	0.2394	0.0018	28.57
25	2	84	47	81.07	0.7240	0.0089	17.25
26	1	85	43	290.08	0.2714	0.0009	52.27
26	2	86	43	122.78	1.2681	0.0103	22.12
27	1	87	41	925.42	0.9945	0.0011	166.74
27	2	88	41	848.24	5.1520	0.0061	152.84
28	1	89	44	196.65	0.1530	0.0008	35.43
28	2	90	44	55.30	1.2736	0.0230	9.96
29	1	91	39	125.94	0.1474	0.0012	22.69
29	2	92	39	150.48	0.9986	0.0066	27.11
30	1	93	38	239.25	0.2862	0.0012	43.11
30	2	94	38	271.01	2.1961	0.0081	48.83
31	1	95	51	358.93	0.4136	0.0012	76.37
31	2	96	51	222.20	3.0919	0.0139	47.28
32	1	97	49	180.25	0.1117	0.0006	38.35
32	2	98	49	193.00	1.6411	0.0085	41.06
33	1	99	57	133.46	0.1673	0.0013	24.05
33	2	100	57	109.49	0.8884	0.0081	19.73
34	1	101	52	839.12	0.9171	0.0011	178.54
34	2	102	52	4111.00	47.700	0.0116	874.70

The thin metal slabs were divided into three nodes. The thicker metal slabs were divided into ten uniformly spaced nodes with one of the ten nodes on the slab surface. The surface coating was not modeled.

In addition to the structural conduction slabs, ten more conductors were used to model the alpha blocks. The data for the alpha block conductor input is given in Table 36. The material properties used for each of the conductors is given in Table 37. The initial conditions for the test are given in Table 38. The break flow and specific enthalpy used in the calculation is given in Table 39. The values in this table are those specified for the standard problem, except that some of the early time values were averaged over a longer time period than the values specified for the standard problem, and the specific enthalpies at early times (0.28 to 2.0 sec) were corrected to give a smooth steam source into the containment. The reason for this is shown in Figure 75. The solid curve in this figure is the steam flow into the containment calculated from the standard problem specified break flow and enthalpy at the containment pressure. There does not appear to be any physical explanation for the sharp drop in total steam flow at 0.5 sec. The total mass flow was assumed to be correct, and the specific enthalpies were corrected to give the smoothed steam flow shown by the dashed line in Figure 75. The standard problem values are shown in parentheses in Table 38.

The slight correction in the enthalpies results in a minor improvement to the predicted pressure response. This will be discussed in the next section. The magnitude of flow and liquid content of the blowdown flow during the first 2 sec of the transient has a significant effect on the differential pressure between the containment rooms. The uncertainty in the blowdown mass flow and enthalpy is probably one of the largest uncertainties in the calculation. The liquid was assumed to enter the containment in the form of drops having an average diameter of 200μm.

7.3 Discussion of Results

COBRA-NC predictions have been made of the short, medium, and long-term containment pressures, atmosphere temperatures, differential pressures, heat transfer coefficients, structural temperatures, air and steam densities, and mass flow between rooms and drop velocities. Along with the "best-estimate" base case for the short-term response, several parametric simulations were made to investigate the sensitivity of various modeling assumptions on the predicted pressure response of the containment. This was done to shed some light on which variables were the most dominant and therefore the most important to model. The results of the base case will first be presented. Then the results of the parametric study will be discussed.

Table 36 Alpha block conduction model input

Zone Number	Conductor Number	Channel Number	Material	Node Locations Surface (m)
7	103	9	Stainless Steel	0.0.00033.00114 .00241.00389 .00496.00688 .00943.01198.01453. 01956 .02706.03593.04619 .06419.08185 .11238.18522 .29019 .39516.5
20	104	29	Stainless Steel	0.0.00013.00087 .00223.00357 .00493.00688 .00943.01198.01453. 01956 .02706.03593.04619 .06419.08185 .11238.18522 .29019 .39516.5
34	105	52	Stainless Steel	0.0.0014.00298 .00473.00688 .00943.01198 .01453.01956.02706.0 3593 .04619.06419.08185 .11238.18522.29019 .39516.5
3	106	4	Lead	0.000027.0017.00430 .00688.00943 .01198 .01453.01956.02706.03593.0 4619.06419.08185 .11238.18522.29019.39516 .5
9	107	15	Lead	0.000 027.0017.00430 .00688.00943 .01198 .01453 .01956.02706.03593 .04619. 06419.08185 .11238.18522.29019.39516 .5
16	108	18	Lead	0.000027. 0017.00430 .00688.00943 .01198 .01453.01956 .02706.03593 .04619.06419 t.08185 .11238.18522.29019.39516.5
19	109	28	Lead	0.000027.0017 .00430 .00688.00943 .01198 .01453.01956 .02706.03593 .04619.06419 .08185 .11238.18522.29019.39516.5
23	110	30	Lead .11238	0.000027.0017.00430T .00688.00943.01198 .01453.01956.02706 .03593 .04619.06419.08185 .18522.29019.39516.5
24	111	37	Lead	0.0 00027.0017.00430 .0068 8.00943 .01198 .01453.01956.02706.03593 .04619.06419.08185 t.11238.18522.29019.39516.5
27	112	41	Lead	0.000027 .0017.00430 .00688.00 943.01198 .01453.01956.02706.03593 .04619 .06419.08185 .11238 .18522.29019.39516.5

Table 37 Material properties

Material	Density kg/m**3	Specific Heat J/kg°C	Conductivity W/m°C
Concrete	2225.0	879.0	2.1
Carbon Steel	7805.9	473.2	51.93
Stainless Steel	7900.0	520.0	20.0
Lead	11388.0	129.4	34.6

Table 38 Initial conditions for test v44

Pressure	1 bar
Atmospheric Temperature (all rooms)	20°C
Relative Humidity (all rooms)	35%

Table 39 Break mass flow and specific enthalpy

Time (sec)	Mass Flow (kg/sec)	Specific Enthalpy (kJ/kg)	
0.0	1391.0	2707.0	
0.1	1355.0	2707.0	
0.2	1281.0	2707.0	
0.3	1268.0	2589.0	(2571.0)
0.4	1497.0	2266.0	(2232.0)
0.5	1688.0	2031.0	(1894.0)
0.6	1879.0	1852.0	(1555.0)
0.7	2039.0	1726.0	(1518.0)
0.8	2152.0	1645.0	(1496.0)
0.9	2227.0	1594.0	(1482.0)
1.0	2282.0	1556.0	(1472.0)
1.1	2324.0	1528.0	(1465.0)
1.2	2352.0	1509.0	(1461.0)
1.3	2375.0	1493.0	(1457.0)
1.4	2388.0	1487.0	(1454.0)
1.5	2401.0	1473.0	(1452.0)
1.6	2406.0	1466.0	(1450.0)
1.7	2409.0	1461.0	(1449.0)
1.8	2404.0	1459.0	(1448.0)
1.9	2400.0	1456.0	(1447.0)
2.0	2395.0	1453.0	(1447.0)
3.0	2283.0	1449.0	
4.0	2149.0	1456.0	
5.0	2016.0	1467.0	
6.0	1884.0	1480.0	
7.0	1751.0	1497.0	
8.0	1623.0	1517.0	
9.0	1460.0	1555.0	
10.0	1365.0	1565.0	
11.0	1263.0	1584.0	
12.0	1159.0	1609.0	
13.0	1057.0	1637.0	
14.0	985.0	1703.0	
15.0	864.01	1703.0	
16.0	774.0	1743.0	
17.0	692.0	1785.0	
18.0	617.0	1832.0	
19.0	547.0	1884.0	
20.0	479.0	1950.0	
21.0	417.0	2028.0	
22.0	364.0	2110.0	
23.0	319.0	2199.0	
24.0	288.9	2267.0	
25.0	259.0	2340.0	

(Table 39, continued)

Time (sec)	Mass Flow (kg/sec)	Specific Enthalpy (kJ/kg)
26.0	236.0	2404.0
28.9	196.0	2527.0
30.0	167.0	2631.0
32.0	148.0	2666.0
34.0	130.0	2700.0
38.0	83.0	2710.0
40.0	68.0	2709.0
42.0	57.0	2709.0
44.0	49.0	2710.0
46.0	42.0	2712.0
48.0	35.0	2714.0
50.0	31.0	2716.0
62.5	0.0	2716.0
1000.0	0.0	2716.9

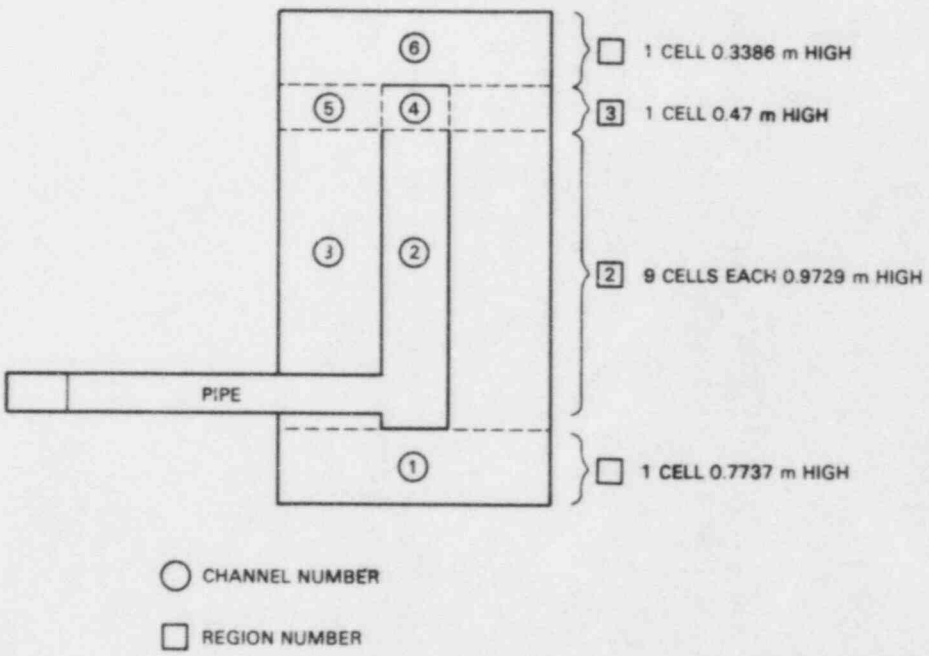

Figure 75 Steam flow into containment

7.3.1 Base-Case Results

The base-case calculation is based on the set of input parameters that appeared to give the best overall comparison with the measured data. The main input variables for this calculation that were varied in the subsequent parametric studies are as follows:

- Net drop disposition rate — 0 (100% carryover)
- Drop size in blowdown nozzle — 200 μm
- Condensation heat transfer — Uchida
- Vent discharge coefficients — GRS values except for vent U0143 and U0140. A value of 8.0 is used for the loss coefficient of these vents.
- Blowdown flow and enthalpy — ISP values except specific enthalpies modified between 0.3 sec and 2.0 sec (see Section 3)

The noding remained constant for all cases. It is possible that equally good results could be obtained with fewer nodes by prudently grouping zones together, but this was not investigated. The drop size specified for the blowdown liquid is the drop size inside the blowdown nozzle at the blowdown vessel pressure. The drop size inside the containment is smaller as a result of drop evaporation at the lower containment pressures.

7.3.1.1 Short-Time Period Results (0-5 sec)

The predicted pressure responses for the short time period for several rooms are shown in Figures 76 through 163. The pressure in the blowdown room, room 1603, is shown in Figure 76. The measured pressure data showed large oscillations. The dashed lines in Figure 76 (and subsequent figures) are the envelope of the measured pressure response. One curve shows the upper bound and the other the lower bound of the oscillation. The solid line is the COBRA-NC-calculated pressure. The calculated pressure falls within or above the envelope of the measured pressure throughout this time period and has the same general shape as an average of the measured data. The pressures for rooms outside of the blowdown room are shown in Figures 77 through 84. In general, the pressure responses in rooms far away from the blowdown room are overpredicted. This probably results from an underprediction of the condensation rate at low steam concentrations. The measured data for some rooms was not available, but the calculated pressures are presented here for completeness.

The calculated differential pressures between rooms are shown in Figures 85 through 92. Again, the envelope of the measured differential pressures is shown with two dashed lines that represent the upper and lower bounds of the measured oscillations. In general, the calculated differential pressures

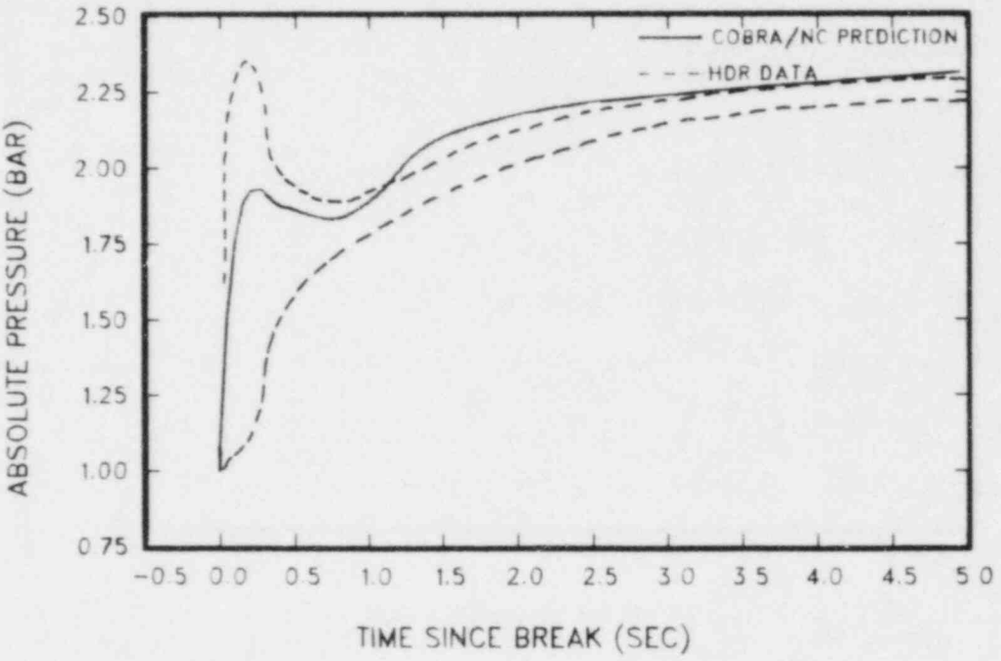

Figure 76 Absolute pressure in room 1603

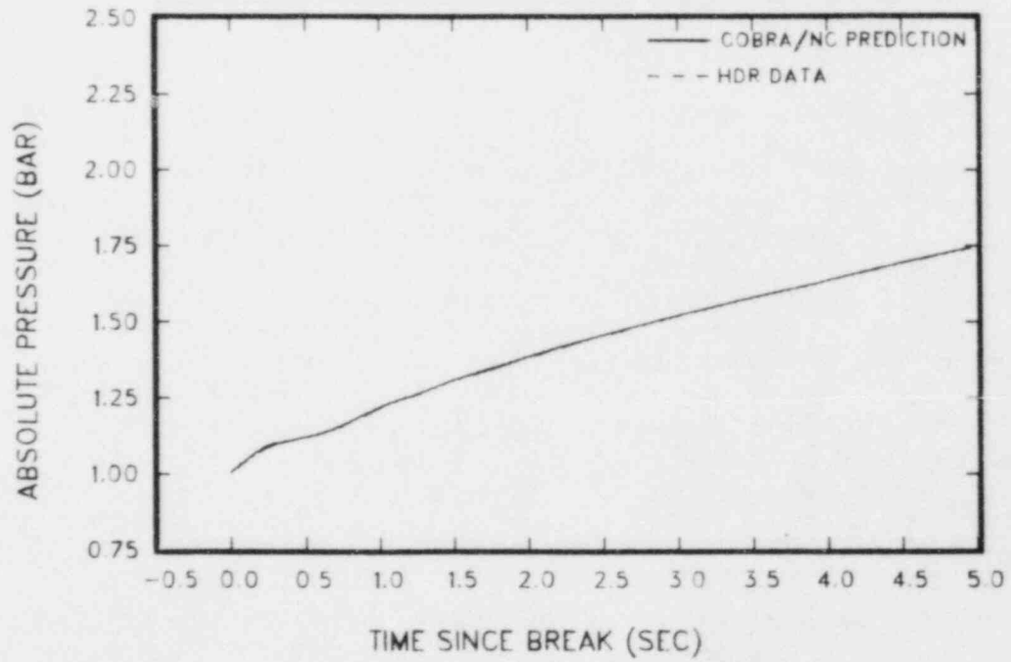

Figure 77 Absolute pressure in room 1708

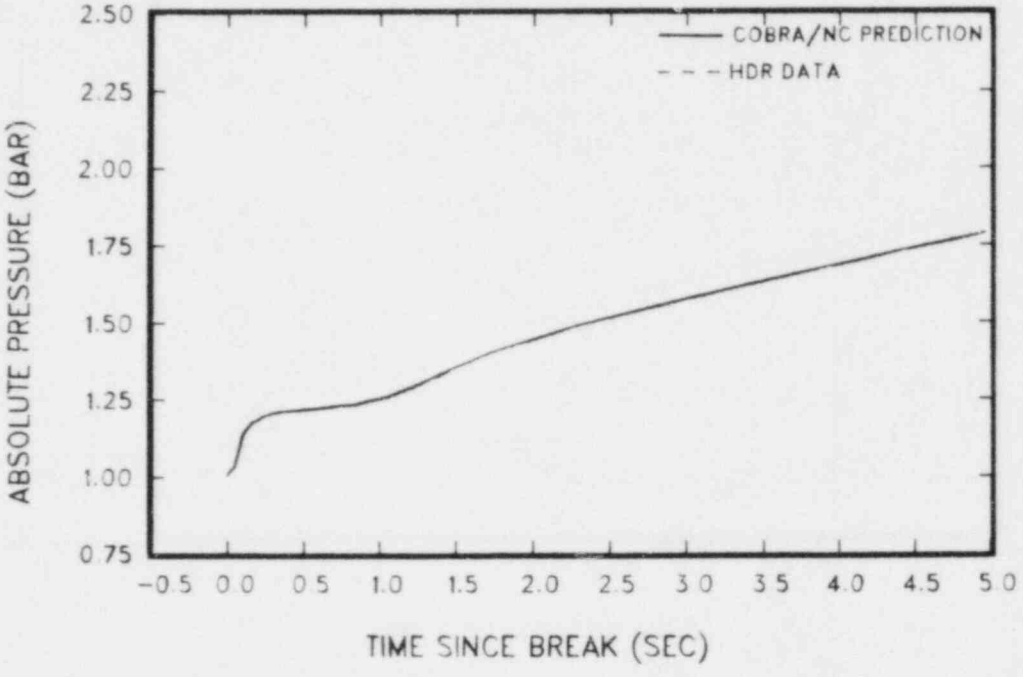

Figure 78 Absolute pressure in room 1605

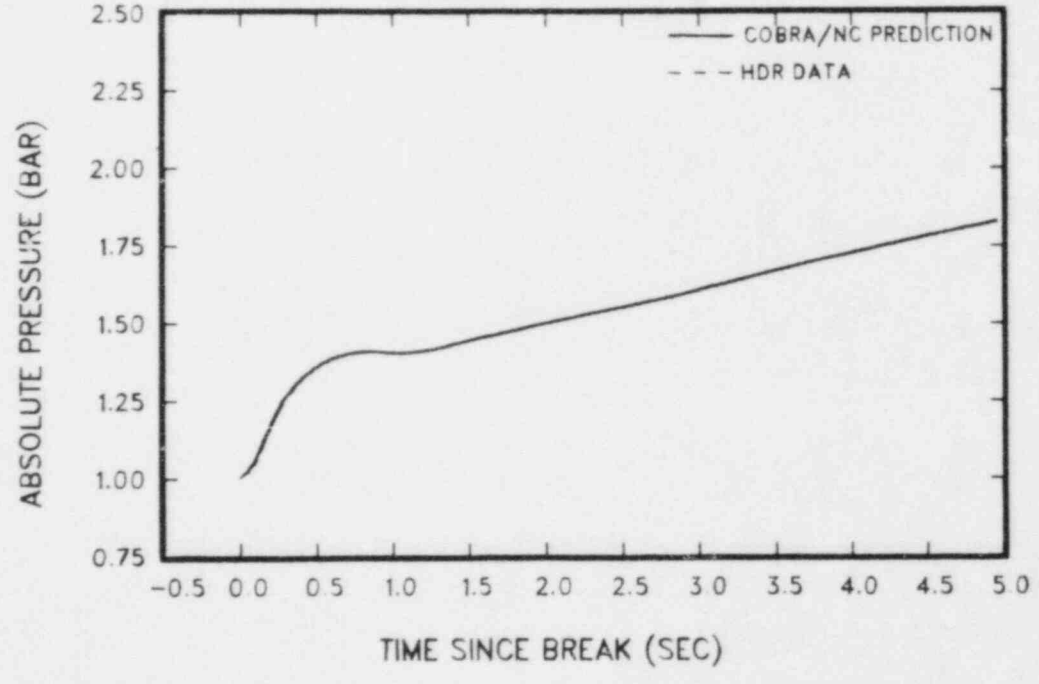

Figure 79 Absolute pressure in room 1704

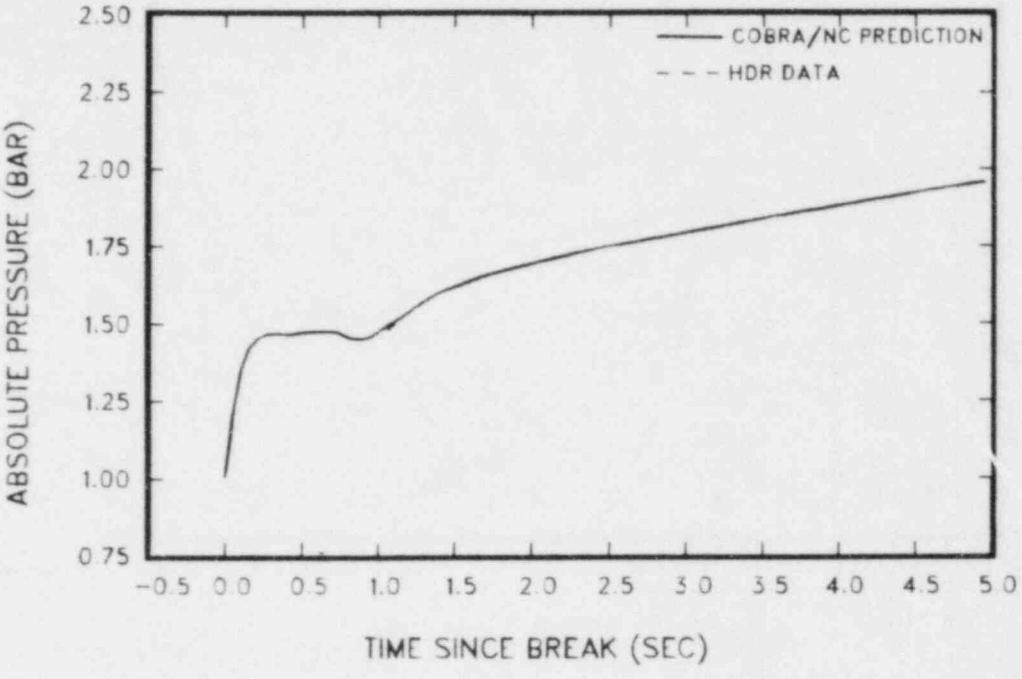

Figure 80 Absolute pressure in room 1704u

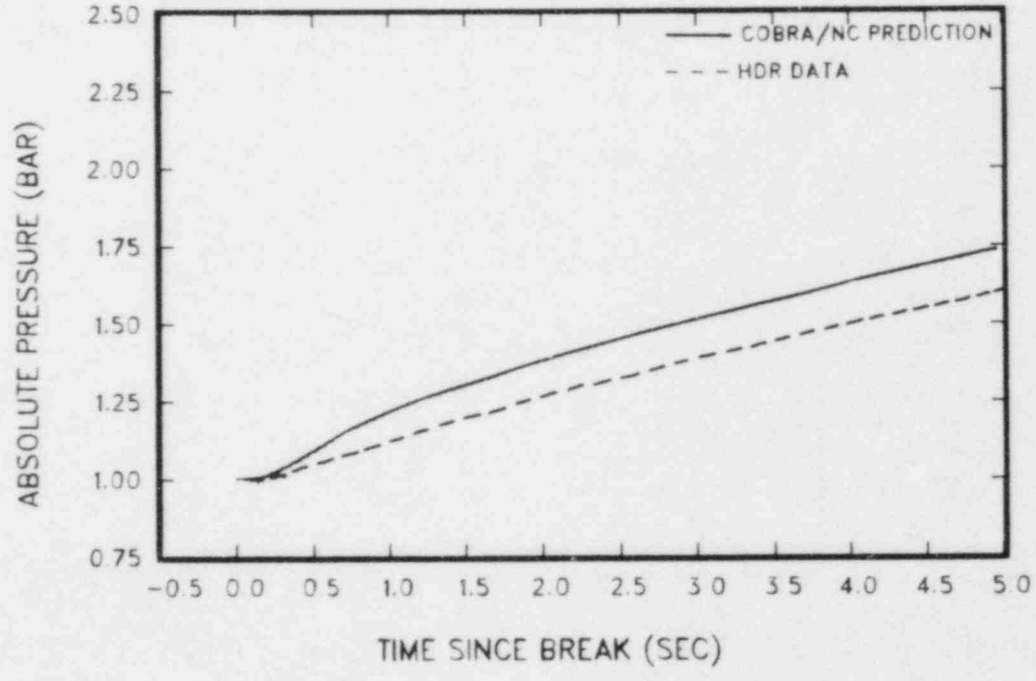

Figure 81 Absolute pressure in room 11004

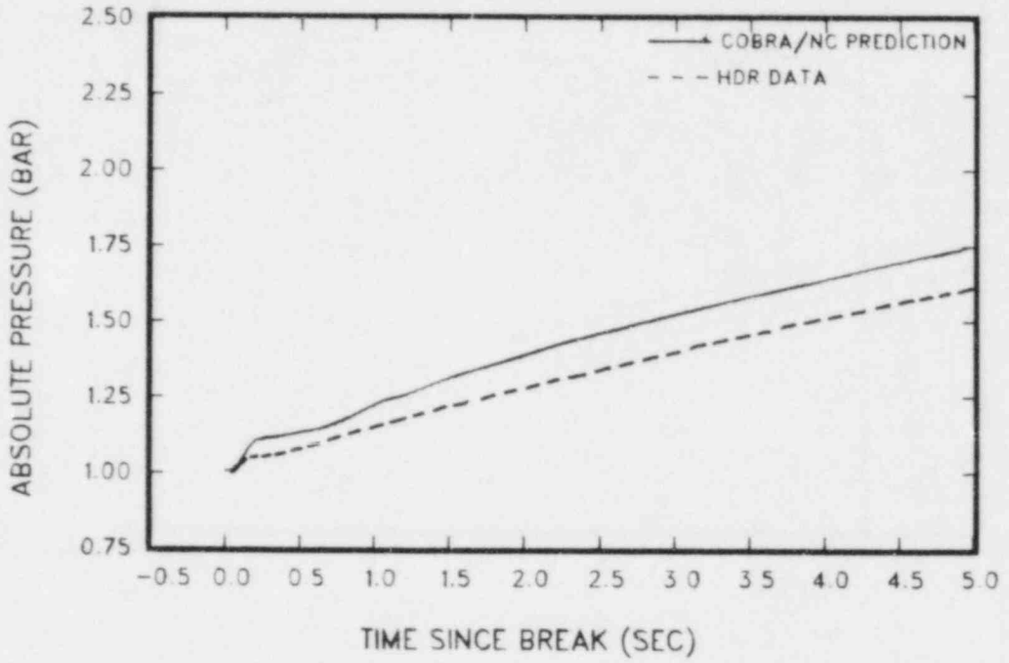

Figure 82 Absolute pressure in room 1602

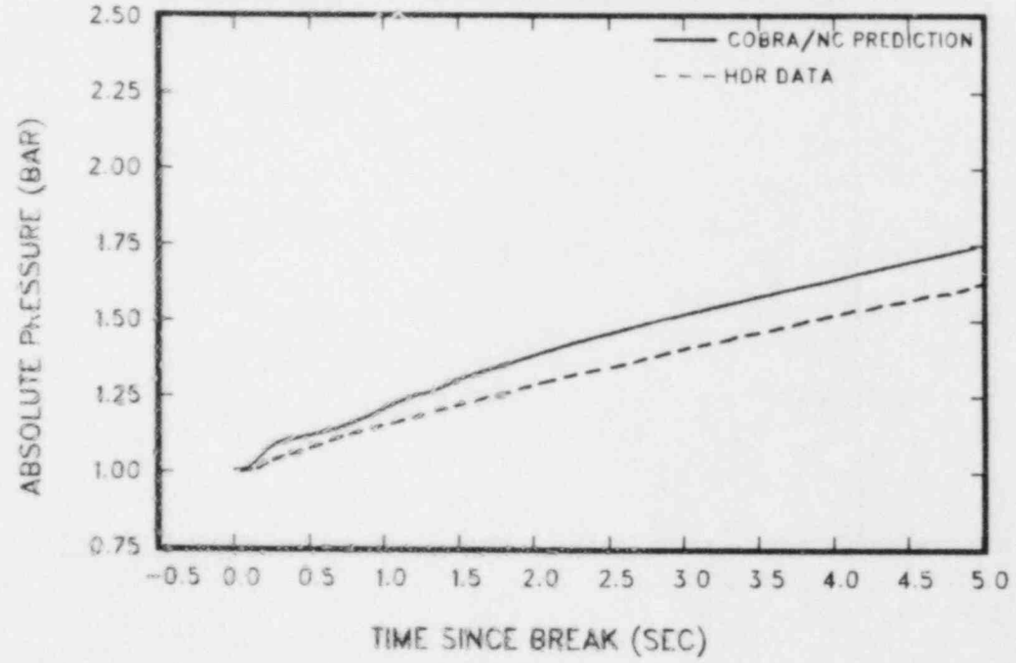

Figure 83 Absolute pressure in room 1508

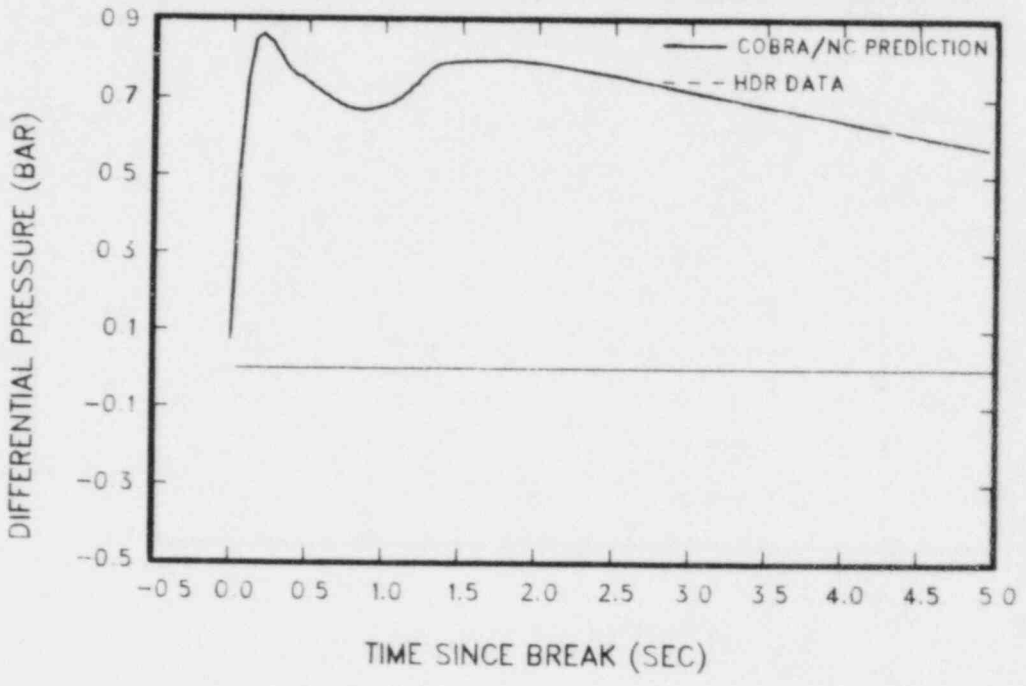

Figure 84 Absolute pressure in room 1305

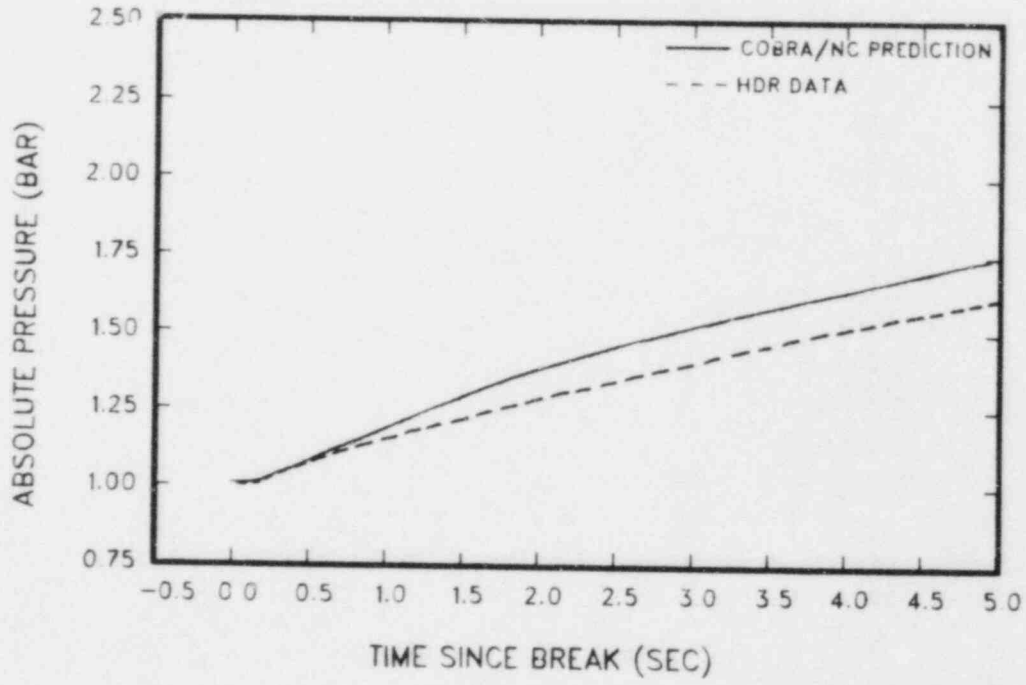

Figure 85 Differential pressure between rooms 1603 and 1508

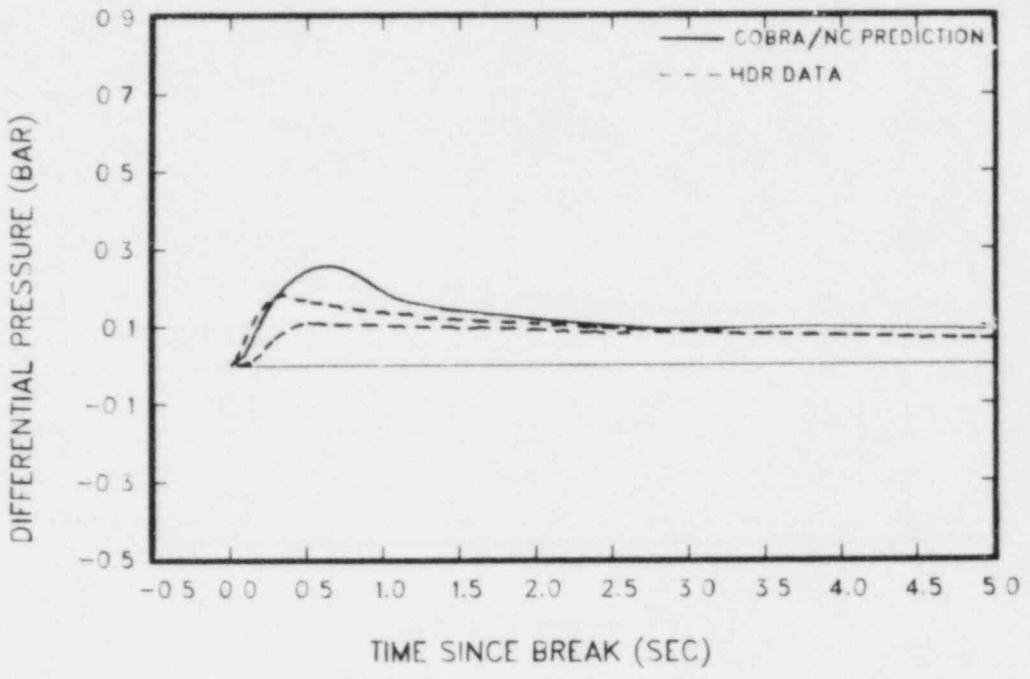

Figure 86 Differential pressure between rooms 1704 and 1804

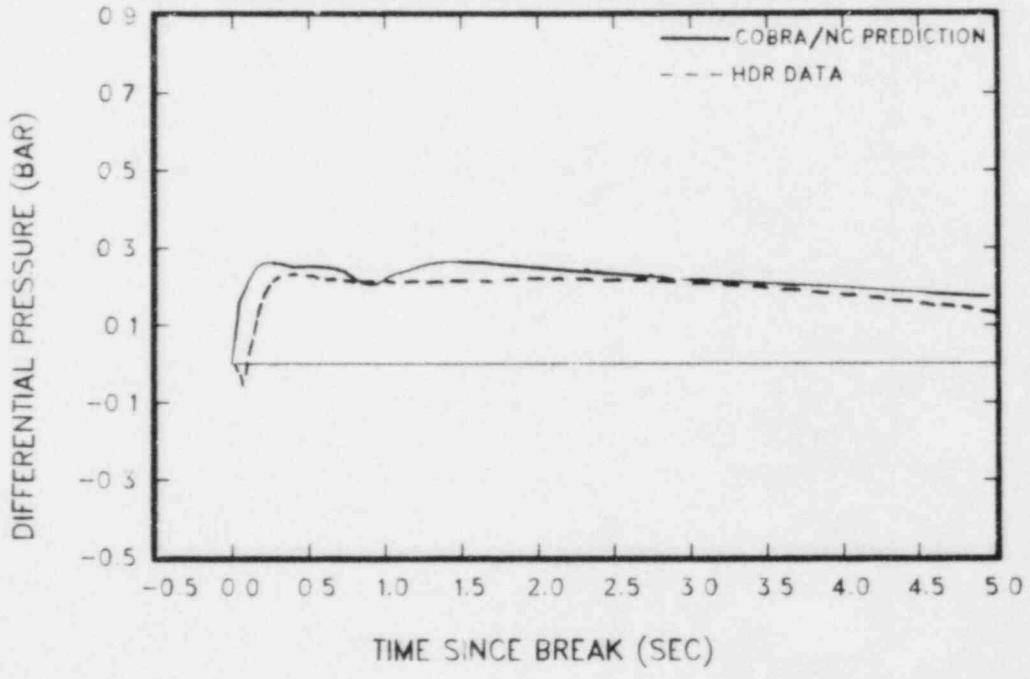

Figure 87 Differential pressure between rooms 1605 and 1701u

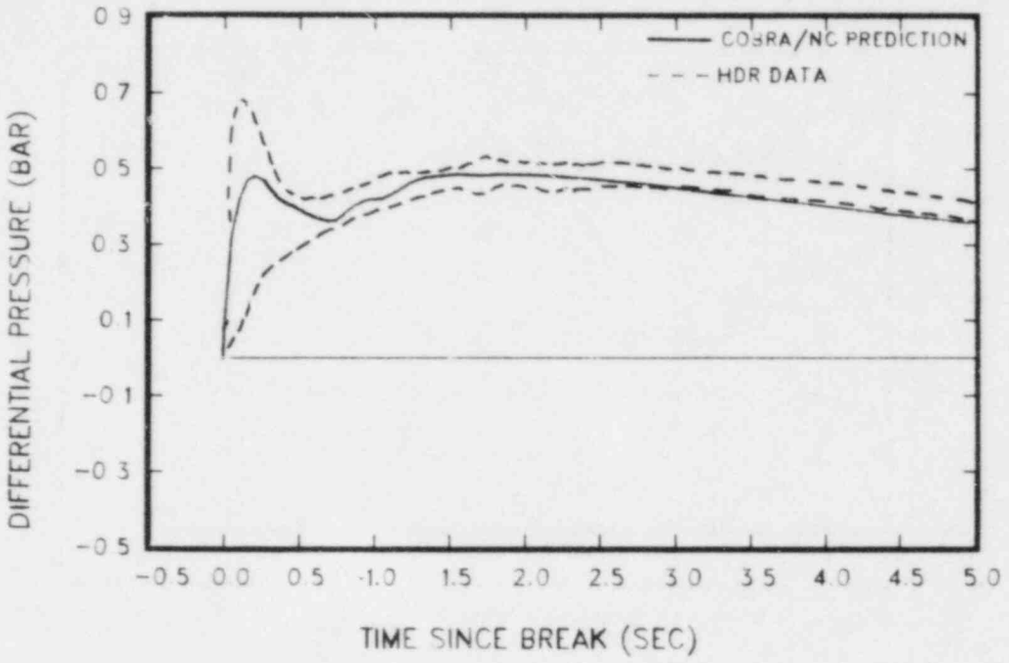

Figure 88 Differential pressure between rooms 1603 and 1701u

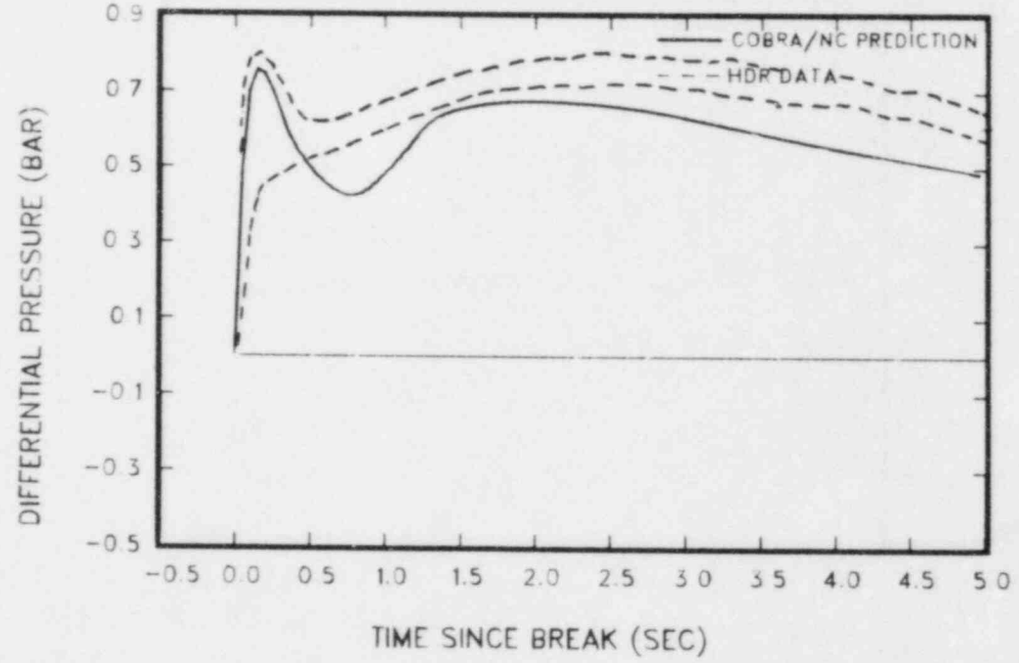

Figure 89 Differential pressure between rooms 1603 and 1704

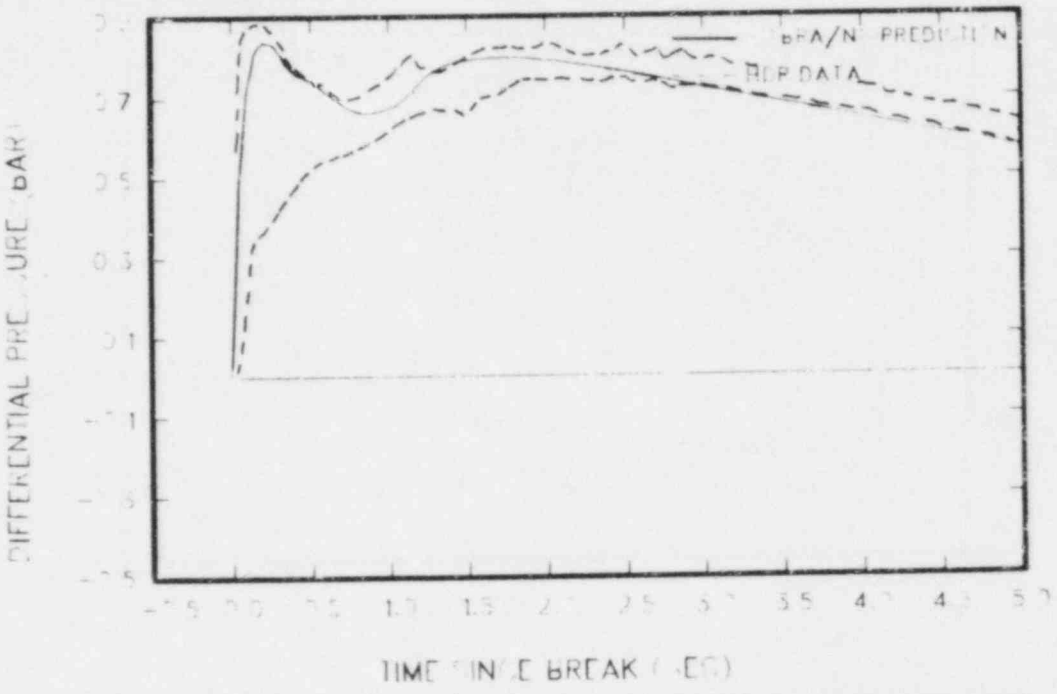

Figure 90 Differential pressure between rooms 1603 and 1708

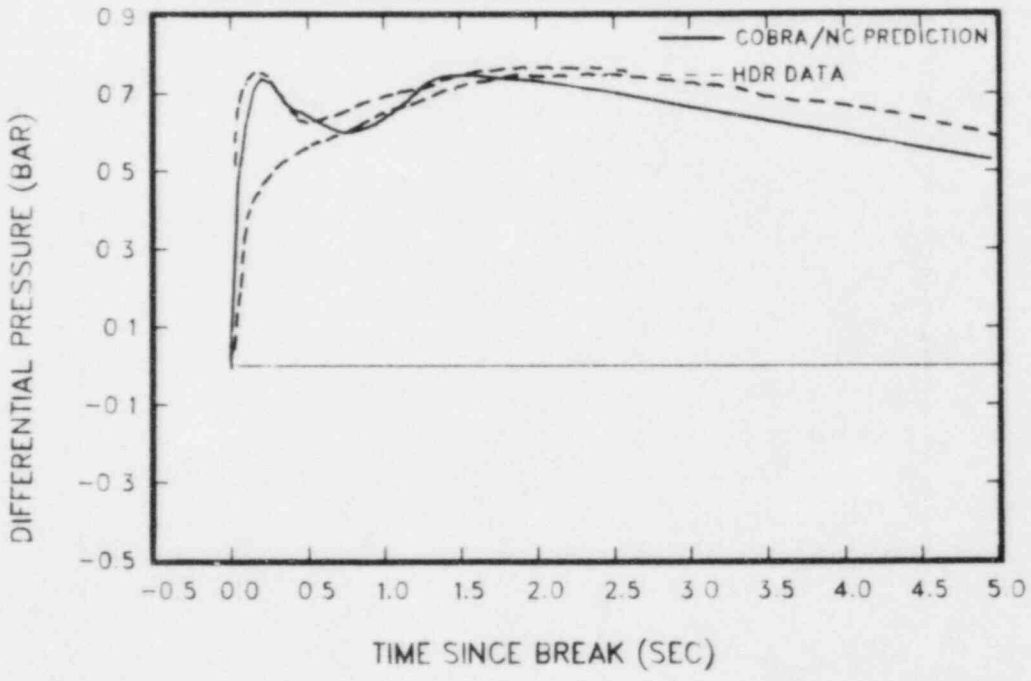

Figure 91 Differential pressure between rooms 1603 and 1605

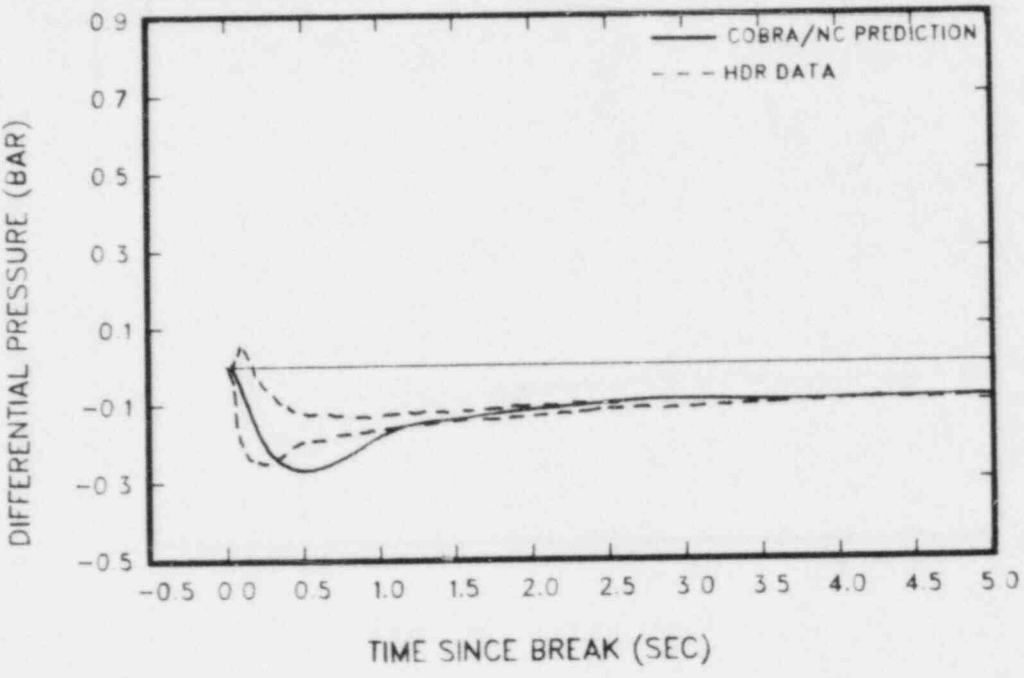

Figure 92 Differential pressure between rooms 1704 and 11004

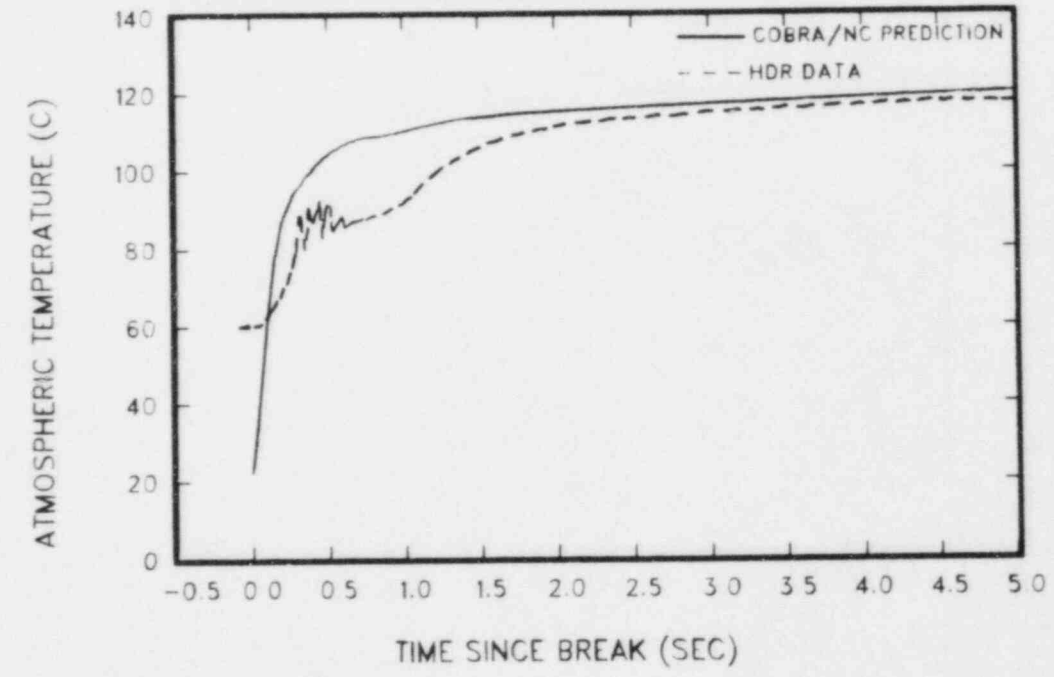

Figure 93 Temperature in room 1701u

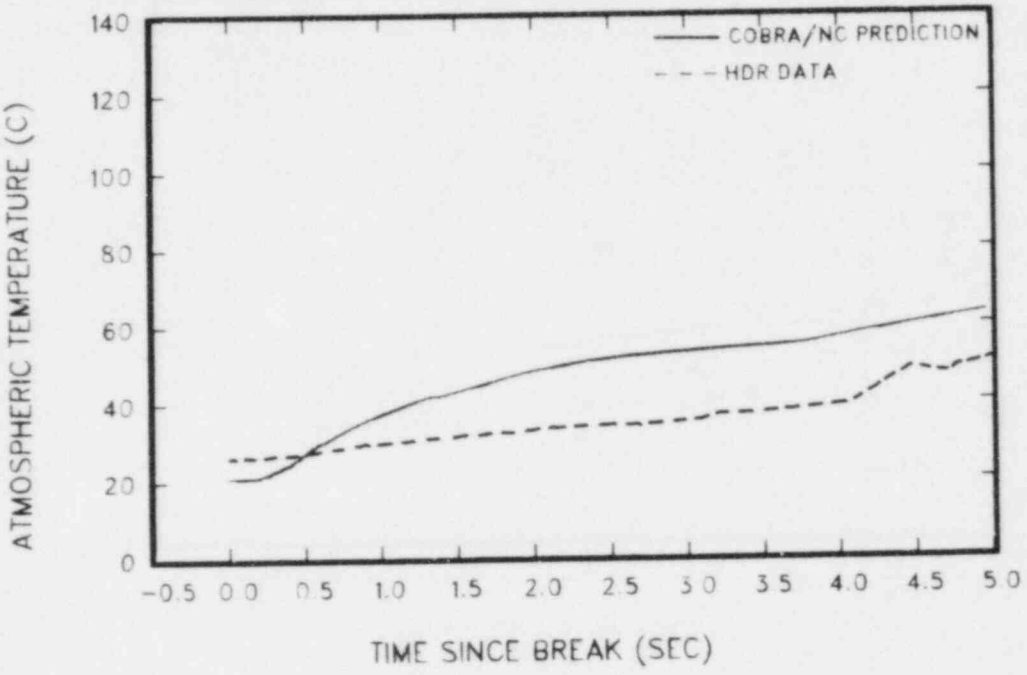

Figure 94 Temperature in room 11004

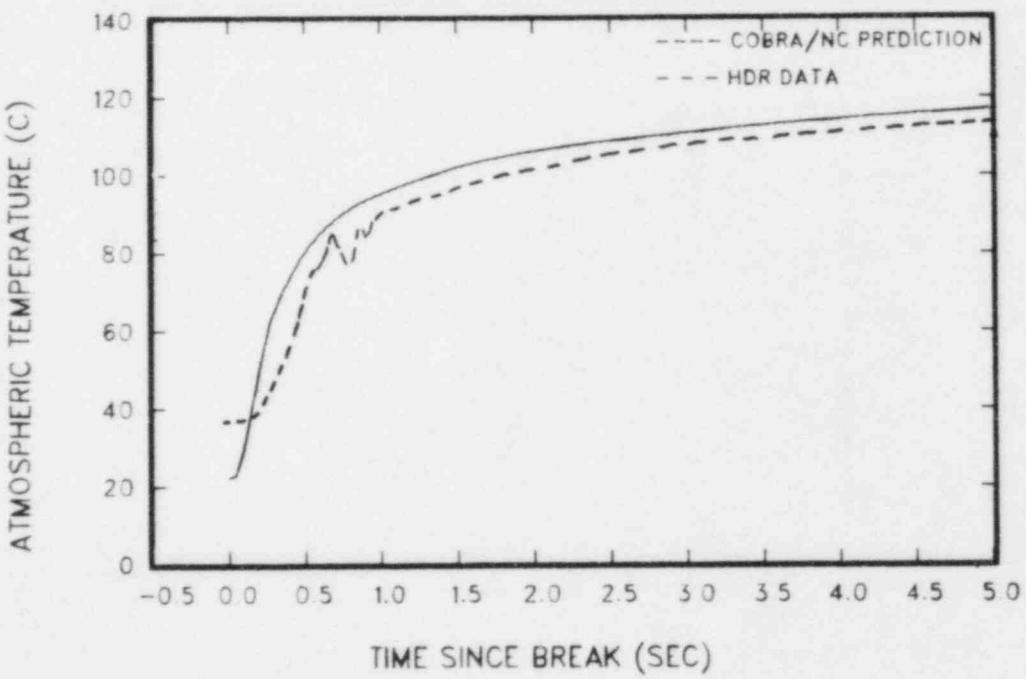

Figure 95 Temperature in room 1704

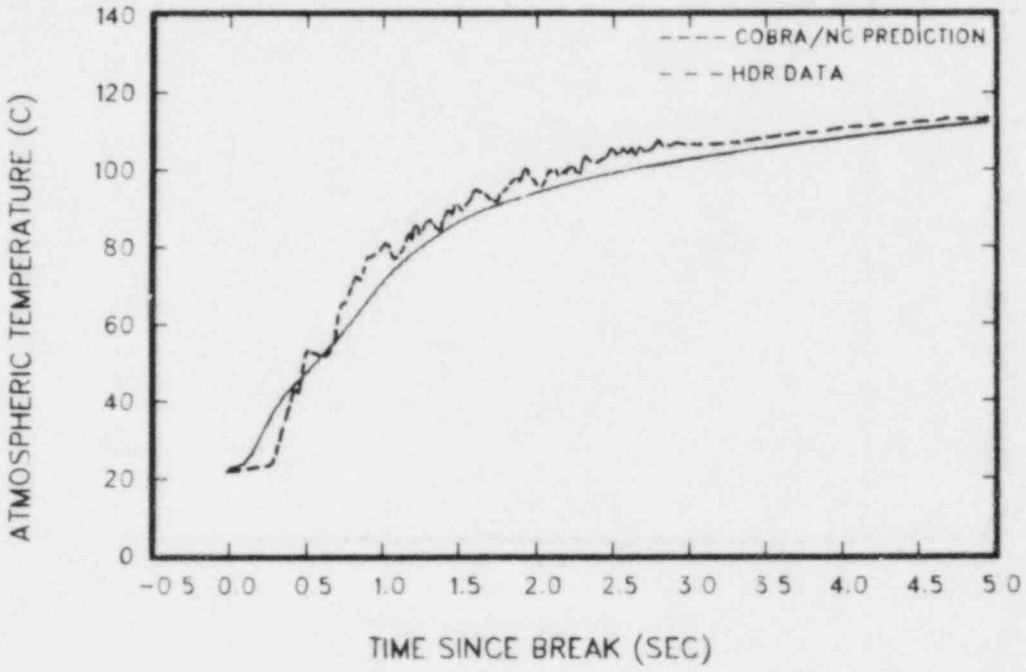

Figure 96 Temperature in room 1606

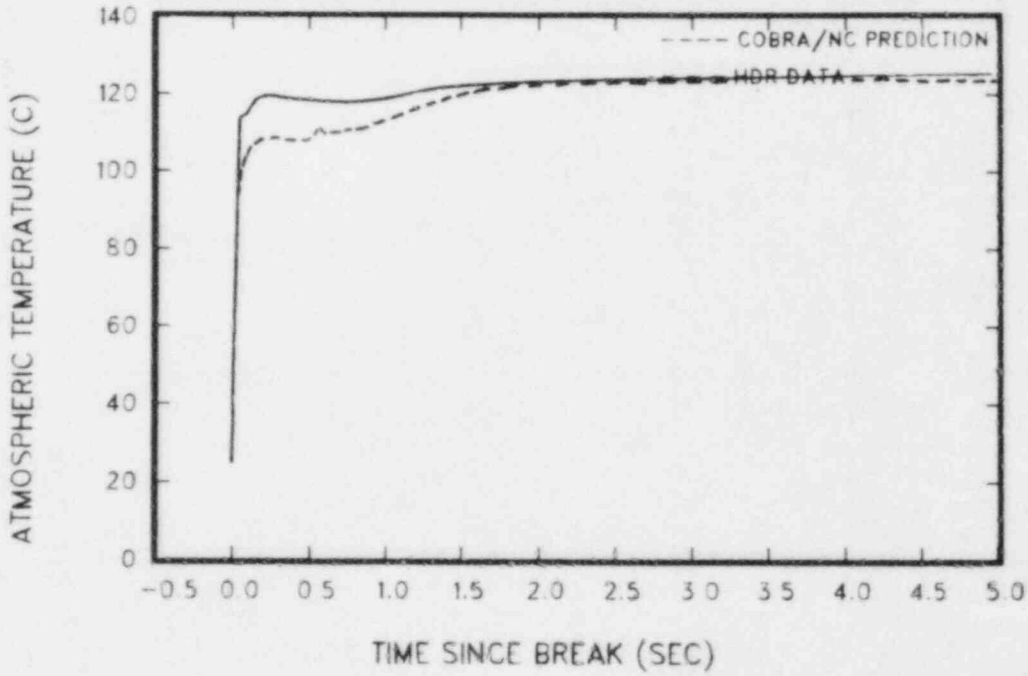

Figure 97 Temperature in room 1603

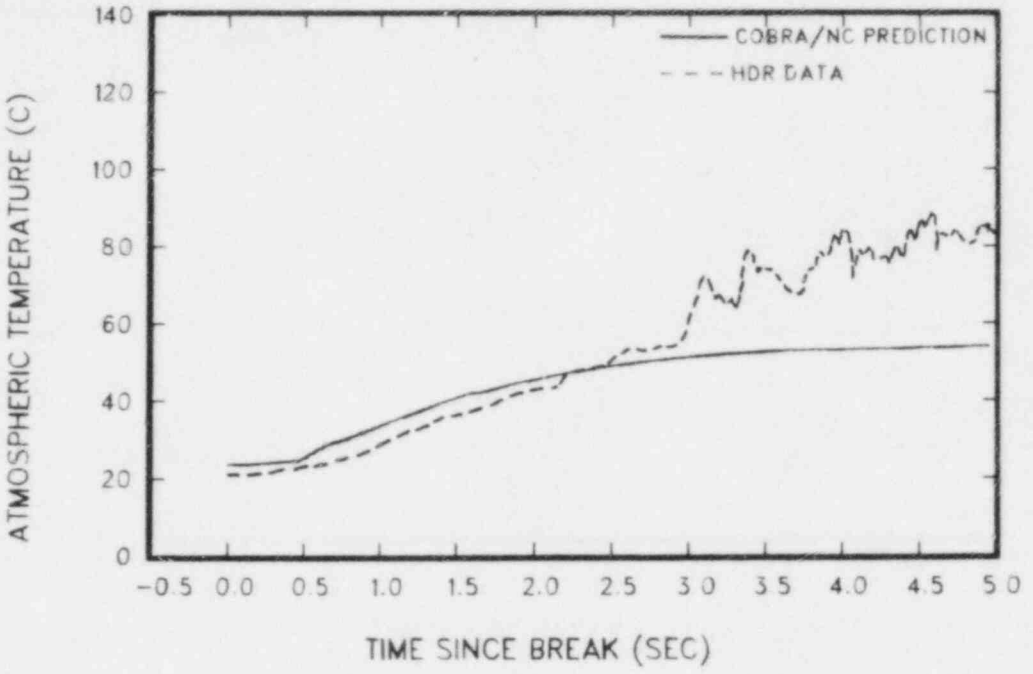

Figure 98 Temperature in room 1305

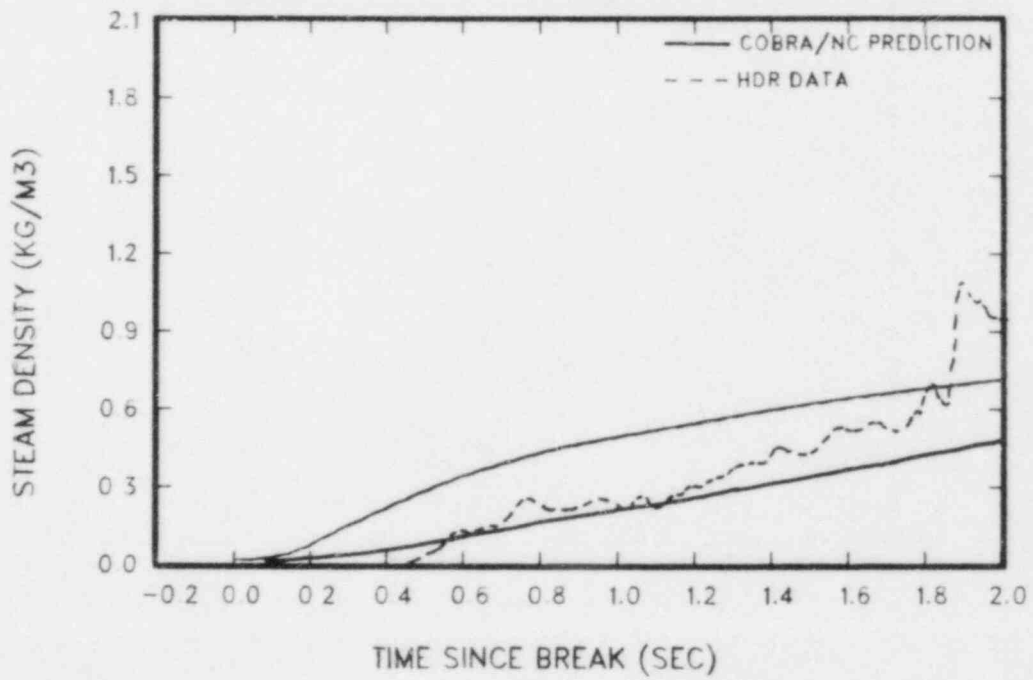

Figure 99 Steam density in room 1704

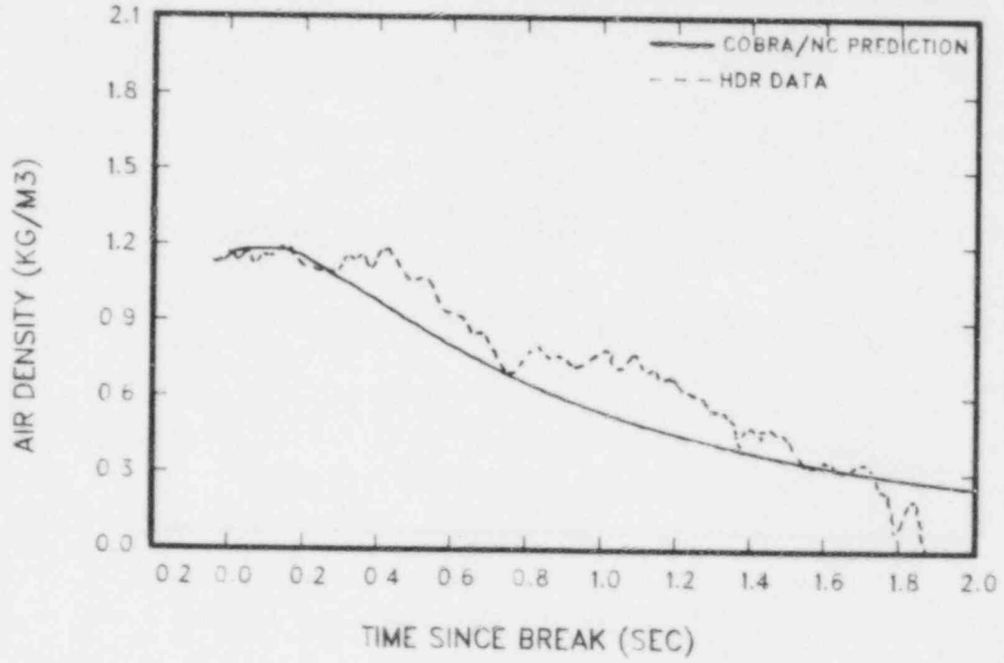

Figure 100 Air density in room 1704

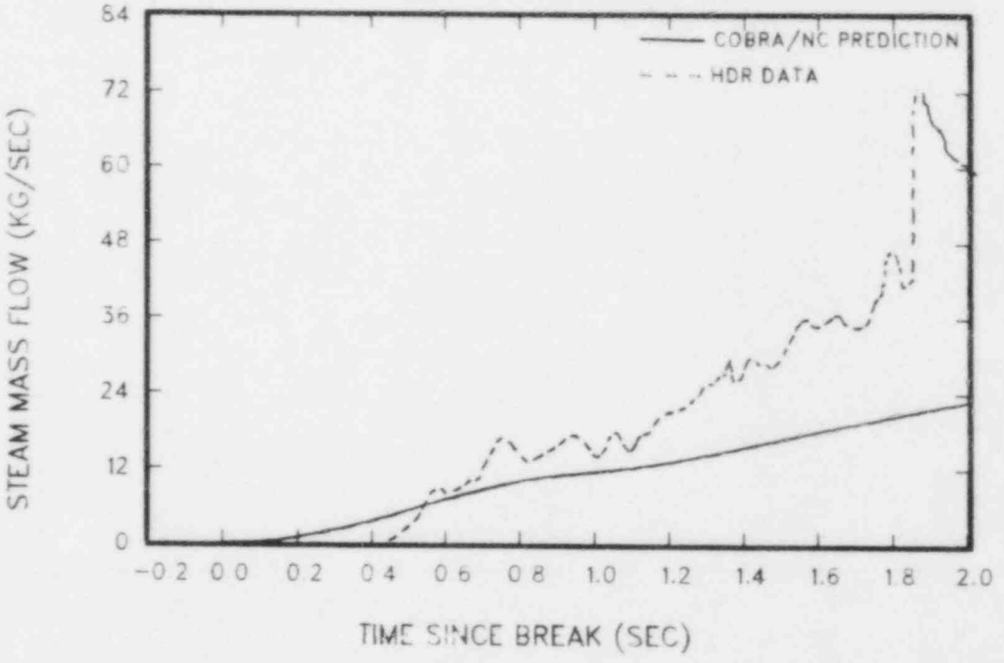

Figure 101 Steam flow between rooms 1704 and 1804

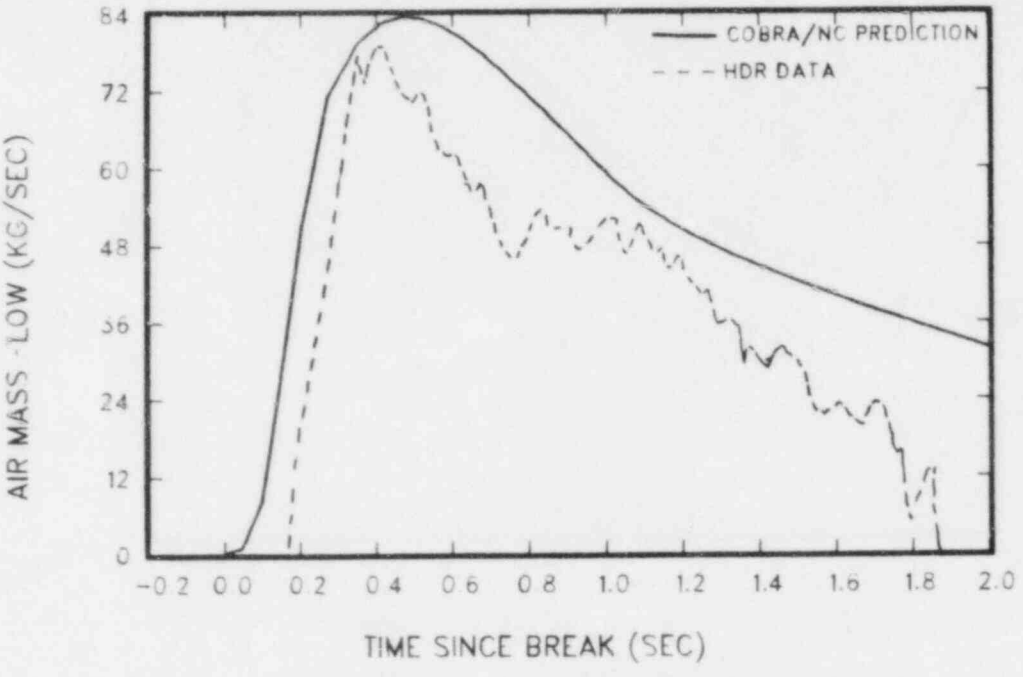

Figure 102 Air flow between rooms 1704 and 1804

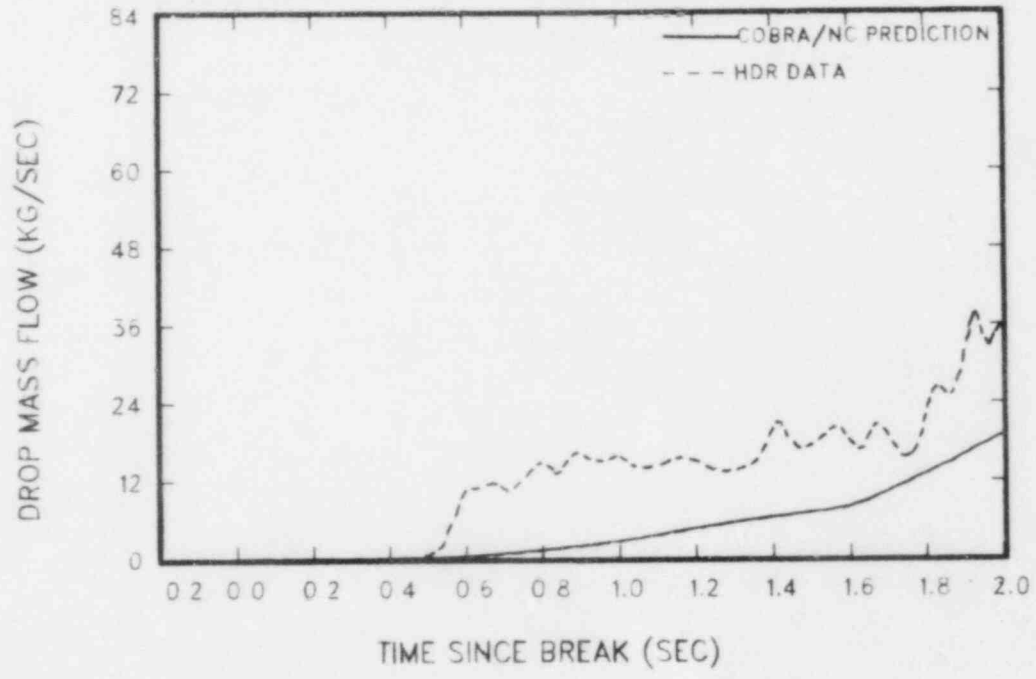

Figure 103 Drop flow between rooms 1704 and 1804

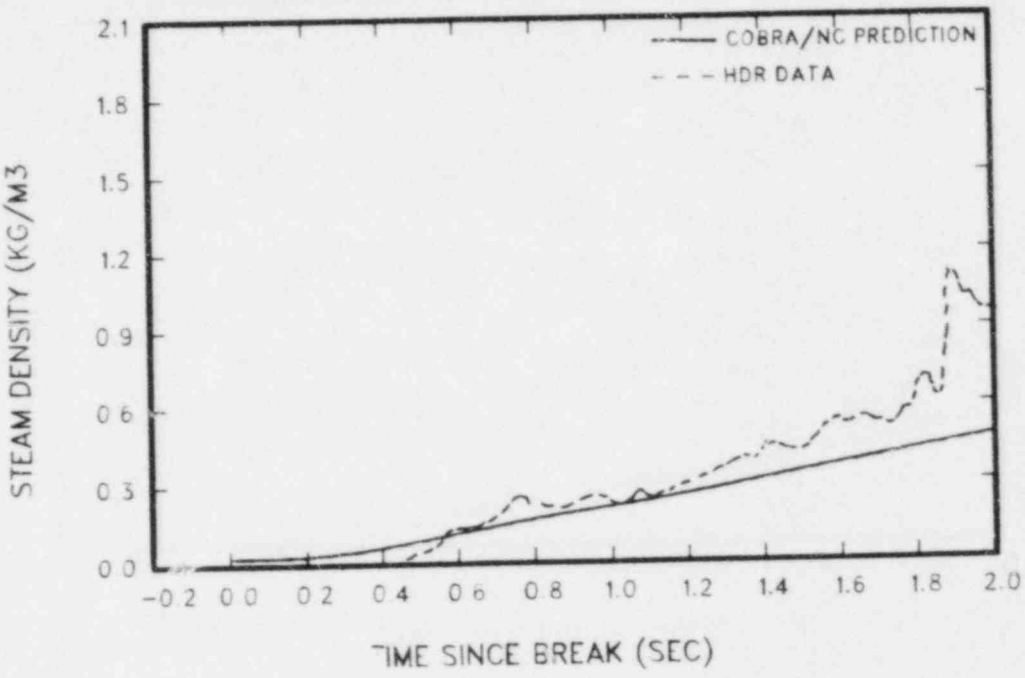

Figure 104 Steam density for flow between rooms 1704 and 1804

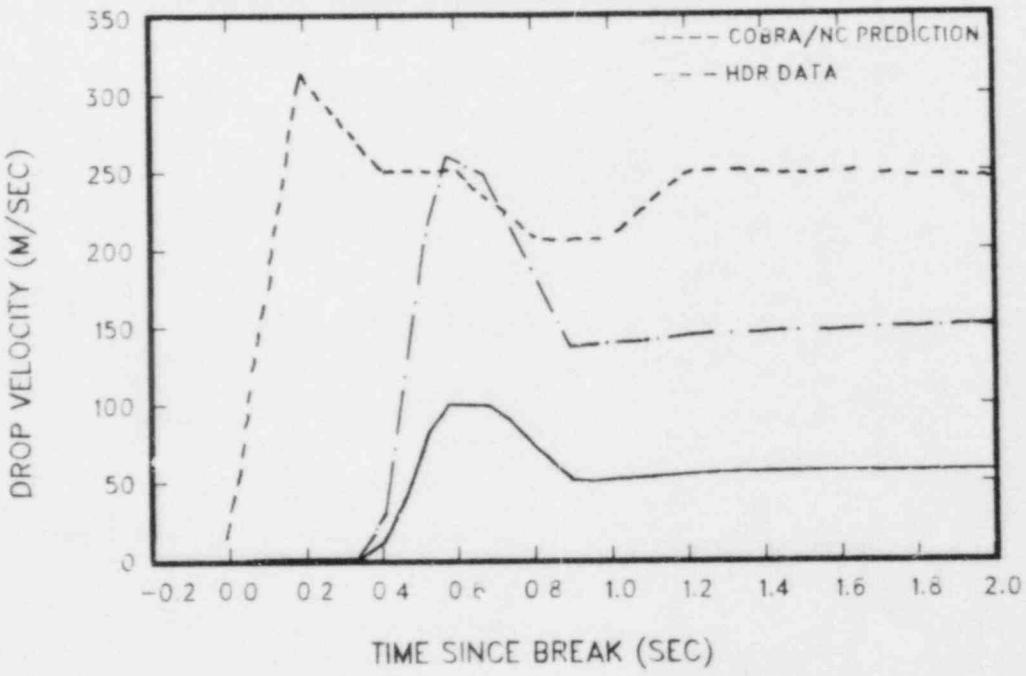

Figure 105 Drop velocity between rooms 1603 and 1704

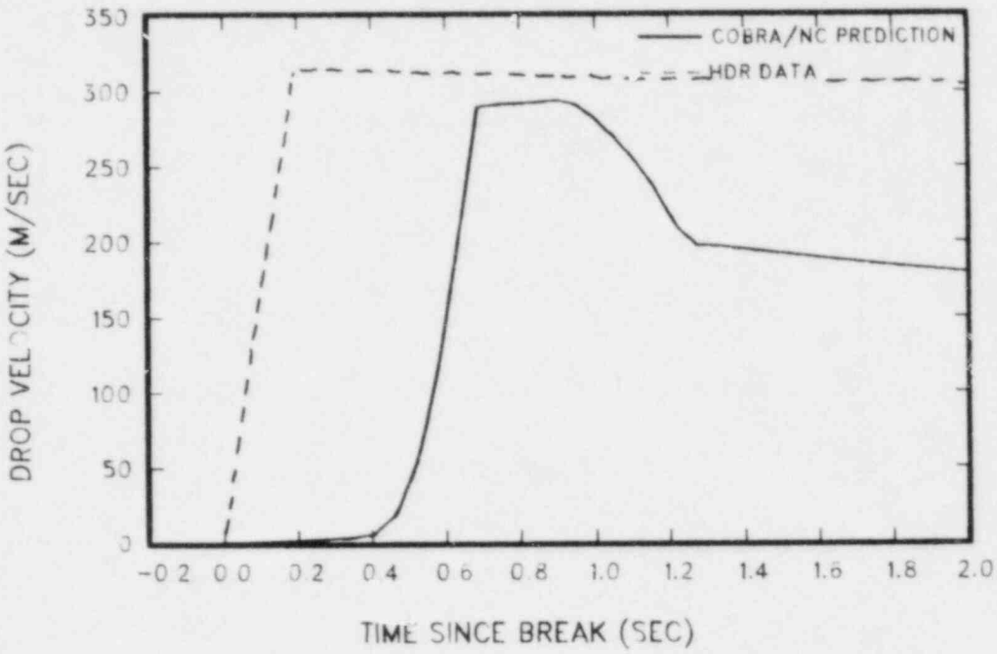

Figure 106 Drop velocity between rooms 1603 and 1708

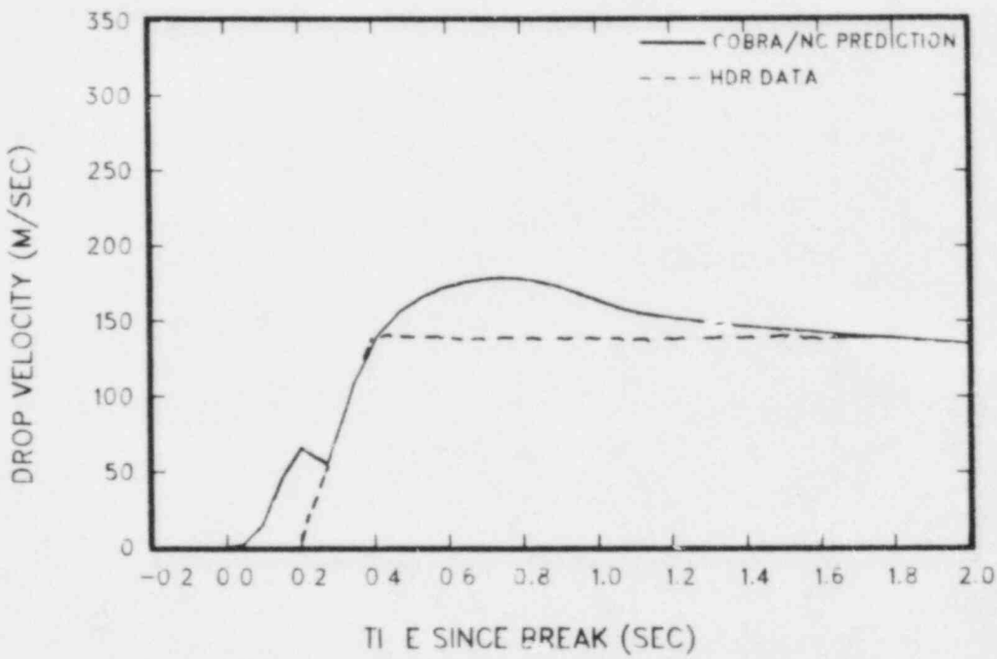

Figure 107 Drop velocity between rooms 1704 and 1804

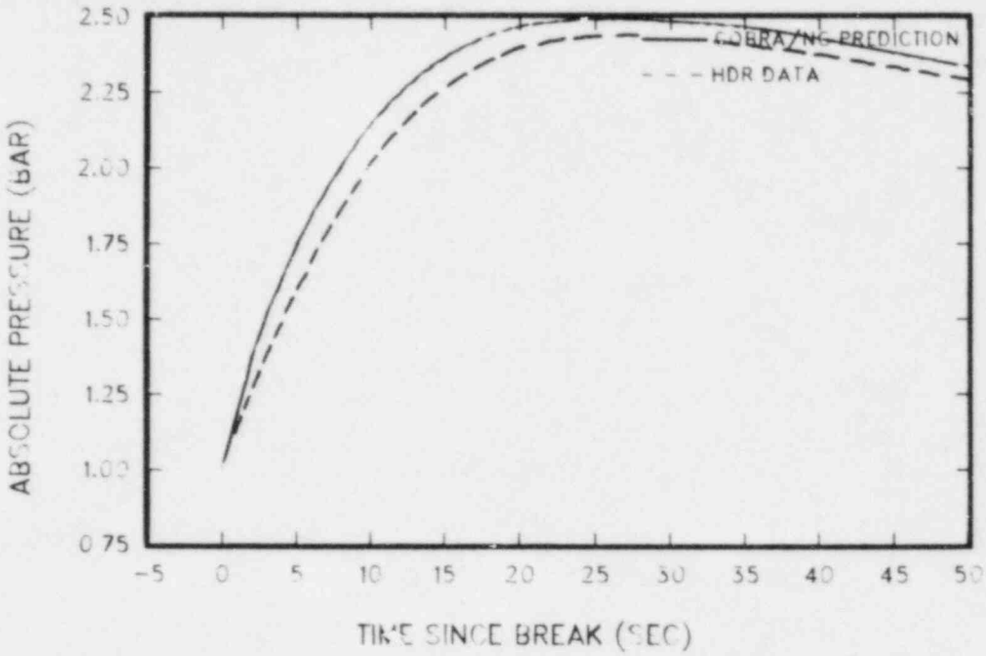

Figure 108 Absolute pressure in room 1305 (0-50 sec)

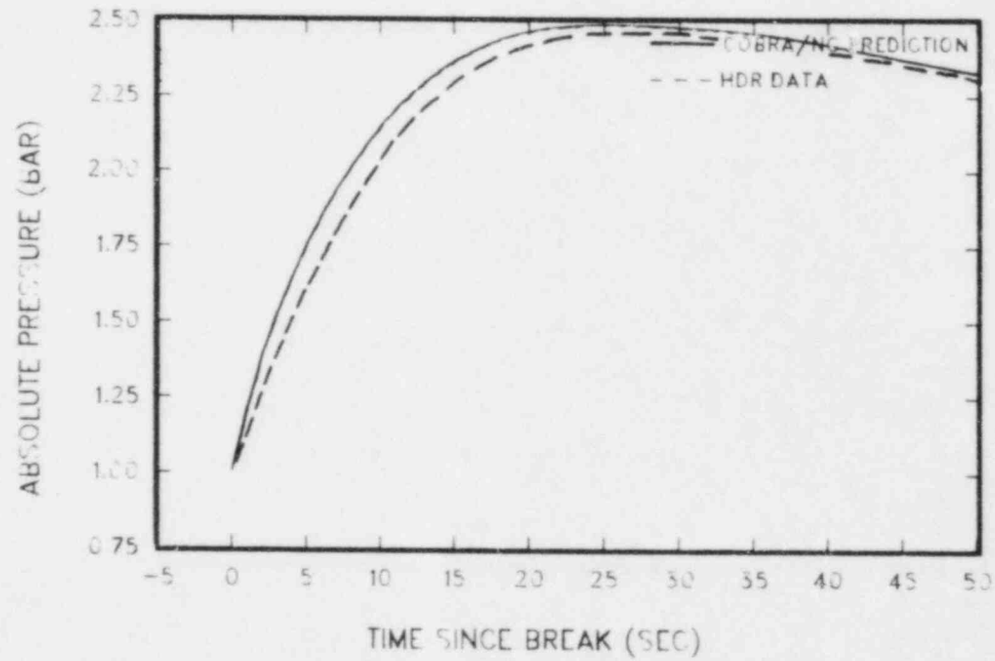

Figure 109 Absolute pressure in room 1508 (0-50 sec)

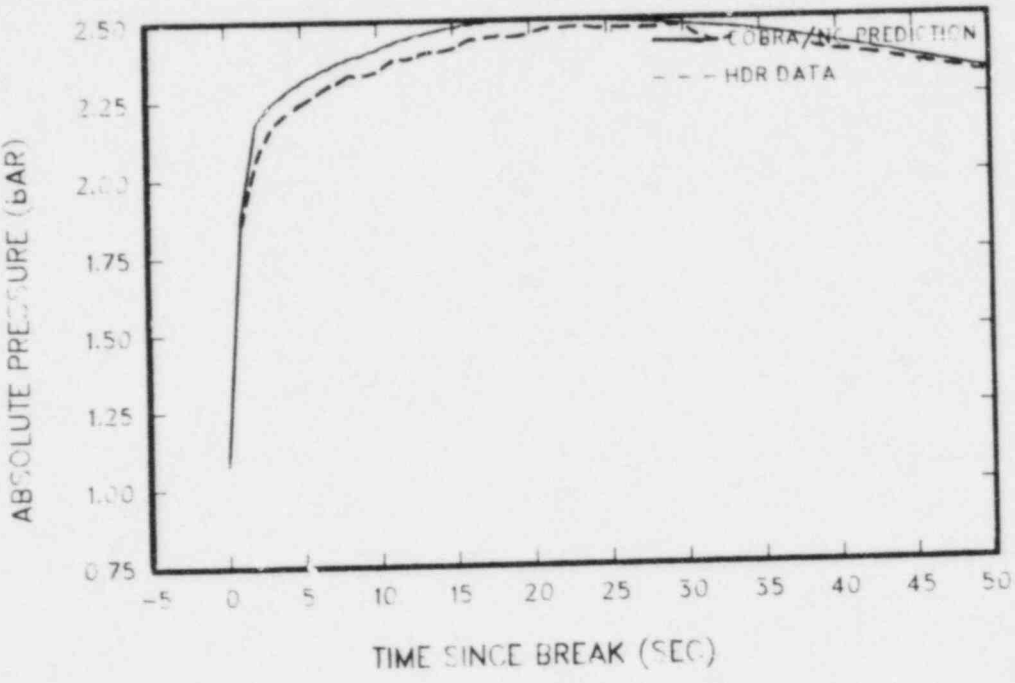

Figure 110 Absolute pressure in room 1603 (0-50 sec)

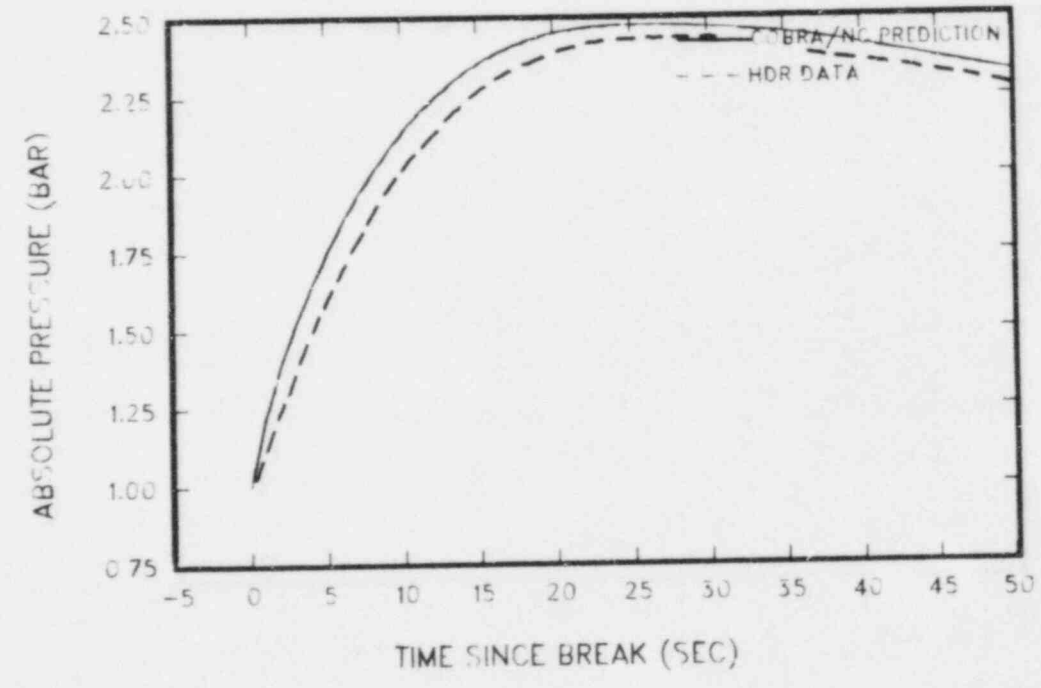

Figure 111 Absolute pressure in room 11004 (0-50 sec)

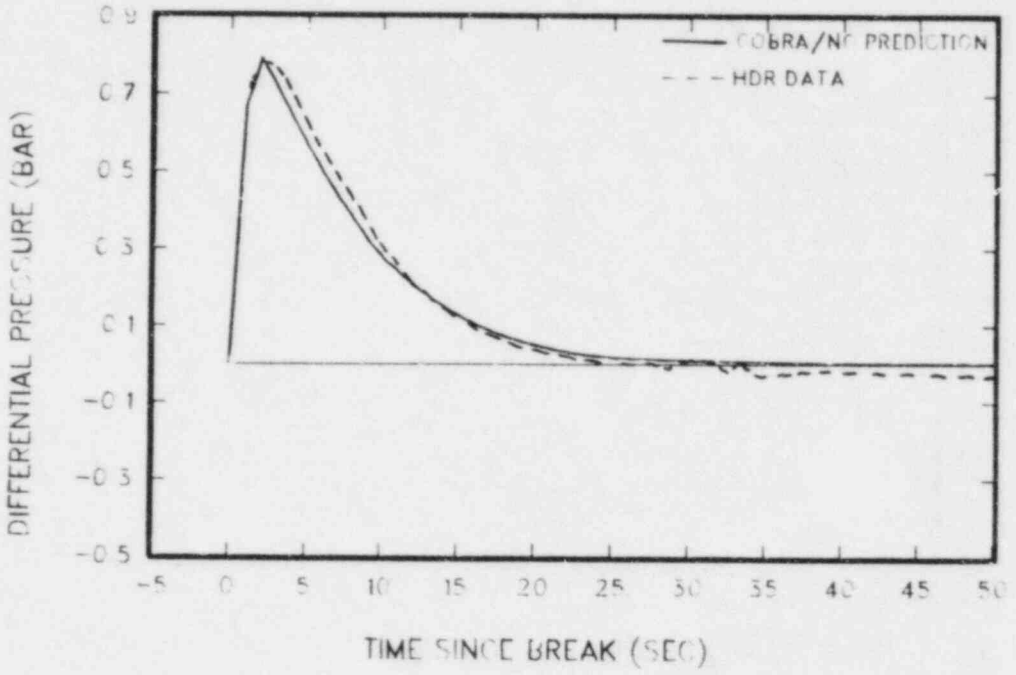

Figure 112 Differential pressure between rooms 1603 and 1708 (0-50 sec)

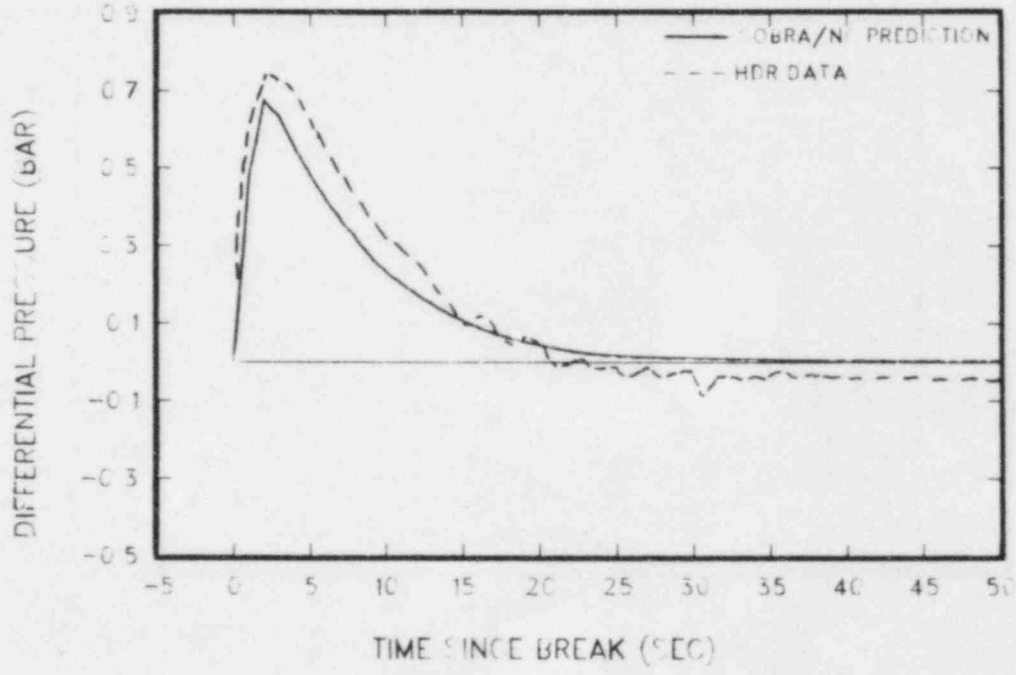

Figure 113 Differential pressure between rooms 1603 and 1704 (0-50 sec)

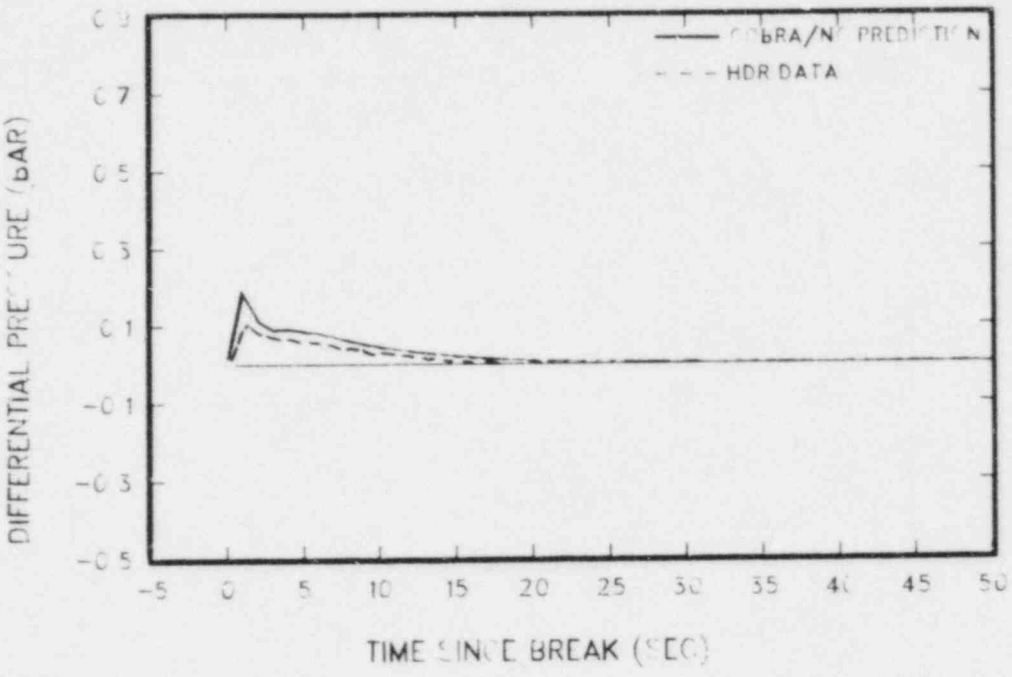

Figure 114 Differential pressure between rooms 1704 and 1804 (0-50 sec)

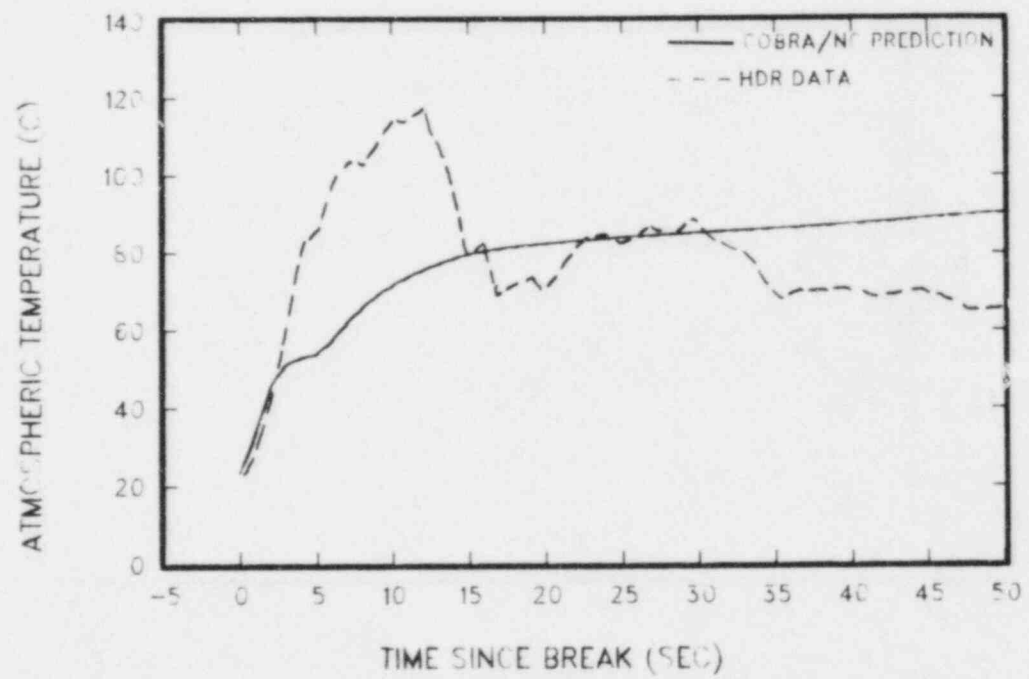

Figure 115 Temperature in room 1305(0-50 sec)

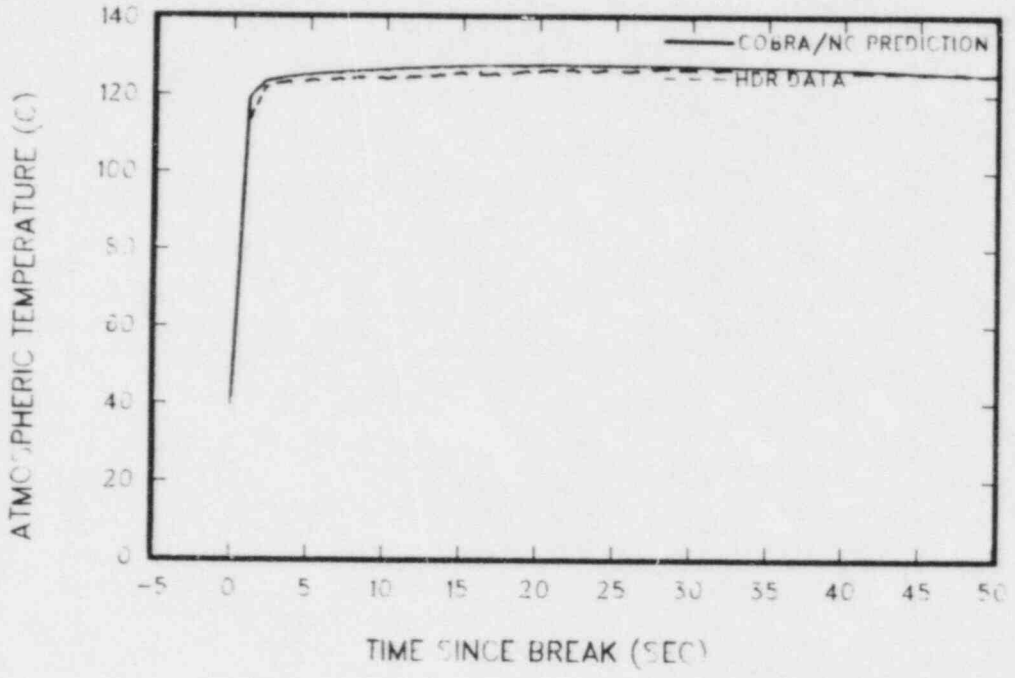

Figure 116 Temperature in room 1603 (0-50 sec)

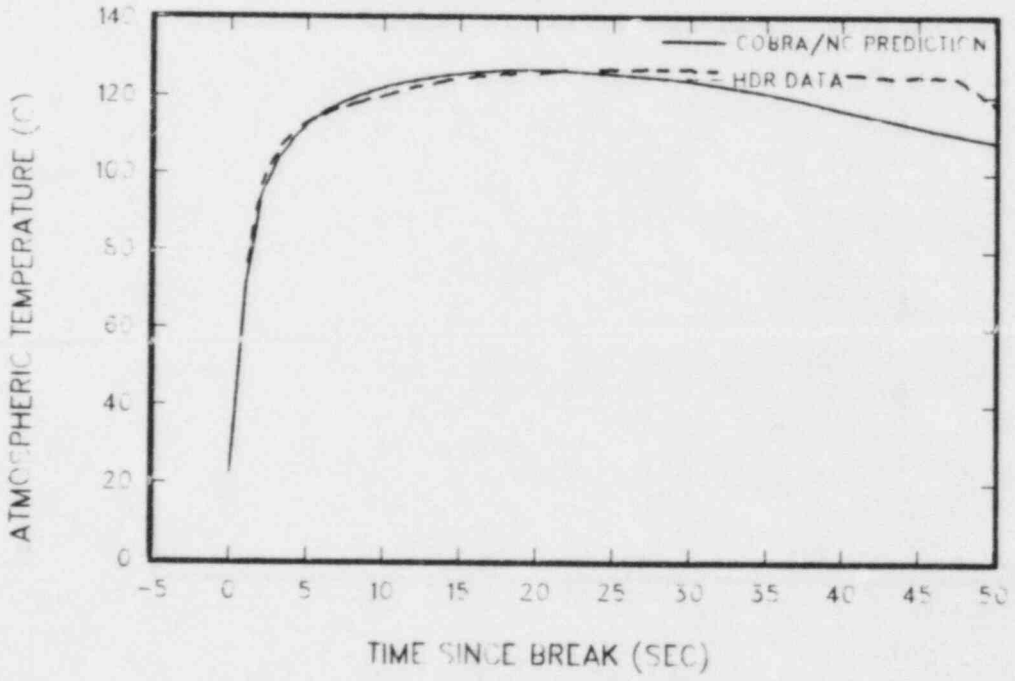

Figure 117 Temperature in room 1606 (0-50 sec)

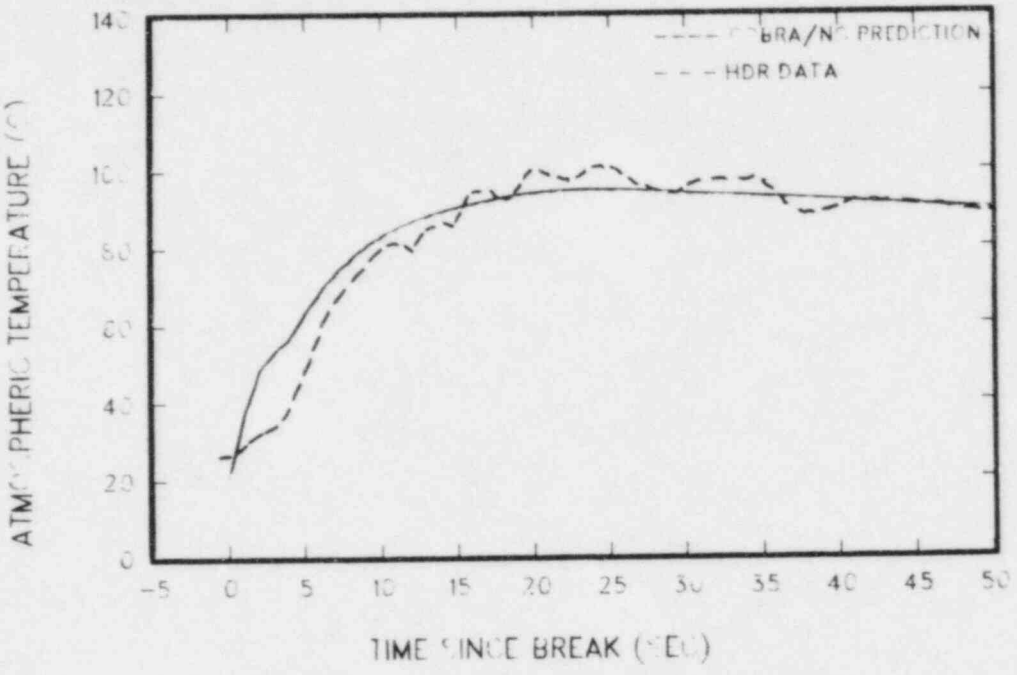

Figure 118 Temperature in room 11004 (0-50 sec)

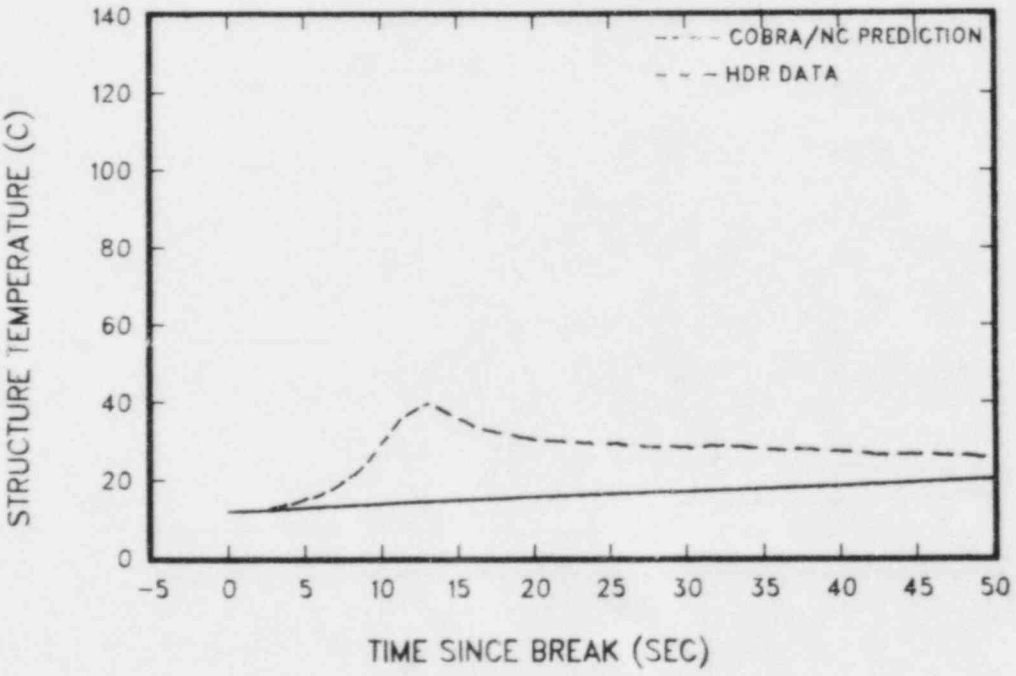

Figure 119 First thermocouple temperature in α block CQ3502 (room 1305)

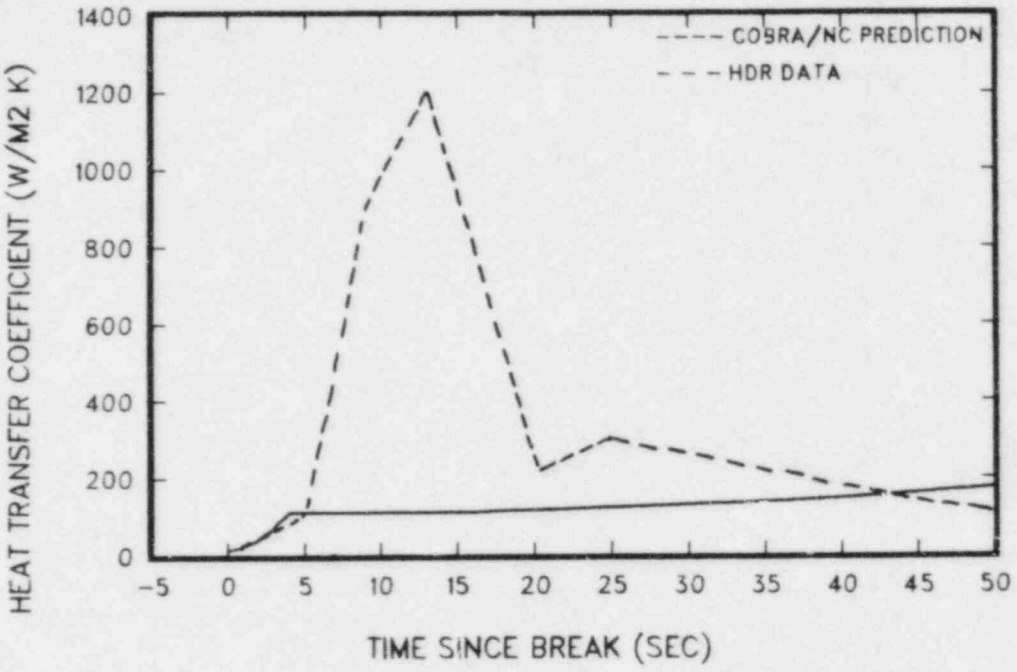

Figure 120 Heat transfer coefficient for α block CQ1035 (room 1305)

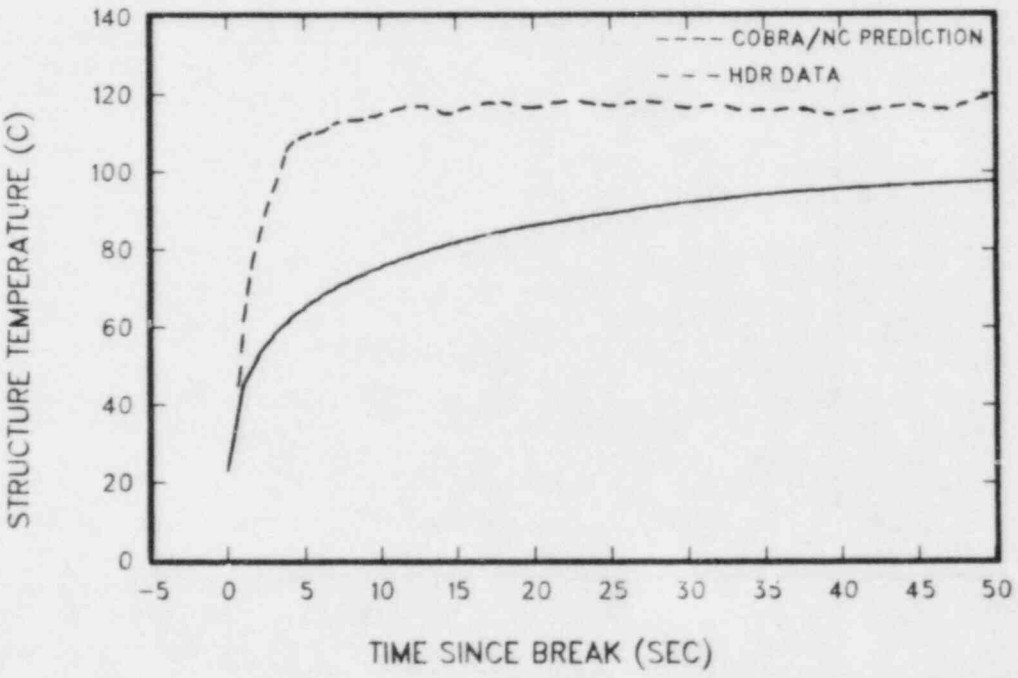

Figure 121 First thermocouple temperature in α block CQ6301 (room 1603)

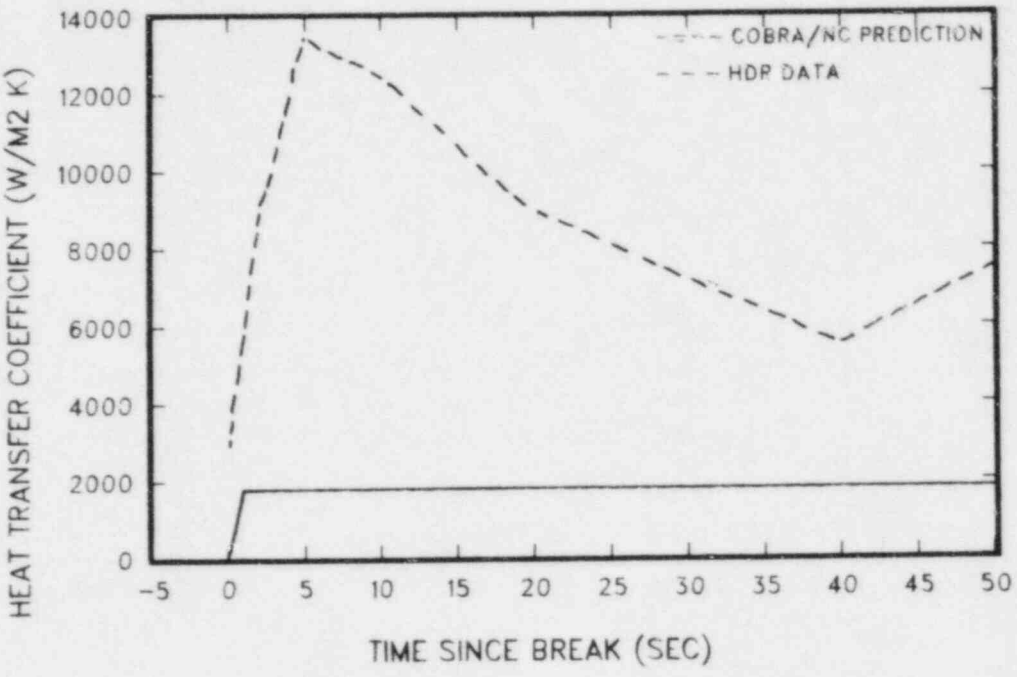

Figure 122 Heat transfer coefficient for α block CQ1263 (room 1603)

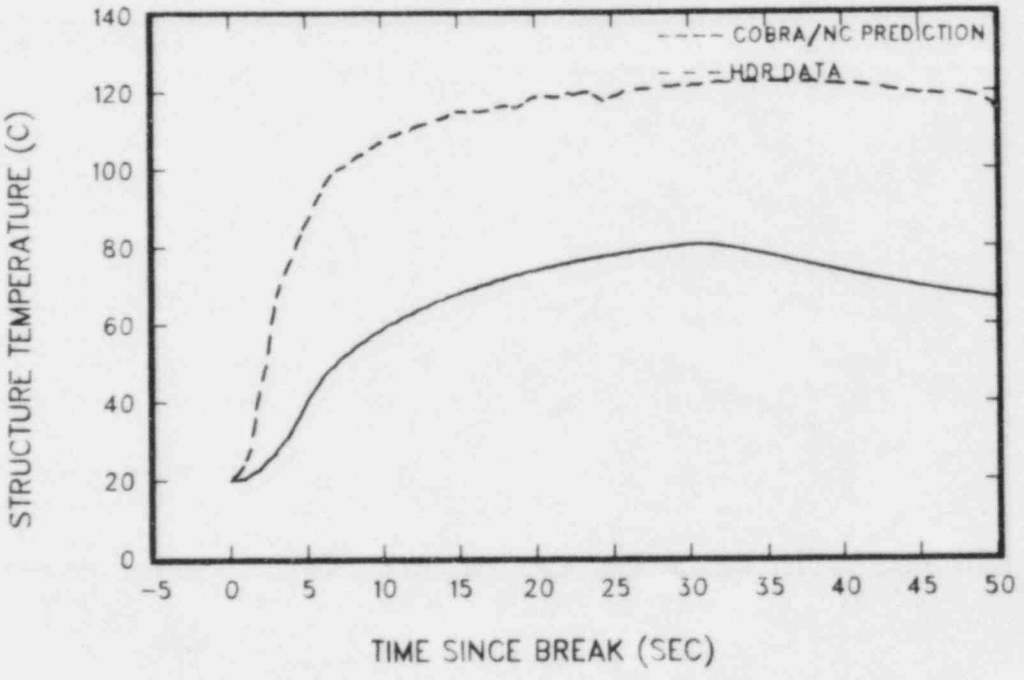

Figure 123 First thermocouple temperature for α block CQ6601 (room 1606)

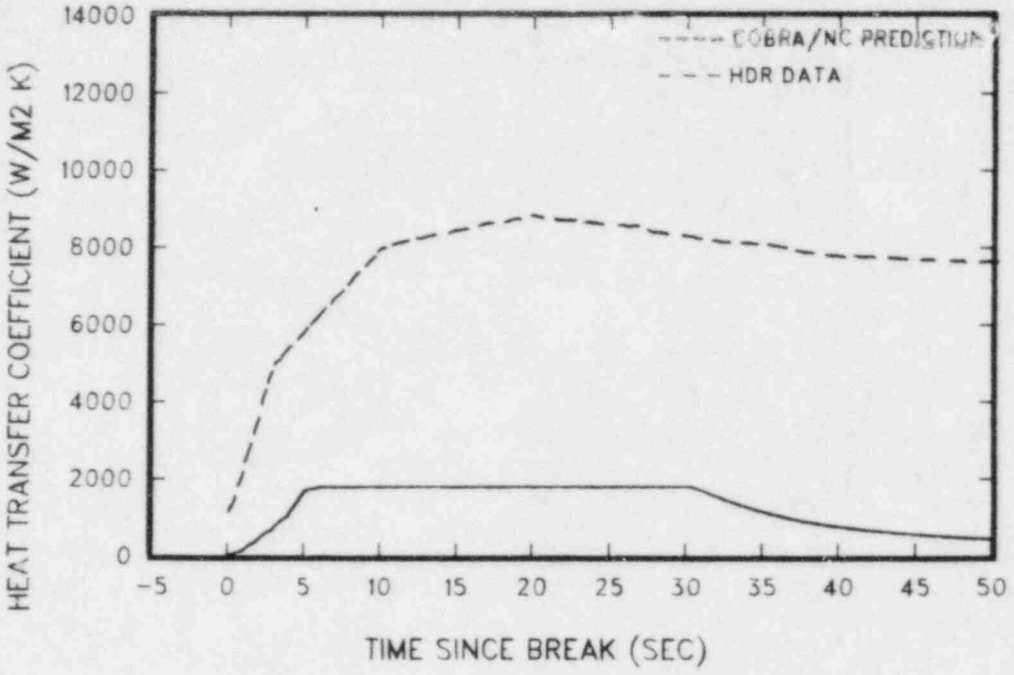

Figure 124 Heat transfer coefficient for α block CQ1266 (room 1606)

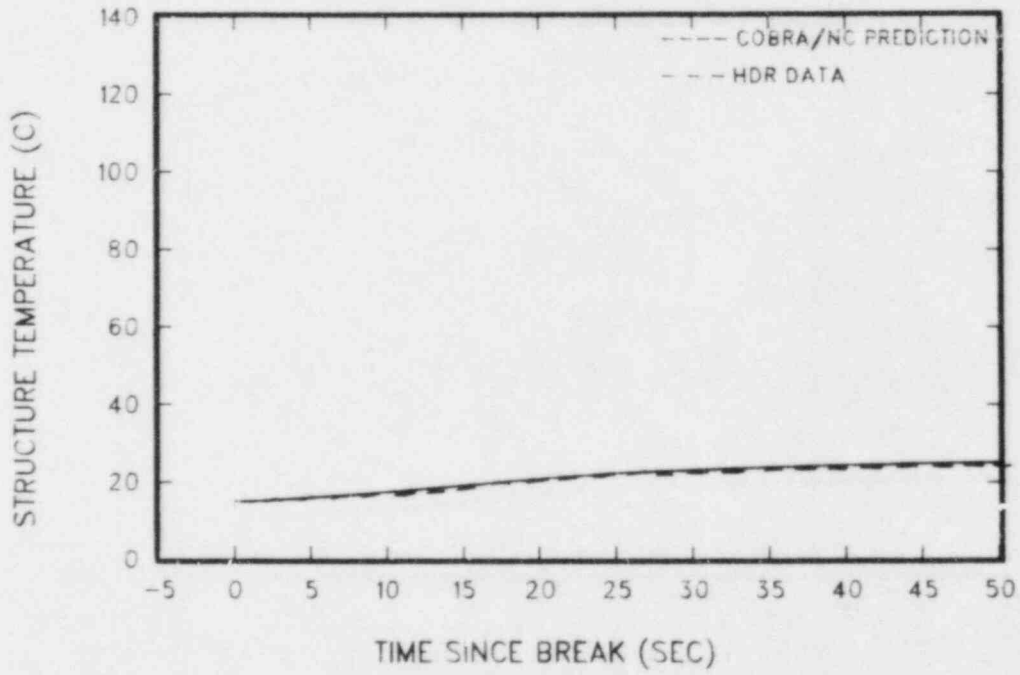

Figure 125 First thermocouple temperature in α block CQ402 (room 11004)

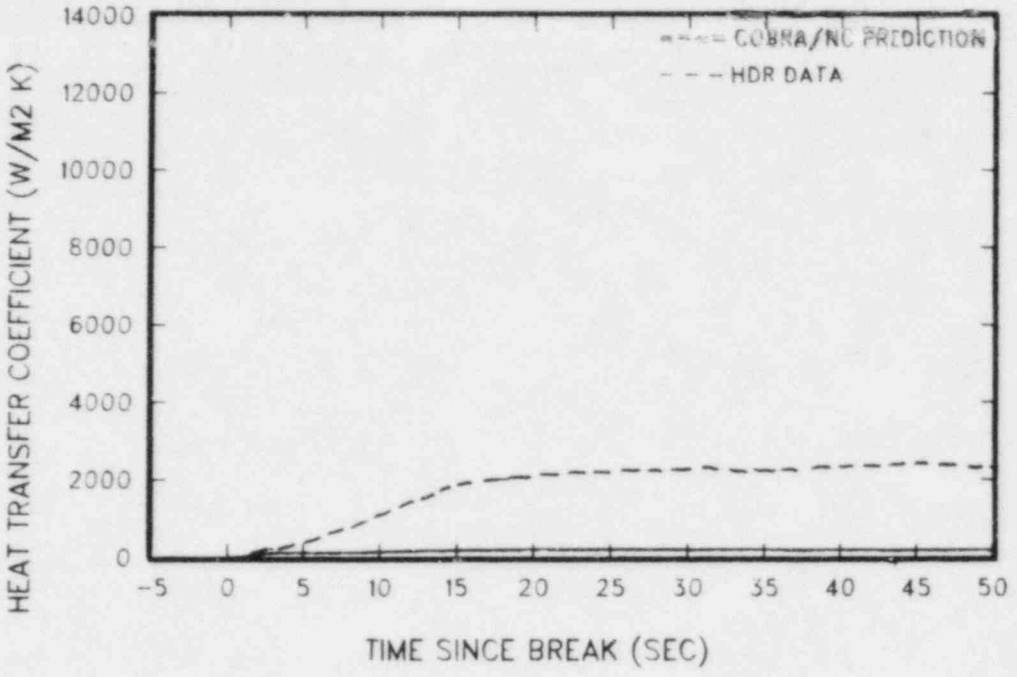

Figure 126 Heat transfer coefficient for α block CQ1104 (room 11004)

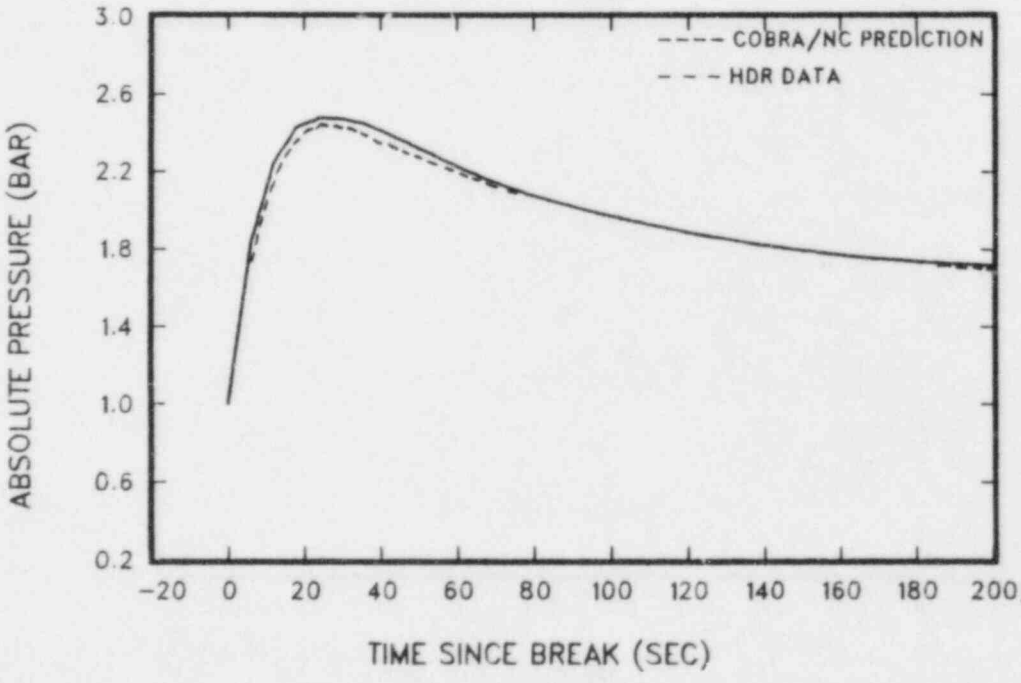

Figure 127 Absolute pressure in room J04 (0-200 sec)

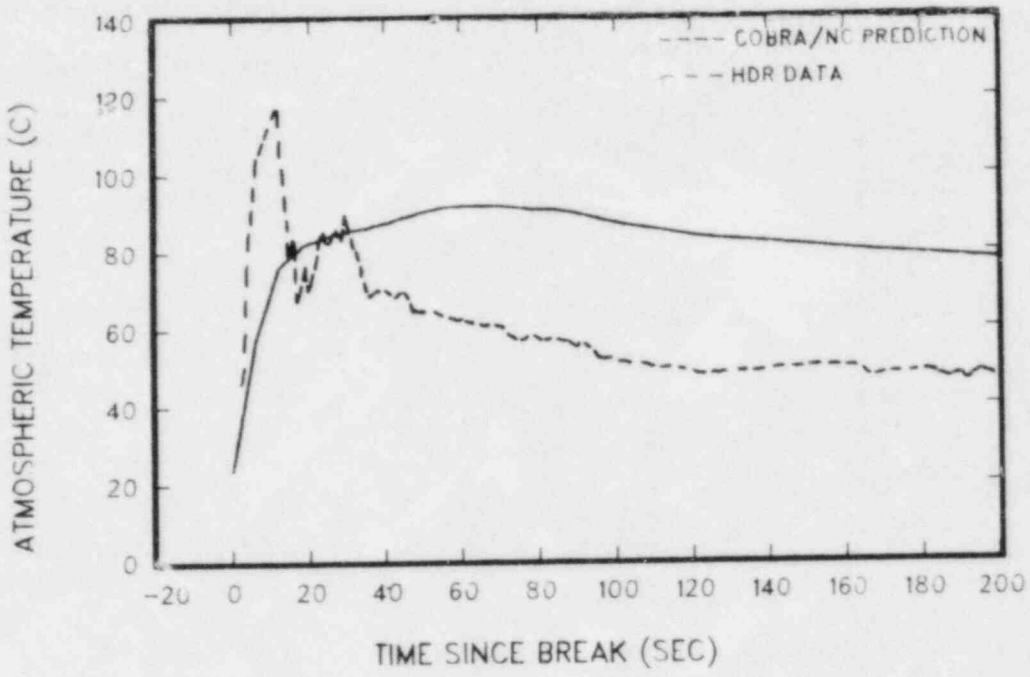

Figure 128 Temperature in room 1305(0-200 sec)

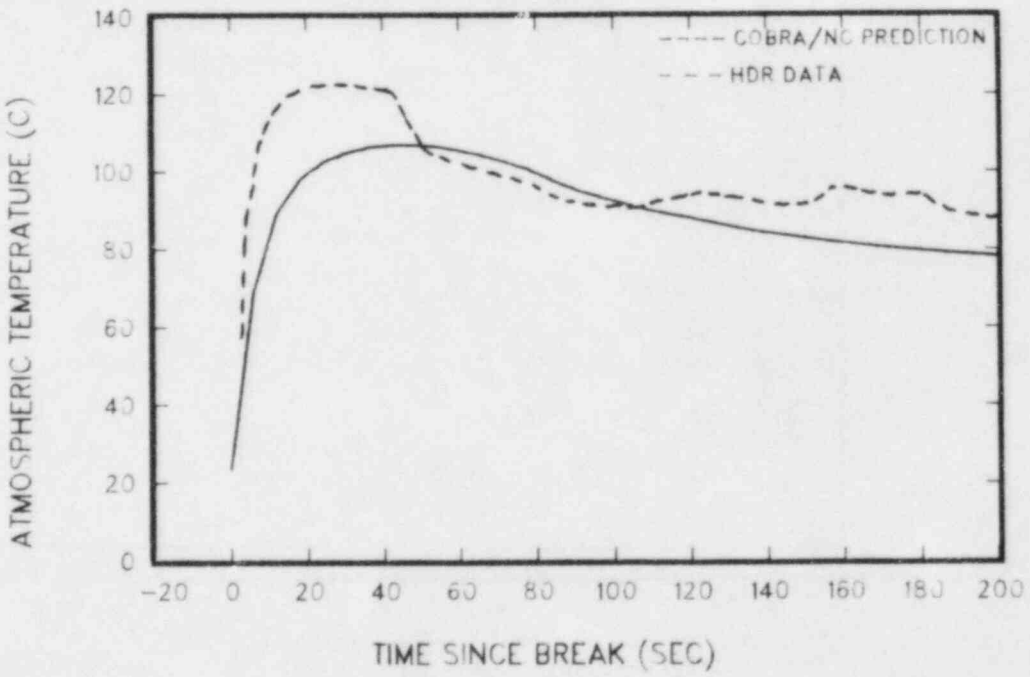

Figure 129 Temperature in room 1307 (0-200 sec)

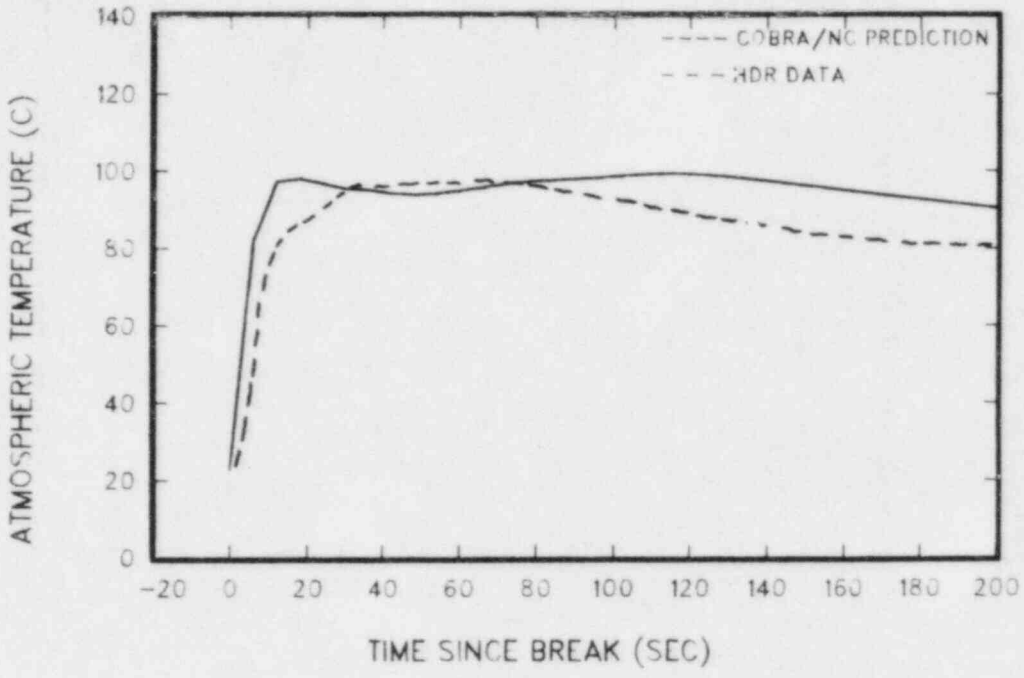

Figure 130 Temperature in room 1511 (0-200 sec)

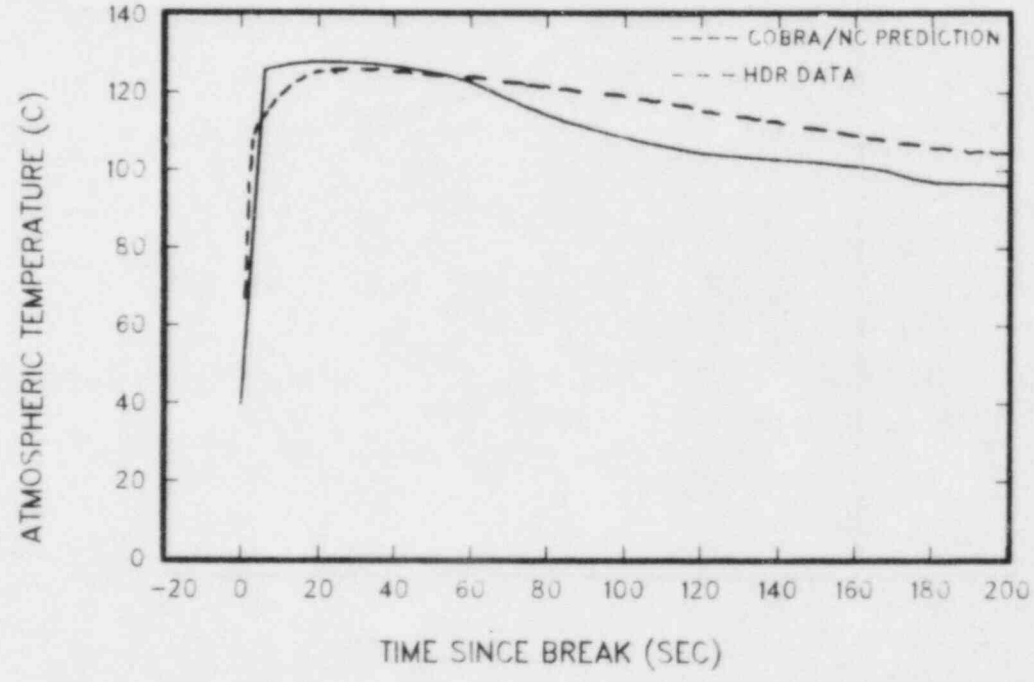

Figure 131 Temperature in room 1603 (0-200 sec)

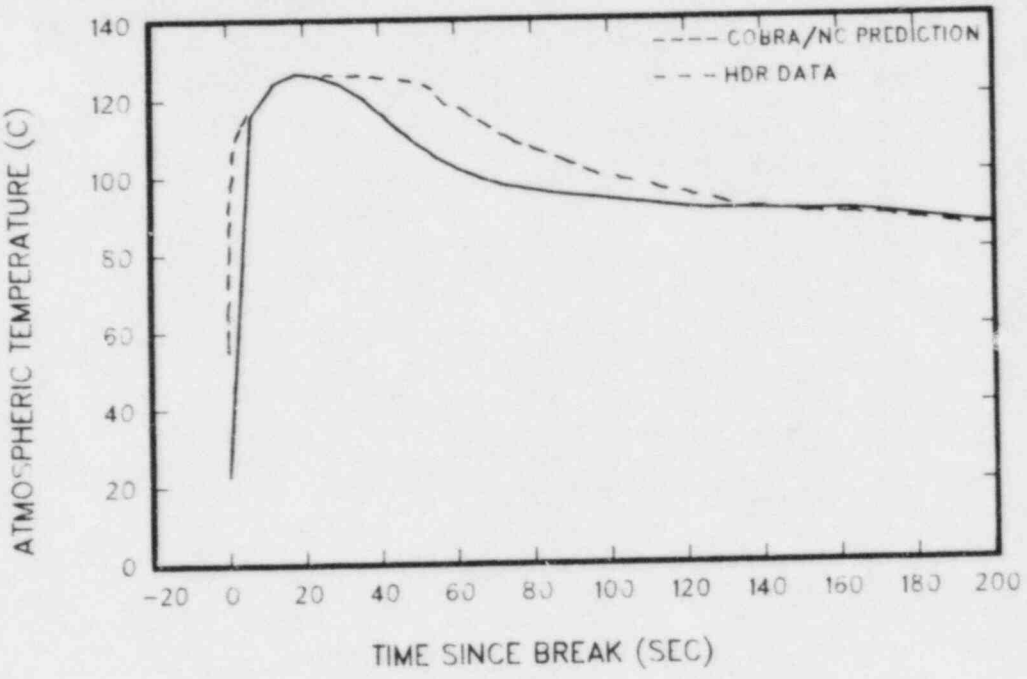

Figure 132 Temperature in room 1606 (0-200 sec)

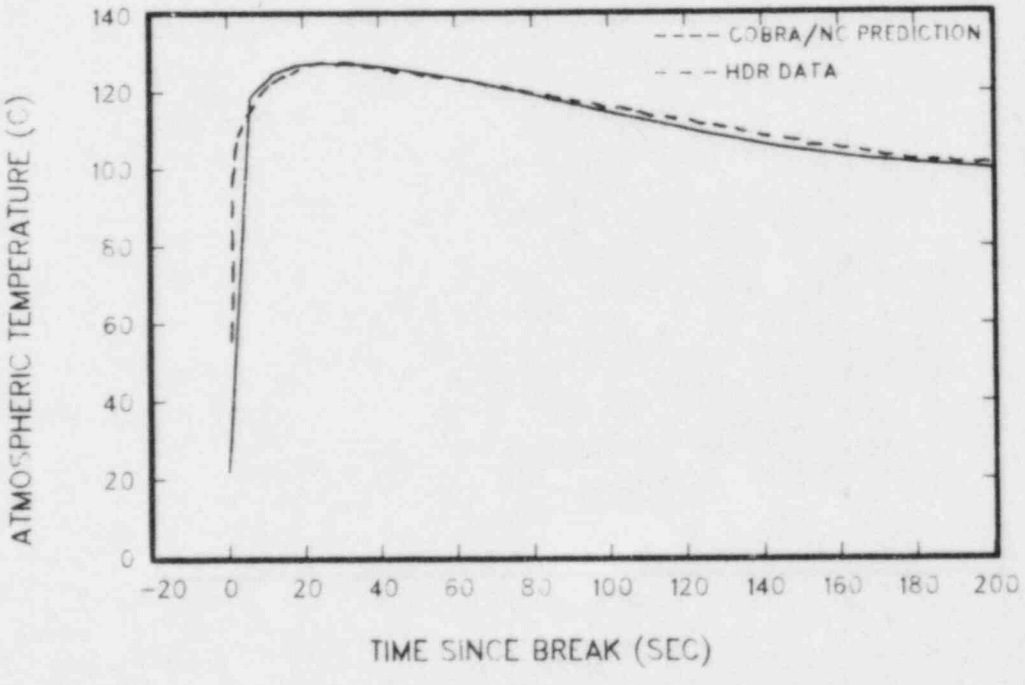

Figure 133 Temperature in room 1704 (0-200 sec)

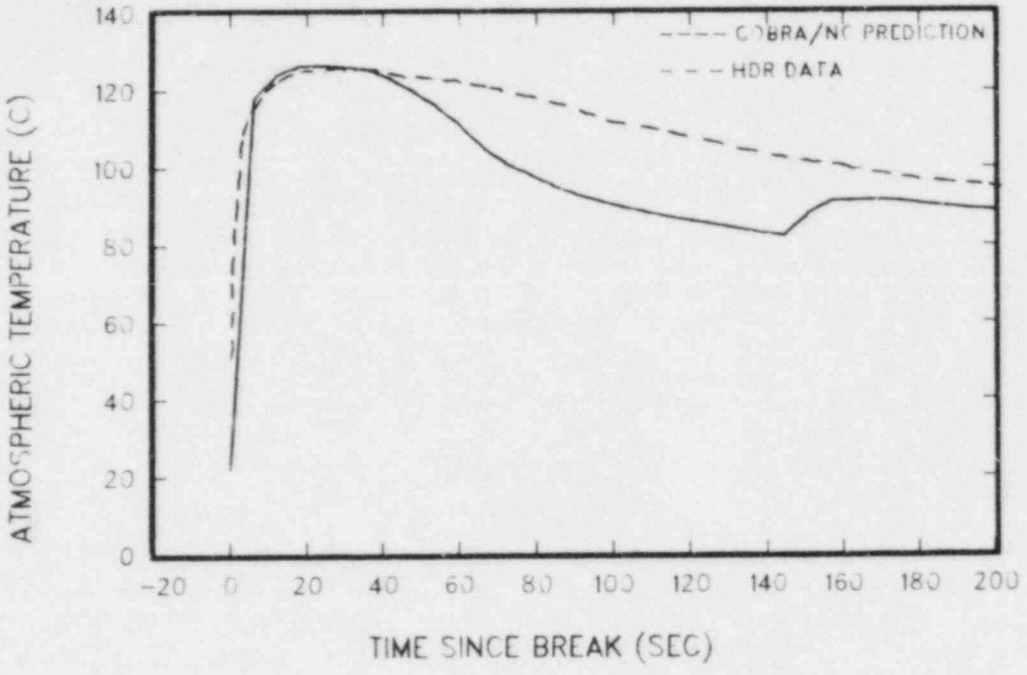

Figure 134 Temperature in room 1804 (0-200 sec)

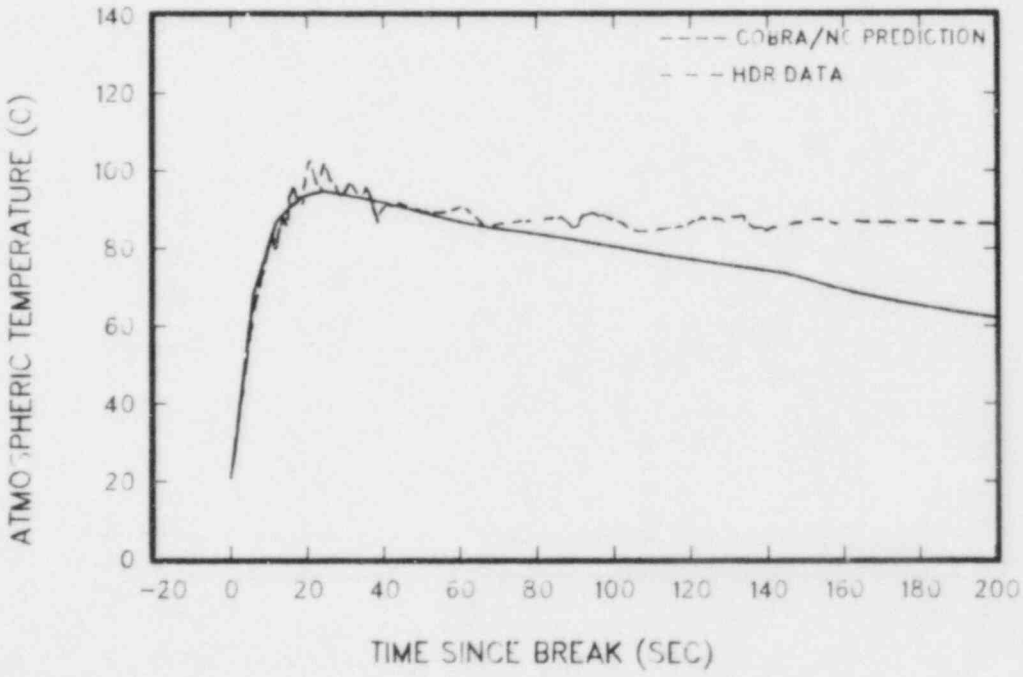

Figure 135 Temperature in room 11004(0-200 sec)

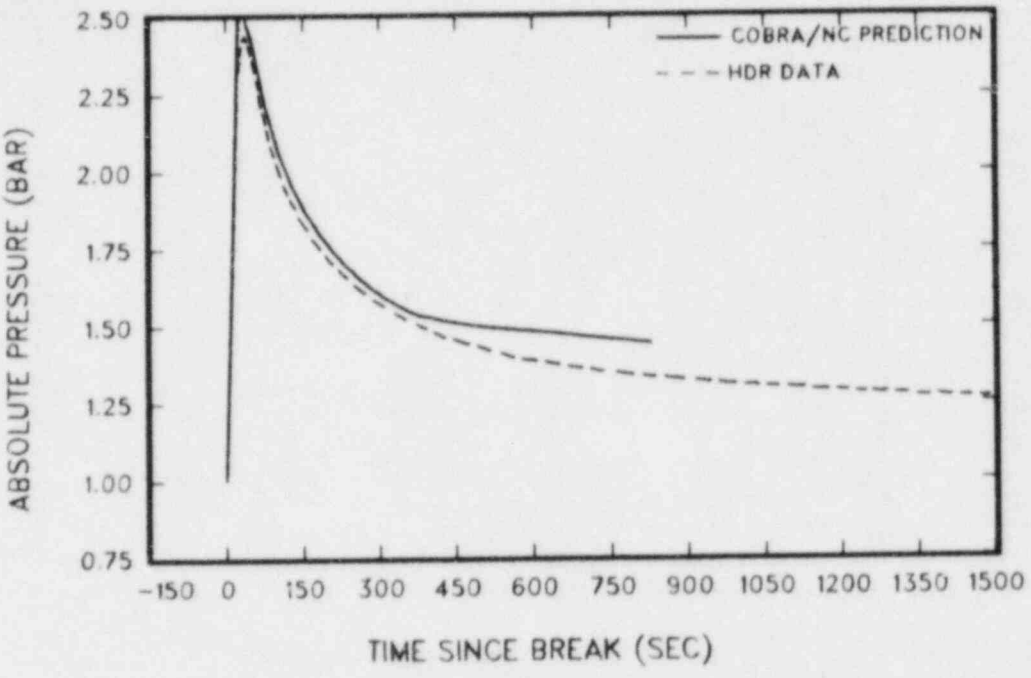

Figure 136 Absolute pressure in room 11004(0-1500 sec)

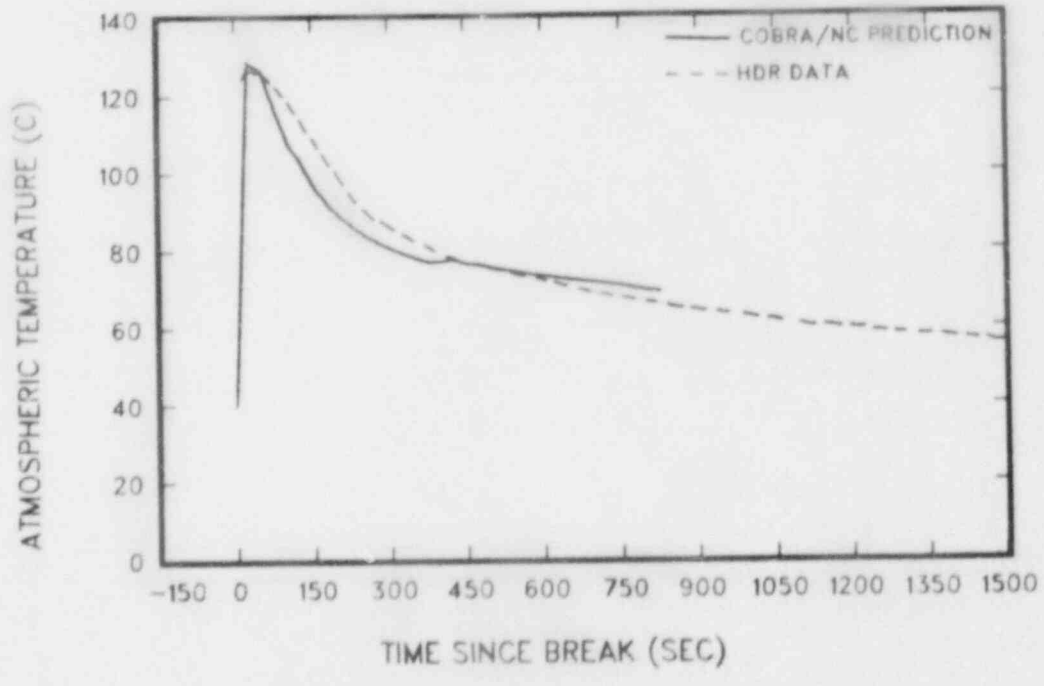

Figure 137 Temperature in Room 1603 (0-1500 sec)

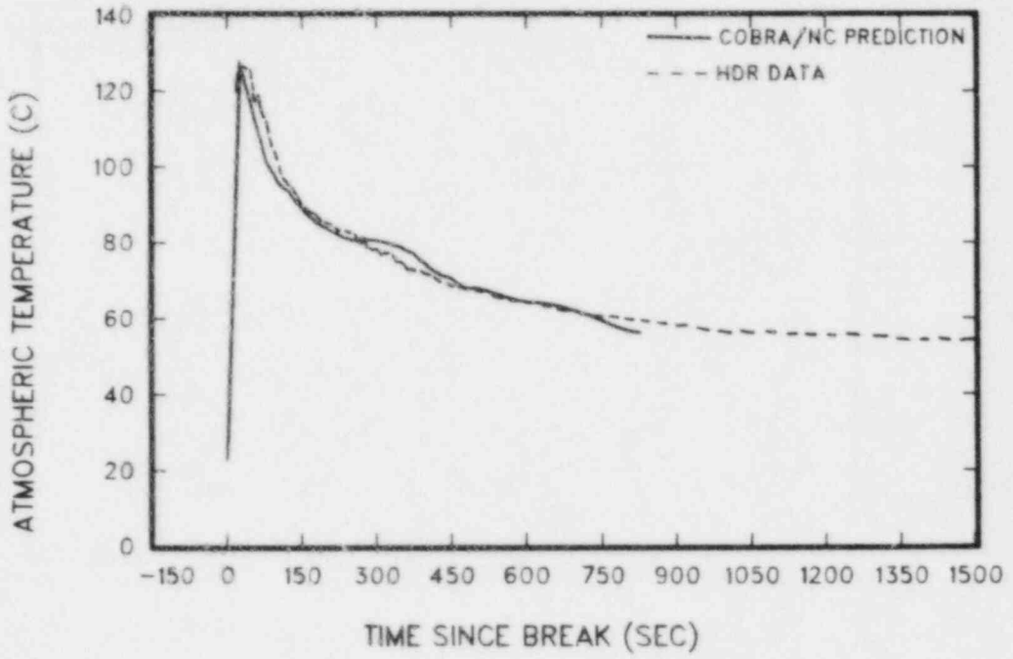

Figure 138 Temperature in room 1606 (0-1500 sec)

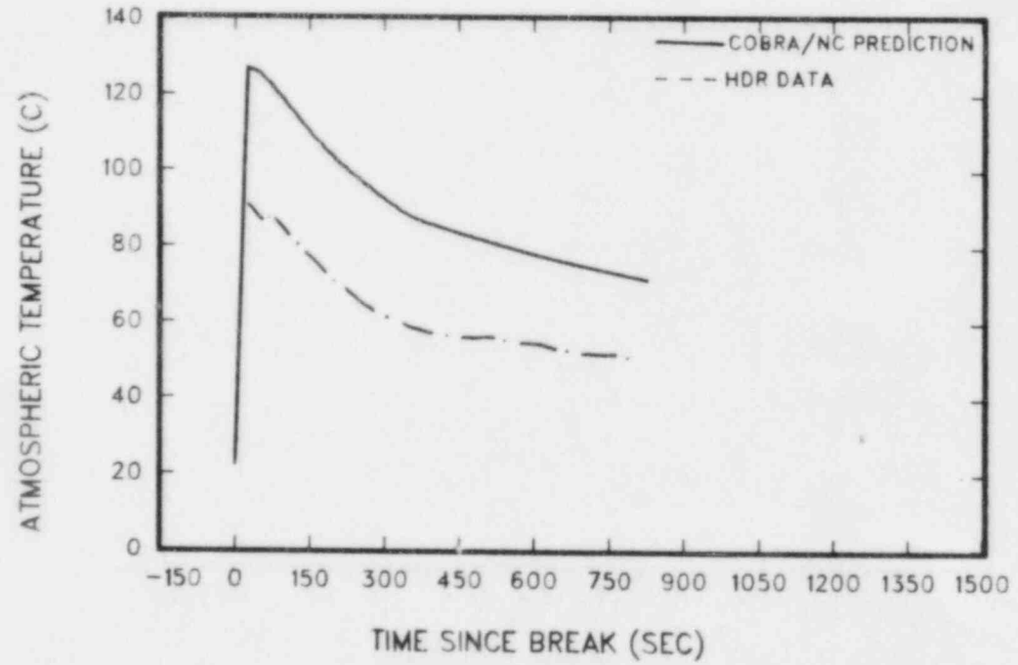

Figure 139 Temperature in room 1704 (0-1500 sec)

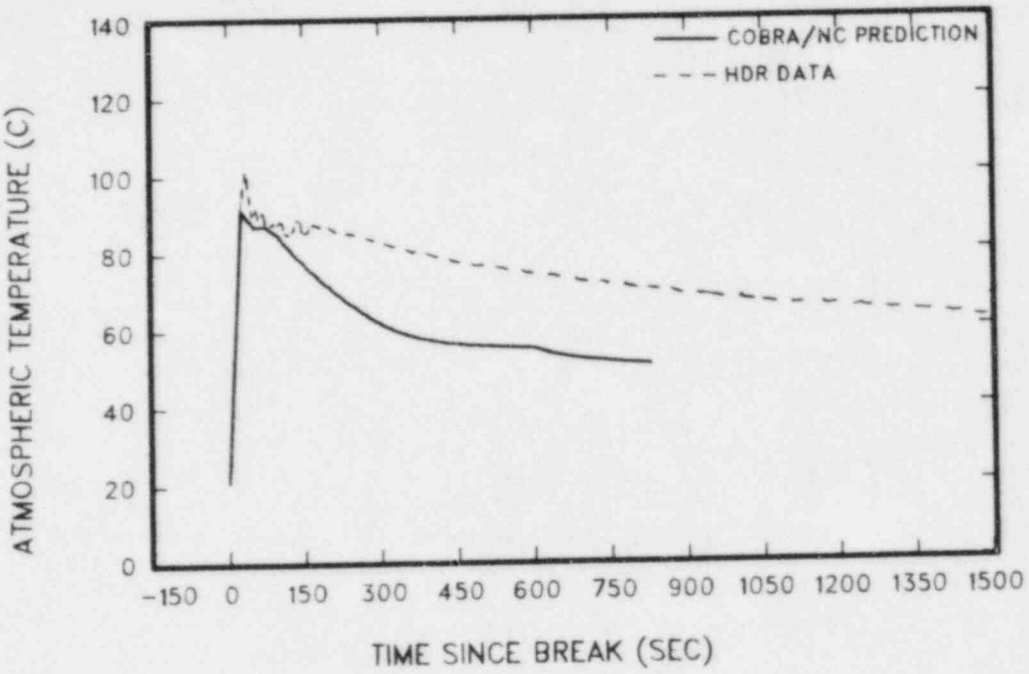

Figure 140 Temperature in room 11004

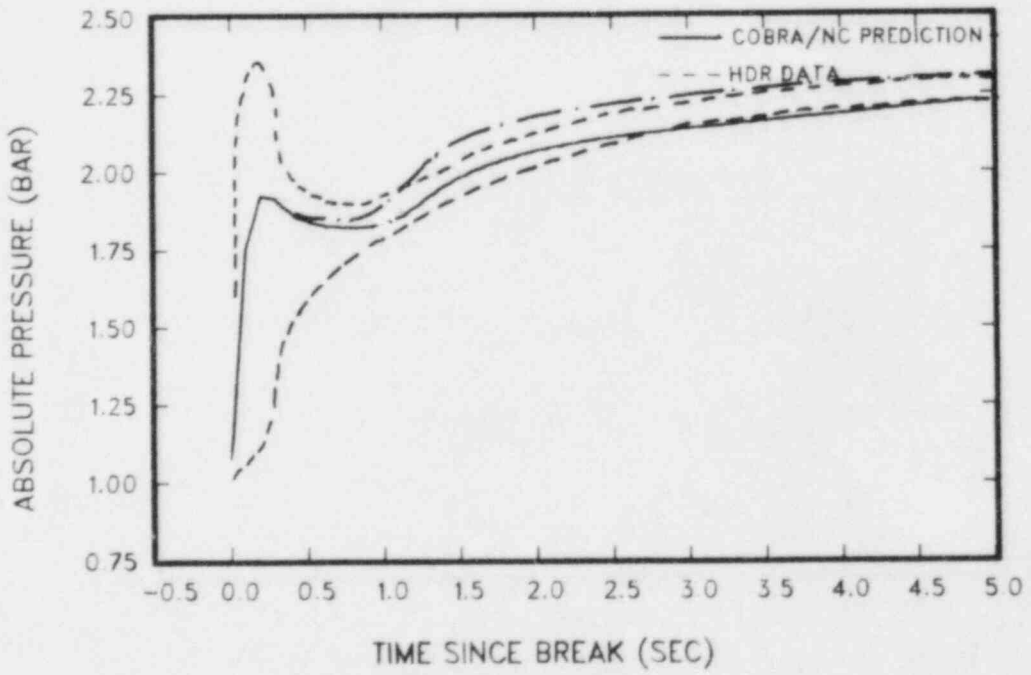

Figure 141 Absolute pressure in room 1603 (2000μm drops)

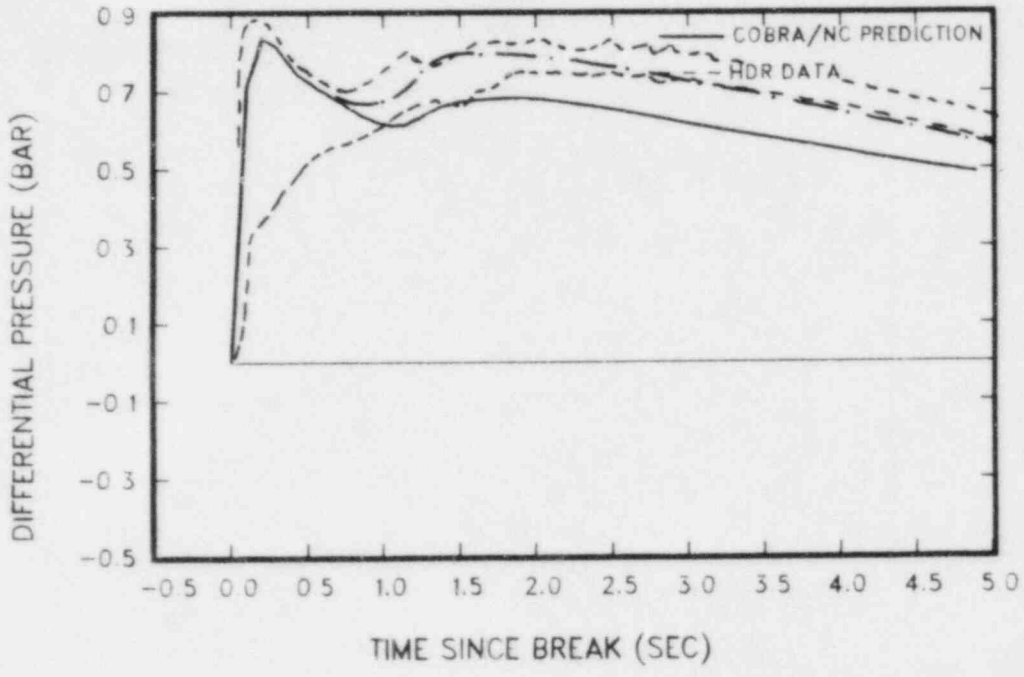

Figure 142 Differential pressure between rooms 1603 and 1708 (2000μm drops)

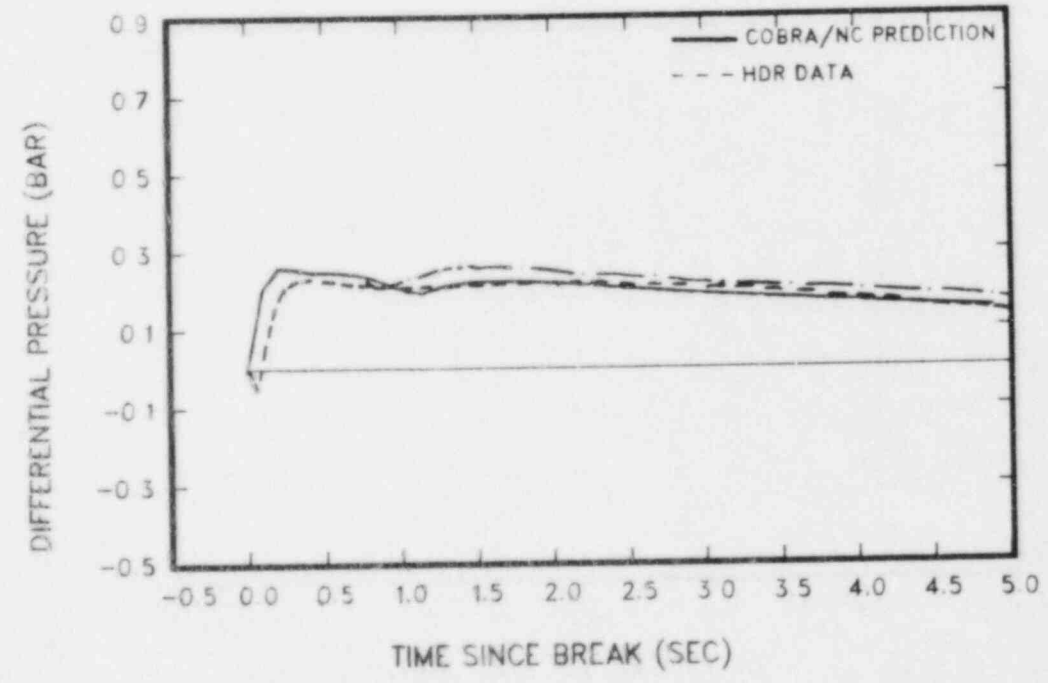

Figure 143 Differential pressure between rooms 1605 and 1701u (2000μm drops)

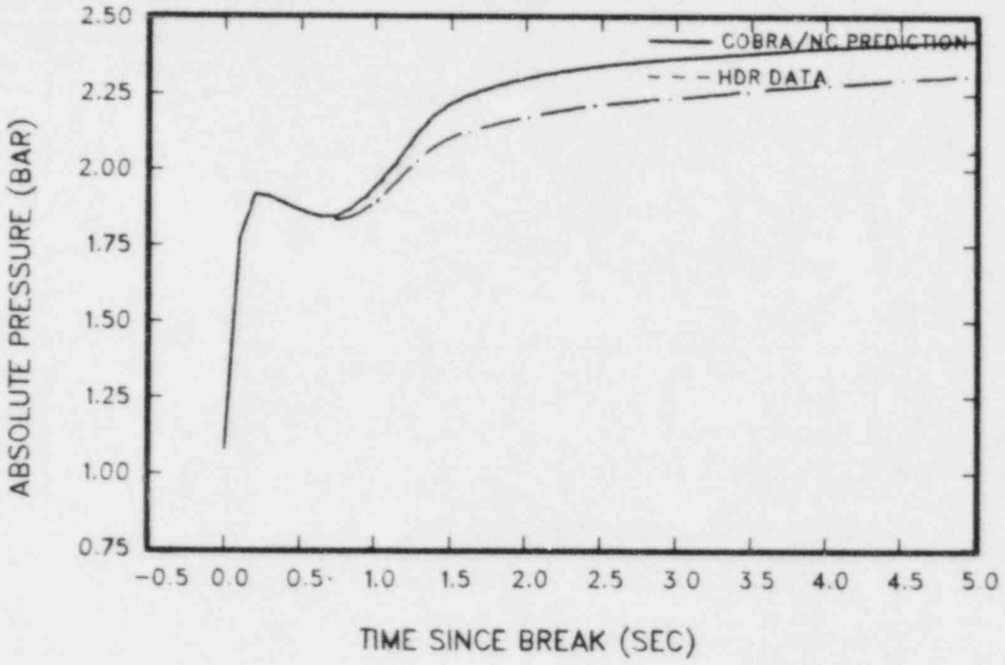

Figure 144 Absolute pressure in room 1603 2μm drops)

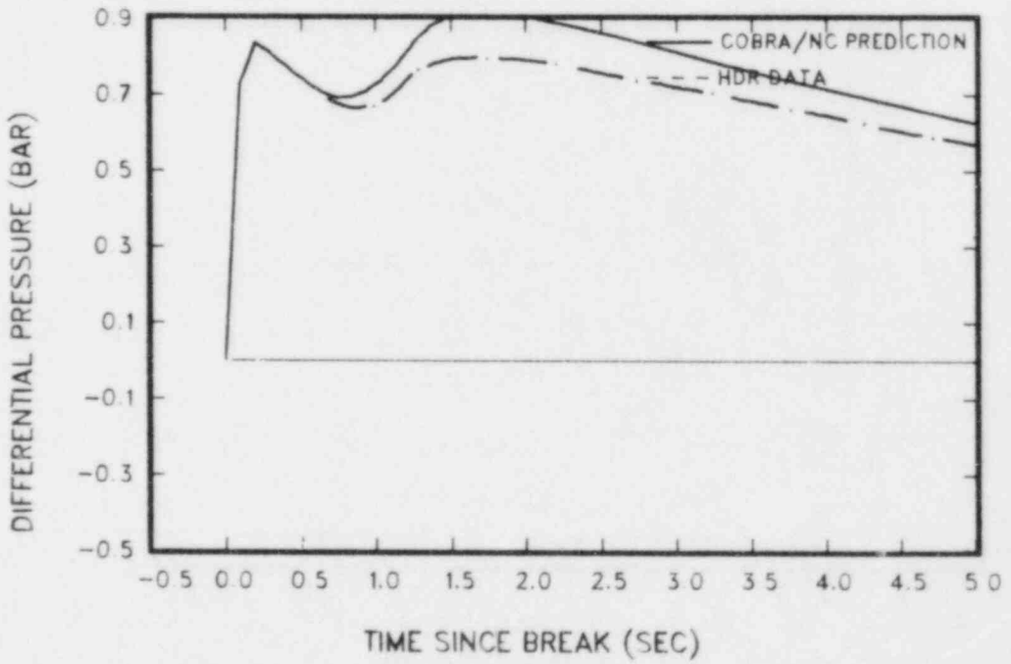

Figure 145 Differential pressure between rooms 1603 and 1708 (2μm drops)

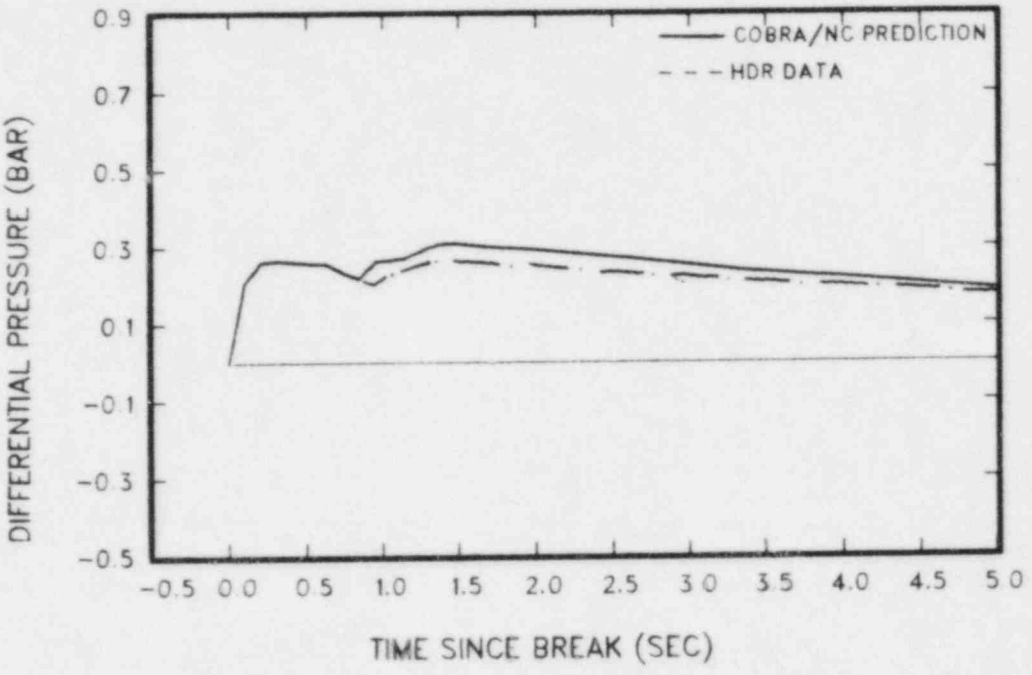

Figure 146 Differential pressure between room 1605 and 1701u (2μm drops)

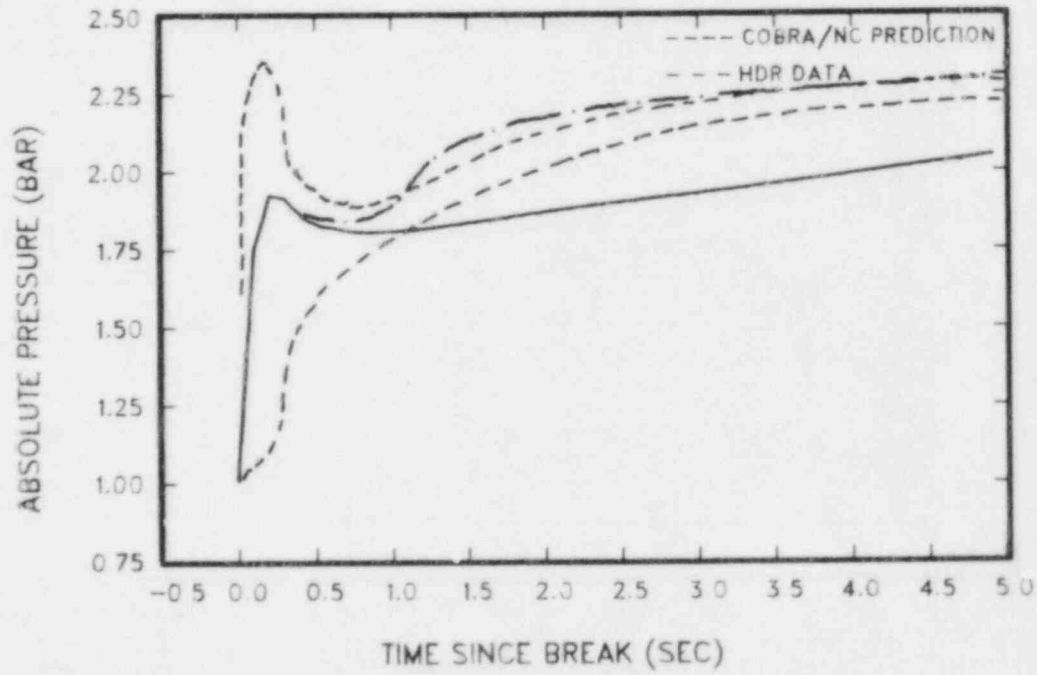

Figure 147 Absolute pressure in room 1603 (no drop carryover)

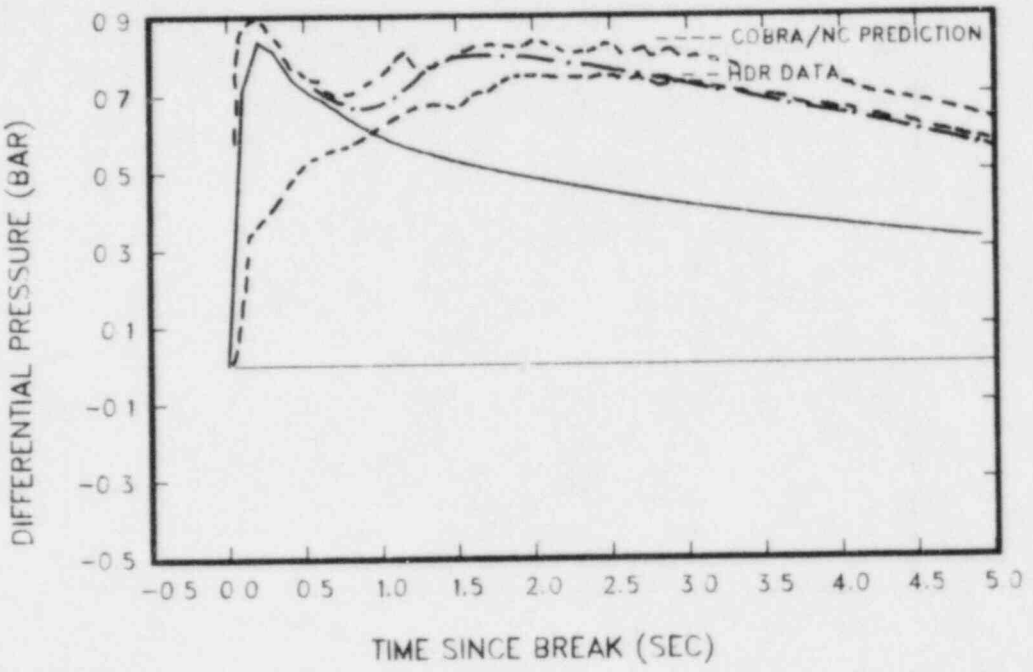

Figure 148 Differential pressure between rooms 1603 and 1708 (no drop carryover)

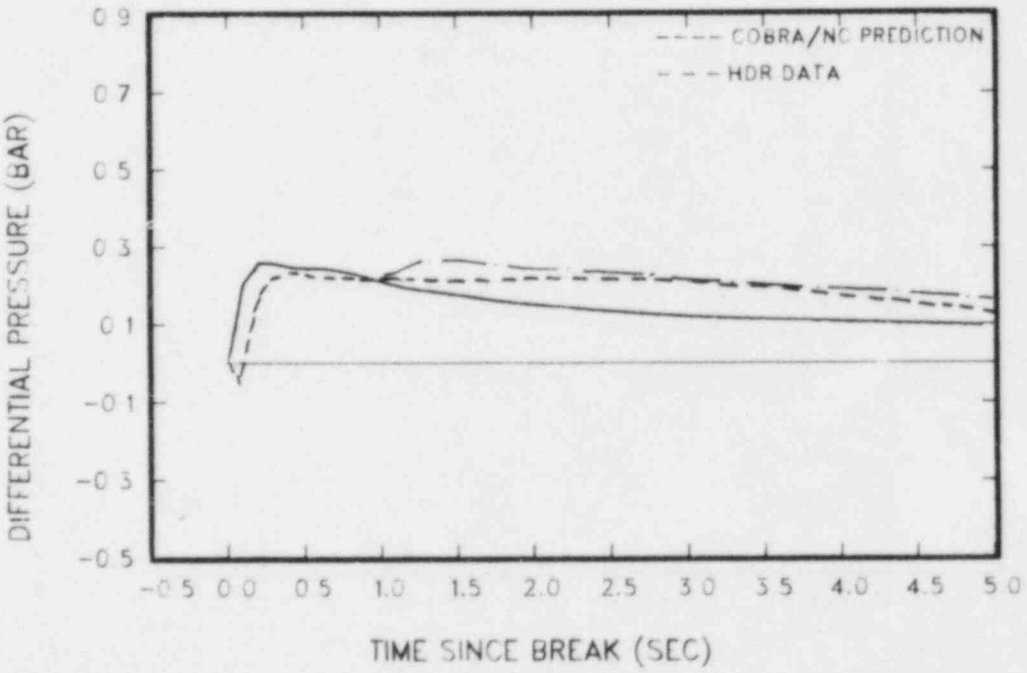

Figure 149 Differential pressure between rooms 1605 and 1701u (no drop carryover)

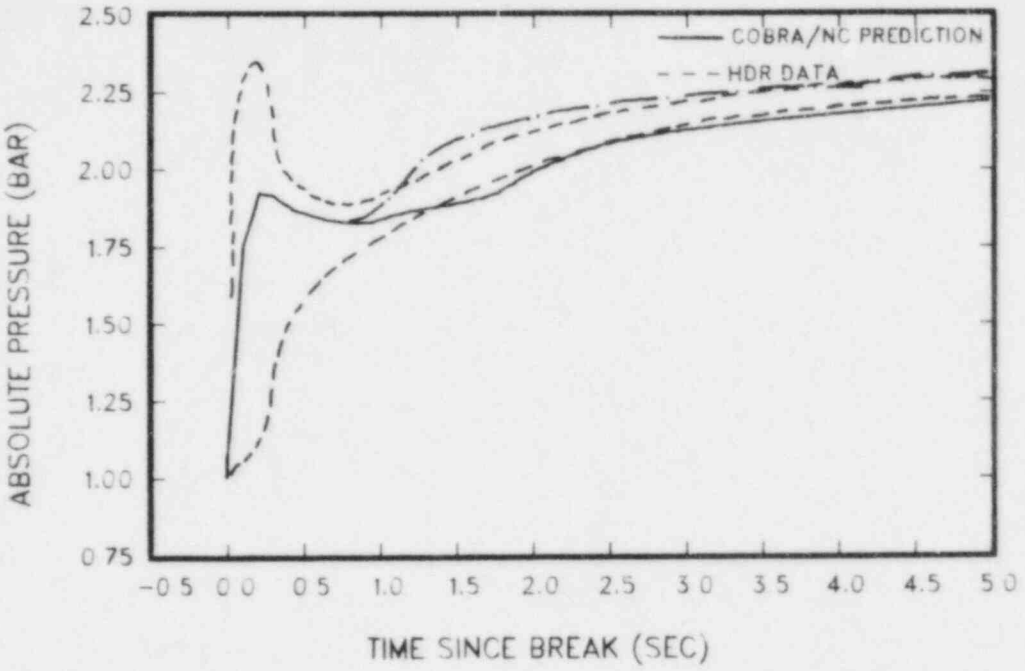

Figure 150 Absolute pressure in room 1603 (drop deposition)

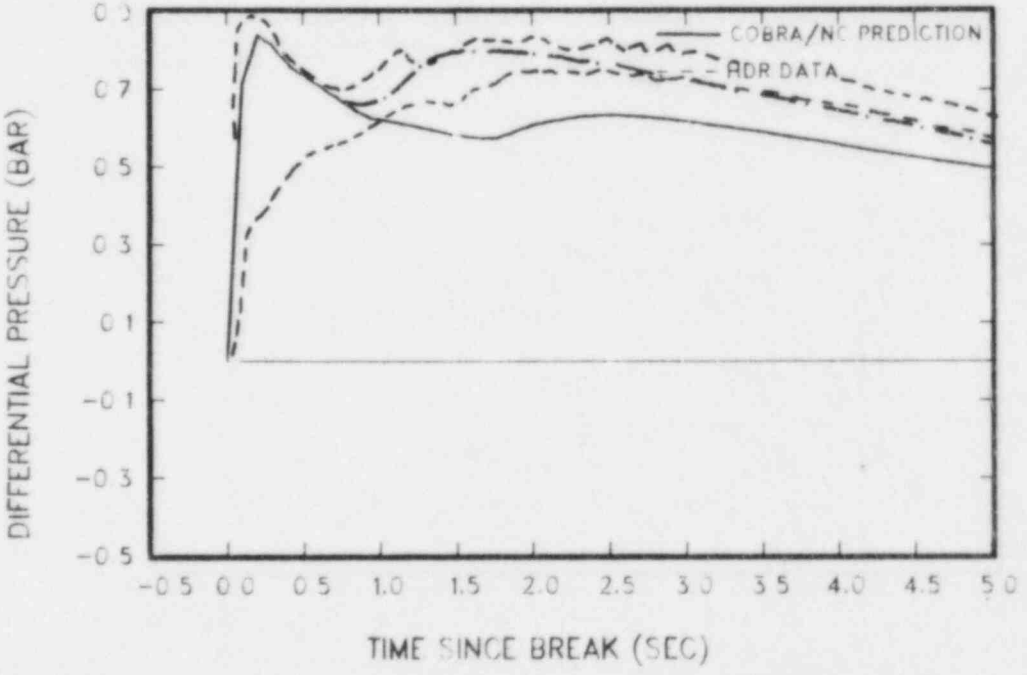

Figure 151 Differential pressure between rooms 1603 and 1708 (drop deposition)

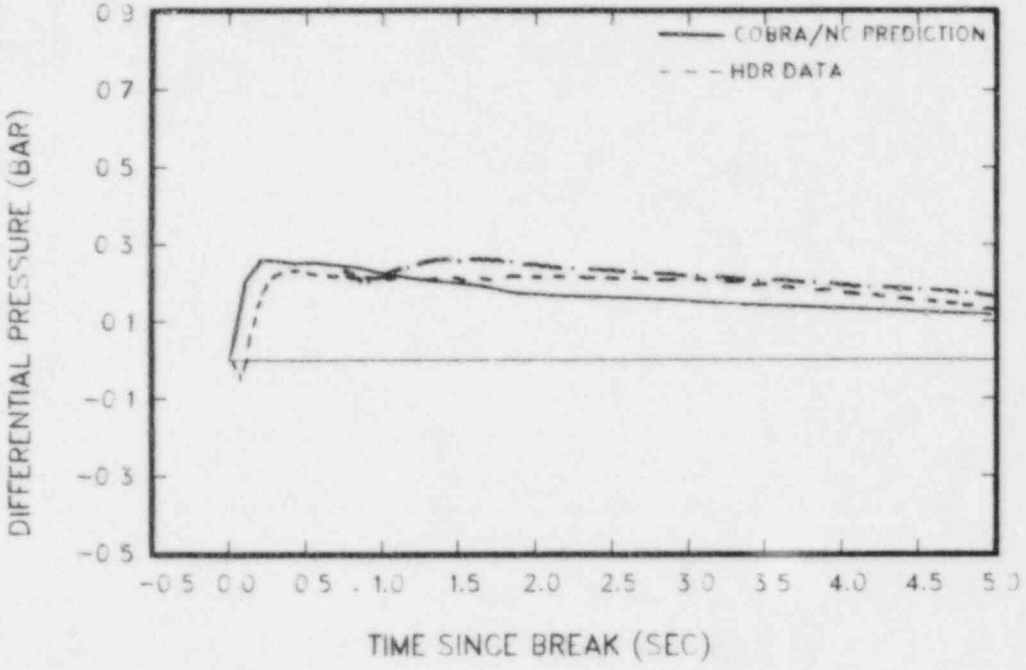

Figure 152 Differential pressure between rooms 1605 and 1701u (drop deposition)

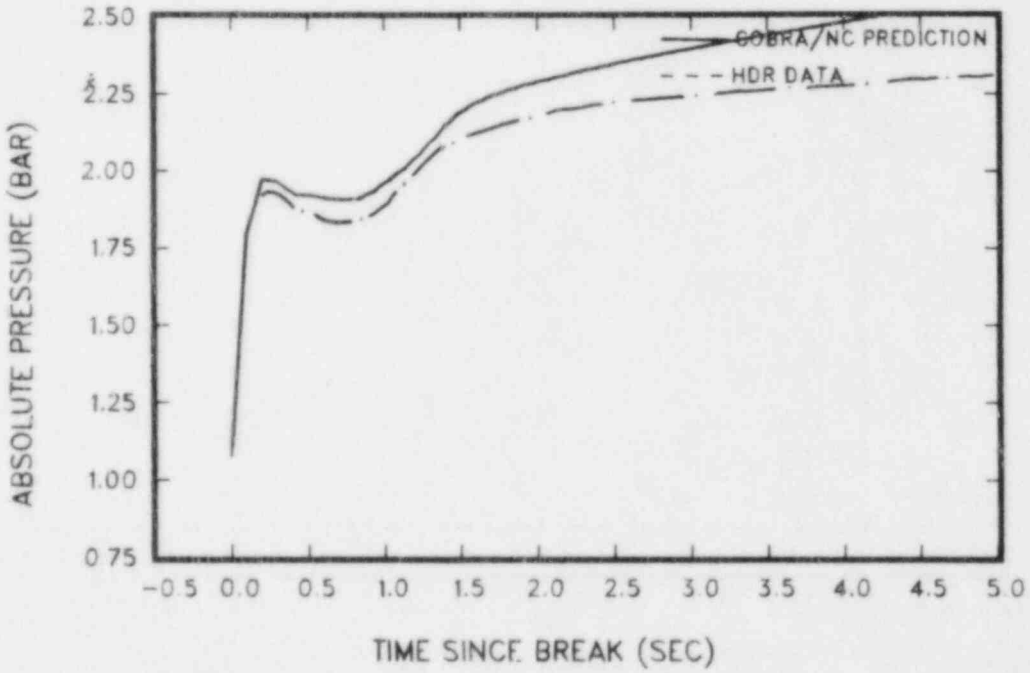

Figure 153 Absolute pressure in room 1603 (no condensation)

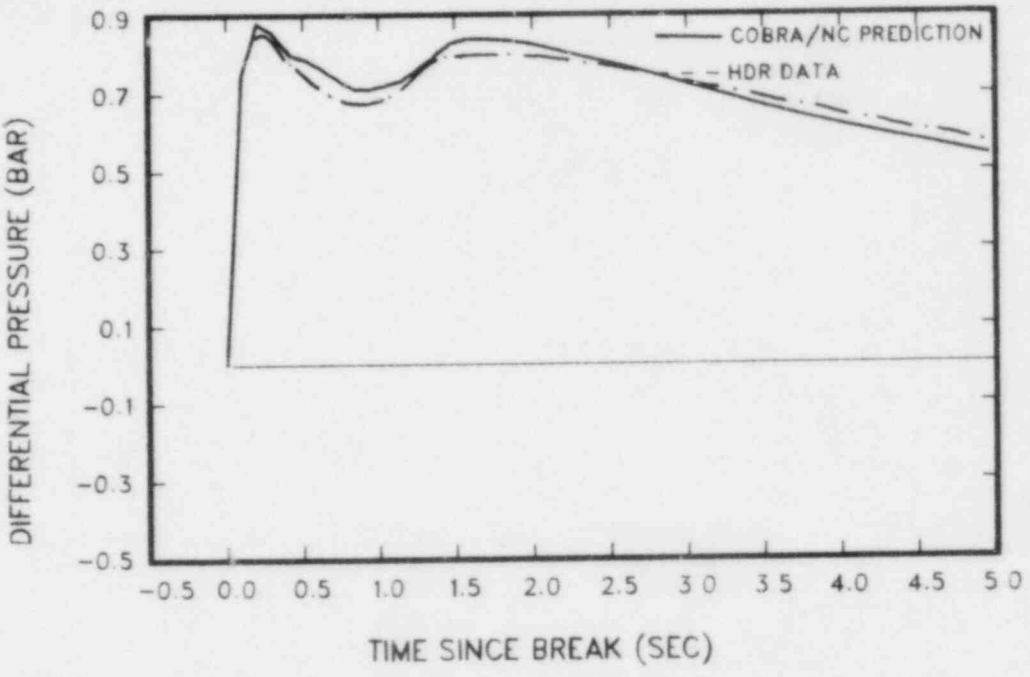

Figure 154 Differential pressure between rooms 1603 and 1708 (no condensation)

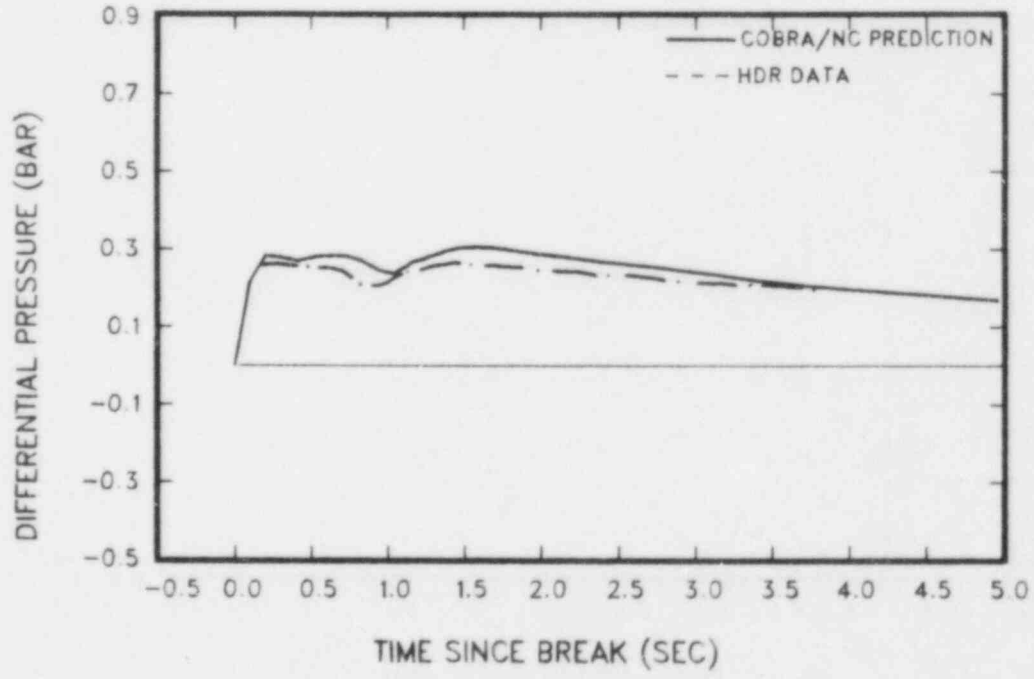

Figure 155 Differential pressure between rooms 1605 and 1701u (no condensation)

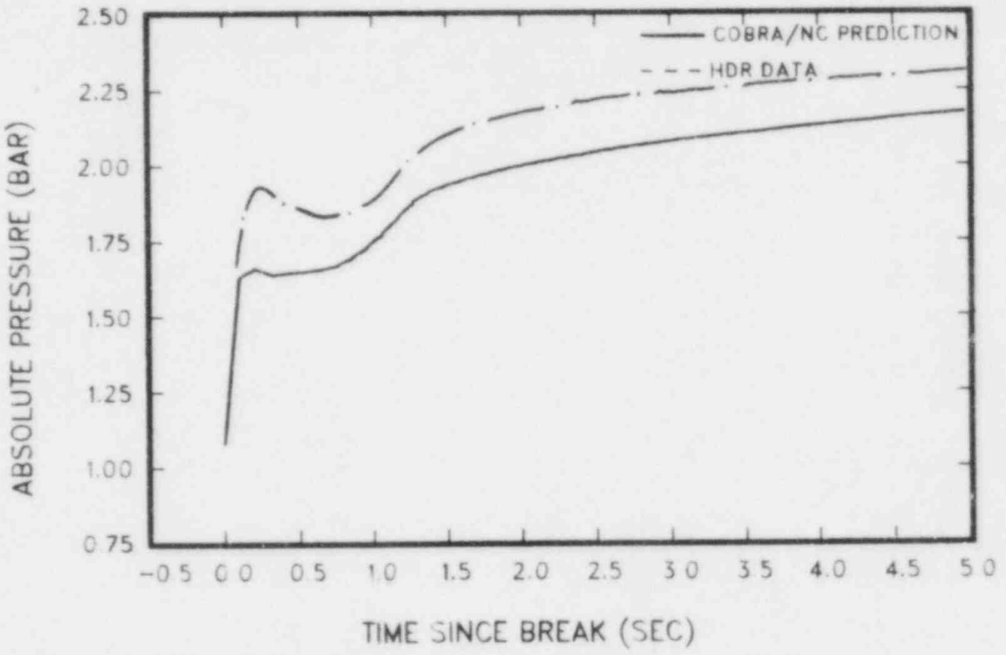

Figure 156 Absolute pressure in room 1603 (100% carryover, 2μm drops, and GRS values for vent loss coefficients)

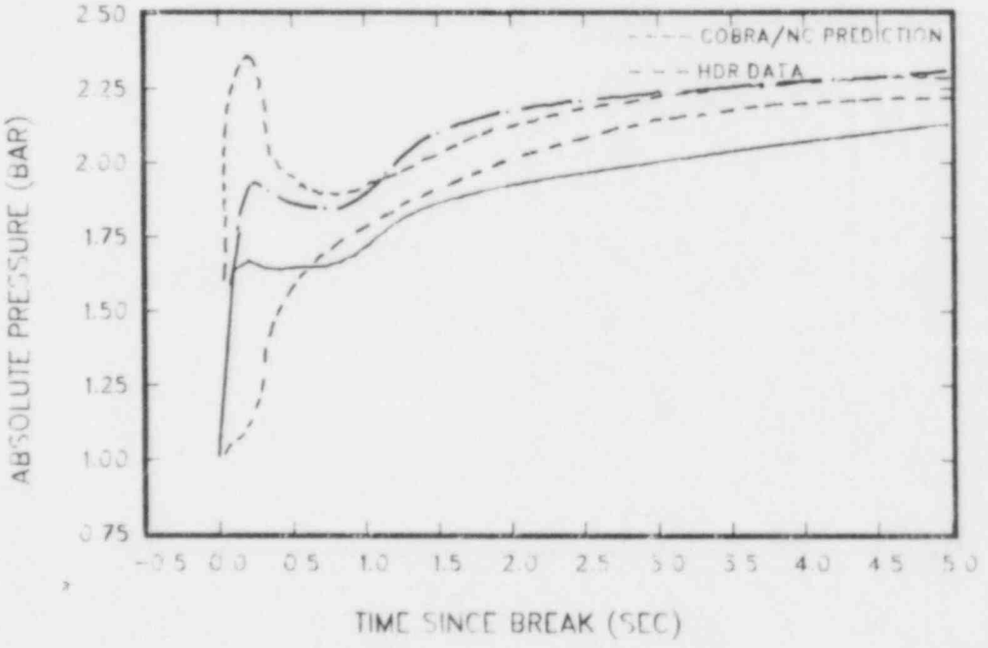

Figure 157 Absolute pressure in room 1603 (GRS loss coefficient)

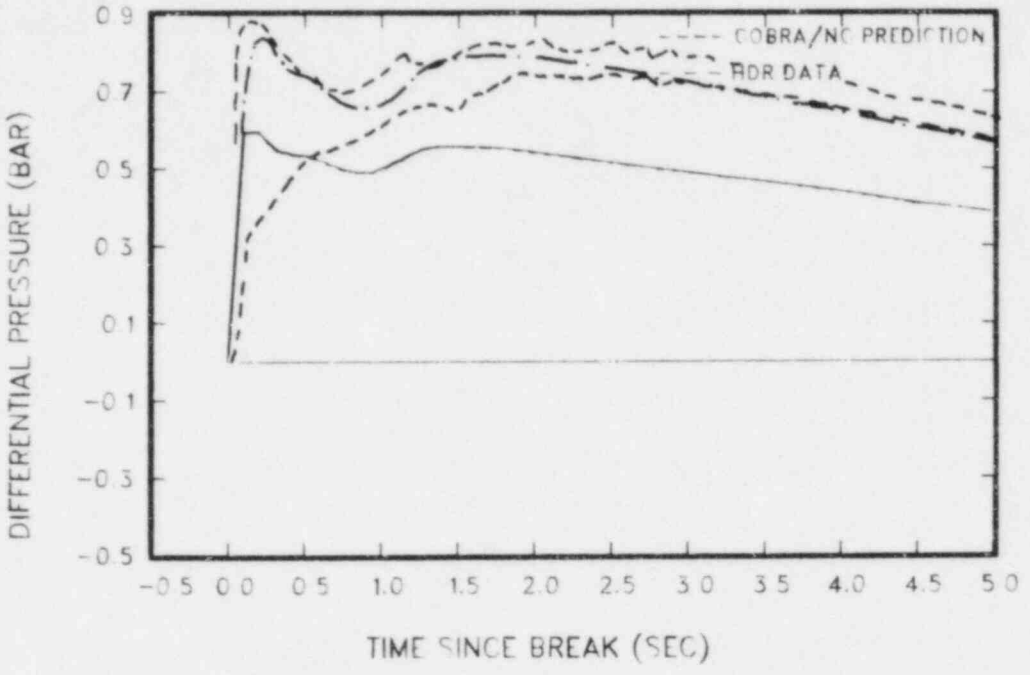

Figure 158 Differential pressure between rooms 1603 and 1708 (GRS loss coefficient)

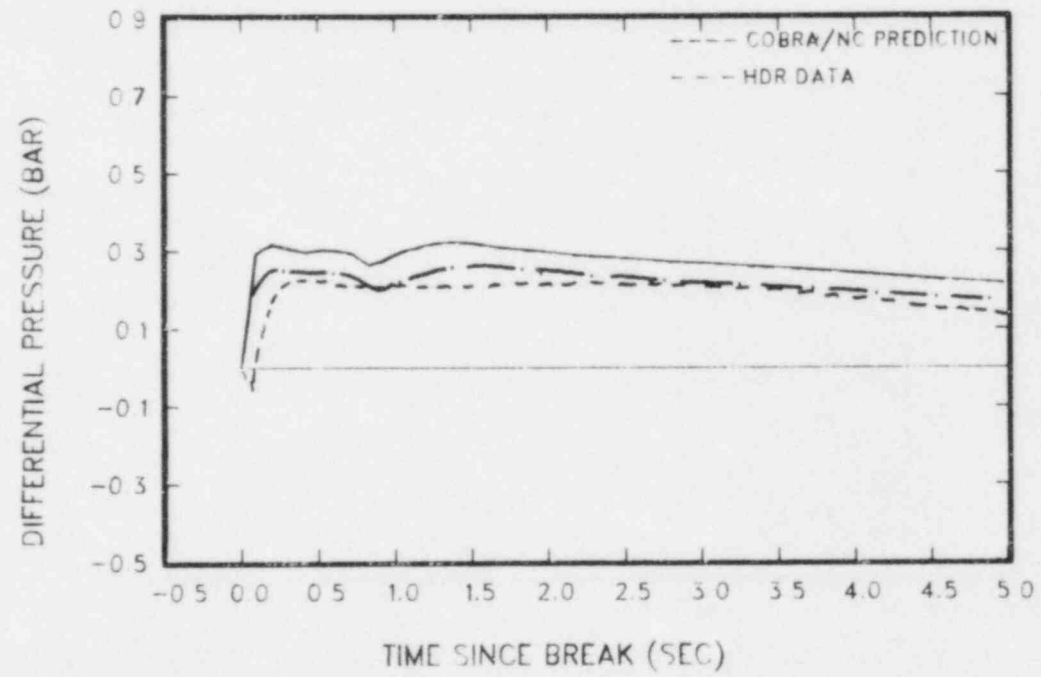

Figure 159 Differential pressure between rooms 1605 and 1701u (GRS loss coefficients)

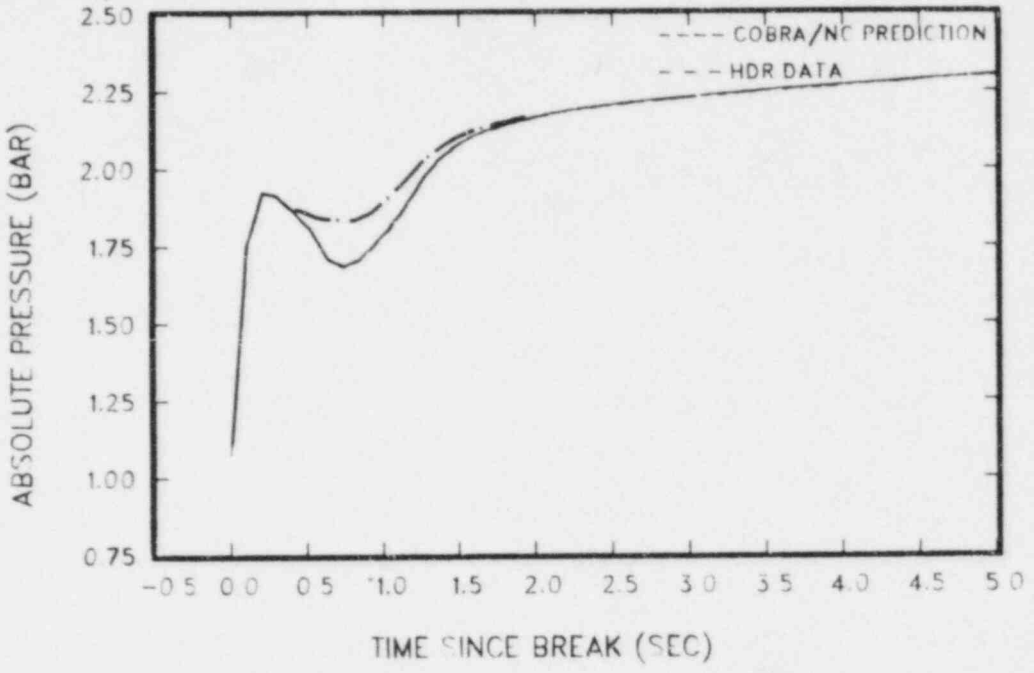

Figure 160 Effect of boundary condition change on the absolute pressure in room 1603

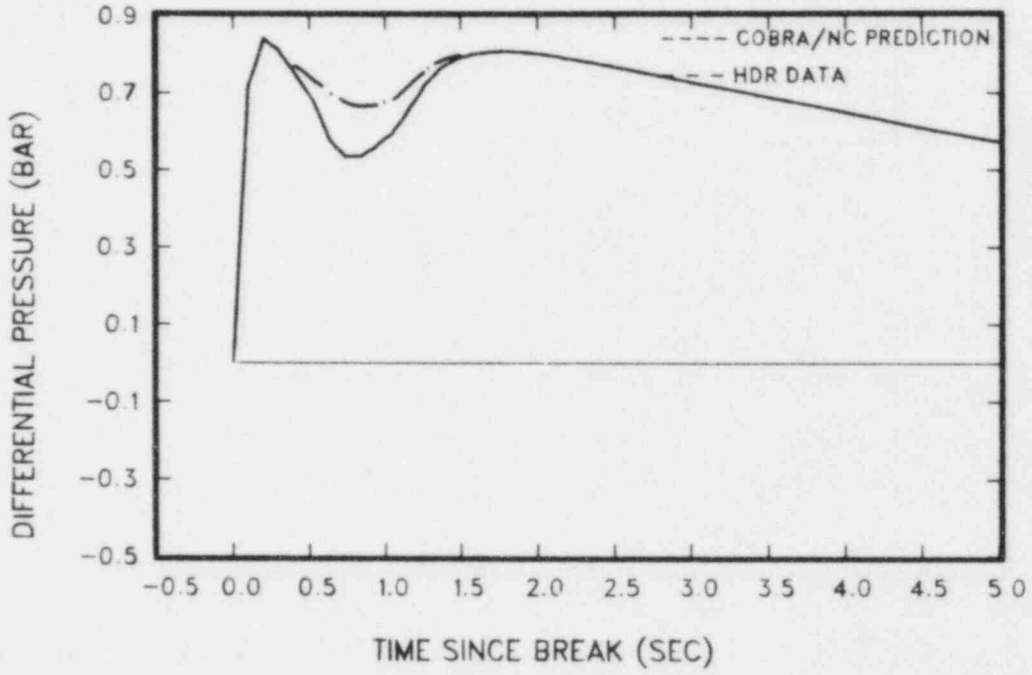

Figure 161 Effect of boundary condition change on the differential pressure between rooms 1603 and 1708

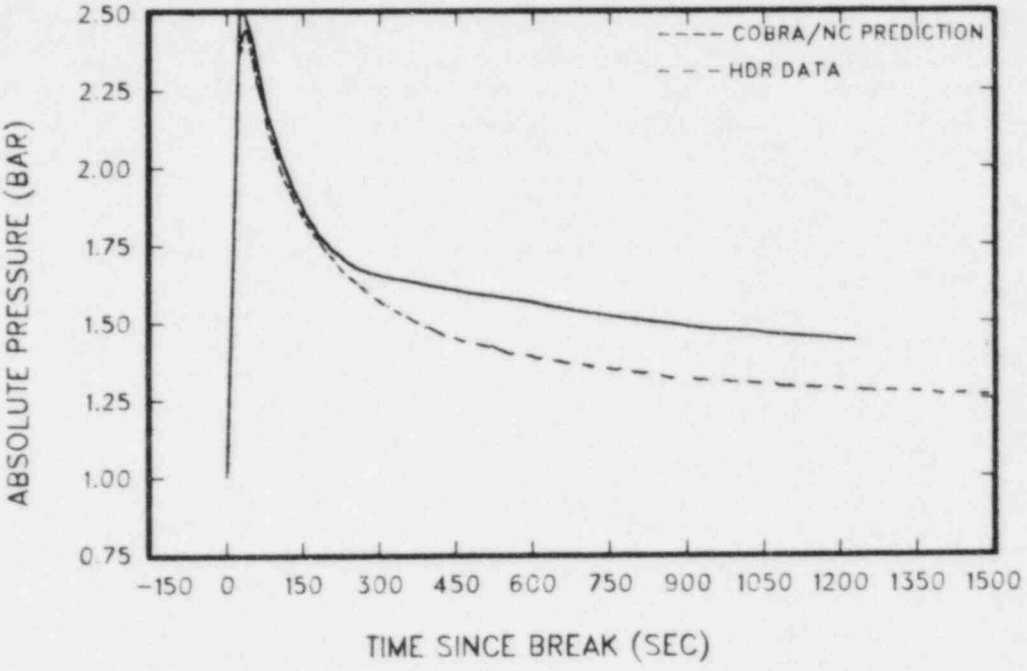

Figure 162 Absolute pressure in room 11004 from earlier calculation

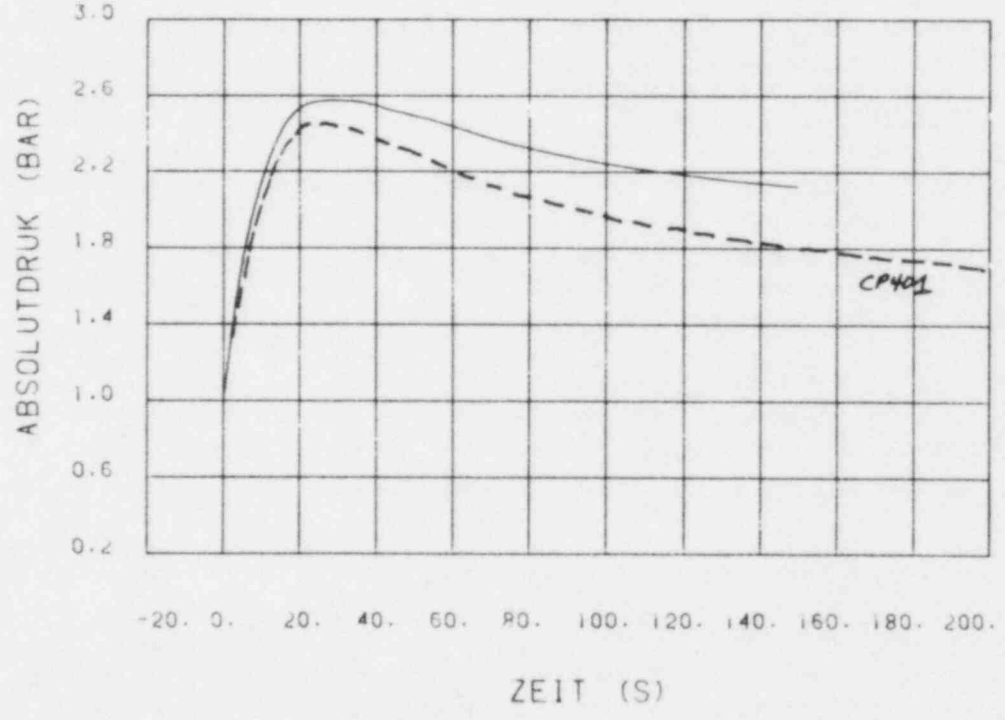

Figure 163 Absolute pressure in room 11004 with steam trapped in part of zone 34

compare well with the measured data throughout the time period in both magnitude and shape. The largest common discrepancy is that the initial peak in the differential pressures seems to be overpredicted in the calculation. This could be a result of the high initial blowdown flow and is an indication that the specified blowdown flow is in error during the first few fractions of a second.

The other notable difference between measured and calculated values is the differential pressure between rooms 1603 and 1704 (Figure 89), which is underpredicted by the code. Since the differential pressure between room 1603 and other rooms is predicted well, and the pressure of room 1603 is predicted well, it must be assumed that the pressure in room 1704 is overpredicted. Since pressure data for room 1704 was not available, this could not be verified.

Calculated temperatures for the short time domain are compared with measured data in Figures 93 through 98. Again, the calculated temperatures are very close to the measured temperatures. The calculated temperatures are initially higher than the measured data in some rooms (Figures 93 through 97). The lower-measured temperatures probably result from air trapped in some of the rooms having highly turbulent flows. This cannot be predicted with the coarse lumped parameter mesh used in the calculation, so the initial underprediction in these rooms is reasonable. The temperature in the dome zone (Figure 94) is overpredicted, indicating that too much steam is in this zone. This results in the high pressure prediction for this zone shown earlier. The condensation heat transfer model (Uchida correlation) probably underpredicts the condensation heat transfer at low vapor fractions during this initial high-flow period. The temperatures in rooms below the blowdown room are underpredicted later in time. The oscillatory nature of the temperature measurements in these regions (Figure 98) indicate that turbulent eddies of steam enter the rooms. The lumped parameter model, of course, is not able to model the turbulent mixing. One interesting point is that the temperature in room 1704 is predicted quite well. However, it is slightly higher than the data. This small difference is equivalent to 0.1 bar pressure, the amount by which the pressure in room 1704 appears to be overpredicted.

The steam density in room 1704 is shown in Figure 99. Two calculated values are shown in this figure, since room 1704 (zone 27) was divided into three separate nodes. The upper curve is the steam density in the lower of the three nodes, and the lower curve is the density in the upper two nodes. An average of these values compares reasonably well with the data. The air density for the lower node is compared with the data in Figure 100. The upper nodes would have a higher air density corresponding to the lower steam density, and the average value, again, is reasonably close to the data. The steam flow between rooms 1704 and 1804, shown in Figure 101, is for a vent located in the middle node of zone 27. Since this node has a lower steam density, the steam flow is underpredicted and the air flow (Figure 102) is overpredicted. The total flow appears to be about right. This concentration gradient in zone 27 may be the cause of the overprediction of room pressure in this zone. This was not investigated further. The drop flow is underpredicted as shown

in Figure 103. Most of the steam and drops entering room 1704 exit through the vents connected to the bottom node of zone 27. The steam density used to calculate the steam flow between rooms 1704 and 1804 is shown in Figure 104. As indicated above, the steam density is slightly low, resulting in the underprediction of the steam flow rate. The drop velocities for three vents are shown in Figures 105 through 107. The drop velocity between room 1603 and 1704 (Figure 105) is greatly underpredicted, because the vent in which the drop velocity is measured was lumped in the calculation with vent U0140, which had an artificially high loss coefficient specified to account for the additional loss caused by the blowdown jet in front of opening U0143.

The actual vent velocity can be estimated by multiplying the calculated vent velocity by the square root of the ratio of the artificial and actual vent loss coefficients. The resultant velocity is also plotted in Figure 105 as the dash-dot line. Three differences between the measured and calculated data shown in Figures 105 and 106 are:

1. The calculated drop velocity starts at about 0.3 sec, whereas the measured data starts at time zero.

2. The calculated velocity shows an initial high peak, whereas the data shows a smaller or no peak.

3. The velocity evens out at a significantly lower value in the calculation than is indicated by the data.

Some explanations for these differences are as follows:

1. Steam-only flow is specified in the boundary conditions for the first 0.3 sec of flow. Therefore, the droplet velocities measured during the first 0.3 sec of the transient are either dust particles in the air or small condensate particles resulting from steam condensation. Flow of drops from the blowdown nozzle through the vents could not possibly start until sometime after 0.3 sec. In this sense, the calculated velocities are more correct than the measured velocities as far as the initiation time of drop flow is concerned. If the measured drop flow is correct, then the blowdown flow contained liquid drops from the initiation of blowdown, and the specified blowdown flow is incorrect.

2. The initial peak in the velocity corresponds to the initial peak in pressure and is an indication that the specified blowdown flow energy is too high in the initial 0.0-0.6 sec of blowdown.

3. The measured drop velocities are even higher than the calculated steam velocities through the vents. Since the vent areas have been verified and the calculated room pressures and room differential pressures are nearly correct, the total calculated vapor flow through the vents must be about right. This means that the calculated vent velocities are the correct average vent velocities. Higher velocities would mean that more flow would pass through the vents. This would cause the pressure in the

blowdown room to decrease. A reasonable explanation for the difference between the measured and calculated velocities would be that the calculated velocities are the average velocities for the entire cross section of the vent, and the measured velocity is the velocity near the vent center line. Since the L/D ratio of the vents is small, it is reasonable to expect that the flow is not fully developed in the vent and that a steep velocity profile exists between the vent centerline and vent walls. The drop velocity sensors are near the centerline and undoubtedly measure a velocity much higher than the vent-average velocity. The calculated drop velocity between room 1704 and 1804 are comparable to the measured values (Figure 107).

7.3.1.2 Medium-Time Period Results (0-50 sec)

The medium-time range calculated pressures are compared with the measured values in Figures 108 through 111. The peak calculated pressure is within 0.05 bar of the peak-measured pressure. This excellent agreement with the data indicates that the Uchida condensation heat transfer correlation is a good model for the average heat transfer coefficient in full-scale containments, provided that the hydrodynamic model has a sufficient number of control volumes to correctly calculate the distribution of steam within the containment. The prediction of circulation flow between the rooms is also important in the correct prediction of the condensation rate. The correct rate of increase of pressure is calculated in room 1603 (Figure 110). This is reflected in the differential pressure predictions (Figures 112 through 114).

The distribution of steam within the containment is reflected in the atmospheric temperatures. Calculated temperatures for various rooms are shown in Figure 115 through 118 for this time period. Measured temperatures in some of the lower rooms exhibit irregular behavior which indicates the existence of turbulent mixing of steam into the lower compartments. The code predicts smooth temperature profiles for this region (Figure 115); however, the average behavior is predicted. Temperatures in the blowdown and surrounding rooms appear to be calculated well, as can be seen from Figures 116 and 117. Also, the temperature in the dome region (Figure 118) is calculated well during this time period, indicating that about the right amount of mixing is occurring between the dome region and the lower rooms on the blowdown room level. These excellent predictions of temperatures in the various regions of the containment provide accurate boundary conditions (temperature and steam concentration) for the room-average condensation heat transfer correlations. Given proper boundary conditions and an accurate description of the structural surface areas and masses, it appears that the Uchida correlation provides a good model for the condensation heat transfer in real containment geometries, as is evident from the good agreement between the calculated and measured pressures during this time period.

Although the Uchida correlation provides a good "room-average" heat transfer coefficient, it does not predict the magnitude of the heat transfer coefficients measured by heat transfer blocks placed at various locations within the facility. In fact, the measured heat transfer coefficients are from four to

ten times larger than the value given by the Uchida correlation. Such large heat transfer coefficients, if applied to all structures within a room, would cause severe underprediction of the peak containment pressure. Evidently, there is a wide variation in the magnitude of the local heat transfer coefficients at various locations within a room such that the average heat transfer coefficient is much lower. High heat transfer coefficients would be expected in areas of high velocity, highly turbulent flow, and with higher than average steam concentrations. Apparently the heat transfer measurement blocks were all located in such regions. Regions with much lower heat transfer coefficients must exist for the average heat transfer coefficient to be given by the Uchida correlation. It is unfortunate (and interesting) that such low values were not measured at any of the measurement locations except those in rooms that had low room-average steam concentration. High local heat transfer coefficients are important for equipment survivability calculations.

No attempt was made in the present calculation to predict these local heat transfer coefficients, so the calculated structural temperatures and heat transfer coefficients shown in Figures 119 through 126 all underpredict the measured values, as expected, since the room-average heat transfer coefficient was used.

7.3.1.3 Medium-Long Time Period Results (0-200 sec)

Although not a part of the international standard problem specification, it is interesting to look at some pressure and temperature plots for the 0-200-sec time range.

The calculated pressure for room 11004, the dome region, is compared with the measured pressure in Figure 127. As can be seen from this figure, the calculated pressure is very close to the measured values throughout this time period. No better comparison should be expected. However, close examination of the room atmosphere temperature (Figures 128 through 135) indicates that the good pressure prediction is not entirely for the right reasons. In particular, the temperature in some of the lower rooms (Figure 128) are overpredicted, compensating for the underprediction of the temperature in some of the upper rooms (Figure 135). In general, however, the temperature distribution throughout the containment is reasonably well predicted, as is illustrated by the temperatures shown in these figures.

7.3.1.4 Long-Time Period Results (0-1500 sec)

The long-term thermal-hydraulic response of the containment was calculated out to about 800 sec. The calculated pressure for this time period is shown in Figure 136. The calculated pressure is in excellent agreement with the data out to about 350 sec. After that the calculated pressure flattens out above the measured data. This is caused by the inadequate prediction of mixing caused by natural convection currents between various rooms in the containment. In particular, the steam concentration in room 1704 is too high and that in room 11004 is too low. This prevents the steam in 1704 from condensing on the cooler structures in room 11004 and causes the slowing of the containment

depressurization. This is a problem when using a multinode lumped parameter model, since it is difficult to predict circulation patterns a priori and to provide adequate flow connections to allow the code to calculate convection currents between rooms. The temperatures for some of the rooms are shown in Figures 137 through 140. The temperatures in rooms 1603 and 1606 are calculated reasonably well. The data for room 1704 was not available for this time period; however, the calculated temperature for room 1704 is compared with the calculated temperature in room 11004. The large temperature difference between these two rooms is evident. When the available measured temperatures are compared, it is evident that the atmospheres of the blowdown room and the upper dome region are completely mixed after 300 sec and presumably so are the atmospheres of room 1704 and room 11004. In fact, the temperature in room 11004 rises above that of the blowdown rooms as the remaining warm steam and air rise to the top of the containment. The calculation could be improved by judiciously choosing the noding connections; however, the only sure way of predicting the actual mixing processes would be to use a finite-difference model with a very large number of nodes. The underprediction of the temperature in room 11004 is shown in Figure 140.

7.3.2 Parametric Study Results

A parametric study over some of the key input variables was conducted to determine the sensitivity of the calculation to these parameters. This was done to shed some light on the relative importance of these parameters in the modeling process with the hope that unnecessary complication of licensing calculations can be avoided. This study was conducted within the limitations of the existing nodalization for the HDR containment and the COBRA-NC lumped parameter model. The influence of each variable is evaluated by comparing the results of each variational calculation with the base case presented in Section 4.1 of this report.

7.3.2.1 Parametric Study Results

The size of droplets suspended in the containment atmosphere that are carried by the atmosphere from one room to the other have an influence on the magnitude of the differential pressure between the two rooms. The relative importance of the drop size has been the subject of much discussion and has led to some suggestions that multiple drop sizes must be considered to correctly predict the vent pressure drops. The COBRA-NC model for suspended liquid is more sophisticated than that of most other containment codes in that the liquid drops are treated as a separate field. This makes it possible to calculate the acceleration and velocity of drops relative to the vapor/air flow. However, only a single average drop size is used in the calculation. The effect of drop size was studied by leaving all of the input parameters the same as for the base case except the drop size. The calculation was then run for three different drop sizes. It is important to remember that the drop size specified is that for drops in the blowdown nozzle and that the actual drop size in the containment is smaller as a result of evaporation from the drop as it comes to equilibrium with the lower containment pressure. The influence of drop

size on vent pressure drops is maximized in this study, since 100% carryover of drops between rooms is assumed.

Three drop sizes have been compared:

- 2μm
- 200μm (base case)
- 2000μm.

The 200μm drop size was used in the base calculation. Results for the 2000μm drops are shown in Figures 141, 142, and 143. The base case calculation is shown in each of these figures with a dash-dot line and the current calculation with a solid line. The absolute pressure in room 1603 is shown in Figure 141. The difference between the calculated pressures in this figure illustrates the overall effect of the larger drop size on the vent pressure drops. The pressure for the drops is lower than for the drops, as should be expected. However, the decrease in pressure is not dramatic. The effect on vents leading from the break room and on vents further away from the break room are typified by the differential pressure shown in Figures 142 and 143. The effect on differential pressures between the break room and surrounding rooms is comparable to the effect on the break room pressure (Figure 142). The effect on the differential pressure across vents away from the break compartment is negligible.

Results for the 2μm drops are shown in Figures 144, 145, and 146. As expected, these results are above the base case predictions, since a smaller drop size is used and the relative velocity between the vapor/air mixture and the drops is lower.

These two drop sizes, 2μm and 2000μm represent the reasonably physical range of drop sizes. The 2000μm drops are the size of drops that would be entrained from a liquid film by the air/vapor velocities in the vents. The 2μm range essentially travels at the same velocity as the air/vapor mixture, so no further change in vent pressure drop can be expected for smaller drop sizes. The total variation in room pressure over this drop size range is about 0.21 bar at 5.0 sec. This is 9.2% of the total room pressure at 5.0 sec. This is not an extremely large change given the large variation in drop size (three orders of magnitude). The variation in vent pressure drop is 0.14 bar or about 24% of the vent pressure drop at 5.0 sec.

7.3.2.2 Effect of Drop Carryover

Vent pressure drops are not only influenced by the size of drops carried by the vent flow but also by the mass (or number) of drops carried in the flow. This value is difficult to determine for lumped parameter simulations and must almost be specified by the analyst. The amount of liquid carried in the flow is a result of the complex interactions of droplet deposition and entrainment. Both of these mechanisms are strongly influenced by the geometry

of the flow path, the presence and geometry of internal structures, and the multidimensional flow patterns within the room. Drop deposition can occur as a result of turbulent diffusion or as a result of direct impact. Entrainment can result from liquid film instabilities caused by gas flow over the film or by backsplatter from drop impaction. These mechanisms are difficult to predict when the three-dimensional flow and geometry are modeled in detail and impossible to predict from the small amount of information provided by a lumped parameter calculation. While the detailed calculation is possible to perform with COBRA-NC, it would be too expensive to use on a routine basis for licensing calculations. It is, therefore, worthwhile to study the sensitivity of the calculation to this parameter.

Three calculations were performed for this study:

- no drop carryover
- deposition by diffusion and by 80% impaction on structures
- 100% carryover (base case).

The results of the calculation with no drop carryover are shown in Figures 147, 148, and 149. The effect of the presence of drops is clearly illustrated in these figures, since the break room pressures and the differential pressures between rooms are significantly underpredicted. Even vents away from the break compartment are affected. This case, with zero-drop carryover, and the 2μm case of Section 4.2.2 represent the entire range of variation possible as a result of drop content in the vent flow, since this case represents infinite slip between the gas and liquid and the 2μm case represents zero slip between the phases. The total possible variation in room 1603 pressure due to liquid carryover is 0.35 bar or 16% of the total pressure at 5.0 sec. The total variation in vent pressure drop is about 0.35 bar or 59% of the total vent pressure drop.

Results for the case that allowed drop deposition by diffusion and by 80% impaction on structures and also re-entrainment off of unstable films are shown in Figures 150, 151, and 152. The results are very interesting. The pressure in Figure 151 is the same as the base case for the first 0.4 sec, since drop flow has not yet occurred in the blowdown nozzle. The case with drop deposition then falls below the prediction for the base case which has no drop deposition, as should be expected. The interesting thing is that from 0.5 to 1.7 sec the prediction for this case is only slightly above the prediction for no drop carryover, indicating most (but not all) of the drops are removed from the flow during this period. However, at about 1.7 to 2.5 sec, the room pressure rises, and from 2.5 sec on the calculation matches the case having 100% carryover and drops. The explanation for this behavior is as follows. From 0.5 to 1.2 sec, drops are depositing on the structural surfaces and forming a liquid film. At 1.7 sec the film reaches the critical thickness and becomes unstable, allowing the re-entrainment of drops. At 2.5 sec the drop re-entrainment rate is equal to the deposition rate. The size of the drops that are re-entrained are determined by the film instability criterion and

are about 2000μm in diameter in this calculation. Thus, except for the period from 0.5 to 1.7 sec, the net effect of drop deposition is to change the drop size carried by the vent flow and not to change the amount of drop carryover! It is doubtful that the velocities used to calculate the stable film thickness are correct, since this is dependent on the local velocities within the room. However, that such a process could take place is very plausible and, if proven, could lead to significant simplification of the analytical model required. The same behavior is observed in the vent pressure drop shown in Figure 151. The vent pressure drop between rooms 1605 and 1701u is below that for the drops, presumably because the critical film thickness has not been achieved in rooms outside of the blowdown room. The total pressure variation possible due to drop carryover is 0.35 bar at 5.0 sec. However, it is possible that the process of re-entrainment could reduce this variation to that given by the variation in drop size (0.21 bar or 9.2% of the total pressure at 5.0 sec). The lower limit of no drop carryover is probably not physically realistic. Judging from the shape of the pressure curve, it is probable that even the 80% impaction overpredicts the amount of droplet deposition.

7.3.2.3 Effect of Condensation

The effect of condensation on the vent pressure drops was studied by setting the wall heat transfer to zero and comparing this result to the base case. The results for this calculation are shown in Figures 153, 154, and 155. The net effect is to increase the absolute pressure in each of the rooms. The difference between the pressures in this calculation and the base case increases with time, since no condensation is allowed. Interestingly, there is only a small effect on the vent pressure drops since the pressure increases in all rooms. Some pressure drops are larger than the base case, and some are smaller, depending on the relative amount of condensation that occurred in each room for the base case. The largest variation in vent pressure drop for all vents was about 0.04 bar or only 6% of the total pressure drop at 5.0 sec.

7.3.2.4 Effect of Vent Loss Coefficients

Perhaps the largest uncertainty in all of the input parameters is the value for the vent loss coefficients. This is particularly true of the loss coefficients for the vents connected to the blowdown nozzle port. Not only is this a complex flow path geometrically, but it is further complicated by the influence of the blowdown jet and impingement plate at the exit of the vent. Even if values of other input variables are specified to cause a maximum vent pressure drop, the geometrical values for the vent loss coefficients specified by GRS are insufficiently large to create the measured pressure drop. This is illustrated in Figure 156, which is the pressure prediction for room 1603 with 100% carryover of drops, a drop diameter of 2μm and the GRS specified vent loss coefficients. It is impossible to determine from this work what the value of each vent loss coefficient should be, but it is apparent that the values specified by GRS are not sufficiently large. A case using the GRS-specified loss coefficients and the base case values for all other parameters is given in Figures 157, 158, and 159.

The variation in the room pressure is 0.18 bar or 8% of the total pressure at 5.0 sec. The variation in the vent pressure drop is 0.13 bar or 22% of the vent pressure drop at 5.0 sec. The uncertainty in the vent pressure drops could be even larger if lower limits on other input parameters are assumed.

7.3.2.5 Effect of Blowdown Boundary Condition Change

The standard problem specified boundary condition was slightly altered between 0.3 sec and 2.0 sec to give a smooth vapor generation rate. This was done by adjusting the specific enthalpy of the flow. This is equivalent to decreasing the liquid content of the flow and increasing the vapor flow rate. The effect of this change on the room pressure and vent pressure drops is illustrated in Figures 160 and 161. The net effect was to diminish the drop in pressure during this time period caused by the sudden sharp drop in steam generation implicit in the standard problem boundary condition specification.

The liquid content of the blowdown flow has a strong effect on the vent pressure drops as does the magnitude of the steam flow. It is difficult to accurately measure the amount of liquid in the flow at high void fractions; however, it is important to determine the uncertainty in the blowdown flow rate boundary condition, since this parameter can have a strong influence on the calculated vent pressure drops. Emphasis should be placed on obtaining accurate blowdown flows and enthalpies in future tests.

7.3.2.6 Effect of Natural Circulation

One of the major difficulties with lumped parameter analysis is to determine an appropriate nodalization and flow connection logic that will allow the code to calculate the correct natural circulation flows between compartments. These circulation flows may follow a path through a chain of rooms and vents, or they may occur due to countercurrent flow within a single vent. Examples of this second type of circulation would be hot air going through the top (or center) of a vent and cold air going the opposite direction through the bottom (or perimeter) of a vent. The effect of natural circulation flow can be illustrated with three cases. The first case is the COBRA-NC pretest calculation of the containment pressure for test V44, shown in Figure 162. The same model for condensation heat transfer was used to obtain the result in this figure as was used to obtain the result shown in Figure 127. However, the peak pressure in Figure 162 is overpredicted by a larger amount than that of Figure 127, and the pressure levels off at a higher value later in time in Figure 162 than in Figure 127. The only difference between these two calculations is that the noding was changed so that the code would predict a convection flow between the dome region and the blowdown room region via the stairwell and circular staircase flow paths allowing mixing between the two volumes.

Another example is shown in Figure 163. The circulation path between the dome region and blowdown region via the stairwells was present in the calculation; however, part of the dome region was modeled with a separate node. This node acted as a steam trap and did not allow mixing with the

remainder of the atmosphere in zone 34. Again, as shown in Figure 163, this caused the pressure to flatten out too early.

Even in the current calculation, the pressure flattens out earlier than it should because steam is trapped in zone 27 or other flow regions. These regions probably mix by countercurrent flow through doorways or other single vents. Additional flow paths would have to be specified to cause these zones to mix. Single volume models may perform better for the long-term pressure response in that the basic assumption in that type of model is that the entire containment atmosphere is well mixed. However, such models will not do well when the atmosphere is not well mixed.

Circulation currents after the end of blowdown are important in the determination of the long-term pressure response of the containment. These currents can be predicted by lumped parameter models only by judicious selection of the nodalization. This task becomes more difficult as the geometry of the containment increases in complexity.

7.4 Conclusions

The results of COBRA-NC post-test calculations of the PHDR test V44 steam blowdown experiment have been presented. These calculations are in excellent agreement with the measured data for absolute pressure, differential pressure, and gas temperature for the short time period from 0-5 sec. There is reasonable agreement with the measured steam and air densities and flows during the period and also with the measured drop velocities. The major differences between the measured and calculated drop velocities can probably be explained as the difference between the vent centerline velocity measured by the instrumentation and the vent-average velocity calculated by the code.

A parametric study was performed for this time period to determine the sensitivity of the calculated pressures to the major input variables. The results of this study are summarized in Table 40.

It is evident from this table that the liquid content of the flow combined with the droplet size gives the largest variation in the calculated room pressures. Physical arguments can be used to show that the variation of this parameter is probably much lower and that the true uncertainty in the room pressure due to the liquid content of the vent flow is much smaller. There is some evidence presented in this report that supports the argument that this variation may be limited to that of drop size, since the drop deposition rate may come into equilibrium with the drop entrainment rate in a very short time. Even the range of drop size is probably limited to between 2 and rather than 2 to 2000μm and the flow is probably a mixture of drop sizes. Both of these factors would reduce the probable effect of the vent flow liquid content. This uncertainty can probably be reduced by a more sophisticated analysis of the flow within the break compartment and more complete measurement of drop flows in all vents leading from the break compartment.

Table 40 Summary of parametric study

Parameter	Range of Parameter Variation	Variation in Computed Results
Drop size	2μm-2000μm	Pressure: 0.21 bar or 9.2% of total ΔP: 0.14 bar or 24% of total
Drop Carryover (combined with drop size)	0 to 100%	Pressure: 0.35 bar or 15% of total ΔP: 0.35 bar or 59% of total
Condensation	0 to Uchida	ΔP: 0.04 bar or 6% of total
Vent Loss* Coefficient	2.0 to 8.0 vent U0140 and U0143	Pressure: 0.18 bar or 8% of total ΔP: 0.13 bar or 22% of total
Blowdown Flow	Figure 7.6	Small effect in 0.3 to 2 sec period. Potential effect is large--uncertainty must be defined.

* Variation is the probable minimum--actual uncertainty could be larger depending on value of other parameters.

One important determination of this study was that, even if all of the input parameters are set to give maximum vent pressure drops, the pressure drops are still underpredicted using the GRS values for vent discharge coefficients. A larger loss coefficient must be specified for the vent containing the blowdown nozzle before reasonable comparisons with the measured vent pressure drops can be obtained. The minimum uncertainty in the loss coefficient of this vent is more significant than the probable uncertainty of the liquid content of the vent flow. This uncertainty should be removed either by closing this vent in future tests or by measurement of the true flow through the vent or true loss coefficient for the vent.

The room pressures and temperatures are calculated very well for the medium (0-50 sec) and medium long (0-200 sec) time periods. The heat transfer block temperatures and heat transfer coefficient calculations were based on the room-average heat transfer coefficients and do not compare well with the higher, measured values evident at the location of the heat transfer blocks. The

calculated temperatures and pressures compare less well with the long-range measurements (0-1500 sec) because of the inability to adequately calculate convection currents with the existing nodalization. The calculation could be improved by a more judicious selection of flow connections.

It can be concluded that:

- The Uchida condensation heat transfer coefficient is an adequate model for large-scale containments provided that the distribution of steam throughout the containment is calculated correctly.

- Many nodes must be used to calculate the correct steam distribution.

- The liquid content of the vent flow is an important parameter, but it can probably be shown that the true uncertainty due to this parameter is small.

- The magnitude of the uncertainty in the effective vent loss coefficients needs to be quantified.
- The convection currents within the containment must be correctly calculated to predict the long-term pressure response of the containment.

8.0 BATTELLE-FRANKFURT HYDROGEN DISTRIBUTION TESTS 6, 12, AND 15

During and after a loss-of-coolant accident (LOCA) in a light water reactor, chemical reactions result in the formation of gaseous hydrogen, the concentration of which may reach the limits of inflammability.

Experiments were carried out in the Battelle-Frankfurt model containment to study experimentally the distribution of hydrogen in air as a result of convection and diffusion (Ref. 8). This is the same model containment that was used for the investigation of steam/water blowdown thermohydraulic processes, and the facility is described in Section 3.0 of this report. The hydrogen distribution tests provide information about the dispersion of hydrogen in air in a relatively large experimental compartment under varied conditions. From these tests the following major conclusions were reached. First, if the hydrogen feed rate does not exceed 2 m^3/hr, and the temperature distribution is uniform, then hydrogen is homogeneously dispersed through the compartment. Second, if the source is located halfway up the compartment wall, a vertical concentration stratification occurs. Equalization of the concentration, essentially through diffusion, proceeds relatively slowly. Third, the openings between the compartments hinder dispersion of the hydrogen only if the cross sections are very small. Fourth, thermal stratification in the compartment clearly restricts hydrogen dispersion and this results in a distinctly higher hydrogen concentration in the cooler region--if the hydrogen source is in the cooler region and, fifth, a high humidity in the hot compartments favors the occurrence of concentration differences.

Simulations of some of these tests were performed with COBRA-NC to assess the codes ability to predict the distribution of hydrogen under various conditions. Tests 6, 12, and 15 were chosen for simulation. Test 6 consisted of two compartments with thermal stratification; test 12 consisted of 6 compartments with uniform temperature; and test 15 consisted of 6 compartments with a thermal stratification between the upper and lower compartments.

These simulations test the codes ability to predict all of the basic conclusions of the experimental program except for the second one. A simulation should be performed in the future to test the code's ability to predict the hydrogen distributions when an elevated hydrogen source is present.

8.1 Description of the Experiment

The experiments were conducted in the Battelle-Frankfurt model containment used for the steam/water blowdown experiments. This facility was briefly described in Section 3.0 of this manual. The central, cylindrical containment compartments R1, R2, and R3 were used for experiment 6. A sketch of these compartments is shown in Figure 164. Tests 12 and 15 were conducted in a 6-compartment configuration of the facility that included the two cylindrical compartments described above and four surrounding annular compartments. Each of these compartments was connected to the surrounding compartments by several vertical and horizontal openings. A sketch of the compartmental arrangement for tests 12 and 15 is shown in Figure 165.

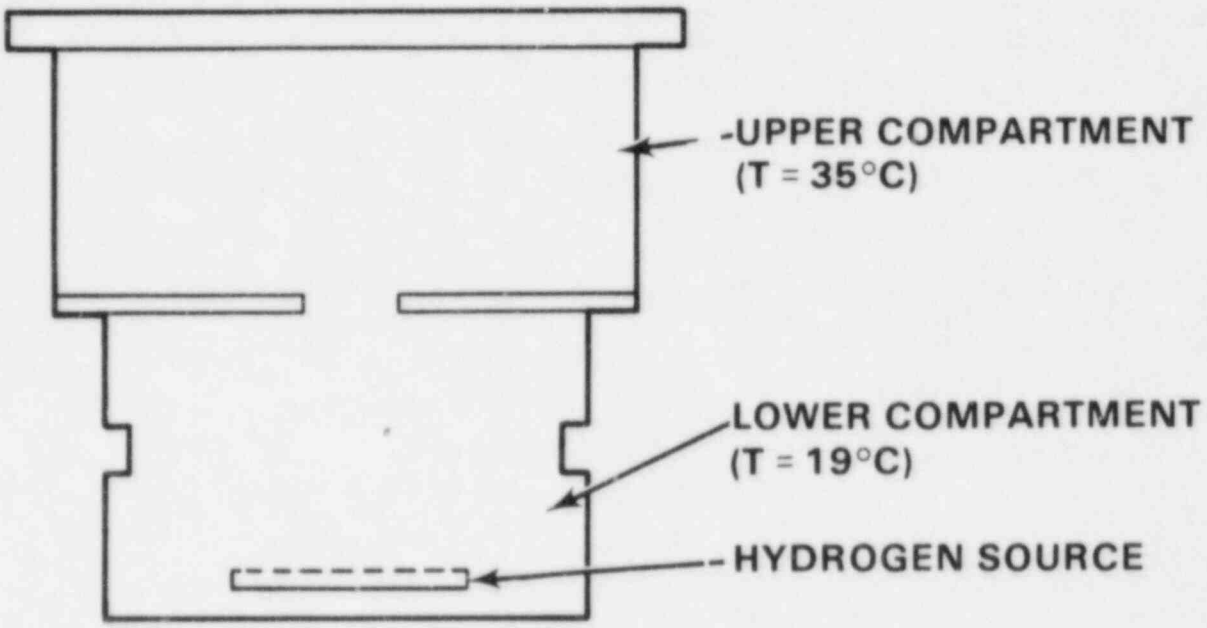

Figure 164 Compartmental arrangement for Battelle-Frankfurt hydrogen test 6

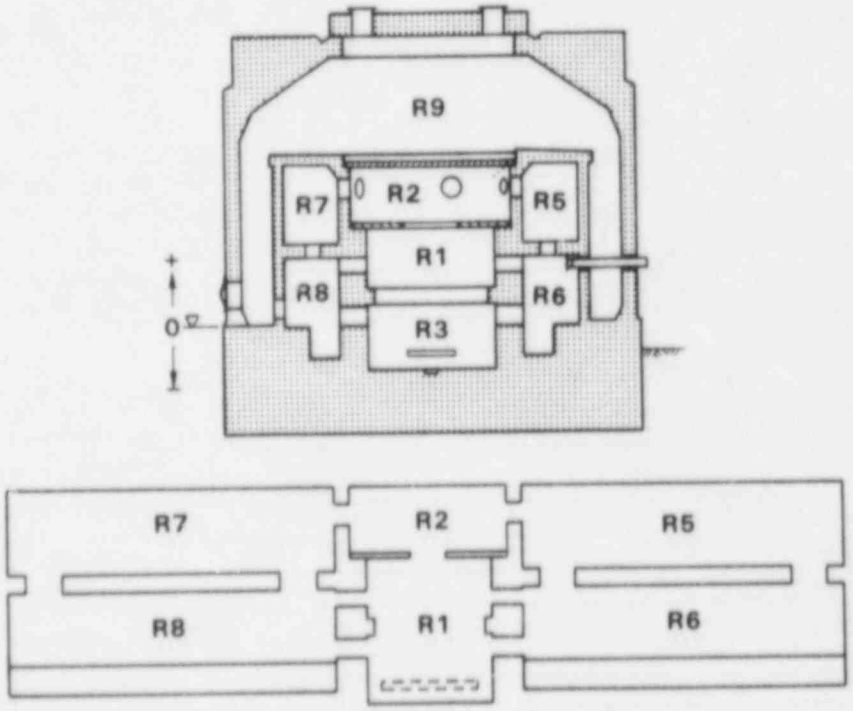

Figure 165 Compartmental arrangements for Battelle-Frankfurt hydrogen tests 12 and 15

Test 6 was conducted by first heating the upper compartment to 35°C while holding the lower compartment to 19°C. These conditions were held until the structure came into thermal equilibrium with the atmosphere in the compartments. A low velocity flow of a nitrogen/hydrogen mixture was injected into the bottom of the lower compartment. The composition of the flow was 34% nitrogen and 66% hydrogen. The input rate was 2.35 m^3/hr for the first 18 min and then 0.98 m^3/hr for the next 1 hr and 48 min. The gas was injected at a temperature of 19°C. The size of the opening between the lower and upper compartments was 1.0 m^2. The total gas volume in the two compartments was 72.0 m^3.

Test 12 was run with a uniform temperature throughout the containment. The gas source was at the floor level of room 1 and consisted of a gas mixture with a volumetric composition of 66.8% hydrogen and 33.2% nitrogen. The gas was injected at a rate of 0.32 m^3/hr at 16°C.

Test 15 was conducted with the upper rooms (rooms 2, 5, and 7) at 35°C and the lower rooms (rooms 1, 6, and 8) at 16°C. The gas source was at the floor level of room 1 and consisted of a gas mixture with a volumetric composition of 67% hydrogen and 33% nitrogen. The gas was injected at a mean rate of 0.30 m^3/hr and a temperature of 17°C. The average relative humidity for the atmosphere prior to the best was 55%.

8.2 COBRA-NC Model Description for Test 6

Test 6 was modeled using the two-dimensional finite-difference model option. The mesh used for test 6 is shown in Figure 166.

The cylindrical test section was modeled with a two-dimensional mesh consisting of four channels each containing six nodes in the lower compartments, two nodes in the opening between the two rooms, and four channels each containing four nodes in the upper compartment. The gap width for the horizontal connection between channels was taken to be the circumference of the circle passing through the boundary between the two channels. The centroid distance was taken to be the radial distance between the center of the two connecting channels. The input data for the channels are given in Table 41, and those for the gaps are given in Table 42.

The concrete walls on the perimeter of the cylindrical compartments were modeled using two thermal conductors. Thermal conduction through the plywood partitions separating the lower compartment from the upper compartment and the upper compartment from the rest of the containment was not modeled. The input data for the thermal conductors is given in Table 43.

A mass flow rate boundary condition was specified at the bottom of channels 1, 2, and 3 to model the hydrogen/nitrogen source. The total flow was 2.9631×10^{-4} kg/sec for the first 18 min and then 1.2357×10^{-4} kg/sec for the next 1 hr and 48 min. These flows were calculated from the volumetric flows specified in Section 8.1 for a gas mixture consisting of 66% by volume of

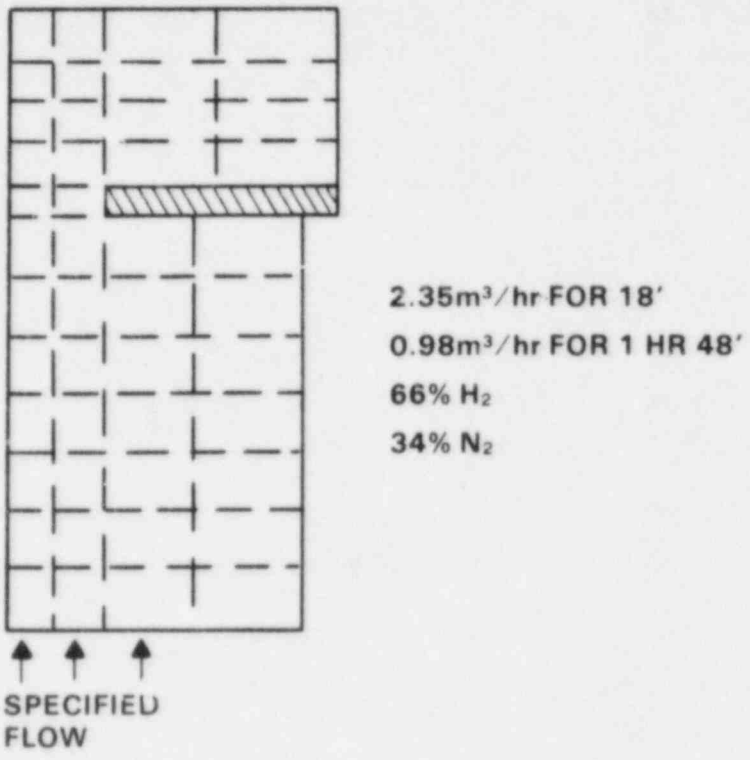

Figure 166 Mesh for Battelle-Frankfurt hydrogen test 6

Table 41 Channel input data for Battelle-Frankfurt hydrogen distribution test 6

Channel No.	Area m^2	Wetted Perimeter m	Height m
1	0.2498		3.56
2	0.7495		3.56
3	3.476		3.56
4	5.965	11.45	3.56
5	0.2498		0.30
6	0.7495	3.54	0.30
7	0.2498		1.85
8	0.7495		1.85
9	5.353		1.85
10	9.979	14.326	1.85

Table 42 Gap input data for Battelle-Frankfurt hydrogen distribution test 6

Gap No.	Connecting Channels	Gap Width (m)	Centroid Distance (m)
1	1&2	1.772	0.282
2	2&3	3.544	0.456
3	3&4	7.499	0.630
4	5&6	1.772	0.282
5	7&8	1.772	0.282
6	8&9	3.544	0.570
7	9&10	8.935	0.858

Table 43 Thermal conductor input data

Conductor Number	Channel Number	Wetted Perimeter (m)	Material Thickness (m)	Material
1	4	11.45	0.80	Concrete*
2	10	14.33	0.37	Concrete*

* Density: 2225.0 kg/m^3
Specific heat: 879.0 J/kg°C
Thermal Conductivity: 2.1 W/m°C

hydrogen and 34% by volume of nitrogen at a temperature of 19°C and a pressure of 1.0 bar.

8.3 COBRA-NC Model Description for Tests 12 and 15

The lumped parameter option was used to model tests 12 and 15. The nodalization used for test 12 is shown in Figure 167, and that for test 15 is shown in Figure 168.

The initial and boundary conditions are also shown in these figures. The mesh for test 12 consisted of two nodes in each of the lower rooms and a single node for each of the upper rooms. Two nodes were provided in each of the lower rooms to accommodate the upper and lower flow vents between the central cylindrical rooms and the outer annular rooms at this level. The temperature

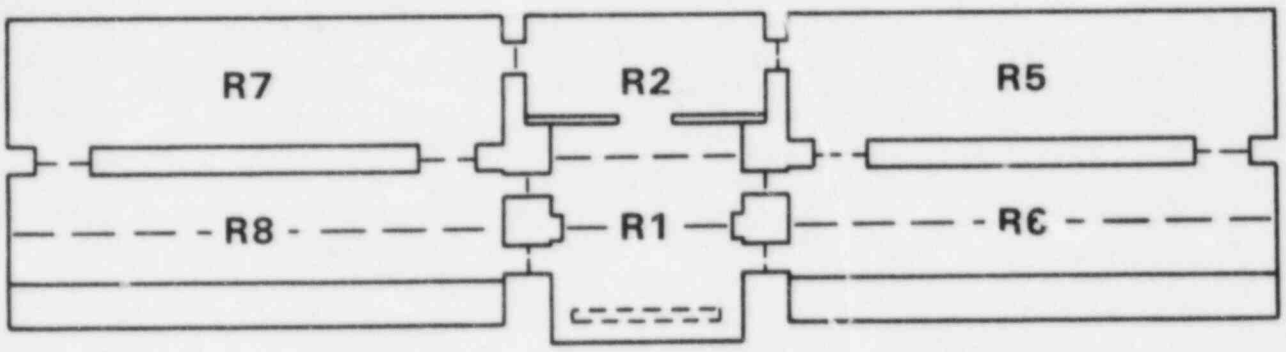

GAS SOURCE
MEAN INJECTION RATE: 0.32m³/h
MIXTURE: 66.8% H_2 BY VOLUME
33.2% N_2 BY VOLUME

Figure 167 Nodalization and boundary conditions for Battelle-Frankfurt test 12

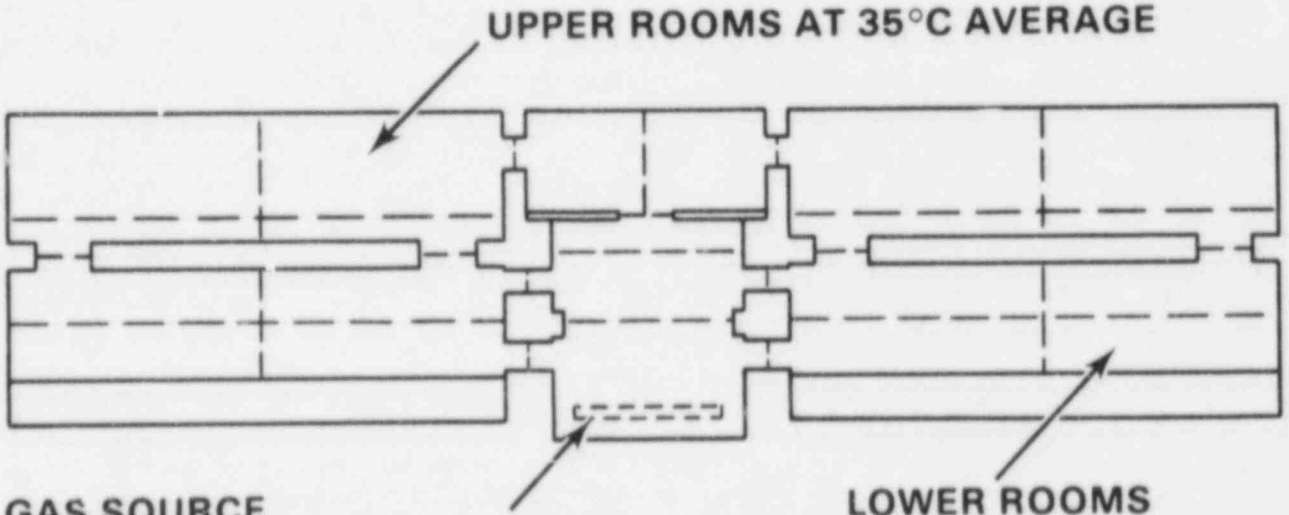

Figure 168 Nodalization and boundary conditions for Battelle-Frankfurt test 15

was uniform throughout the containment, and a constant flow rate boundary condition was specified at the bottom of room 1.

Initially, the mesh for test 12 was used for test 15, except that the upper rooms were initialized to 35°C, and the gas source flow rate was adjusted slightly to match the flow specified for test 15. However, since the mesh for test 12 only has a single connection between each lower room and the room directly above it, the code could not predict convection currents between these rooms. The hydrogen introduced by the gas source remained in the lower rooms and no mixing occurred. The upper rooms were then modeled with two channels so that upflow and downflow could simultaneously occur between the lower compartments and the compartments directly above them. This is the nodalization shown in Figure 168.

The initial and boundary conditions are also shown in this figure. The heat transfer to (or from) structural surfaces was neglected in the initial simulation of test 15.

8.4 Discussion of Results

Predictions were made for the hydrogen concentration in each of the rooms of Test 12 as a function of time. The code predictions for rooms 1, 2, 7, and 6 are shown in Figures 169 through 172, respectively. The code predictions are very good for this isothermal test using the lumped parameter approach. The calculation was sensitive to very large time step sizes. The analyst should be cautioned to test the solution for accuracy by varying the time step size when using the lumped parameter approach. A maximum time step size of 10 s was used in this calculation. Some unsteadiness in the solution was observed when using 50 s time step sizes.

Both the magnitude and trends of the data are predicted well by COBRA-NC. Notice that the initial jump in the concentration in room 1 (Figure 169) was predicted. The concentration in the lower, outer rooms was underpredicted later in time. This is probably a result of using a time average injection rate of 0.32 m^3/hr. The actual injection rate was 0.334 m^3/hr for the first 23 hr and then was adjusted down to 0.311 m^3/hr.

The simulation of test 15 neglected the heat transfer between the containment atmosphere and the containment walls. The hydrogen concentrations in rooms 1 and 2 are compared with the experimental concentration for these rooms in Figure 173. The data shows a concentration difference between the upper and lower room for the duration of the test with the magnitude of the difference decreasing in time. The COBRA-NC calculation also shows a concentration gradient, but it is smaller in magnitude. Also, at about 4×10^4 s into the transient a complete mixing of the upper and lower compartments was predicted. The major difference between the calculation and the experiment is the lack of heat transfer from the wall to the atmosphere in the calculation. The solid structures in the upper rooms contain a large amount of heat which

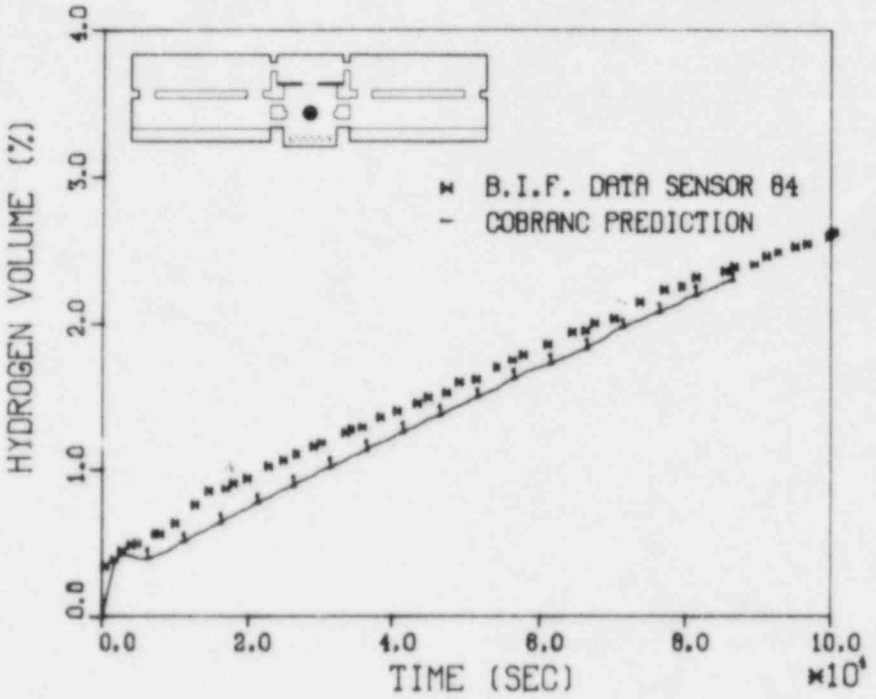

Figure 169 Test 12 hydrogen concentration in room 1

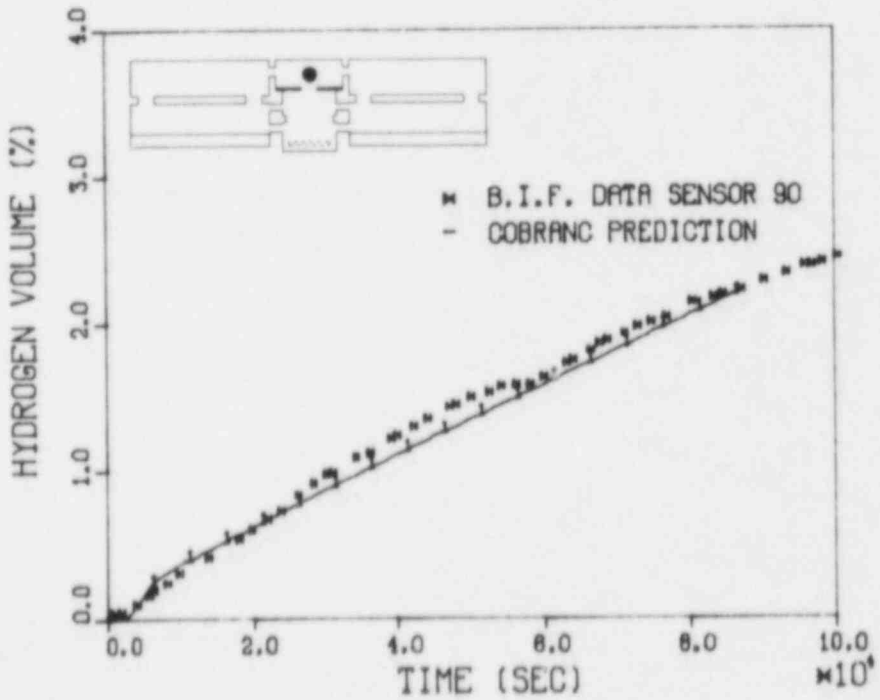

Figure 170 Test 12 hydrogen concentration in room 2

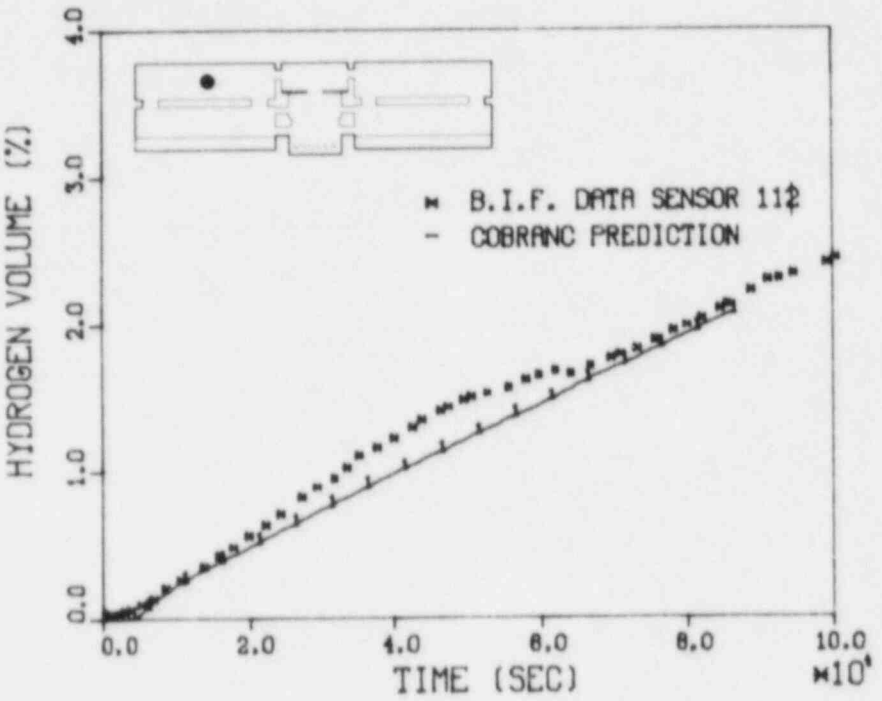

Figure 171 Test 12 hydrogen concentration in room 7

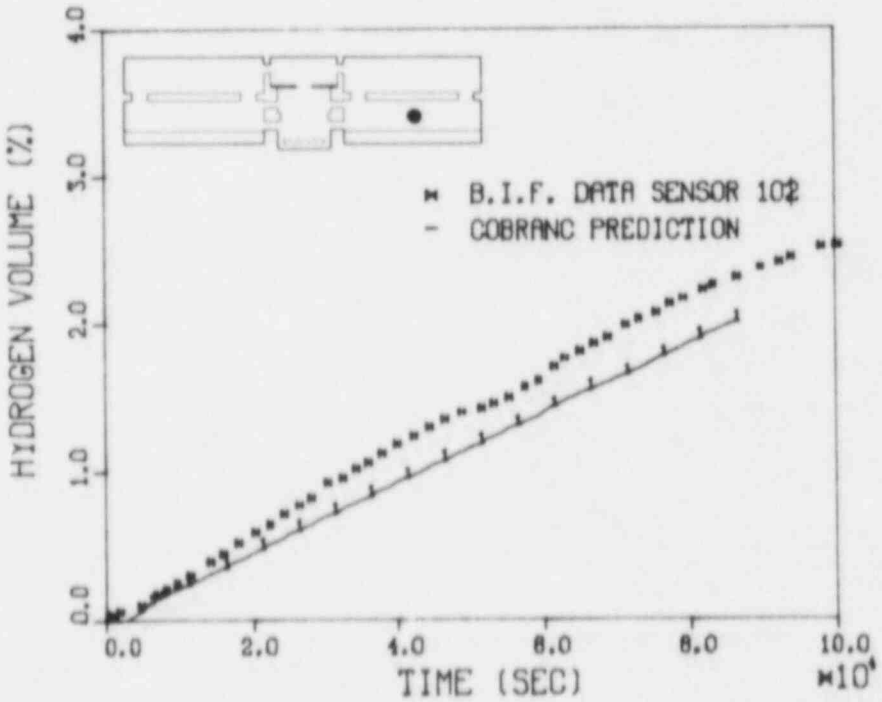

Figure 172 Test 12 hydrogen concentration in room 6

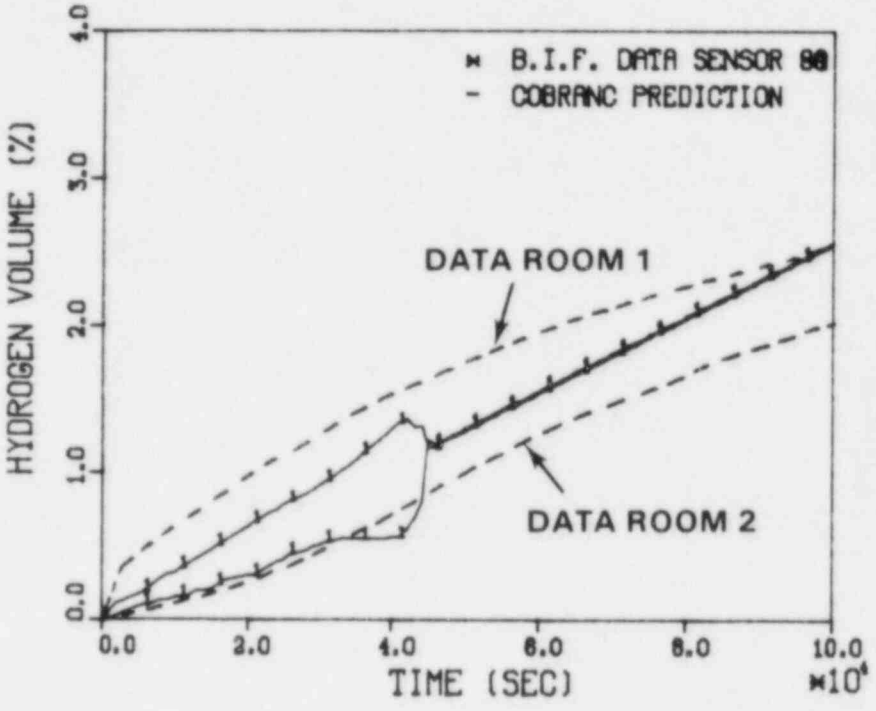

Figure 173 Test 15 hydrogen concentrations in room 1 and 2 without heat transfer

maintains the temperature of the atmosphere in the upper rooms near the initial temperature. Thus, heat transfer from the wall maintains the thermal stratification and prevents the mixing of the upper and the lower compartment atmosphere.

The results of the simulation of test 6 are shown in Figures 174 and 175. The predicted hydrogen concentration at the top center of the lower compartment is compared with the experimental data in Figure 174. The predicted concentration at the top center of the upper room is shown in Figure 175. The concentration gradient between the upper and lower room were predicted both qualitatively and quantitatively quite well by the code.

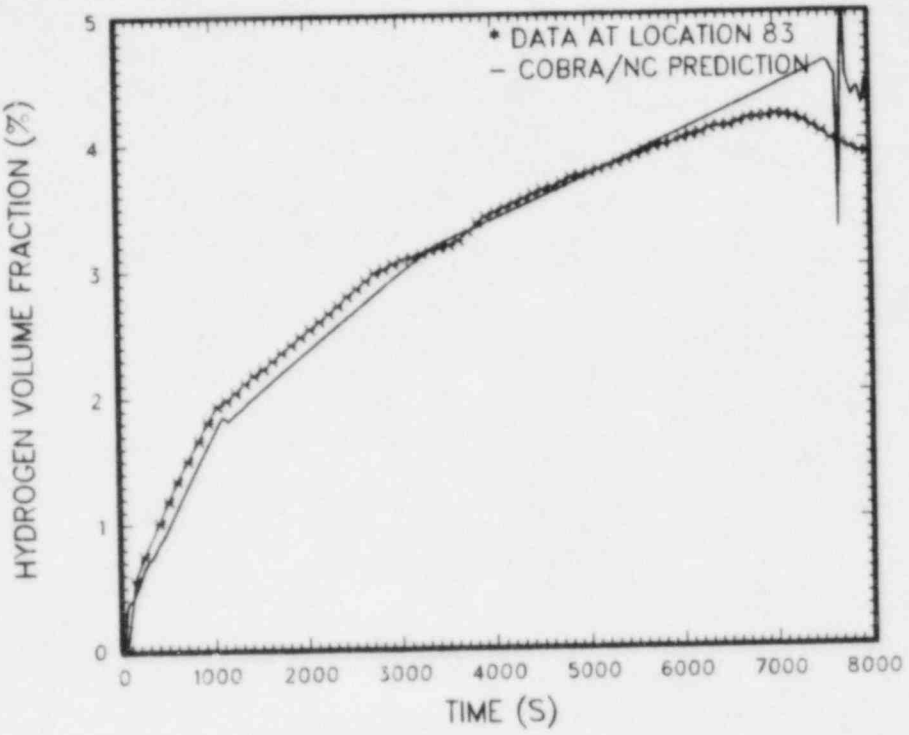

Figure 174 Test 6 hydrogen concentration in room 1

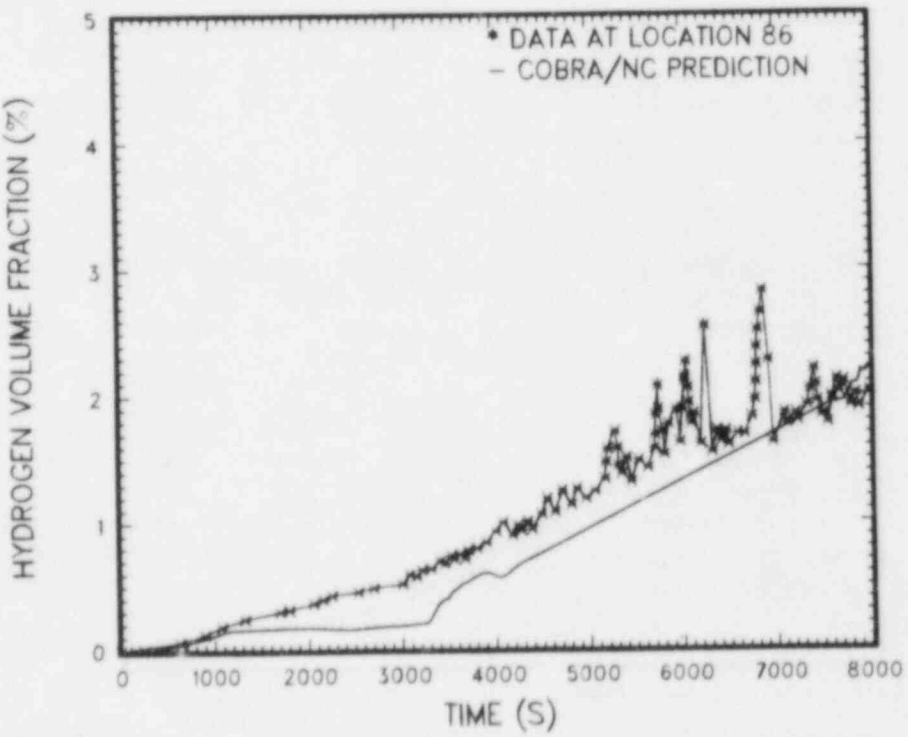

Figure 175 Test 6 hydrogen concentration at top of room 2

9.0 HEDL HYDROGEN DISTRIBUTION TESTS HM-5 AND HM-6

The results of COBRA-NC predictions of the Hanford Engineering Development Laboratory's (HEDL's) hydrogen distribution tests HM-5 and HM-6 (Ref. 9) are presented in this section. These tests were conducted in the Containment System Test Facility (CSTF) under the sponsorship of the Electric Power Research Institute (EPRI). The tests were performed in an annular compartment constructed within an 850 m^3 vessel. A recirculation system provided forced flow between the annular test compartment and the large vessel volume above the test compartment. Compartment temperatures typical of reactor accident situations were maintained during the tests. A horizontal, high velocity jet of steam and hydrogen was released in test HM-5. A vertical, lower velocity jet of steam and helium was released in test HM-6.

The code was used to predict the noncondensable gas concentrations and temperature at five circumferential measurement stations around the test section and for three vertical elevations at each station. These calculations were made as a blind pretest prediction to test the ability to correctly predict the hydrogen distribution within the annular compartment. A brief description of the experiment will first be given. This will be followed by a description of the COBRA-TF model used in the calculation and then by a discussion of the results.

9.1 Description of the Experiment

The CSTF contains a large coded vessel 20.4 m high and 7.6 m in diameter having a volume of 850 m^3. The test compartment, which simulated a simplified lower compartment area of an ice condenser plant, was fabricated in the lower area of the vessel and contained no major geometrical objects such as pipes, tanks, or structural elements. Figure 176 shows a schematic of the annular test compartment whose outer diameter was 7.62 m. The inside wall of the annulus was 3 m in diameter by 4.7-m high and was fabricated from corrugated steel sheet. A lower deck was provided inside the test vessel to act as the floor of the annular compartment and an upper deck represented the ceiling. The test compartment volume occupied a 300° section of the annulus leaving a 60° sector to represent the refueling area of the referenced plant. The containment vessel walls were constructed of steel approximately 1.65-cm thick and the heads were standard elliptical heads 1.9-cm thick. The outside of the vessel was insulated with 2.54 cm of glass fiber, aluminum foil covered insulating board with the following physical properties (density = 96 Kg/m^3) and k = 0.0467 watt/m-°C at 100°C).

The horizontal, Jet A, nozzle was located 25° from one radial wall of the annulus and was centered at a height of 1.52 m from the floor. The nozzle inside diameter was 7.77 cm and was directed 60° to the radius as shown in Figure 176.

The vertical, Jet B, nozzle was directed vertically into the test compartment and had an inside diameter of 7.77 cm. The nozzle was 120° from one radial

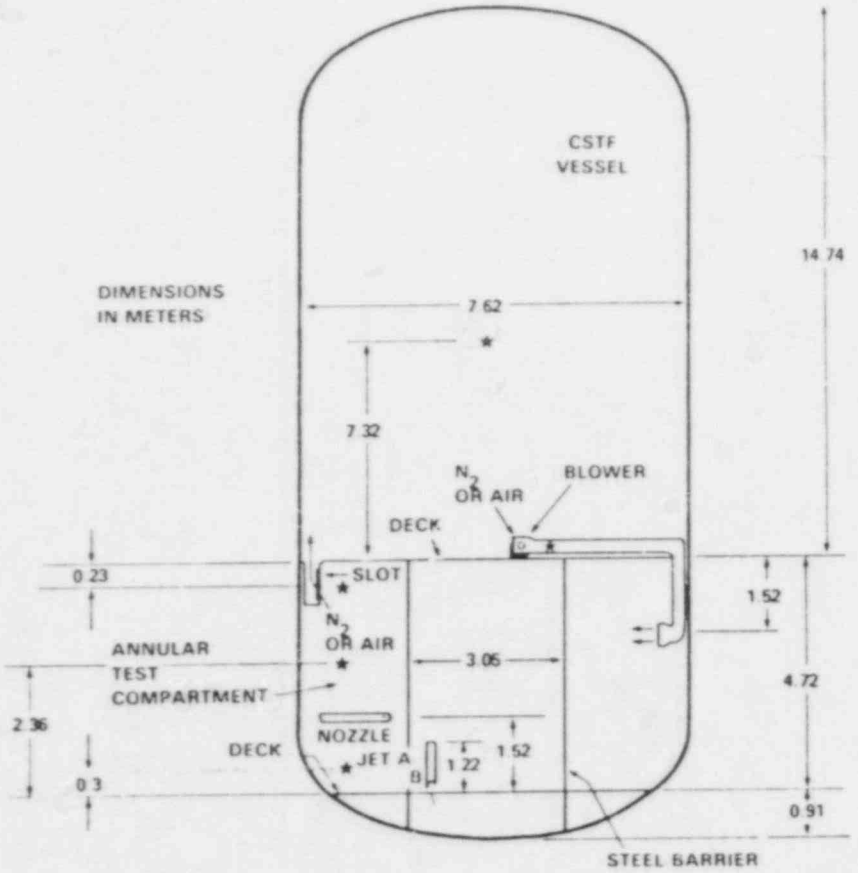

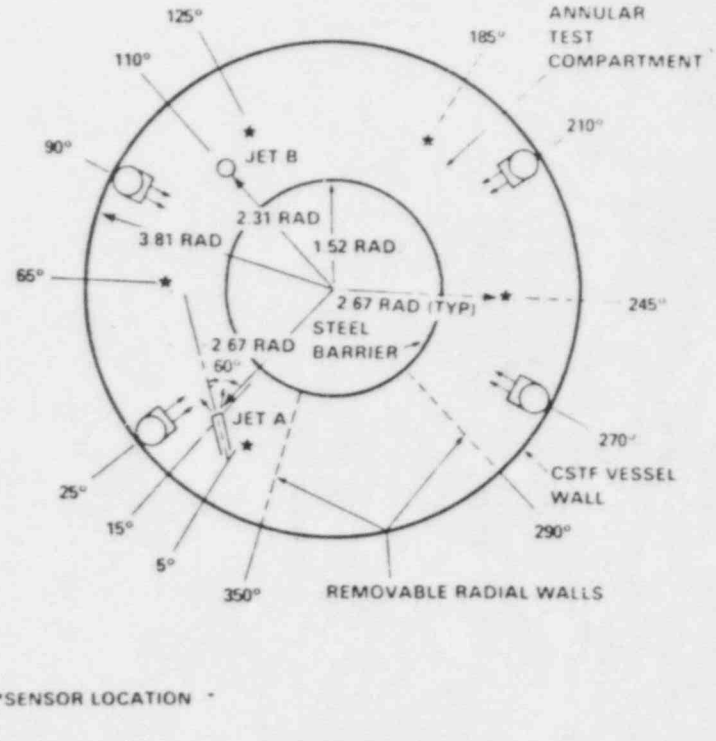

Figure 176 Test compartment geometry

wall and 1.2 m from the lower deck. The radius from the vessel axis to the nozzle was 2.31 m. A blower at the vessel axis on the upper containment deck provided air recirculation from the upper to lower compartment atmosphere. The lower compartment inlet ducts were arranged, as shown in Figure 176, at 25°, 90°, 210°, and 270°. The air flow rate with the blower operating was 109 m^3/min distributed through four openings each 0.73 m in height by 1.41-m wide.

The outlet air flow passages were 24 vertical slots 0.64-m high by 4.3-cm wide. The slots were made in the wall of circular duct segments suspended from the ceiling of the compartment. The slots were spaced along the periphery of the compartment, over the 300° segment, as shown in Figure 177.

Fifteen instrumentation locations for the lower containment test compartment are illustrated schematically in Figure 176. There were three height locations for each of the five annular locations (5°, 65°, 125°, 185°, and 245°) (see Table 44 and Table 45) all at a radius of 2.7 m. The instrumentation for each measurement station is listed in Table 9.2. Additional gas sample points and thermocouples were located at 7.32 m above the upper deck at the vessel axis and at the blower discharge.

The test vessel was vented through a 25-cm diameter pipe located at 290° and 7.9 m above the test compartment ceiling. The hydrogen-steam-nitrogen gas mixture was vented through a water bubbler to the building exhaust system during test HM-5. A nitrogen purge was provided upstream of the water bubbler during test HM-5 to dilute the hydrogen-nitrogen mixture and to prevent any possibility of air inleakage. The helium-steam-air gas mixture was vented directly to the exhaust system during test HM-6. The exhaust system included a scrubber system, HEPA filters, building exhaust tunnel, sand filter, blower, and 61-m stack.

Containment vessel pressure relative to atmospheric was measured with a differential pressure transducer. The vessel pressure was measured at a point 6.4 m above the test compartment ceiling. The test sequence for the two standard problem experiments includes the following steps:

1. place temporary seals over the test compartment outlet vents.
2. purge with N_2 for test HM-5 only
3. heat test compartment volume to near 66°C while maintaining upper containment near 35°C until steady state reached
4. start data acquisition system
5. remove temporary seals
6. start recirculation blower

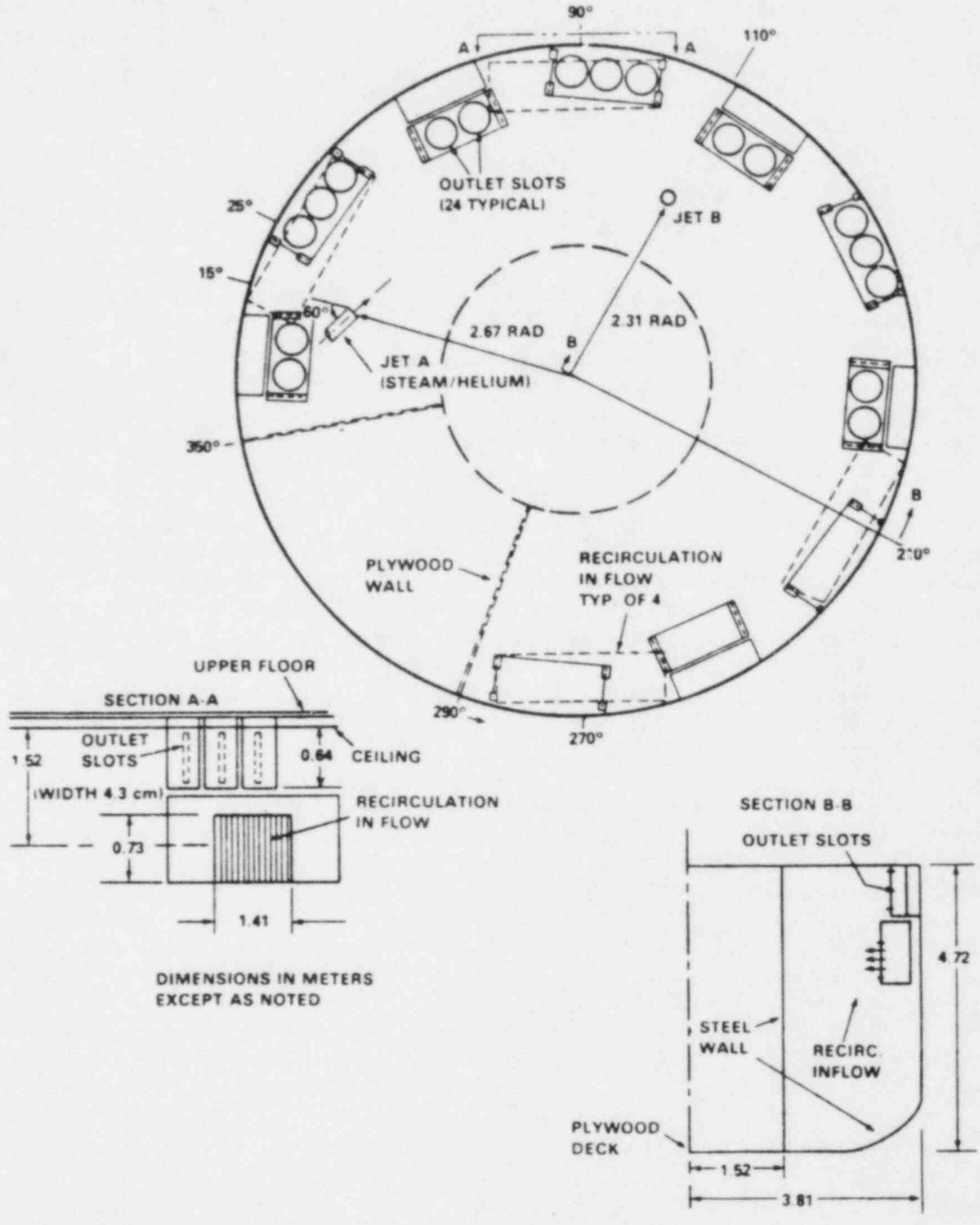

Figure 177 Test compartment air recirculation system details

Table 44 Lower test compartment height locations

Designation	Location
Top	0.23 m below the ceiling
Midplane	2.36 m up from the lower deck
Bottom	0.3 m up from the lower deck

Table 45 Instrumentation lower containment test compartment

Sensor Location	Point No	Gas Velocity Probe	Gas Sample
5°, Top	1	Yes	Yes
65°, Top	2	No	Yes
125°, Top	3	No	Yes
185°, Top	4	No	Yes
245°, Top	5	No	Yes
5°, Midplane	15	No	No
65°, Midplane	16	No	No
125°, Midplane	8	Yes	Yes
185°, Midplane	17	No	No
245°, Midplane	18	No	No
5°, Bottom	6	Yes	Yes
65°, Bottom	14	No	No
125°, Bottom	7	Yes	Yes
185°, Bottom	9	Yes	Yes
245°, Bottom	10	Yes	Yes
Total sensors		6	10

7. start steam injection
8. start H_2 or He flow and continue for approximately 10 minutes
9. stop H_2 or He flow
10. stop steam flow
11. continue data logging until one hour after start of H_2 or He flow.

Test HM-5 consisted of a horizontal high-velocity hydrogen-steam jet into a nitrogen atmosphere. Test HM-6 involved a vertical helium-steam jet release into an air atmosphere. The panel seal was removed at 11 min for test HM-5

and at 1 min for test HM-6. The blower was turned on at 11.8 min for test HM-5 and at 4.8 min for test HM-6.
The hydrogen-steam and helium-steam source jet time-dependent parameters are plotted in Figures 178 and 181 for tests HM-5 and HM-6 respectively. Hydrogen or helium flow was measured with a thermal mass flowmeter. Differential pressure drop across an orifice was measured to calculate steam mass flow. The nozzle temperature was measured both 1 m upstream of the nozzle and at the nozzle opening, with good agreement. The gas-steam line was preheated prior to the jet release. The nozzle gas temperature cooled when steam flow was initiated, probably due to the presence of some condensed steam. After condensed steam was blown from the steam supply line the jet gas temperature increased rapidly. Test compartment initial air and wall temperatures prior to testing are shown in Table 46.

The gas recirculation system provided 108 m^3/min of upper containment nitrogen or air to the lower compartment region during both tests. The time-dependent H_2 or He concentration at the blower discharge is plotted in Figure 179 for test HM-5 and Figure 182 for test HM- 6. It was assumed that the recirculation nitrogen or air is saturated with water vapor once steam release has started. The H_2 or He concentrations provided for the blower discharge location are on a dry basis with all water vapor removed. The recirculation nitrogen and air temperatures are shown in Figures 180 and 183. The recirculation air temperature for test HM-5 is relatively high prior to the blower being turned on due to back flow of some heated gas through the recirculation system.

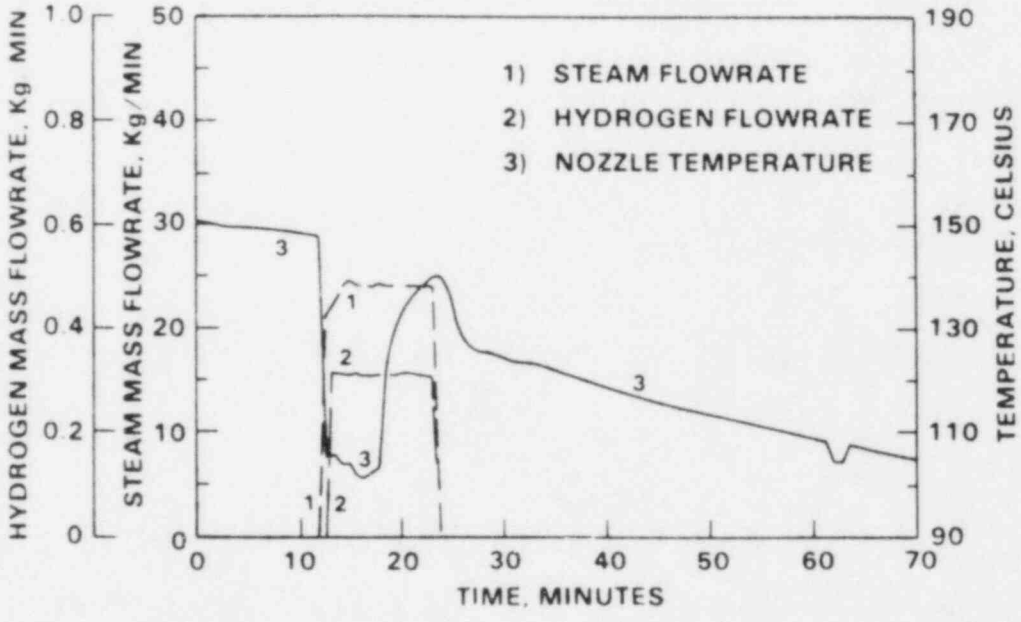

Figure 178 HM-5 nozzle flow rates and temperatures

Table 46 Initial temperatures

Test Number	Location	Temperature, °C
HM-5	Gas Temperature:	
	upper level	64.0
	middle level	62.0
	lower level	60.0
	Inner Wall Temperature:	
	upper level	65.2
	middle level	65.0
	lower level	61.2
	Outer Wall Temperatures:*	
	upper level	58.0 - 86.2
	middle level	47.6 - 65.0
	lower level	58.7 - 77.1
HM-6	Gas Temperature:	
	upper level	64.0
	middle level	62.8
	lower level	61.7
	Inner Wall Temperature:	
	upper level	64.0
	middle level	64.5
	lower level	62.7
	Outer Wall Temperature:*	
	upper level	57.8 - 73.4
	middle level	50.6 - 66.1
	lower level	62.3 - 82.3

* Temperature range given because of wide variation in measured wall temperatures

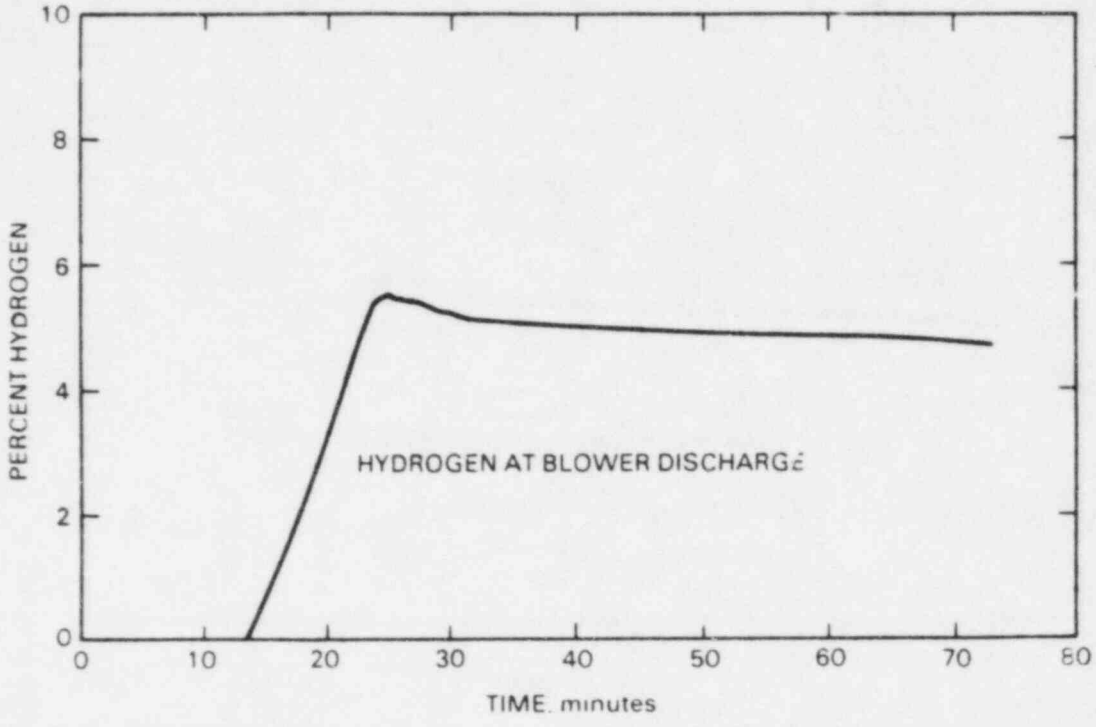

Figure 179 Hydrogen concentration at blower discharge for test HM-5

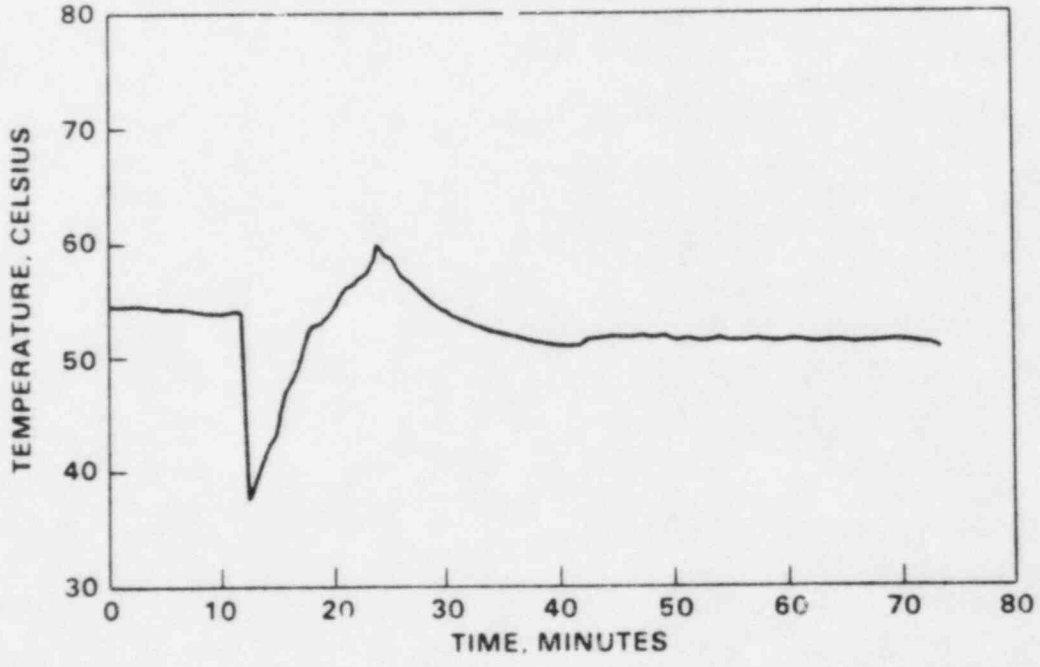

Figure 180 Nitrogen temperature at blower discharge for test HM-5

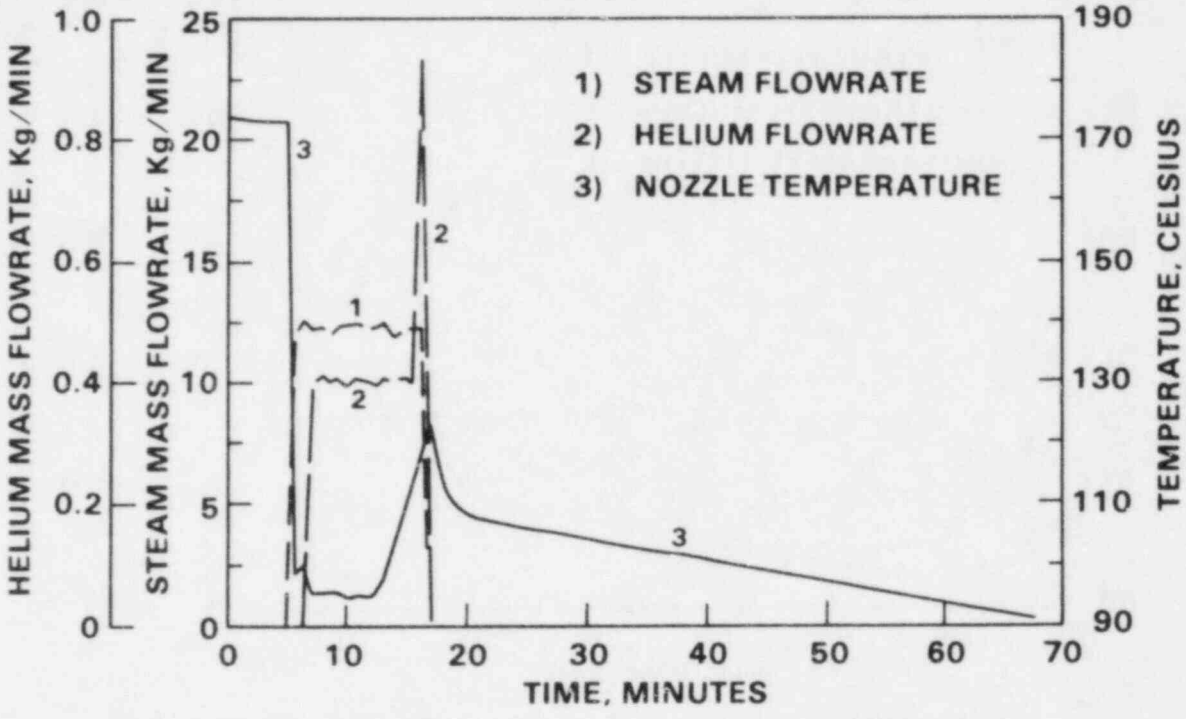

Figure 181 Test HM-6 nozzle flow rates and temperatures

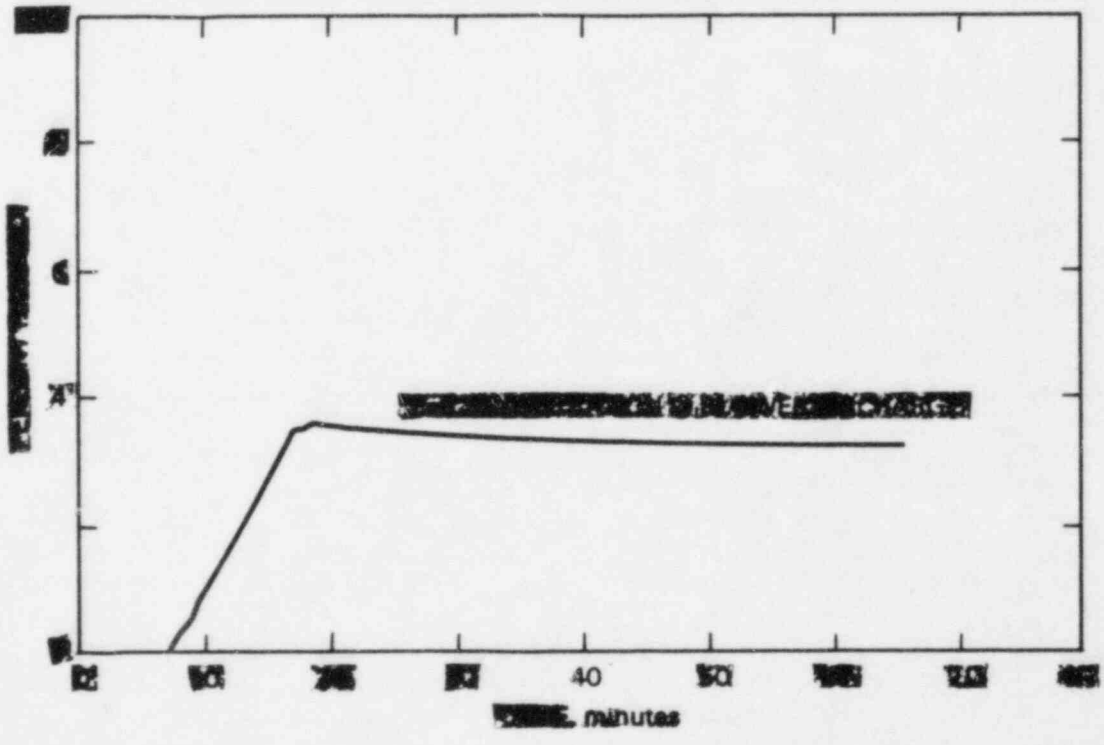

Figure 182 Helium concentration at blower discharge for test HM-6

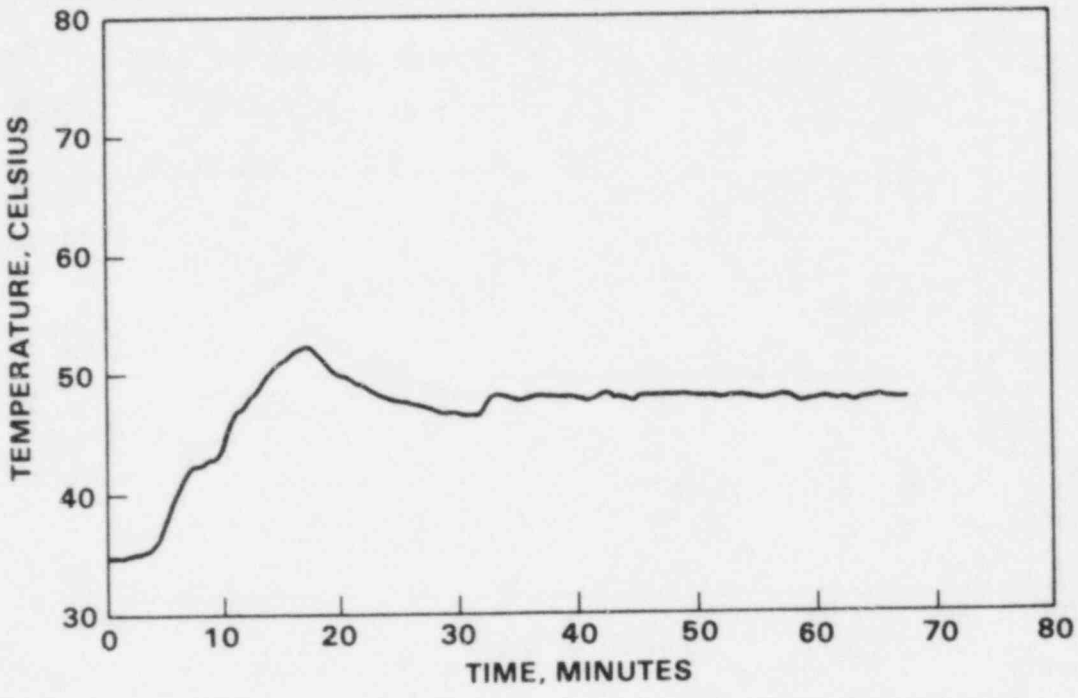

Figure 183 Air temperature at blower discharge for test HM-6

9.2 COBRA-TF Model Description

9.2.1 Pretest Blind Calculation

Two separate meshes were used to model the CSTF. The first mesh was used to perform blind, pretest predictions for tests HM-5 and HM-6. This mesh is shown in Figures 184, 185, and 186. Part (a) of Figure 184 shows a cross-sectional view of the mesh and part (b) shows the vertical height of the mesh. The annular test section was divided into five vertical sections. This was done to accommodate the location of the horizontal jet (Jet A in Figure 184), the locations of the blower discharge vents, and the locations of the outlet slots. The five sections permitted the use of a different vertical length increment for the mesh at each level. Each section was divided into 50 mesh cells (or channels 1 node high) as shown in Figure 184(a). Additional channels were added to sections 4 and 5 (Figures 185 and 186) to model the blower inlet vents and outflow slots at the top of the test section. A finer mesh was used in the vicinity of the horizontal jet, so that the momentum of the jet would be conserved in the calculation. This was done because it was believed that the momentum of the jet would be a predominant factor in the mixing behavior of the test section. The same mesh was used for test HM-6, the vertical jet test (Jet B in Figure 184), as there was

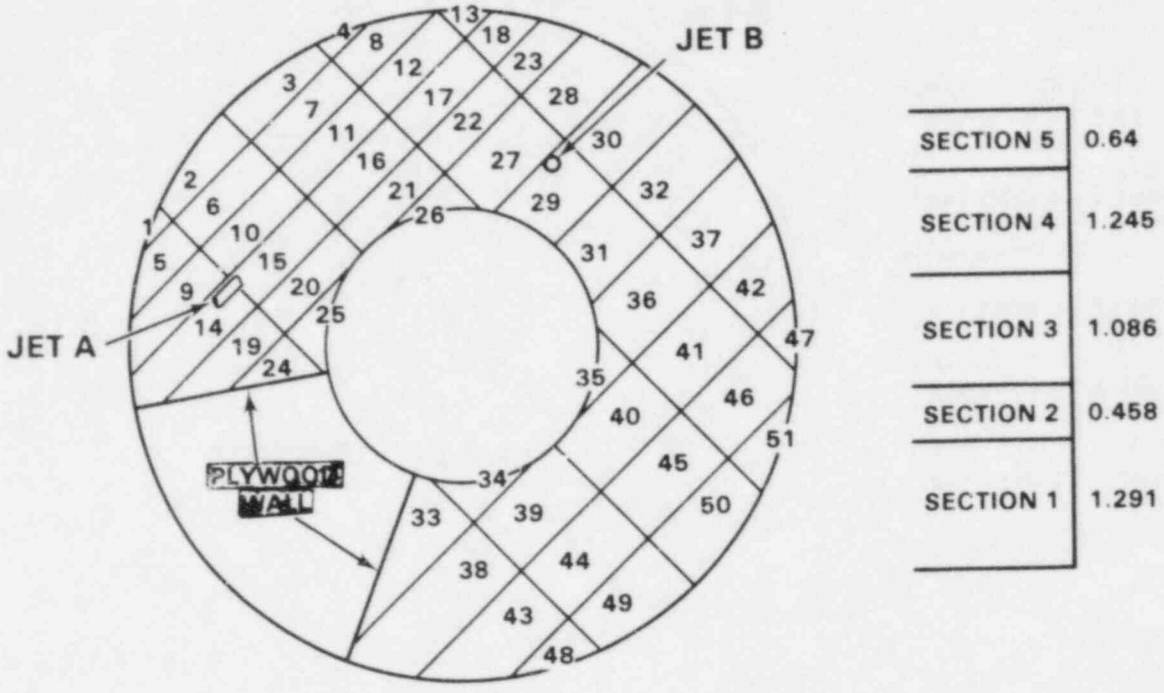

Figure 184 COBRA-TF mesh for CSTF pretest predictions

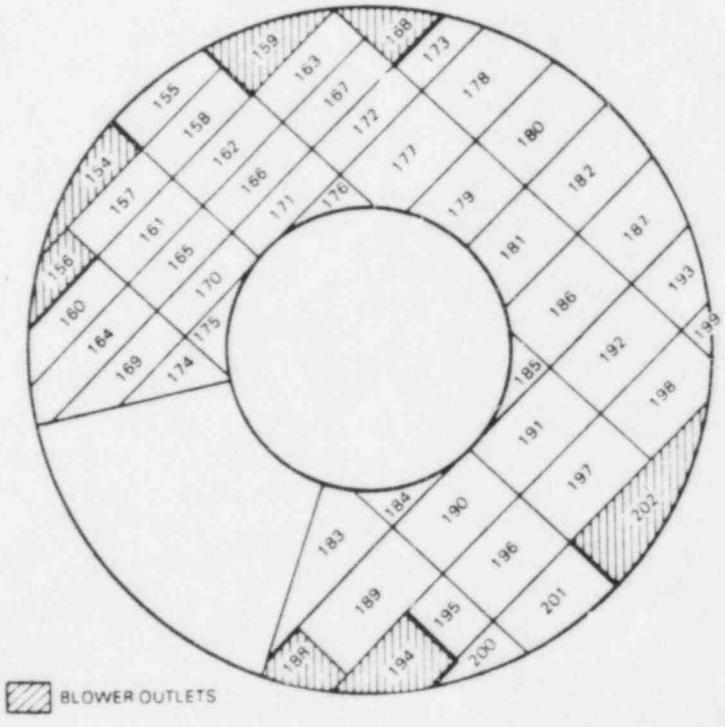

Figure 185 Mesh for section 4

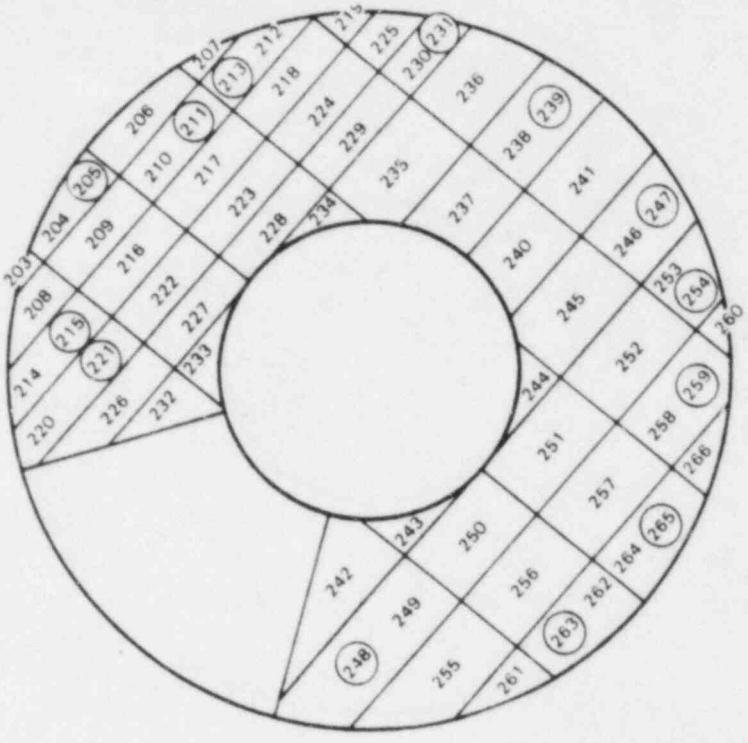

Figure 186 Mesh for section 5

insufficient time before the pretest calculations were due to generate a new mesh. Thus, a coarser mesh was used in the vicinity of the vertical jet. This would result in a more rapid dissipation of the jet momentum. Therefore, less mixing due to jet momentum should be expected. A total of 266 mesh cells were used to model the test section. Each mesh cell was modeled with a single channel, one node high. The area for each channel was calculated from the dimensions provided in Figures 176 and 177 using the assumption that the mesh lines shown in Figure 184 were perpendicular to the horizontal nozzle in the one direction and parallel to the nozzle in the other. The channel input data are given in Table 47. Channels in the second and third sections have the same flow area and wetted perimeter as channels occupying the same location in the first section. Sections 4 and 5 contain additional channels to model blower inlet or outlet ducts. Channels with the same flow areas are listed together in Table 47, while unique channels containing blower inlet or outlet ducts are listed separately. The first section was modeled with channels 1 through 51, the second with channels 52 through 102, the third with channels 103 through 153, the fourth with channels 154 through 202, and the fifth with channels 203 through 266. The input data for the gaps are given in Table 48. The thermal conductor geometry type locations are shown in Figure 187. There are 18 geometry types. The input data for each geometry type is provided in Table 49. The thickness of the inner wall was assumed to be 0.2 in. The outer wall was modeled as a composite wall consisting of 0.65 in. of steel in the inside covered by 1.0 in. of glass fiber insulation. The inner wall was

Table 47 Channel input data

Channel Numbers	Area ($in.^2$)	Wetted P (in.)	Comments
1, 52, 103, 203	107.7	23.32	
2, 53, 104	760.3	50.95	
3, 54, 105, 206	760.3	50.95	
4, 55, 106, 207	107.7	23.32	
5, 56, 107, 156, 208	838.9	31.90	
6, 57, 108, 157, 209	901.1	0.001	18.027 x 49.987 = 901.1 in.2
7, 58, 101	901.1	0.001	
8, 59, 110	838.9	31.90	
9, 60, 111, 160	1027.0	25.33	
10, 61, 112, 161, 216	901.1	0.001	
11, 62, 113, 162, 217	901.1	0.001	
12, 63, 114, 163, 218	899.0	3.24	
13, 64, 115, 219	127.9	22.10	
14, 65, 116, 164	1257.0	26.63	
15, 66, 117, 165, 222	901.1	0.001	
16, 67, 118, 166, 223	901.1	0.001	
17, 68, 119, 167, 224	901.1	0.001	
18, 69, 120, 225	396.4	19.159	
19, 70, 121, 168, 226	871.6	31.43	
20, 71, 122, 169, 227	901.1	0.001	
21, 72, 123, 171, 228	901.1	0.001	
22, 73, 124, 172, 229	901.1	0.001	
23, 74, 125, 173	598.1	20.32	
24, 75, 126, 174, 232	440.3	43.26	
25, 76, 127, 175, 233	397.9	57.43	
26, 77, 128, 176, 234	399.1	59.17	
27, 78, 129, 177, 235	1493.0	3.47	
28, 79, 130, 178, 236	1282.0	31.41	
29, 80, 131, 179, 237	1279.0	31.32	
30, 81, 132, 180	1466.0	30.11	
31, 82, 133, 181, 240	1283.0	31.41	
32, 83, 134, 182, 241	1470.0	30.19	
33, 84, 135, 183, 242	1422.0	90.80	
34, 85, 136, 184, 243	407.0	59.17	
35, 86, 137, 185, 244	407.0	59.17	
36, 87, 138, 186, 245	1497.0	3.385	
37, 88, 139, 187	1284.0	31.52	
38, 89, 140	2370.0	31.06	
39, 90, 141, 190, 250	1499.0	0.001	29.992 x 49.987 = 1499.0 in.2
40, 91, 142, 191, 251	1499.0	0.001	
41, 92, 143, 192, 252	1499.0	0.001	
42, 93, 144, 193	885.5	34.79	
43, 94, 145, 255	1693.0	42.56	

(Table 47, continued)

Channel Numbers	Area ($in.^2$)	Wetted P (in.)	Comments
44, 95, 146, 196, 256	1499.0	0.001	
45, 96, 147, 197, 257	1499.0	0.001	
46, 97, 148, 198	1464.0	20.57	
47, 98, 149, 199, 260	450.5	29.63	
48, 99, 150, 200, 261	480.7	45.53	
49, 100, 151, 201	1359.0	50.96	
50, 101, 152	1359.0	50.96	
51, 102, 153, 266	480.7	45.53	
154,	868.0	74.27	Blower outlet at 25°
155	868.0	74.27	
158	1320.5	0.001	
159	419.5	31.9	Blower outlet at 90°
168	524.3	41.3	Blower outlet at 90°
188	1185.0	31.06	Blower outlet at 270°
189	1185.0	0.001	
194	1129.0	42.56	Blower outlet at 270°
195	564.0	0.001	
205	397.51	122.4	Outlet slots at 25°
204	362.8	173.4	
211	132.5	40.8	Outlet slot at 70°
210	768.6	40.8	
213	132.5	40.8	Outlet slot at 70°
212	706.4	72.7	
215	132.5	40.8	Outlet slot at 5°
214	894.5	66.13	
221	132.5	40.8	Outlet slot at 5°
220	1124.5	67.4	
231	132.5	40.8	Outlet slot at 90°
230	465.6	61.1	
239	265.0	81.6	Outlet slot at 115°
238	1201.0	111.7	
247	265.0	81.6	Outlet slot at 160°
246	1019.0	113.0	
248	397.5	122.4	Outlet slot at 275°
249	1972.5	153.5	
258	1199.0	102.2	
263	265.0	81.6	Outlet slot at 250°
262	1094.0	132.6	
265	265.0	81.6	Outlet slot at 220°
264	1094.0	132.6	
259	265.0	81.6	Outlet slot at 190°
258	1199.0	102.2	
254	132.5	40.8	Outlet slot at 160°
253	753.0	75.6	
202	1839.7	96.49	Blower outlet at 210°

Table 48 Gap Input Data

Gap No.	Channels Connected by Gap		Width (in.)	Length (in.)	Loss Coefficients	FWALL	IGAPB	IGAPA	FACTOR	IGAP	JGAP
1	1	2	9.45	39.19		0.0	0.25		81		
2	1	5	21.30	15.31		0.0	0.25		82		
3	2	3	18.03	49.99		0.0	0.5		83		
4	2	6	49.99	18.03		0.0	0.0		84		
5	3	4	9.45	39.19		0.0	0.25		85		
6	3	7	49.99	18.03		0.0	0.0		86		
7	4	8	21.30	15.31		0.0	0.25		87		
8	5	6	18.03	46.29		0.0	0.0		88		
9	5	9	47.55	18.03		0.0	0.5		89		
10	6	7	18.03	49.99		0.0	0.0		90		
11	6	10	49.99	18.03		0.0	0.0		91		
12	6	10	18.03	46.29		0.0	0.0		92		
13	7	11	49.99	18.03		0.0	0.0		93		
14	8	12	47.55	18.03		0.0	0.0		94		
15	9	10	18.03	53.21		0.0	0.0		95		
16	9	14	65.31	18.03		0.0	0.5		96		
17	10	11	18.03	49.99		0.0	0.0		97		
18	10	15	49.99	18.03		0.0	0.0		98		
19	11	12	18.03	49.99		0.0	0.0		99		
20	11	16	49.99	18.03		0.0	0.0		100		
21	12	13	15.89	32.65		0.0	0.25		101		
22	12	17	49.99	18.03		0.0	0.0		102		
23	13	18	15.33	18.03		0.0	0.25		103		
24	14	15	18.03	58.22		0.0	0.0		104		
25	14	19	61.2	18.03		0.0	0.5		105		
26	15	16	18.03	49.99		0.0	0.0		106		
27	15	20	49.99	18.03		0.0	0.0		107		
28	16	17	18.03	49.99		0.0	0.0		108		
29	16	21	49.99	18.03		0.0	0.0		109		
30	17	18	18.03	35.87		0.0	0.0		110		
31	17	22	49.99	18.03		0.0	0.0		111		
32	18	23	28.19	18.03		0.0	0.5		112		
33	19	20	18.03	49.15		0.0	0.0		113		
34	19	24	35.45	18.03		0.0	0.5		114		
35	20	21	18.03	49.99		0.0	0.5		115		
36	20	25	49.99	18.03		0.0	0.0		116		
37	21	22	18.03	49.99		0.0	0.0		117		
38	21	26	49.99	18.03		0.0	0.0		118		
39	22	23	18.03	41.43		0.0	0.0		119		
40	22	27	49.99	18.03		0.0	0.0		121		
41	23	28	37.54	18.03		0.0	0.5		121		
42	24	25	24.82	30.22		0.0	0.5		122		
43	26	27	26.95	27.49		0.0	0.0		123		
44	27	28	29.91	46.87		0.0	0.0		124		

(Table 48, continued)

Gap No.	Channels Connected by Gap		Width (in.)	Length (in.)	Loss Coefficients	FWALL	IGAPB	IGAPA	FACTOR	IGAP	JGAP
45	27	29	48.16	29.91		0.0	0.5		125		
46	28	30	46.97	29.91		0.0	0.5		126		
47	29	30	29.91	46.31		0.0	0.0		127		
48	29	31	40.15	29.95		0.0	0.5		128		
49	30	32	49.99	29.95		0.0	0.5		129		
50	31	32	29.99	46.31		0.0	0.0		130		
51	31	36	48.21	29.99		0.0	0.5		131		
52	32	37	46.96	29.99		0.0	0.5		132		
53	33	34	26.96	51.82		0.0	0.5		133		
54	33	38	76.65	29.99		0.0	0.5		134		
55	34	39	49.99	24.16		0.0	0.0		135		
56	35	36	26.96	34.49		0.0	0.0		136		
57	35	40	49.99	24.16		0.0	0.0		137		
58	36	37	29.99	46.10		0.0	0.0		138		
59	36	41	49.99	29.97		0.0	0.0		139		
60	37	42	37.47	29.99		0.0	0.5		140		
61	38	39	29.99	64.08		0.0	0.0		141		
62	38	43	69.98	29.99		0.0	0.5		142		
63	39	40	29.99	49.99		0.0	0.0		143		
64	39	40	49.99	29.99		0.0	0.0		144		
65	40	41	29.99	49.99		0.0	0.0		145		
66	40	45	49.99	29.99		0.0	0.0		146		
67	41	42	29.99	39.36		0.0	0.0		147		
68	41	46	49.99	29.99		0.0	0.0		148		
69	42	47	29.99	25.89		0.0	0.25		149		
70	43	44	29.99	52.49		0.0	0.0		150		
72	44	45	29.99	49.99		0.0	0.0		152		
73	44	49	49.99	27.85		0.0	0.0		153		
74	45	46	29.99	49.99		0.0	0.0		154		
75	45	50	29.99	27.85		0.0	0.0		155		
76	46	47	21.80	34.99		0.0	0.25		156		
77	46	51	39.99	25.70		0.0	0.25		157		
77	46	51	39.99	25.70		0.0	0.25		157		
78	48	49	21.42	49.99		0.0	0.25		158		
79	49	50	29.99	49.99		0.0	0.5		159		
80	50	51	21.42	49.99		0.0	0.25		160		
81	50	51	9.45	39.19		0.0	0.25		161		
82	52	53	21.30	15.31		0.0	0.25		162		
83	52	56	18.03	49.99		0.0	0.5		163		
84	53	54	49.99	18.03		0.0	0.0		164		
85	53	57	9.45	39.19		0.0	0.25		165		
86	54	55	49.99	18.03		0.0	0.0		166		
87	54	58	21.30	15.31		0.0	0.25		167		
88	55	59	18.03	46.29		0.0	0.0		168		

(Table 48, continued)

Gap No.	Channels Connected by Gap		Width (in.)	Length (in.)	Loss Coefficients	FWALL	IGAPB	IGAPA	FACTOR	IGAP	JGAP
89	56	57	47.55	18.03		0.0	0.5		169		
90	56	60	18.03	49.99		0.0	0.0		170		
91	57	58	49.99	18.03		0.0	0.0		171		
92	58	59	18.03	46.29		0.0	0.0		172		
93	58	62	49.99	18.03		0.0	0.0		173		
94	59	63	47.55	18.03		0.0	0.0		174		
95	60	61	18.03	53.21		0.0	0.0		175		
96	60	65	65.31	18.03		0.0	0.5		176		
97	61	62	18.03	49.99		0.0	0.0		177		
98	61	66	49.99	18.03		0.0	0.0		178		
99	62	63	18.03	49.99		0.0	0.0		179		
100	62	67	49.99	18.03		0.0	0.0		180		
101	63	64	15.89	32.65		0.0	0.25		181		
102	63	68	49.99	18.03		0.0	0.0		182		
103	64	69	15.33	18.03		0.0	0.25		183		
104	65	66	18.03	58.22		0.0	0.0		184		
105	65	70	61.2	18.03		0.0	0.5		185		
106	66	67	18.03	49.99		0.0	0.0		186		
107	66	71	49.99	18.03		0.0	0.0		187		
108	67	68	18.03	49.99		0.0	0.0		188		
109	67	72	49.99	18.03		0.0	0.0		189		
110	68	69	18.03	35.87		0.0	0.0		190		
111	68	73	49.99	18.03		0.0	0.0		191		
112	69	74	28.19	18.03		0.0	0.5		192		
113	70	71	18.03	49.15		0.0	0.0		193		
114	70	75	35.45	18.03		0.0	0.5		194		
115	71	72	18.03	49.99		0.0	0.5		195		
116	71	76	49.99	18.03		0.0	0.0		196		
117	72	73	18.03	49.99		0.0	0.0		197		
118	72	77	49.99	18.03		0.0	0.0		198		
119	73	74	18.03	41.43		0.0	0.0		199		
120	73	78	49.99	18.03		0.0	0.0		200		
121	74	79	37.54	18.03		0.0	0.5		201		
122	75	76	24.82	30.22		0.0	0.5		202		
123	78	79	26.95	27.49		0.0	0.0		203		
124	78	79	29.91	46.87		0.0	0.0		204		
125	78	80	48.16	29.91		0.0	0.5		205		
126	79	81	46.97	29.91		0.0	0.5		206		
127	80	81	29.91	46.31		0.0	0.0				
128	80	82	40.15	29.95		0.0	0.5		208		
129	81	83	49.99	29.95		0.0	0.5		209		
130											
131	82	87	48.21	29.99		0.0	0.5		211		
132	83	88	46.96	29. 99		0.0	0.5		212		

(Table 48, continued)

Gap No.	Channels Connected by Gap		Width (in.)	Length (in.)	Loss Coefficients	FWALL	IGAPB	IGAPA	FACTOR	IGAP	JGAP
133	84	85	26.96	51.82		0.0	0.5		213		
134	84	89	76.65	29.99		0.0	0.5		214		
135	85	90	49.99	24.16		0.0	0.0		215		
136	86	87	26.96	34.49		0.0	0.0		216		
137	86	91	49.99	24.16		0.0	0.0		217		
138	87	88	29.99	46.10		0.0	0.0		218		
139	87	92	49.99	29.97		0.0	0.0		219		
140	88	93	37.47	29.99		0.0	0.5		220		
141	89	90	29.99	64.08		0.0	0.0		221		
142	89	94	69.98	29.99		0.0	0.5		222		
143	90	91	29.99	49.99		0.0	0.0		223		
144	90	95	49.99	29.99		0.0	0.0		224		
145	91	92	29.99	49.99		0.0	0.0		225		
146	91	96	49.99	29.99		0.0	0.0		226		
147	92	93	29.99	39.36		0.0	0.0		227		
148	92	97	49.99	29.99		0.0	0.0		228		
149	93	98	29.99	25.89		0.0	0.25		229		
150	94	95	29.99	52.49		0.0	0.0		230		
151	94	99	39.99	25.70		0.0	0.25		231		
152	95	96	29.99	49.99		0.0	0.0		232		
153	95	100	49.99	27.85		0.0	0.0		233		
154	96	97	29.99	49.99		0.0	0.0		234		
155	96	101	29.99	27.85		0.0	0.0		235		
156	97	98	21.80	34.99		0.0	0.25		236		
157	97	102	39.99	25.70		0.0	0.25		237		
158	99	100	39.99	25.70		0.0	0.25		238		
159	100	101	21.42	49.99		0.0	0.25		239		
160	101	102	9.45	39.19		0.0	0.25		240		
161	103	104	9.45	39.19		0.0	0.25		0		
162	103	107	21.30	15.31		0.0	0.25		0		
163	104	105	18.03	49.99		0.0	0.5		0		
164	104	108	49.99	18.03		0.0	0.0		0		
165	105	106	9.45	39.19		0.0	0.25		0		
166	105	109	49.99	18.03		0.0	0.0		242		
167	106	110	21.30	15.31		0.0	0.25		0		
168	107	108	18.03	46.29		0.0	0.0		0		
169	107	111	47.55	18.03		0.0	0.5		0		
170	108	109	18.03	49.99		0.0	0.0		244		
171	108	112	49.99	18.03		0.0	0.0		245		
172	109	110	18.03	46.29		0.0	0.0		0		
173	109	113	49.99	18.03		0.0	0.0		246		
174	110	114	47.55	18.03		0.0	0.0		0		
175	111	112	18.03	53.21		0.0	0.0		248		
176	111	116	65.31	18.03		0.0	0.5		249		

(Table 48, continued)

Gap No.	Channels Connected by Gap		Width (in.)	Length (in.)	Loss Coefficients	FWALL	IGAPB	IGAPA	FACTOR	IGAP	JGAP
177	112	113	18.03	49.99		0.0	0.0		250		
178	112	117	49.99	18.03		0.0	0.0		251		
179	113	114	18.03	49.99		0.0	0.0		252		
180	113	118	49.99	18.03		0.0	0.0		253		
181	114	115	15.89	32.65		0.0	0.25		0		
182	114	119	49.99	18.03		0.0	0.0		255		
183	115	120	15.33	18.03		0.0	0.25		0		
184	116	117	18.03	58.22		0.0	0.0		256		
185	116	121	61.2	18.03		0.0	0.5		257		
186	117	118	18.03	49.99		0.0	0.0		258		
187	117	122	49.99	18.03		0.0	0.0		259		
188	118	119	18.03	49.99		0.0	0.0		260		
189	118	123	49.99	18.03		0.0	0.0		261		
190	119	120	18.03	35.87		0.0	0.0		0		
191	119	124	49.99	18.03		0.0	0.0		263		
192	120	125	28.19	18.03		0.0	0.5		0		
193	121	122	18.03	49.15		0.0	0.0		264		
194	121	126	35.45	18.03		0.0	0.5		265		
195	122	123	18.03	49.99		0.0	0.5		266		
196	122	127	49.99	18.03		0.0	0.0		267		
197	123	124	18.03	49.99		0.0	0.0		268		
198	123	128	49.99	18.03		0.0	0.0		269		
199	124	125	18.03	41.43		0.0	0.0		270		
200	124	129	49.99	18.03		0.0	0.0		271		
201	125	130	37.54	18.03		0.0	0.5		272		
202	126	127	24.82	30.22		0.0	0.5		273		
203	128	129	26.95	27.49		0.0	0.0		274		
204	129	130	29.91	46.87		0.0	0.0		275		
205	129	131	48.16	29.91		0.0	0.5		276		
206	130	132	46.97	29.91		0.0	0.5		277		
207	131	132	29.91	46.31		0.0	0.0		278		
208	131	133	40.15	29.95		0.0	0.5		279		
209	132	134	49.99	29.95		0.0	0.5		280		
210	133	134	29.99	46.31		0.0	0.0		281		
211	133	138	48.21	29.99		0.0	0.5		282		
212	134	139	46.96	29.99		0.0	0.5		283		
213	135	136	26.96	51.82		0.0	0.5		284		
214	135	140	76.65	29.99		0.0	0.5		285		
215	136	141	49.99	24.16		0.0	0.0		286		
216	137	138	26.96	34.49		0.0	0.0		287		
217	138	142	49.99	24.16		0.0	0.0		288		
218	138	139	29.99	46.10		0.0	0.0		289		
219	138	143	49.99	29.97		0.0	0.0		290		
220	139	144	37.47	29.99		0.0	0.5		291		

(Table 48, continued)

Gap No.	Channels Connected by Gap		Width (in.)	Length (in.)	Loss Coefficient	FWALL	IGAPB	IGAPA	FACTOR	IGAP	JGAP
221	140	141	29.99	64.08		0.0	0.0		293		
222	140	145	69.98	29.99		0.0	0.5		294		
223	141	142	29.99	49.99		0.0	0.0		295		
224	141	146	49.99	29.99		0.0	0.0		296		
225	142	143	29.99	49.99		0.0	0.0		297		
226	142	147	49.99	29.99		0.0	0.0		298		
227	143	144	29.99	39.36		0.0	0.0		299		
228	143	148	49.99	29.99		0.0	0.0		300		
229	144	149	29.99	25.89		0.0	0.25		301		
230	145	146	29.99	52.49		0.0	0.0		303		
231	145	150	39.99	25.70		0.0	0.25		304		
232	146	147	29.99	49.99		0.0	0.0		305		
233	146	151	49.99	27.85		0.0	0.0		306		
234	147	148	29.99	49.99		0.0	0.0		307		
235	147	152	29.99	27.85		0.0	0.0		0		
236	148	149	21.80	34.99		0.0	0.25		309		
237	148	153	39.99	25.70		0.0	0.25		0		
238	150	151	39.99	25.70		0.0	0.25		312		
239	151	152	21.42	49.99		0.0	0.25		0		
240	152	153	29.99	49.99		0.0	0.5		0		
241	154	157	21.69	18.03		0.0	0.5		0		
242	155	158	49.99	18.03		0.0	0.5		319		
243	156	157	10.84	46.29		0.0	0.0		0		
244	157	158	18.03	49.99		0.0	0.5		323		
245	159	161	49.99	18.03		0.0	0.0		324		
246	158	162	49.99	18.03		0.0	0.0		327		
247	159	163	46.27	18.03		0.0	0.0		0		
248	160	161	18.03	53.21		0.0	0.0		331		
249	160	164	65.31	18.03		0.0	0.5		332		
250	161	162	18.03	49.99		0.0	0.0		333		
251	161	165	49.99	18.03		0.0	0.0		334		
252	162	163	18.03	49.99		0.0	0.0		335		
253	162	166	49.99	18.03		0.0	0.0		336		
254	163	168	8.14	32.65		0.0	0.5		0		
255	163	167	49.99	18.03		0.0	0.5		338		
256	164	165	18.03	58.22		0.0	0.0		341		
257	164	169	61.20	18.03		0.0	0.5		342		
258	165	166	18.03	49.99		0.0	0.0		343		
259	165	170	49.99	18.03		0.0	0.0		344		
260	166	167	18.03	49.99		0.0	0.0		345		
261	166	171	49.99	18.03		0.0	0.0		346		
262	167	168	8.14	35.87		0.0	0.0		0		
263	167	172	49.99	18.03		0.0	0.0		347		
264	169	170	18.03	49.15		0.0	0.0		348		

(Table 48, continued)

Gap No.	Channels Connected by Gap		Width (in.)	Length (in.)	Loss Coefficients	FWALL	IGAPB	IGAPA	FACTOR	IGAP	JGAP
265	169	174	35.45	18.03		0.0	0.5		349		
266	170	171	18.03	49.99		0.0	0.5		350		
267	170	175	49.99	18.03		0.0	0.0		351		
268	171	172	18.03	49.99		0.0	0.0		352		
269	171	176	49.99	18.03		0.0	0.0		353		
270	172	173	18.03	41.43		0.0	0.0		354		
271	172	177	49.99	18.03		0.0	0.0		355		
272	173	178	37.54	18.03		0.0	0.5		357		
273	174	175	24.82	30.22		0.0	0.5		358		
274	176	177	26.95	37.49		0.0	0.0		359		
275	177	178	29.91	46.87		0.0	0.0		360		
276	177	179	48.16	29.91		0.0	0.5		361		
277	178	180	46.97	29.91		0.0	0.5		362		
278	179	180	29.91	46.31		0.0	0.0		363		
279	179	181	40.15	29.95		0.0	0.5		364		
280	180	182	49.99	29.95		0.0	0.5		366		
281	181	182	29.99	46.31		0.0	0.0		367		
282	181	186	48.21	29.99		0.0	0.5		368		
283	182	187	46.96	29.99		0.0	0.5		369		
284	183	184	26.96	51.82		0.0	0.5		370		
285	183	189	57.56	29.99		0.0	0.5		371		
286	184	190	49.99	24.16		0.0	0.0		372		
287	185	186	26.96	34.49		0.0	0.0		373		
288	185	191	49.99	24.16		0.0	0.0		374		
289	186	187	29.99	46.10		0.0	0.0		375		
290	186	192	49.99	29.99		0.0	0.0		376		
291	187	193	37.47	29.99		0.0	0.5		378		
292	188	189	8.14	29.99		0.0	0.25		0		
293	189	190	49.99	29.99		0.0	0.0		380		
294	189	195	19.18	29.99		0.0	0.5		381		
295	190	191	29.99	49.99		0.0	0.5		382		
296	190	196	49.99	29.99		0.0	0.0		383		
297	191	192	29.99	49.99		0.0	0.0		384		
298	191	197	49.99	29.99		0.0	0.0		385		
299	192	193	29.99	39.36		0.0	0.0		386		
300	192	198	49.99	29.99		0.0	0.0		387		
301	193	199	19.99	25.89		0.0	0.25		389		
302	194	195	18.14	19.19		0.0	0.0		0		
303	195	196	29.99	34.58		0.0	0.0		390		
304	195	200	19.18	25.70		0.0	0.25		391		
305	196	197	29.99	49.99		0.0	0.0		392		
306	196	201	49.99	27.85		0.0	0.0		393		
307	197	198	29.99	49.99		0.0	0.0		394		
308	197	202	49.99	27.85		0.0	0.0		0		

(Table 48, continued)

Gap No.	Channels Connected by Gap		Width (in.)	Length (in.)	Loss Coefficients	FWALL	IGAPB	IGAPA	FACTOR	IGAP	JGAP
309	198	199	21.80	34.99		0.0	0.5		397		
310	198	202	39.99	25.70		0.0	0.25		0		
311	189	194	16.27	29.99		0.0	0.25		0		
312	200	201	21.42	44.99		0.0	0.25		399		
313	203	204	9.45	39.19		0.0	0.25		0		
314	203	208	21.30	15.31		0.0	0.25		0		
315	204	205	5.08	12.98		1.5	0.0		0		
316	204	206	18.03	49.99		0.0	0.0		0		
317	204	208	49.99	18.03		0.0	0.0		0		
318	206	207	9.45	39.19		0.0	0.25		0		
319	206	210	49.99	18.03		0.0	0.0		0		
320	207	212	21.30	15.31		0.0	0.25		0		
321	208	209	18.03	46.29		0.0	0.0		0		
322	208	214	47.55	18.03		0.0	0.5		0		
323	209	210	18.03	49.99		0.0	0.0		0		
324	209	216	49.99	18.03		0.0	0.0		0		
325	210	211	1.693	12.98		1.5	0.0		0		
326	210	212	18.03	46.29		0.0	0.0		0		
327	210	217	49.99	18.03		0.0	0.0		0		
328	212	213	1.693	12.98		1.5	1.5		0		
329	212	218	47.55	18.03		0.0	0.5		0		
330	214	215	1.693	12.98		1.5	1.5		0		
331	214	216	18.03	53.21		0.0	0.0		0		
332	214	220	65.31	18.03		0.0	0.5		0		
333	216	217	18.03	49.99		0.0	0.0		0		
334	216	222	49.99	18.03		0.0	0.0		0		
335	217	218	18.03	49.99		0.0	0.0		0		
336	217	223	49.99	18.03		0.0	0.0		0		
337	218	219	15.89	32.65		0.0	0.25		0		
338	218	224	49.99	18.03		0.0	0.0		0		
339	219	225	3.386	12.98		1.5	0.0		0		
340	220	221	1.693	12.98		1.5	0.0		0		
341	220	222	18.03	58.22		0.0	0.0		0		
342	220	226	61.20	18.03		0.0	0.5		0		
343	222	223	18.03	49.99		0.0	0.0		0		
344	222	227	49.99	18.03		0.0	0.0		0		
345	223	224	18.03	49.99		0.0	0.0		0		
346	223	228	49.99	18.03		0.0	0.0		0		
347	224	229	49.99	18.03		0.0	0.0		0		
348	226	227	18.03	49.15		0.0	0.0		0		
349	226	232	35.45	18.03		0.0	0.5		0		
350	227	228	18.03	49.99		0.0	0.5		0		
351	227	233	49.99	18.03		0.0	0.0		0		
352	228	229	18.03	49.99		0.0	0.0		0		

(Table 48, continued)

Gap No.	Channels Connected by Gap		Width (in.)	Length (in.)	Loss Coefficients	FWALL	IGAPB	IGAPA	FACTOR	IGAP	JGAP
265	169	174	35.45	18.03		0.0	0.5		349		
266	170	171	18.03	49.99		0.0	0.5		350		
267	170	175	49.99	18.03		0.0	0.0		351		
268	171	172	18.03	49.99		0.0	0.0		352		
269	171	176	49.99	18.03		0.0	0.0		353		
360	235	236	29.91	46.87		0.0	0.0		0		
361	235	237	48.16	29.91		0.0	0.5		0		
362	236	238	46.97	29.91		0.0	0.5		0		
363	237	238	29.91	46.31		0.0	0.0		0		
364	237	240	40.15	29.95		0.0	0.5		0		
365	238	239	3.386	12.98		1.5	0.0		0		
366	238	241	49.99	29.95		0.0	0.5		0		
367	240	241	29.99	46.31		0.0	0.0		0		
368	240	245	48.21	29.99		0.0	0.5		0		
369	241	246	46.96	29.99		0.0	0.5		0		
370	242	243	26.96	51.82		0.0	0.5		0		
371	242	249	76.65	29.99		0.0	0.5		0		
372	243	250	49.99	24.16		0.0	0.0		0		
373	244	245	26.96	34.49		0.0	0.0		0		
374	244	151	49.99	24.16		0.0	0.0		0		
375	245	246	29.99	46.10		0.0	0.0		0		
376	245	152	49.99	29.99		0.0	0.0		0		
377	246	247	3.386	12.98		1.5	0.0		0		
378	246	253	37.47	29.99		0.0	0.5		0		
379	248	249	5.079	12.98		1.5	0.0		0		
380	249	150	29.99	64.08		0.0	0.0		0		
381	249	155	69.98	29.99		0.0	0.5		0		
381	250	151	29.99	49.99		0.0	0.5		0		
383	250	156	49.99	29.99		0.0	0.0		0		
384	251	252	29.99	49.99		0.0	0.0		0		
385	251	257	49.99	29.99		0.0	0.0		0		
386	252	253	29.99	39.36		0.0	0.0		0		
387	252	258	49.99	29.99		0.0	0.0		0		
388	253	254	1.693	12.98		1.5	0.0		0		
389	253	260	19.99	25.89		0.0	0.25		0		
390	255	256	29.99	52.49		0.0	0.0		0		
391	255	261	39.99	25.70		0.0	0.25		0		
392	256	257	29.99	49.99		0.0	0.0		0		
393	256	262	49.99	27.85		0.0	0.0		0		
394	257	258	29.99	49.99		0.0	0.0		0		
395	257	264	49.99	27.85		0.0	0.0		0		
396	158	259	3.386	12.98		1.5	0.0		0		
397	258	260	21.80	34.99		0.0	0.25		0		
398	258	266	39.99	25.70		0.0	0.25		0		

(Table 48 continued)

Gap No.	Channels Connected by Gap		Width (in.)	Length (in.)	Loss Coefficients	FWALL	IGAPB	IGAPA	FACTOR	IGAP	JGAP
399	261	262	21.42	44.99		0.0	0.25		0		
400	262	263	3.386	12.98		1.5	0.0		0		
401	262	264	29.99	49.99		0.0	0.5		0		
402	264	265	3.386	12.98		1.5	0.0		0		
403	264	266	21.42	49.99		0.0	0.25		0		

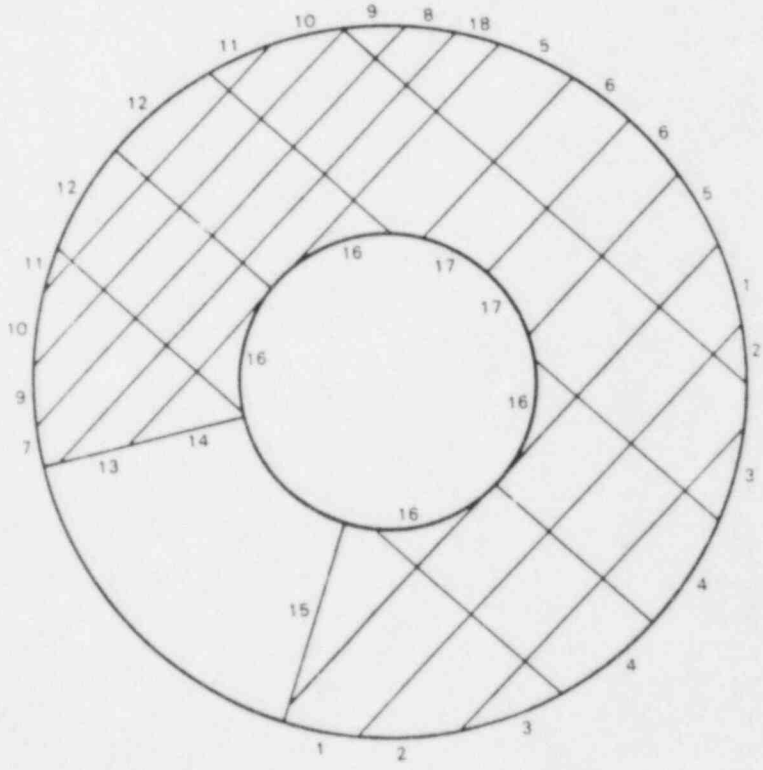

Figure 187 Location of thermal conductor geometry types

Table 49 Input data for thermal conductor geometry types

Geometry Type	Heated Perimeter (inches)	Total Thickness (inches)	Number of Nodes and (thickness) of each region (inches)		
1	34.79	1.65	5(.1)	5(.55)	5(1.0)
2	29.63	1.65	5(.1)	5(.55)	5(1.0)
3	45.54	1.65	5(.1)	5(.55)	5(1.0)
4	50.96	1.65	5(.1)	5(.55)	5(1.0)
5	31.42	1.65	5(.1)	5(.55)	5(1.0)
6	30.11	1.65	5(.1)	5(.55)	5(1.0)
7	26.65	1.65	5(.1)	5(.55)	5(1.0)
8	19.16	1.65	5(.1)	5(.55)	5(1.0)
9	25.34	1.65	5(.1)	5(.55)	5(1.0)
10	31.90	1.65	5(.1)	5(.55)	5(1.0)
11	23.32	1.65	5(.1)	5(.55)	5(1.0)
12	50.96	1.65	5(.1)	5(.55)	5(1.0)
13	31.43	1.65	5(.1)	5(.55)	5(1.0)
14	43.28	1.65	5(.1)	5(.55)	5(1.0)
15	90.13	1.65	5(.1)	5(.55)	5(1.0)
16	59.17	0.2	5(.1)	5(.1)	
17	31.41	0.2	5(.1)	5(.1)	
18	20.32	1.65	5(.1)	5(.55)	5(1.0)

modeled with two regions each 0.1 in. thick and each containing 5 heat transfer nodes. The outer wall was modeled with three regions each having 5 heat transfer nodes through the thickness. The inner region was 0.1 in. thick, the second 0.55 in. thick and the last 1.0 in. thick. The steel wall was modeled with the first two regions and the insulation with the third region.Here the boundary conditions at the jet nozzle for test HM-5 are given in Table 50. Since the nozzle flows were reported separately for each species of the gas/vapor jet (Figure 162, these had to be converted into the total mass flow rate, and the volume fraction and enthalpy of each species had to be calculated for input to the code. The jet was injected into channel 66 in the horizontal direction for test HM-5.

The boundary conditions for the blower discharge vent are given in Table 50. The volume fractions given in Table 51 are slightly lower than the measured volume fractions since the measured volume fractions were reported on a dry basis. The volume fraction given in Table 51 are based on the assumption that the recirculated nitrogen and hydrogen are saturated with water vapor. The equivalent data for test HM-6 are given in Tables 52 and 53.

The simulation was started for each test prior to the initiation of flow into the test nozzle. The simulation was continued until the jet flow was terminated and the concentrations began to level out.

Table 50 Nozzle boundary condition input for test HM-5

Time (sec)	Total Flow (lbm/sec)	Volume Fraction H_2	Volume Fraction H_2O	Time (sec)	Enthalpy (Btu/lbm) H_2	Enthalpy (Btu/lbm) H_2O
703.0	0.0	0.0	1.0	741.8	2297	1155.0
722.2	0.4012	0.0	1.0	967.2	2280	1150.5
743.2	0.7194	0.0	1.0	1060.0	2284	1151.1
746.6	0.7719	0.0115	0.9885	1123.0	2435	1173.5
780.9	0.8180	0.1082	0.8918	1183.0	2465	1178.3
840.2	0.8878	0.1053	0.8947	1243.0	2495	1181.0
880.3	0.9110	0.1024	0.8976	1303.0	2504	1183.5
927.4	0.8962	0.1038	0.8962	1375.0	2519	1185.0
1018.7	0.8927	0.1046	0.8954	2400.0	2519	1185.0
1066.4	0.9022	0.1031	0.8969			
1126.3	0.8920	0.1046	0.8954			
1369.9	0.8925	0.1046	0.8954			
1375.2	0.8917	0.0942	0.9058			
1417.0	0.0	0.0942	0.9058			

Table 51 Blower discharge boundary condition input for test HM-5

Time (sec)	Volume Fractions N_2	Volume Fractions H_2	Volume Fractions Steam	Enthalpy (Btu/lbm) $N_2 + H_2$	Enthalpy (Btu/lbm) Steam
0.0	0.9438	0.0	0.0562	132.6	1102.9
750.0	0.9438	0.0	0.0562	132.66	1102.9
803.4	0.9438	0.0	0.0562	134.81	1100.1
1080.0	0.8557	0.0180	0.1254	143.14	1116.8
1440.0	0.7883	0.0441	0.1660	147.61	1122.0
1698.0	0.8181	0.472	0.1364	147.63	1118.2
2040.0	0.8322	0.0449	0.1215	147.15	1116.3
2400.0	0.8401	0.0451	0.1140	147.12	1115.3

Table 52 Nozzle boundary condition input for test HM-6

Time (sec)	Total Flow (lbm/sec)	Volume Fraction		Time (sec)	Enthalpy (Btu/lbm)	
		He	H_2O		He	H_2O
0.0	0.0	0.0	1.0	0.0	689.0	1150.0
288.0	0.0	0.0	1.0	750.0	689.0	1150.0
330.0	0.5317	0.0	1.0	1008.0	724.0	1172.0
372.0	0.5317	0.0	1.0	1110.0	705.8	1160.0
420.0	0.5467	0.1125	0.8875	1230.0	691.0	1150.0
912.0	0.5467	0.1125	0.8875	1320.0	688.0	1150.0
960.0	0.5662	0.2259	0.7741			
1014.0	0.0	0.2259	0.7741			
1320.0	0.0	0.2259	0.7741			

Table 53 Blower discharge boundary condition input for test HM-6

Time (sec)	Volume Fractions			Enthalpy (Btu/lbm)	
	Air	He	Steam	Air + He	Steam
0.0	0.9468	0.0	0.0532	132.6	1150.0
426.0	0.9265	0.0	0.0735	135.5	1157.0
1020.0	0.8483	0.0308	0.1210	143.0	1173.0
1080.0	0.849	0.0335	0.1175	141.9	1172.0
1740.0	0.8775	0.0308	0.0937	139.8	1165.0

9.2.2 Post-Test Calculation

A post-test calculation was made of test HM-5 to 1) determine the cause of a spike in the calculated hydrogen calculation in the pretest calculation and 2) to evaluate the effect of mesh size on the accuracy of the prediction.

The cause of the concentration spike will be discussed more in the next section of this report.

A coarser mesh for the post-test calculation was obtained by lumping mesh cells together to form larger mesh cells. The mesh thus obtained is shown in Figure 188. The area of channel 8, for example, was obtained by adding the flow area of channels 10, 11, 15, and 16 of Figure 184(a) together, etc. The mesh was divided into five equal mesh cells vertically. The circular cells were used to model the blower discharge and outlet slot flows (i.e. channels 3, 5, 7, 10, 15, 16, 20, 22, 24, and 26). The nozzle and blower discharge boundary conditions and the initial wall and gas temperatures remained unchanged from the values used in the pretest calculation.

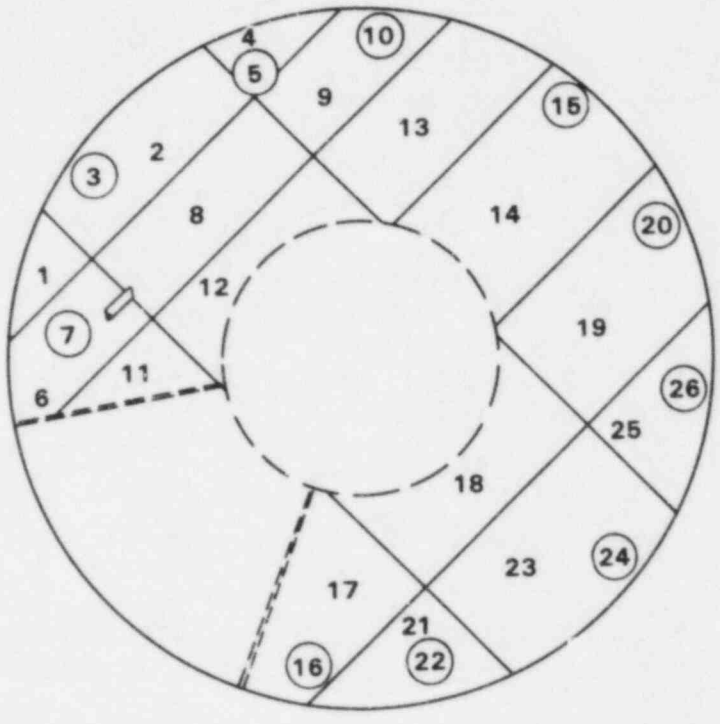

Figure 188 Mesh for post-test calculation of test HM-5

9.3 Discussion of Results

The main parameters that were measured in the experiments were the hydrogen (or helium) concentration on a dry basis and the gas temperature. The COBRA-TF pretest prediction of the hydrogen concentration for the top elevation of the 125° measurement location is shown in Figure 189. The measured data is shown as a solid curve and the code prediction as a dashed curve. The code prediction for the lower elevation at the 125° measurement location is shown in Figure 190. The prediction at the lower elevation is in reasonable agreement with the data both in shape and magnitude. The observed time shift between the data and the calculation is accounted for by a time lag in the experimental measurement system for which the data shown here has not been corrected. The magnitude of the predicted concentration at the top elevation is a little low; however, even more significantly, the shape of the calculation differs from the measured data. The irregular spiked shape of the calculation curve shown in Figure 189 is the result of a restart error in the code. The calculation was run in two segments, and data from the first segment was dumped to a restart file. This file was read by the code in the second restart run, and the calculation was continued. A variable was left out of the restart dump causing the perturbation to the flow field observed in Figure 189. That this was the problem was demonstrated by a post-test calculation in which the restart was

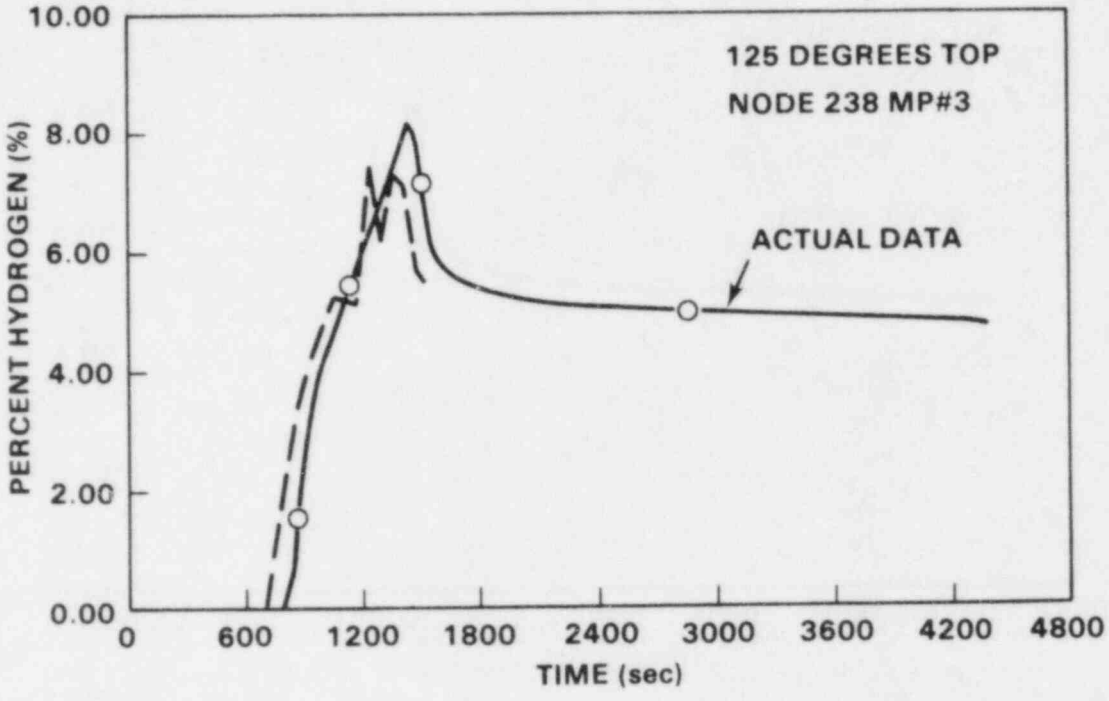

Figure 189 Hydrogen concentration at 125° top elevation--blind calculation

not used. A coarser mesh was also used in the post-test calculation, Figure 188. All other initial and boundary conditions remained the same, and nc changes were made to the code between the "blind" and "post-test" calculation. The post-test prediction for the 125° top elevation is shown in Figure 191. (The measured data is shown as a dashed curve in this figure.) Notice that the shape and magnitude of the prediction compares very well with the measure data. Also, there is no disturbing jaggedness to the curve (compare with Figure 189). All calculated values at the top and middle elevations showed the same concentration as did the experimental data. The bottom elevation was underpredicted using the coarse mesh (Figure 192), while they were predicted very well using the fine mesh (Figure 190). The bottom concentrations were underpredicted by 17% using the coarse mesh. The coarse mesh causes the jet momentum to be rapidly dissipated resulting in less circulation within the test compartment. However, one should consider the additional computational cost required to obtain the more accurate solution. The fine-mesh calculation required 8 CPU hours on a CDC 7600 computer for 15 transient minutes, while the coarse mesh calculations only required 0.72 hours of CPU time for a 23.3 minute transient. Note that the full set of two-fluid equations is solved, even though they are not necessarily needed for this test, and so one should expect this code to be slower than corresponding single-phase codes. The predicted temperatures at the corresponding measurement locations for the fine-mesh calculation are shown in Figures 193 and 194.

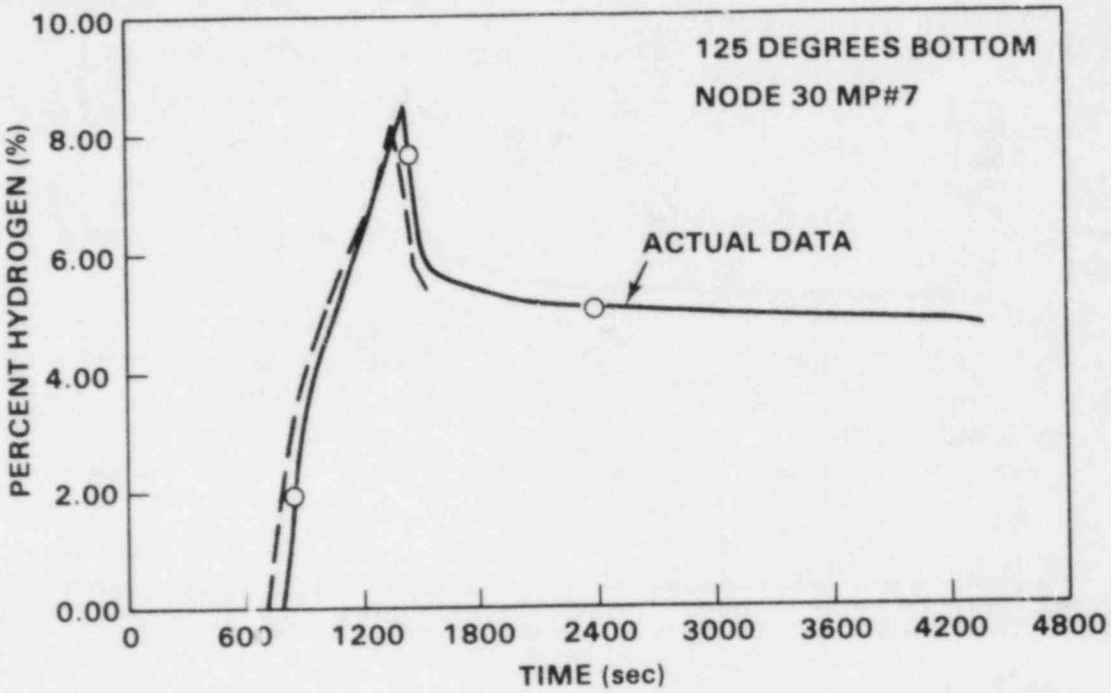

Figure 190 Hydrogen concentration at 125° bottom elevation--blind calculation

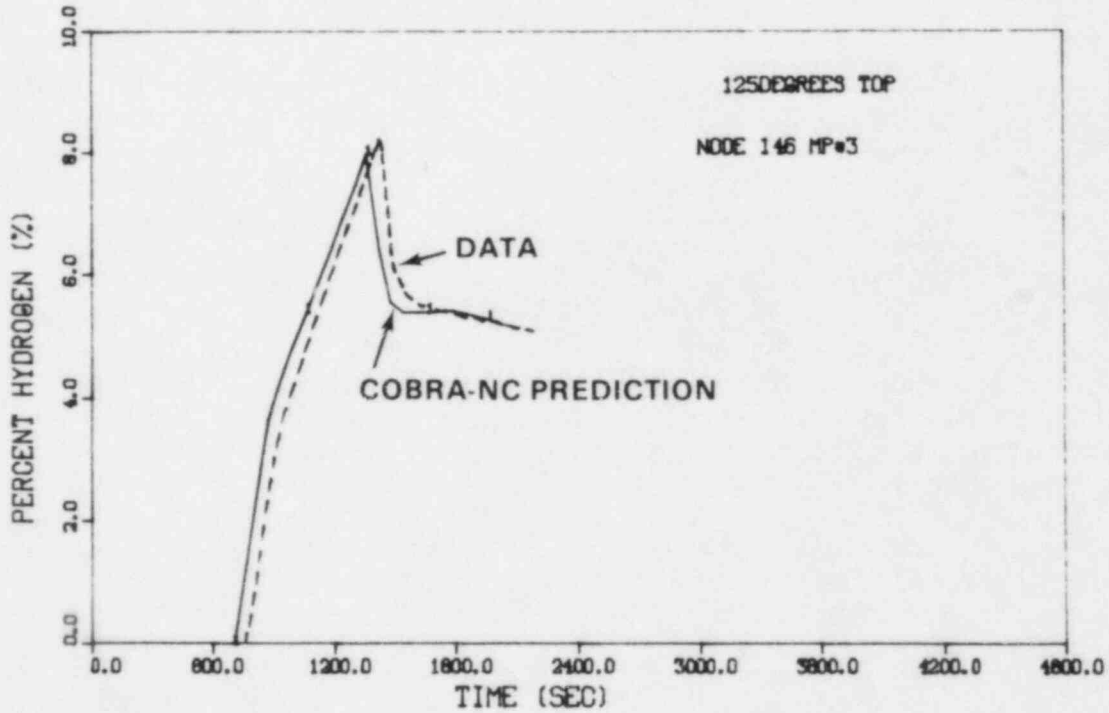

Figure 191 Hydrogen concentration at 125° top elevation--post-test calculation

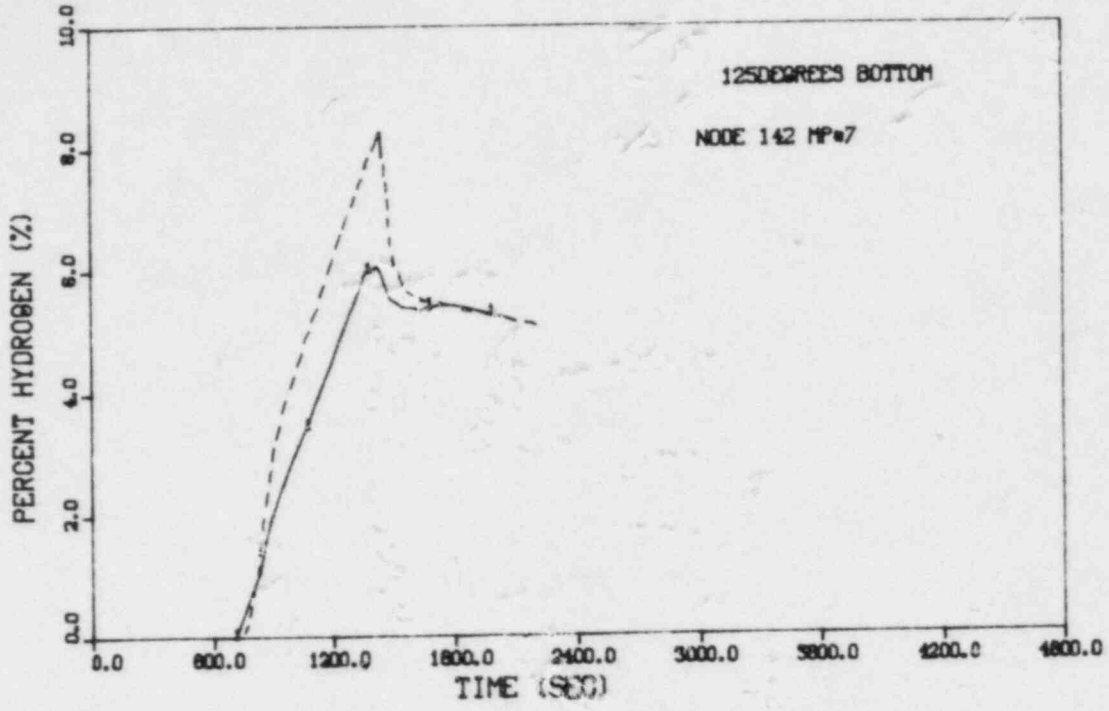

Figure 192 Hydrogen concentration at the 125° bottom elevation--post-test calculation

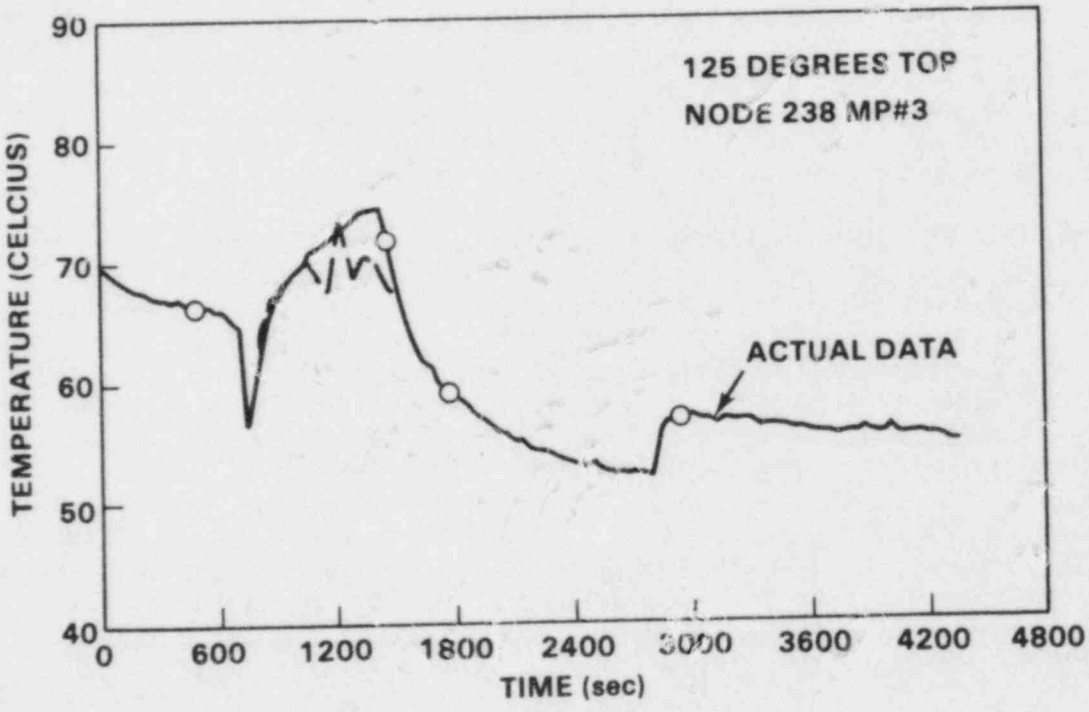

Figure 193 Gas temperature at the 125° top elevation--pretest calculation

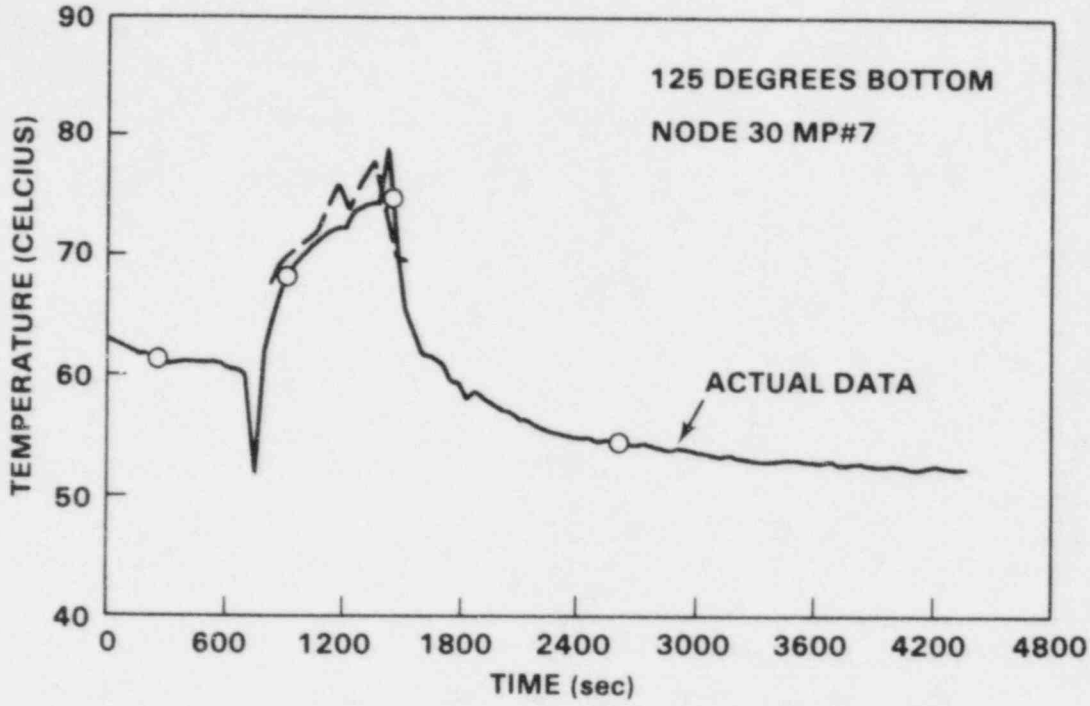

Figure 194 Gas temperature at the 125° bottom elevation--pretest calculation

The reasonable comparison with the data is a good indication that about the right amount of condensation, thermal mixing, and wall heat transfer has been calculated.

No appreciable concentration gradient was measured around the circumference of the test section. The code predictions also show little concentration gradient around the circumference of the test section.

The "blind" results for the vertical helium Jet B using the original mesh are shown in Figures 195 through 198. The location of the jet was artificially raised in the calculation to avoid the jet crossing over the narrow level of mesh cells provided for Jet A. This was done to avoid the small time step dictated by the Courant limitation at this location, thereby reducing the computational time. The predicted concentrations at the top elevation compare very well with the data in shape and magnitude (Figure 195). The concentrations at the middle and lower elevations were underpredicted. This is a result of Figure 198 Gas temperature at the 125° top elevation-pretest calculation the high jet elevation and the coarseness of the mesh in the vicinity of Jet B. It can be assumed that if a finer mesh were used to preserve the momentum of Jet B, then there would be increased mixing within the compartment. The temperature predictions for this test were also reasonable (Figure 198).

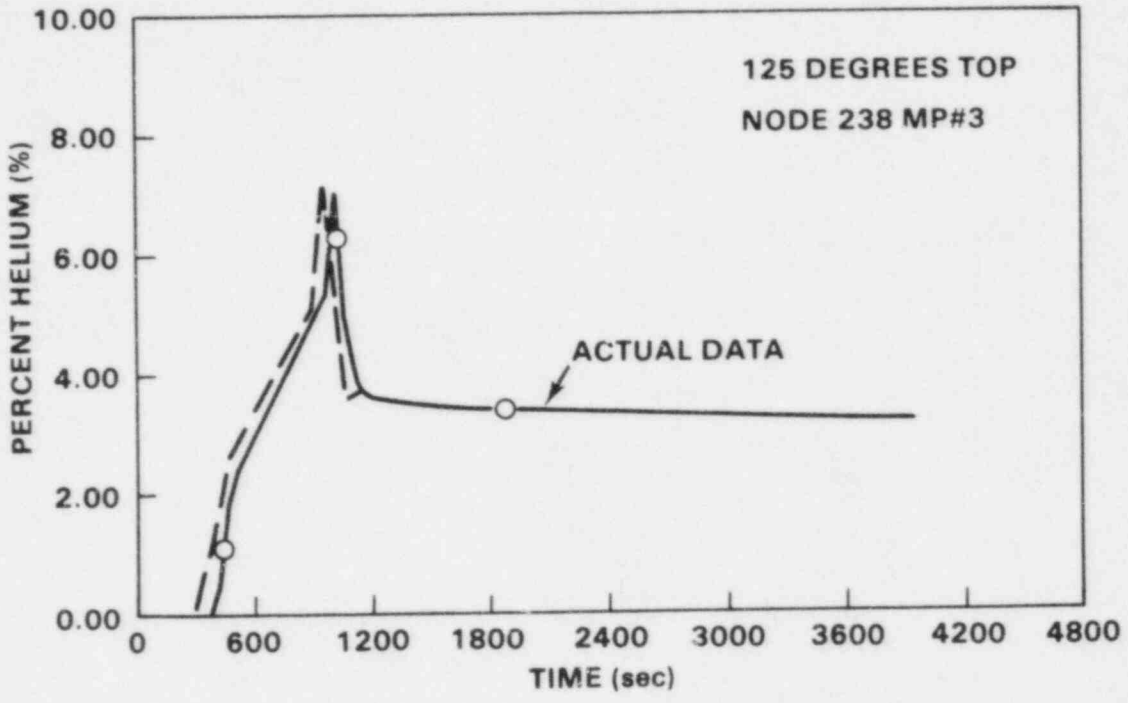

Figure 195 Helium concentration at the 125° top elevation--pretest prediction

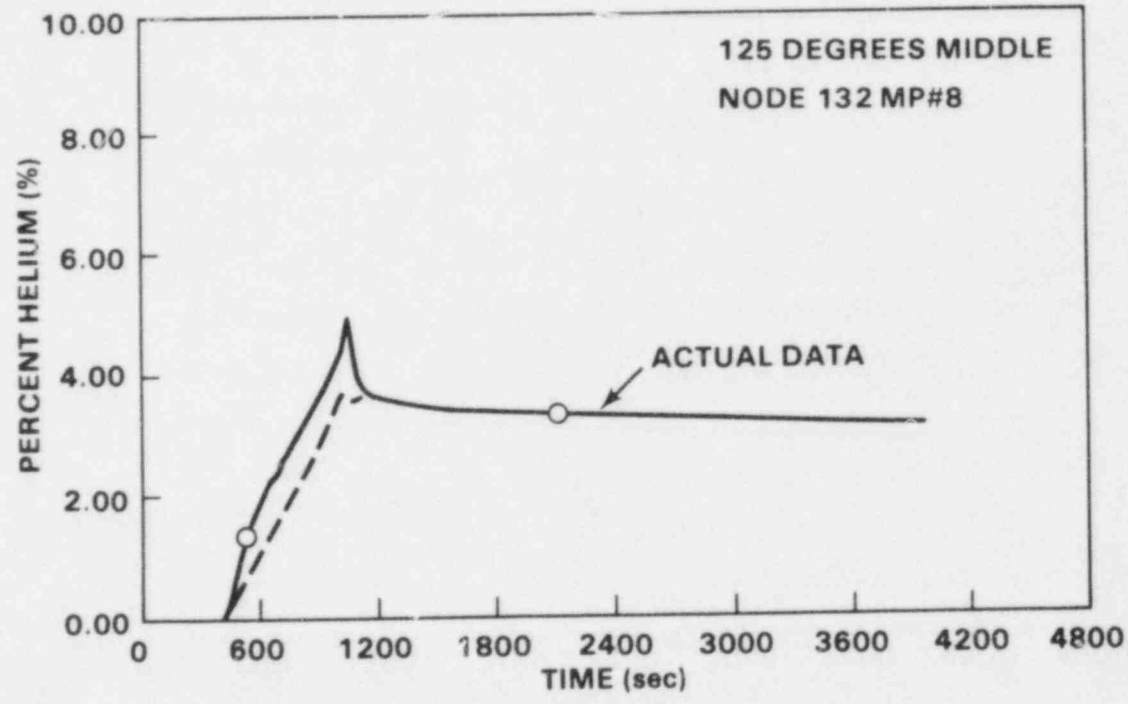

Figure 196 Helium concentration at the 125° middle elevation--pretest calculation

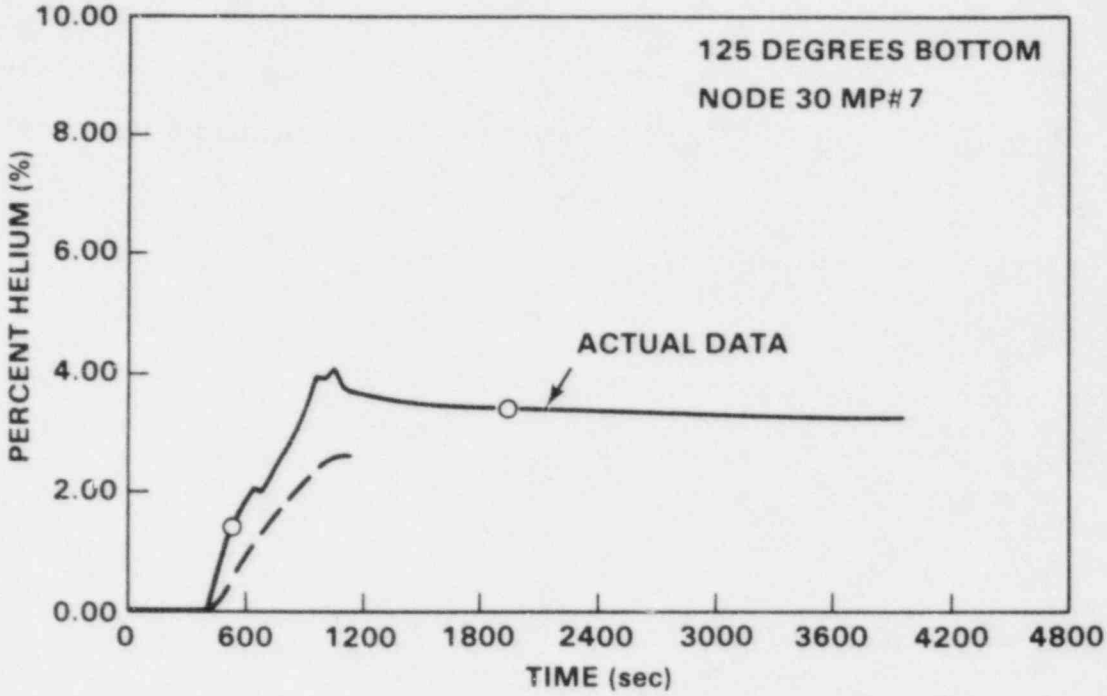

Figure 197 Helium concentration at the 125° bottom elevation--pretest calculation

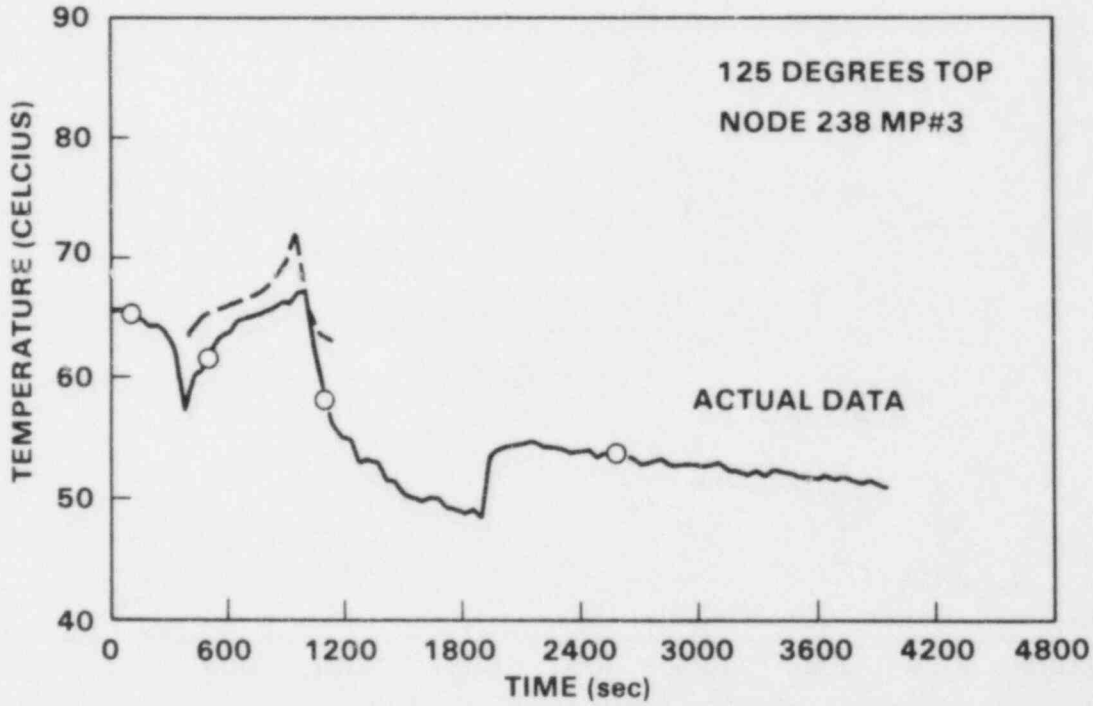

Figure 198 Gas temperature at the 125° top elevation--pretest calculation

9.4 Conclusions

COBRA-TF has been used to predict the concentration of hydrogen (or helium) in two tests involving high-velocity steam jet releases. A reasonable pretest prediction was obtained of both the gas concentration and gas temperature. A coding error in the restart subroutines caused an irregularity in the prediction for test HM-5. This irregularity did not appear when the restart option was not used. The results of these data comparisons indicate that COBRA-TF can predict the hydrogen concentration in a containment compartment with a high-velocity jet release. The data comparisons can be improved by using a fine enough mesh to preserve the jet's momentum. This must be done at large additional computational expense, however. The gas temperature predictions are reasonable by may be improved by modeling the recirculation period prior to the initiation of flow in the jet nozzle.

10.0 CONCLUSIONS

In this report, COBRA-NC predictions were compared with tests conducted in model containments that were scaled to investigate: 1) the behavior of steam/water blowdown into the containment and, 2) the behavior of steam/water hydrogen releases into the containment. These tests were conducted in a variety of test facility sizes and geometries. In general, the code predictions compare very favorably with the experimental data from both types of experiments. In particular, the blind pretest predictions made by COBRA-NC were very reasonable for both types of tests and provide confidence that reasonably conservative predictions can be made with the code. Even so, some insights have been obtained as a result of this code assessment effort that will enable us to obtain even better code predictions in the future. Some of these insights warrant further discussion.

First we will consider the prediction of steam/water blowdown phenomena. The following major conclusions can be drawn as a result of the steam/water blowdown data comparisons.

- The number of control volumes used to model the containment is very important in determining the proper boundary conditions for condensation heat-transfer coefficient correlations. A sufficient number of control volumes must be used so that the steam concentration gradients throughout the containment will be predicted. Large concentration differences will exist during blowdown in multicompartment containments as can be seen from the temperature measurements taken in the HDR facility tests (see Section 7 of this report). The COBRA-NC model for these tests consisted of 61 control volumes. This is a significantly larger number of volumes than was used by other codes that were also used to perform pretest predictions of these experiments. The use of several control volumes in the COBRA-NC model provided the correct steam concentration for each room of the containment during the early stages at the blowdown, thus providing correct boundary conditions (steam concentration and temperature) to the wall condensation heat-transfer model. This cannot be achieved by one- or two-node models of a containment, since they would produce homogeneously mixed values for the steam concentration and temperature. Even for five or ten node models, it is somewhat of a guess as to how different compartments should be grouped together to obtain "correct" boundary conditions for the heat-transfer solution.

- The natural convection currents that tend to mix the containment atmosphere following blowdown cannot be adequately predicted using a lumped parameter model. The large number of control volumes used in the COBRA-NC model of the HDR containment allowed the nonhomogeneous distribution of steam in the containment during the blowdown phase of the transient, but it did not predict the mixing of the atmosphere between the upper cooler rooms and the break area rooms caused by natural convection currents following blowdown. Following blowdown, natural convection currents apparently mix the steam in the near blowdown reaction with air in the compartments further away. This is particularly true of compartments

above the blowdown region. This mixing is important in reducing the pressure during the post-blowdown periods, since it brings steam into contact with cooler structural surfaces in upper containment regions and enhances the total condensation rate. Single or few node models, while inadequate for predicting the heat transfer during the initial stages of the transient, provide a more homogenized atmosphere that is more representative of the post-blowdown period. One may be tempted to return to a one- or two-node model in order to mix the atmosphere. However, one would be faced with the problem of how to group compartments together to obtain a correct steam concentration distribution, since, although mixing does occur, it is not complete. Therefore, a fine enough mesh has to be provided to allow the code to calculate natural circulation flows into and out of individual rooms. This could be done by using the three-dimensional finite-difference code option, but this could be very expensive computationaly. If a lumped parameter model is used, as in the case of the HDR model, the calculation essentially becomes vapor locked with hot air and steam trapped below colder, more dense air. Therefore, when using a lumped parameter model, multiple computational flow paths must exist between rooms at each level of the containment to permit cold dense gas to fall down and hot gases to rise. The reader should realize, however, that natural convection currents can only be correctly calculated by solving the equations of motion using the three-dimensional finite-difference option of the code.

- The Uchida correlation for the condensation heat transfer coefficient provides a conservative prediction of the containment peak pressure provided that the hydrodynamics model uses enough nodes to correctly predict the steam concentration for each region of the containment. Further work must be done to understand the correction between the integral heat transfer coefficient and the local distribution of steam within each individual compartment. These studies can be done using the three-dimensional finite-difference option in COBRA-NC to study the flow patterns in individual rooms.

The following conclusions can be made as a result of the hydrogen distribution data comparisons:

- Lumped parameter models can adequately predict the hydrogen concentration in rooms where no model stratification is present and the hydrogen source is at the floor level.

- The heat transfer to and from walls and structures must be modeled when thermal stratification is present, since this heat transfer tends to maintain the stratification and causes significant differences in hydrogen concentration between the stratified layers.

- A sufficiently fine mesh must be provided to predict the natural convection currents that drive the mixing of compartment atmospheres when thermal stratification or elevated hydrogen sources are present. This will, in

some cases, require the use of the three-dimensional finite-difference option of the code.

The COBRA-NC computer code has additional capabilities that have not been demonstrated by the present set of data comparisons. These include the capability to model BWR suppression pools and containment sprays. These capabilities will be assessed as applicable data becomes available.

In summary, the results of the data comparisons presented in this report indicate that COBRA-NC can be used to reliably predict the response of nuclear containments to steam/water blowdown and hydrogen release provided that appropriate mesh sizes are used to resolve the gradients expected to occur. One of the strong points of COBRA-NC is that it can be used in either a lumped parameter or finite-difference mode. This allows the user to perform noding studies that will allow him to select the optimum model for the problem under consideration.

RELATED DOCUMENTS

COBRA/TRAC - A Thermal Hydraulics Code for Transient Analysis of Nuclear Reactor Vessels and Primary Coolant Systems, NUREG/CR-3046, March 1983

Volume 1: Equations and Constitutive Models

Volume 2: Numerical Solution Methods

Volume 3: Users' Manual

Volume 4: Developmental Assessment and Data Comparison

Volume 5: Programmers' Manual

COBRA-NC: A Thermal-Hydraulic Code for Transient Analysis of Nuclear Reactor Components

Volume 1: Equations and Constitutive Models NUREG/CR-3262

Volume 2: Numerical Solution Methods NUREG/CR-3262

Volume 3: Users' Manual for General Two-Phase Thermal Hydraulics (to be published)

Volume 4: Users' Manual for Containment Analysis (COBRA-NC), NUREG/CR-3262

Volume 5: Users' Manual for Flow Blockage and Hot Bundle Analysis (to be published)

Volume 6: Assessment Manual for General Two-Phase Thermal-Hydraulic Applications (to be published)

Volume 7: Assessment Manual for Containment Applications, NUREG/CR-3262

Volume 8: Assessment Manual for Flow Blockage and Hot Bundle Applications (to be published)

Volume 9: Programmers' Manual (to be published)

11.0 REFERENCES

1. "Numerical Benchmark Problem on Containment Codes," Organization for Economic Cooperation and Development, Nuclear Energy Agency, SINDOC(80)263, Paris, December 4, 1980.

2. D. L. Nguyen, "Comparison Report on OECD-CSNI Containment Standard Problem No. 2", CSNI Report No. 65, May 1981.

3. J. Marshall, et al., "OECD/CSNI Containment Analysis Standard Problem No. 3," CASP3-1, December 1981.

4. "Investigation of Phenomena Occurring within a Multicompartment Containment After Rupture of the Primary Cooling Circuit in Water-Cooled Reactors," Battelle-Institute e.V. Frankfurt/Main West Germany, Technischer Bericht BF-R550-32-D1, May 1977, and Technischer Bericht BF-R550-32-D15-2, November 1978.

5. "Investigation of Phenomena Occurring within a Multicompartment Containment After Rupture of the Primary Cooling Circuit in Water-Cooled Reactors," Battelle-Institute e.V. Frankfurt/Main West Germany, Technical Report BF-R550-32-C13-1, July 1976, and Technical Report BF-R550-32-C15-1, July 1976.

6. M. Schall, "Design Report for the HDR Containment Experiments V21.2 to V21.3 and V42 to V44 with Specifications for the Pretest Computations," HDR Safety Program Report No. 3.280/82, January 1982.

7. M. Schall and L. Valencia, "Data Compilation on the HDR Containment for Input Data Processing for Pretest Calculations," HDR Safety Program Report No. 3.279/82, January 1982.

8. G. Langer, et al., "Experimental Investigation of the Hydrogen Distribution in the Containment of a Light Water Reactor Following a Coolant Loss Accident," Battelle-Frankfurt Technical Reports BF-R-63.363-3 and BF-R-64.036-2.

9. G. R. Bloom, et al., "Hydrogen Mixing and Distribution in Containment Atmospheres," EPRI NP-2669, March 1983.

10. M. J. Thurgood, et al., "COBRA/TRAC - A Thermal-Hydraulics Code for Transient Analysis of Nuclear Reactor Vessels and Primary Coolant Systems, Volume 1: Equations and Constitutive Models," NUREG/CR-3046, November 1982.

APPENDIX A

Geometrical Data

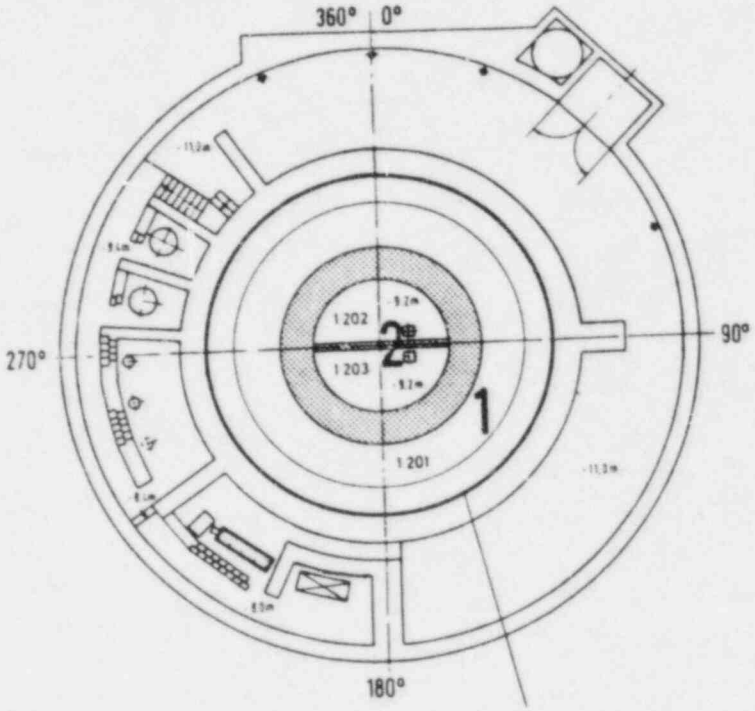

Figure A.1 Plan of HDR containment at level B-B (-0.8 m) (34-zones model)

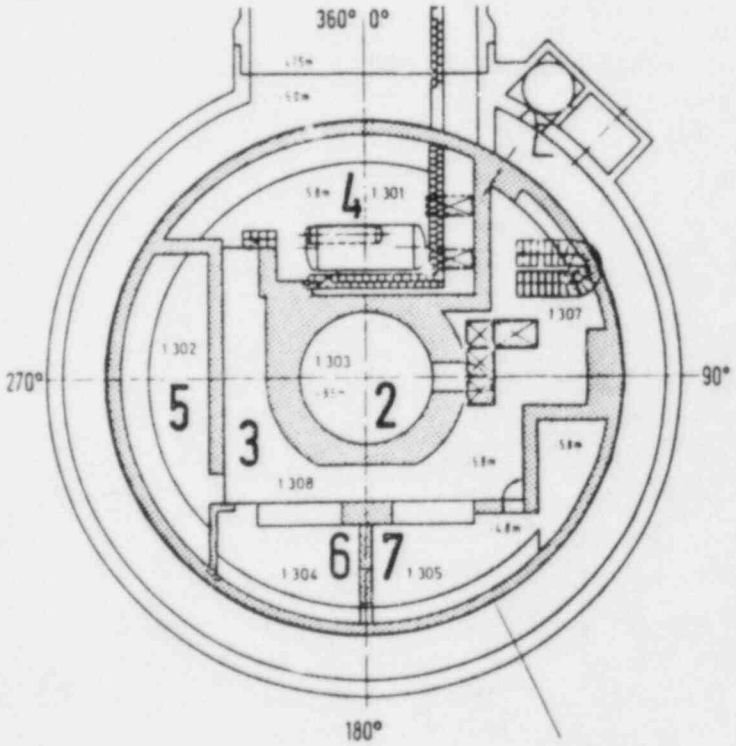

Figure A.2 Plan of HDR containment at level C-C (-5.0 m) (34-zones model)

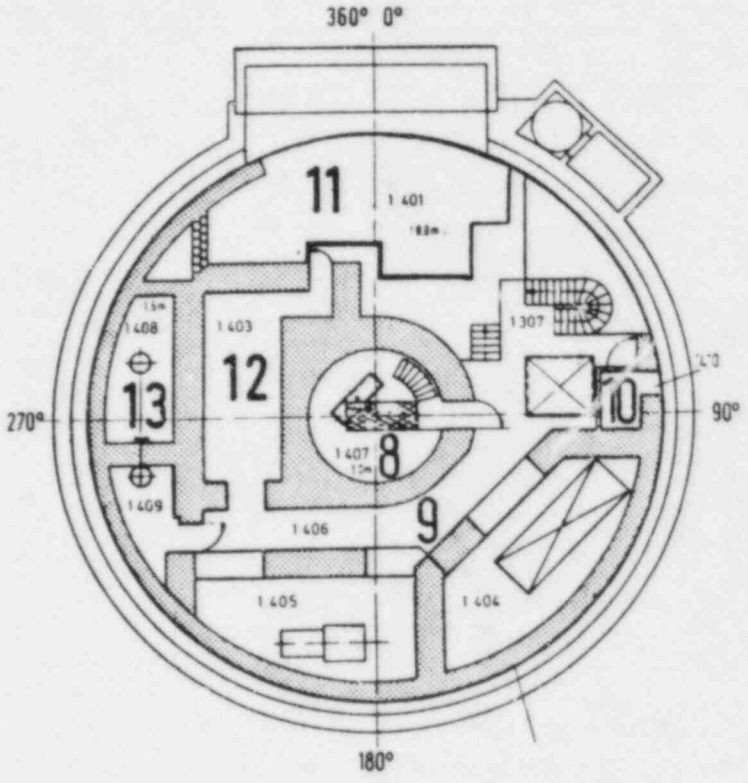

Figure A.3 Plan of HDR containment at level D-D (+0 m) (34-zones model)

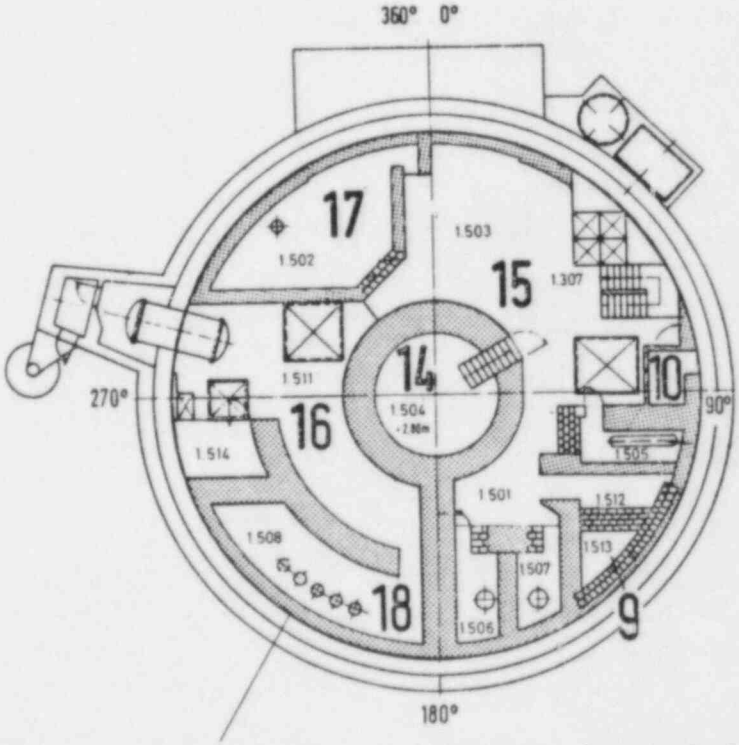

Figure A.4 Plan of HDR containment at level E-E (+5.4 m) (34-zones model)

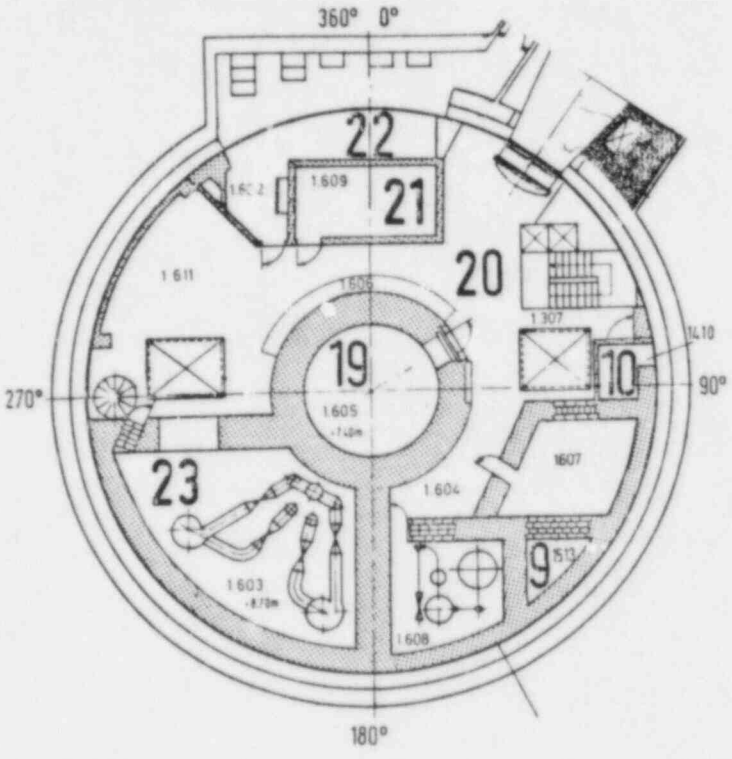

Figure A.5 Plan of HDR containment at level F-F (+11.5 m) (34-zones model)

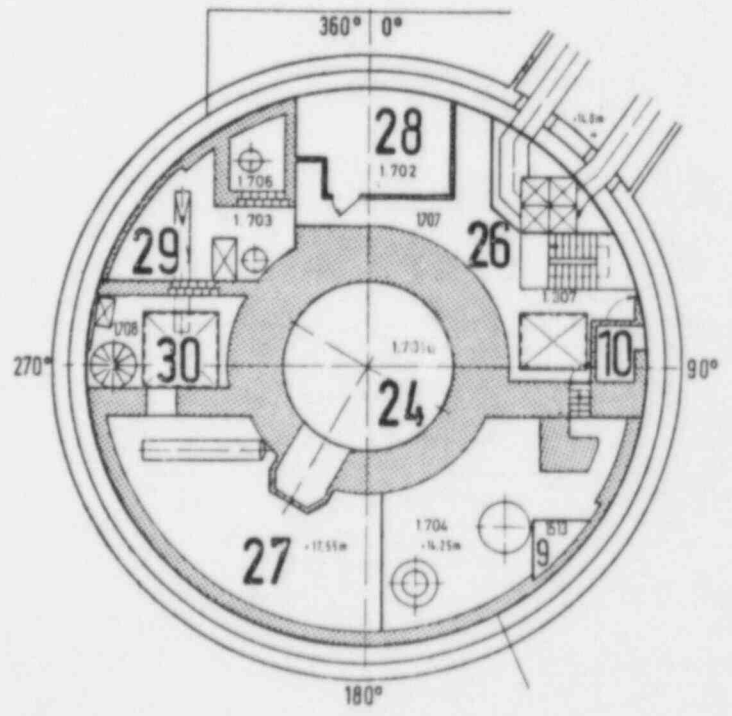

Figure A.6 Plan of HDR containment at level G-G (+18.0 m) (34-zones model)

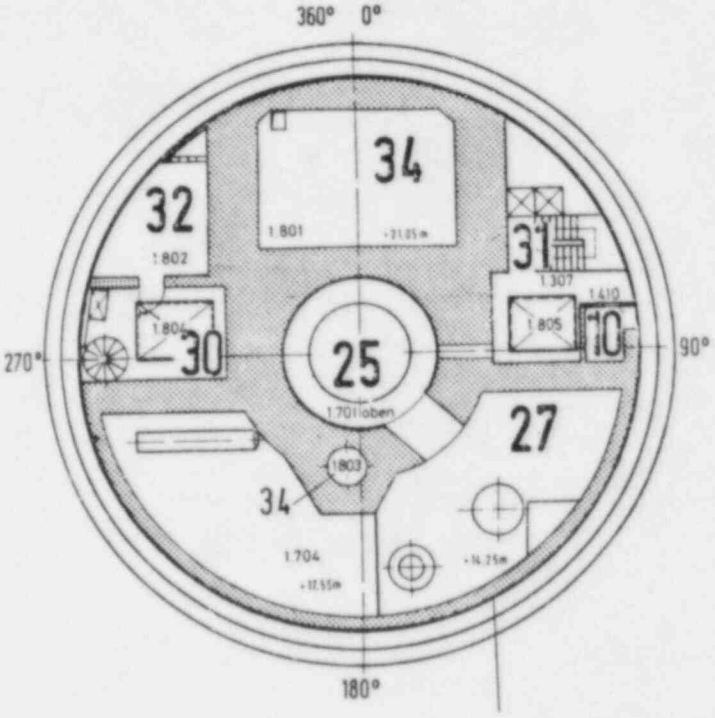

Figure A.7 Plan of HDR containment at level H-H (+20.6 m) (34-zones model)

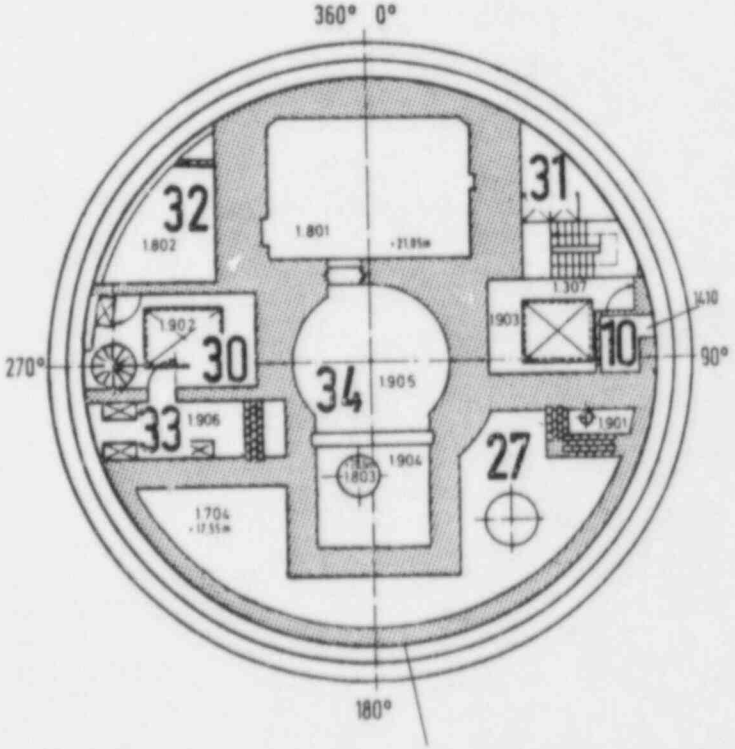

Figure A.8 Plan of HDR containment at level J-J (+25.3 m) (34-zones model)

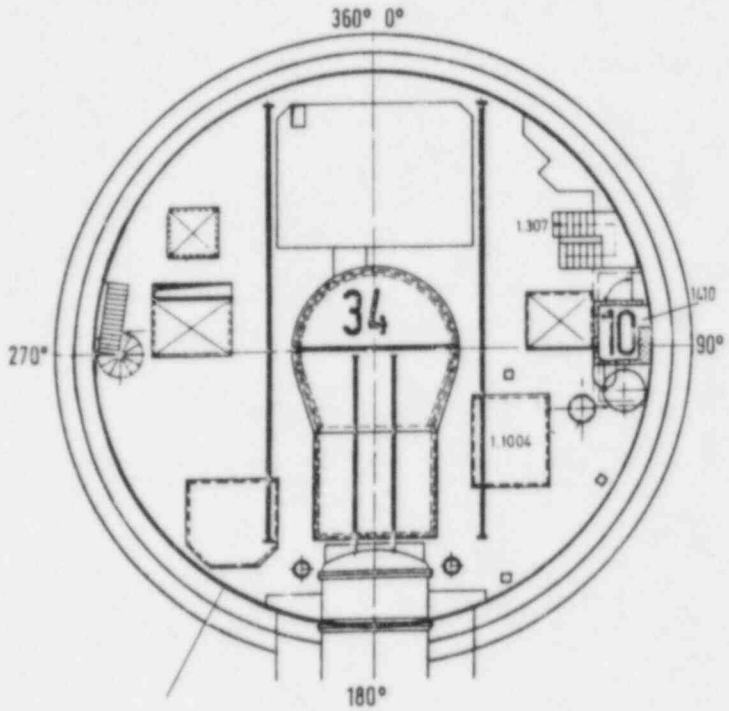

Figure A.9 Plan of HDR containment at level K-K (+31.0 m) (34-zones model)

Table A.1 List of original HDR compartments and their function

Room Nr.	Purpose During Reactor Operation	Room Nr.	Purpose During Reactor Operation	Room Nr.	Purpose During Reactor Operation
1201	Reactor annulus	1202	Building sump I	1203	Building sump II
1301	Overflow facility	1302	Valve room	1303	Active water vessel
1304	Primary water pump	1305	Primary water pump	1307	Stair well
1308	Service room	1311	Water level regulator		
1401	Cable spreading room	1403	Primary loop pump	1404	Primary loop pump
1405	Primary loop pump	1406	Service, assembly room	1407	Neutron flux measurement
1408	Main mixed-bed filter	1409	Precoat tank	1410	Elevator
1501	Service room	1502	Standby cooling	1503	Control rod drives
1504	Neutron flux measurement	1505	Aftercooler, condensator I	1506	Main cleanup pump
1507	Main cleanup pump	1508	Cleanup preheater	1511	Remote valve drives
1512	Aftercooler, condensator II	1513	Pipe tunnel	1514	Cooling water distribution
1602	Measurement cable dist.	1603	Circulation pump room	1604	Service room
1605	Control rods radiator	1606	Reactor measurement	1607	Steam radiator
1608	Steam radiator II, recombiner	1609	Measurement cable boxes	1611	Auxiliary cooling
1701	Reactor (upper)	1701	Reactor (lower)	1702	HVAC
1703	Spent fuel pool cooling	1704	Steam generator	1706	Spent fuel pool filter
1707	Service room	1708	Service room		
1801	Spent fuel pool	1802	New fuel storage	1803	Transfer pool
1804	Service room	1805	Service room		
1901	Superheated steam filter	1902	Service room	1903	Service room
1904	Fuel transfer pool	1905	Flood room	1906	Cladding tube surveillance
11004	Compartment above +30.85 m				

Table A.2 List of 34 containment zones

Model Room No.	Room Description	Containment Room Number	Volume	Remarks
1	Annulus at -8.5 m	1201	152	
2	Sump	1202, 1203, 1303	78	
3	Stairs and landing at -5.8 m	1307, 1308	160	
4	Overflow facility	1301	206	
5	Valve room	1302	93	
6	Primary water pump	1304	39	
7	Neutron flux measurement	1305, 1311	63	
8	Neutron flux measurement	1407	84	
9	Stairs, compartments, and landing at -1.1 m	1307, 1404-1406, 1409, 1513	585	
10	Elevator	1410	113	
11	Cable spreading	1401	296	
12	Primary loop pump	1403	76	
13	Primary filter	1408	59	
14	Neutron flux measurement	1504	57	
15	Stairs, compartments, and landing at +4.5 m	1307, 1501, 1503, 1505-1507, 1512	543	
16	Portion of landing at + 4.5 m	1511, 1514	235	
17	Standby cooling	1502	107	
18	Transfer pool	1508	57	
19	Control rod compartment	1605	93	
20	Stairs, compartments, and landing at +10 m	1307, 1604, 1606-1608, 1611	507	
21	Condensate discharge	1609	59	
22	Measurement cable distribution	1602	61	
23	Circulation pumps	1603	280	
24	Lower RPV annulus	1701 u	44	
25	Upper RPV annulus	1701 o	64	
26	Stairs and landing at +15 m	1307, 1707	131	
27	Superheated steam generator and filter	1704, 1901	848	
28	HVAC facility	1702	54	
29	Spent fuel cooling and filter	1703, 1706	169	
30	Assembly tunnel and circular stairs	1708, 1804, 1902	269	
31	Stairs and landing at 20 m and 25.3 m	1307, 1805, 1903	279	
32	New fuel storage	1802	125	
33	Cladding tube surveillance	1906	62	
34	Dome and transfer pool	1801, 1803, 1904, 1905, 11004	5293	

Table A.3 Compilation or the vent flow openings of the 34-zones model

Open No.	From Comp.	To Comp.	From Zone	To Zone	F min in m**2	DC @ GRS	Delta p bar	Description
1	1201	1202	01	02	0.04	0.65		opening in wall to compartment No. R 1202
2	1201	1203	01	02	0.028	0.65		opening in wall to compartment No. R 1203
3	1202	1302	02	05	0.12	0.6		pipe channel with bending, leading from side wall in R 1202 to floor in R 1302
4	1203	1305	02	07	0.149	0.6		pipe channel with bending, leading from side wall in R 1202 to floor in R 1205
5	1303	1308	02	03	0.164	0.7		21 bores in wall of R 1308
6	1303	1308	02	03	0.007	0.7		bore choked by rock wool and with logitudinal cable
7	1301	1303	04	02	0.214	0.6		pipe channel with oblique inlet in ceiling of R 1301
8	1301	1303	04	02	0.09	0.6		pipe channel with vertical inlet in side wall of R 1301
9	1303	1407	02	08	0.042	0.6		pipe channel
10	1303	1407	02	08	0.224	0.6		pipe channel in floor, covered by grating
11.1	1303	1407	02	08	0.071	0.7		ventilation duct No. 3 (see Fig. 3.7-25)
11.2	1401	1407	11	08	0.03	0.7		ventilation duct No. 3 (see Fig. 3.7-25)
11.3	1401	1406	11	09	0.24	0.75		ventilation duct No. 3 (see Fig. 3.7-25)
12.1	1303	1308	02	03	0.2	0.7		ventilation duct No. 6 (see Fig. 2.7-28)
12.2	1203	1303	02	02	0.017	0.7		ventilation duct No. 6 (see Fig. 3.7-28)
13	1303	1308	02	03	1.824	0.8		open steel door
14	1201	1308	01	03	0.178	0.6		pipe channel in floor, covered by grating
15	1201	1308	01	03	0.1	0.6		pipe channel (with ledge in its interior) in floor
16	1201	1301	01	04	0.089	0.7		cylindrical pipe channel, oblique in floor
17	1201	1301	01	04	0.09	0.65		oblique opening in floor near opening No. 51
18	1201	1301	01	04	0.051	0.7		cylindrical pipe channel
19	1304	1305	06	07	0.149	0.7		pipe channel
20	1304	1305	06	07	5.775	0.85		large opening covering the total height of the compartments
21	1301	1308	04	03	1.991	0.8		opening (passage)
22	1302	1308	05	03	0.157	0.7		20 bores
23	1302	1308	05	03	0.013	0.7		two bores
24	1301	1302	04	05	0.015	0.7		two openings
25	1302	1308	05	03	1.3	0.8		open door
26.1	1302	1308	05	03	0.081	0.7		ventilation duct No. 3 (see Fig. 3.7-25)
26.2	1303	1308	02	03	0.07	0.7		ventilation duct No. 3 (see Fig. 3.7-25)
27	1304	1308	06	03	1.064	0.8		open steel door
28	1301	1302	04	05	0.246	0.5		pipe channel with bending
29	1301	1302	04	05	0.0367	0.6		pipe channel
30.1	1201	1301	01	04	0.063	0.7		ventilation duct No. 1 (see Fig. 3.7-23)
30.2	1301	1308	04	03	0.16	0.75		ventilation duct No. 1 (see Fig. 3.7-23)
31	1304	1308	06	03	2.4	0.85		opening in equipment concrete block wall
32	1305	1308	07	03	3.04	0.85		opening in equipment concrete block wall
33	1305	1308	07	03	1.129	0.85		open steel door (closed in V44)
34	1301	1408	04	13	1.199	0.65		hole leading to the lower end of pipe channel (opening No. 151)
35	1302	1408	05	13	0.626	0.7		opening in floor
36	1302	1408	05	13	0.487	0.65		opening in floor
37	1302	1408	05	13	0.194	0.65		cable shaft in floor
38	1302	1408	05	13	0.636	0.6		pipe channel in floor

(Table A.3, continued).

Open No.	From Comp.	To Comp.	From Zone	To Zone	F min in m**2	DC @ GRS	Delta p bar	Description
39	1304	1405	06	09	0.03	0.65		ventilation duct No. 5 (see Fig. 3.7-27)
40.1	1304	1405	06	09	0.06	0.75		ventilation duct No. 4 (see Fig. 3.7-26)
40.2	1305	1405	07	09	0.06	0.75		ventilation duct No. 4 (see Fig. 3.7-26)
40.3	1404	1405	09	09	0.1	0.75		ventilation duct No. 4 (see Fig. 3.7-26)
41.1	1305	1404	07	09	0.02	0.75		ventilation duct No. 5 (see Fig. 3.7-27)
41.2	1404	1405	09	09	0.12	0.75		ventilation duct No. 5 (see Fig. 3.7-27)
42	1304	1405	06	09	0.17	0.55		pipe channel
43	1304	1405	06	09	0.017	0.65		bore in ceiling
44	1311	1404	07	09	0.03	0.75		ventilation duct No. 4 (see Fig. 3.7-26)
45	1305	1404	07	09	1.535	0.6		pipe channel
46	1302	1409	05	09	0.023	0.7		two bores in floor, plated with zinc sheeting
47	1308	1406	03	09	0.01	0.6		cable duct in floor
48	1201	1301	01	04	0.732	0.6	+0.02 -0.5	oblique floor opening, covered by iron slab
49	1201	1301	01	04	0.034	0.6	+0.02 -0.5	oblique floor opening, covered by iron slab
50	1201	1301	01	04	0.231	0.6	+0.02 -0.5	oblique floor opening, covered by iron slab
51	1201	1301	01	04	0.4515	0.6	+0.02 -0.5	oblique floor opening, covered by iron slab
52	1308	1406	03	09	4.39	0.85	+0.2 -0.6	transport hatch in floor, covered by iron slabs
53	1406	1410	09	10	1.36	0.8		open elevator door at level -1.1 m
54	1406	1407	09	08	0.921	0.75		open steel door
55	1403	1406	12	09	0.623	0.65		pipe channel, crossed by ventilation duct
56	1401	1406	11	09	2.965	0.85	+-0.05	cable shaft, partially covered with zinc plate
57	1403	1406	12	09	0.442	0.8		passage through concrete block wall
58.1	1308	1409	03	09	0.02	0.7		ventilation duct No. 6 (see Fig. 3.7-28)
58.2	1408	1409	13	09	0.02	0.7		ventilation duct No. 6 (see Fig. 3.7-28)
59	1403	1408	12	13	0.099	0.7		cable duct in wall
60	1403	1406	12	09	0.637	0.8		open steel door with L-bended passage
61.1	1403	1406	12	09	0.48	0.75		ventilation duct No. 5 (see Fig. 3.7-27)
61.2	1403	1404	12	09	0.36	0.75		ventilation duct No. 5 (see Fig. 3.7-27)
62.1	1308	1406	03	09	2.49	0.8		stair case (compartment No. 1307) at level -1.1 m
62.2	1308	1406	03	09	1.8	0.8		stair case (compartment No. 1307) at level -1.1 m
62.3	1308	1406	03	09	1.627	0.8		stair case (compartment No. 1307) at level -1.1 m
63.1	1501	1511	15	16	0.06	0.75		ventilation duct No. 7 (see Fig. 3.7-29)
63.2	1406	1501	09	15	0.06	0.75		ventilation duct No. 7 (see Fig. 3.7-29)
63.3	1501	1503	15	15	0.16	0.75		ventilation duct No. 7 (see Fig. 3.7-29)
64	1501	1511	15	16	0.0028	0.7		bore
65	1406	1504	09	14	0.048	0.7		opening
66	1406	1504	09	14	0.04	0.7		opening with cable duct
67	1503	1504	15	14	1.913	0.8		open steel door leading to stair case
68	1502	1503	17	15	0.0028	0.7		bore
69	1502	1503	17	15	0.00975	0.7		two bores

(Table A.3, continued).

Open No.	From Comp.	To Comp.	From Zone	To Zone	F min in m**2	DC @ GRS	Delta p bar	Description
70	1502	1503	17	15	0.975	0.7		open door and adjacent passage
71	1502	1503	17	15	0.0038	0.7		bore
72	1502	1503	17	15	0.0007	0.7		steel pipe in wall
73	1502	1511	17	16	0.033	0.6		seven bores, plated with zinc sheeting
74	1502	1511	17	16	0.1	0.6		channel, crossed by ventilation duct
75	1502	1511	17	16	0.0012	0.7		bore, plated with zinc sheeting
76	1502	1511	17	16	0.013	0.5		channel with cables
77	1503	1511	15	16	3.646	0.85		passage, covering the total compartments height
78	1301	1308	04	03	0.1	0.75		ventilation duct No. 2 (see Fig. 3.7-29)
79	1302	1304	05	06	3.068	0.85	+-0.05	opening covered by zinc plate
80	1606	1609	20	21	0.0057	0.7		bore
81	1606	1609	20	21	0.00933	0.65		bore
82.1	1403	1404	12	09	0.4	0.75		ventilation duct No. 4 (see Fig. 3.7-26)
82.2	1403	1406	12	09	0.1	0.75		ventilation duct No. 4 (see Fig. 3.7-26)
83.1	1308	1406	03	09	0.18	0.7		ventilation duct No. 6 (see Fig. 3.7-28)
83.2	1401	1406	11	09	0.08	0.7		ventilation duct No. 6 (see Fig. 3.7-28)
84.1	1401	1606	11	20	0.08	0.6		ventilation duct No. 6 (see Fig. 3.7-28)
84.2	1401	1606	11	20	0.14	0.6		ventilation duct No. 6 (see Fig. 3.7-28)
85	1301	1302	04	05	2.826	0.85	+-0.05	opening covered by zinc plate
86	1602	1606	22	20	1.43	0.8		open steel door
87	1606	1609	20	21	1.43	0.8		open steel door
88.1	1602	1609	22	21	0.044	0.75		ventilation duct No. 12 (see Fig. 3.7-30)
88.2	1604	1609	20	21	0.15	0.75		ventilation duct No. 12 (see Fig. 3.7-30)
89	1401	1406	11	09	2.09	0.8		open steel door
90	1702	1707	28	26	1.44	0.8		open steel door
91	1703	1707	29	26	1.69	0.8		open lead-shielded door
92	1704	1707	27	26	1.3	0.7	+-0.1 closed	zigzag passage with stairs (lateral edges rounded) and instrumented door (initially closed)
93.1	1404	1704	09	27	1.5	0.6		vertical pipe channel leading from R 1704 (level +14.25 m) to R1404 (+3.5 m) separated from R 1607 and R 1512 by concrete block walls
93.2	1513	1607	09	20	0.5	0.65	+-0.4	concrete block wall
93.3	1512	1513	15	09	0.5	0.65	+-0.4	concrete block wall
94	1606	1704	20	27	0,05	0.7		ventilation duct in concrete block wall leading from R 1606 (ceiling) to main ventilation duct
95	1704	11004	27	34	8.0	0.85	+1 closed	opening covered by heavy concrete slab (20 to 30.000 kg)
96	1704	1804	27	30	0.43	0.9		instrumented (DK) channel with rounded inlet
97	1701 o	1704	25	27	0.15	0.65		pipe channel close to opening No. 96
98	1704	1504	27	30	0.02	0.6		bore with measured cables
99	1607	1704	20	27	0.21	0.6		pipe channel covered by grating
100	1704	1904	27	34	0.0148			bore
101	1704	1904	27	34	0.0676	0.6		bore
102	1701 o	1704	25	27	1.62	0.75		opening in biological shield
103	1704	1805	27	31	0.088	0.6		two bores close to opening No. 102

(Table A.3, continued).

Open No.	From Comp.	To Comp.	From Zone	To Zone	F min in m**2	DC @ GRS	Delta p bar	Description
104	1701 o	1704	25	27	0.07	0.65		two bores close to opening No. 102
105	1701 o	1704	25	27	0.11	0.6		two bores close to opening No. 102
106.1	1701 o	1704	25	27	0.35	0.65		opening close to opening No. 102
106.2	1701 o	1704	25	27	0.0314	0.65		pipe below opening No. 106.1
107	1704	11004	27	34	0.18	0.6		opening
108	1701 o	1704	25	27	0.25	0.7		opening below opening No. 106
109	1704	1903	27	31	0.31	0.7		ventilation duct leading from compartment R 1704 via two elbows to R 1903 and to main ventilation duct
110	1603	1704	23	27	0.37	0.55		pipe channel with weir sill in R 1704
111	1704	1903	27	31	0.04	0.7		two steel pipes
112	1704	1906	27	33	0.19	0.7		channel adjacent to opening No. 96
113.1	1704	1906	27	33	0.206	0.65		branched cable duct in ceiling of R 1704
113.2	1701 o	1704	25	27	0.206	0.65		branched cable duct in ceiling of R 1704
114.1	1704	1901	27	27	0.48	0.7		opening
114.2	1704	1901	27	27	0.038	0.7		ventilation duct
115	1906	11004	33	34	0.03	0.65	+0.02 -1 closed	service channel, covered by metal slab
116	1903	11004	31	34	0.03	0.65	+0.02 -1 closed	service channel, covered by metal slab
117.1	1903	11004	31	34	2.06	0.8		ventilation channel (see Fig. 3.7-4)
117.2	1903	11004	31	34	2.72	0.8		stair case (see Fig. 3.7-4)
117.3	1903	11004	31	34	4.54	0.85	closed +0.2 -0.6	closed transport hatch (see Fig. 3.7-5)
117.4	1903	11004	31	34	0.3	0.8		opening
118.1	1707	1805	26	31	4.99	0.85		main ventilation channel, like opening No. 121.1
118.2	1707	1805	26	31	2.98	0.85		stair case, like opening No. 121.2
118.3	1707	1805	26	31	4.54	0.85	+0.2 -0.6 closed	close transport hatch, like opening No. 121.3
119.1	1606	1707	20	26	3.58	0.85		main ventilation channel, like No. 121.1
119.2	1606	1707	20	26	3.39	0.85		stair case, like No. 121.2
119.3	1606	1707	20	26	4.54	0.85	+0.2 -0.6 closed	closed transport hatch, like No. 121.3
120.1	1501	1606	15	20	2.55	0.8		main ventilation channel, like No. 121.1
120.2	1501	1606	15	20	3.2	0.8		stair case, like No. 121.2
120.3	1501	1606	15	20	4.54	0.85	+0.2 -0.6 closed	closed transport hatch, like No. 121.3
121.1	1406	1501	09	15	4.0	0.85		main ventilation channel, see Fig. 3.7-5
121.2	1406	1501	09	15	3.38	0.85		stair case, see Fig. 3.7-5

(Table A.3, continued).

Open No.	From Comp.	To Comp.	From Zone	To Zone	F min in m**2	DC @ GRS	Delta p bar	Description
121.3	1406	1501	09	15	4.54	0.85	-0.2 +0.6 closed	closed transport hatch, see Fig. 3.7-5
122.1	1902	11004	30	34	4.81	0.85		open transport hatch
122.2	1902	11004	30	34	0.6	0.8		opening
122.3	1902	11004	30	34	2.06	0.8		spiral staircase
123	1902	1906	30	33	0.083	0.65		opening to spiral staircase
123.1	1902	1906	30	33	0.114	0.65		opening to spiral staircase
124	1902	1906	30	33	1.47	0.8		door partially (40%) opened
125	1802	1906	32	33	0.064	0.7		ventilation duct No. 9 (see Fig. 3.7-15)
126	1701 o	1804	25	30	0.24	0.65		zigzag ventilation duct
127	1802	11004	32	34	1.624	0.85	+0.3 -0.6 closed	closed transport hatch
128.1	1703	1708	29	30	0.06	0.7		ventilation duct No. 10 (see Fig. 3.7-16)
128.2	1703	1706	29	29	0.03	0.7		ventilation duct No. 10 (see Fig. 3.7-16)
128.3	1609	1703	21	29	0.06	0.7		ventilation duct No. 10 (see Fig. 3.7-16)
129	1902	11004	30	34	0.235	0.7	+0.02 -0.6 closed	openings covered by steel plates, adjacent to opening No. 122.1
130	1606	1708	20	30	0.22	0.7		pipe and cable duct
131.1	1606	1708	20	30	3.77	0.85		open transport hatch
131.2	1606	1708	20	30	1.77	0.85		openings parallel to 131.1
132	1606	1708	20	30	1.22	0.75		spiral stair case
133	1603	1708	23	30	0.43	0.85		upper part of opening No. 162
134	1701 o	1701 u	25	24	1.7	0.7		gap between RPV and biological shield
135	1701 o	1805	25	31	0.0806	0.65		three bores of different diameters
136	1701 o	1707	25	26	0.0327	0.65		bores for measuring cable protection tube
137.1	1802	1902	32	30	1.26	0.85		open steel door to compartment No. R 1802
137.2	1802	1902	32	30	1.76	0.85		open steel door to compartment No. R 1802
138	1605	1701 u	19	24	1.374	0.6		17 bores and three grooves in the floor
139	1701 o	1704	25	27	0.3	0.55	+-0.5	choked pipe channel
140	1603	1704	23	27	1.64	0.8	-0.5 +0.2 closed	opening situated in opening No. 143 and covered by steel slab (open for test V44)
141	1802	1902	32	30	0.09	0.7		opening and ventilation duct
142	1405	1506	09	15	0.14	0.65		pipe channel
143	1603	1701 u	23	24	3.02	0.7		opening in the upper part of break compartment R 1603, crossed by break pipe
144.1	1506	1508	15	18	1.42	0.65	+-0.2	ventilation duct No. 8 (see Fig. 3.7-14)
144.2	1506	1508	15	18	0.17	0.65		ventilation duct No. 8 (see Fig. 3.7-14)
144.3	1506	1508	15	18	0.056	0.7		ventilation duct No. 8 (see Fig. 3.7-14)
145	1603	1701 u	23	24	0.17	0.65		channel parallel to opening No. 143

(Table A.3, continued).

Open No.	From Comp.	To Comp.	From Zone	To Zone	F min in m**2	DC @ GRS	Delta p bar	Description
146.1	1502	1508	17	18	0.18	0.7		ventilation duct No. 8 (see Fig. 3.7-14)
146.2	1508	1514	18	16	0.18	0.65		ventilation duct No. 8 (see Fig. 3.7-14)
147	1508	1511	18	16	1.056	0.8		open lead-shielded door
148	1403	1511	12	16	3.5	0.8		floor opening covered by grating
149	1502	1611	17	20	1.4	0.75		pipe channel
150	1502	1603	17	23	0.28	0.55		pipe channel with weir sill in R 1603
151.1	1302	1502	05	17	0.93	0.7		pipe channel
151.2	1408	1502	13	17	0.276	0.7		pipe channel
152	1511	1611	16	20	0.14	0.7		cable duct and openings in ceiling
153.1	1407	1504	08	14	0.209	0.65		rectangular opening and bores
153.2	1503	1504	15	14	0.08	0.7		zigzag opening in R 1503 leading to ventilation duct
153.3	1407	1504	08	14	0.17	0.65		six cylindrical U-channels
154.1	1504	1605	14	19	0.078	0.65		rectangular openings and bores in ceiling
154.2	1503	1605	15	19	0.229	0.65		four cylindrical U-channels, like No. 153.3
155.1	1505	1607	15	20	0.77	0.7		two openings in ceiling of R 1505
155.2	1512	1607	15	20	0.052	0.65		opening in ceiling of R 1512
156	1503	1602	15	22	0.1	0.7		cable duct and gap by the side of ventilation duct
157.1	1802	1904	32	34	0.06	0.6		ventilation duct No. 11 (see Fig. 3.7-17)
157.2	1904	1906	34	33	0.075	0.6		ventilation duct No. 11 (see Fig. 3.7-17)
157.3	1801	1903	34	31	0.42	0.7		ventilation duct No. 11 (see Fig. 3.7-17)
158.1	1404	1512	09	15	0.072	0.65		circular gap
158.2	1512	1513	15	09	0.11	0.65		gap
159	1507	1608	15	20	0.041	0.65		pipe channel, almost completely covered by ventilation duct
160	1404	1507	09	15	0.085	0.65		trapezoidal pipe channel
161	1406	1501	09	15	0.133	0.65		pipe channels and circular gap
162	1603	1606	23	20	0.90	0.85		opening (upper part see No. 133) (closed in V44)
163	1603	1606	23	20	1.10	0.7		zigzag passage with stairs and open lead-shielded door
164.1	1603	1608	23	20	0.58	0.65	+-0.2 closed	opening covered by sheeting
164.2	1603	1608	23	20	0.072	0.7	closed	ventilation duct
164.3	1603	1604	23	20	0.018	0.65	closed	ventilation duct
165	1603	1605	23	19	0.19	0.7		wall opening and steel pipe
166.1	1603	1608	23	20	0.282	0.7		rectangular wall opening (closed in V44)
166.2	1603	1608	23	20	0.03	0.7	closed	rectangular wall opening
167	1605	1606	19	20	1.99	0.85		open lead-shielded door
168	1605	1606	19	20	0.23	0.6		four cylindrical S-channels
169	1605	1606	19	20	0.05	0.55		oblique bore, see Fig. 3.7-13
170	1503	1605	15	19	0.163	0.65		ventilation duct, covered by grating and leading through compartment R 1503 to ventilation duct No. 8
171.1	1608	1704	20	27	0.036	0.6		opening in ceiling of R 1608
171.2	1513	1608	09	20	0.066	0.7		opening in ceiling of R 1608
172.1	1606	1609	20	21	0.06	0.7		ventilation duct No. 10 (see Fig. 3.7-16)
172.2	1602	1609	22	21	0.06	0.7		ventilation duct No. 10 (see Fig. 3.7-16)

(Table A.3, continued).

Open No.	From Comp.	To Comp.	From Zone	To Zone	F min in m**2	DC @ GRS	Delta p bar	Description
172.3	1606	1606	20	20	0.14	0.7		ventilation duct No. 10 (see Fig. 3.7-16)
173	1606	1707	20	26	0.18	0.7		vertical ventilation duct in ceiling of R 1606, leading without protection via R 1703 and R 1707 to main ventilation duct
174	1611	1703	20	29	0.304	0.65		pipe channel
175.1	1706	1802	29	32	0.032	0.7		ventilation duct No. 9 (see Fig. 3.7-15)
175.2	1703	1802	29	32	0.04	0.7		ventilation duct No. 9 (see Fig. 3.7-15)
175.3	1706	1707	29	26	0.15	0.75		ventilation duct No. 9 (see Fig. 3.7-15)
176	1603	1704	23	27	0.24	0.9		instrumented (DK) channel with rounded inlet
177	1508	1603	18	23	1.145	0.8	closed	floor opening
178	1508	1603	18	23	2.78	0.85	+-1 closed	floor opening
179	1508	1603	18	23	0.98	0.8	+-1 closed	floor opening
180.1	1603	1704	23	27	0.0	0.7	closed	zigzag channel in ceiling of R 1603, closed by PD-transfer
180.2	1603	1704	23	27	0.15	0.7		zigzag channel in ceiling of R 1603, open
180.3	1608	1704	20	27	0.0	0.7		zigzag channel in ceiling of R 1603, closed
181	Spalt	1603	Spalt	23	0.51	0.65		rectangular opening (with weir sill in R 1603) and 13 bores leading to gap between concrete wall and steel shell
182	1701 o	11004	25	34	3.0	0.8	+-4	membrane seal (2.5 mm thick) at the upper end of RPV
183.1	1603	1704	23	27	0.183	0.7		rectangular opening
183.2	1603	1704	23	27	0.0	0.7		closed bores
183.3	1603	1704	23	27	0.01	0.65		five bores
184.1	1506	1508	15	18	0.033	0.6		open sheet metal sleeve, filled with rock wool
184.2	1506	1508	15	18	0.006	0.7		channel with crushed edges
185	1508	1511	18	16	0.0056	0.6		two pipes

Table A.4 Compilation of structural elements of HDR-containment (zones)

Zone Number	Material Type	Coating Thickness in mm	Inner-/INTERWALL Area in m**2	Inner-/INTERWALL Volume in m**3	Outer Wall Area in m**2	Outer Wall Volume in m**3
01	B	0.15	28.09	11.24		
01	B	0.15	94.61	45.16	98.90	69.91
02	B	0.15	130.06	50.08	25.00	20.55
03	B	0.15	342.52	112.82	52.56	38.39
03	S	0.15			4.00	0.07
03	T	0.15	23.30	4.22		
04	B	0.15	214.10	71.20	66.30	33.15
04	S	0.15			4.30	0.17
04	T	0.15	34.30	2.11		
05	B	0.15	80.00	16.05	60.10	36.86
06	B	0.15	42.20	14.39	32.10	19.26
06	B	0.00	10.49	3.33		
06	T	0.15	7.61	1.52		
07	B	0.15	65.13	20.60	51.07	31.08
07	B	0.00	11.74	5.98		
07	T	0.15	7.61	1.52.		
08	B	0.15	127.30	55.10		
09	B	0.15	544.55	177.72	109.11	58.10
09	B	1.50	54.51	22.63		
09	B	0.00	11.56	5.78		
09	S	0.15			39.25	1.18
09	T	0.15	57.77	19.61	57.36	29.33
10	B	0.00	245.95	40.58	48.92	32.94
10	S	0.00			35.29	1.05
11	B	0.15	141.55	69.33	17.96	11.67
11	B	1.50	2.10			
11	S	0.15			44.21	1.33
11	T	0.15	7.11	1.78		
11	Z	0.15	90.26	6.56		
12	B	0.15	149.65	75.00		
12	B	1.50	2.24	1.68		
12	B	0.00	2.76			
12	T	0.15	1.62	0.41		

(Table A.4, continued).

Zone Number	Material Type	Coating Thickness in mm	Inner-/INTERWALL Area in m**2	Inner-/INTERWALL Volume in m**3	Outer Wall Area in m**2	Outer Wall Volume in m**3
13	B	0.15	86.39	28.00	42.49	22.73
13	S	0.15			0.25	0.01
13	T	0.15	11.20	2.30		
14	B	0.15	118.75	41.04		
15	B	0.15	485.80	145.28	52.58	24.27
15	B	1.50	78.58	14.23		
15	B	0.00	13.03	2.65	2.94	1.18
15	S	0.15			38.52	1.16
15	T	0.15	40.67	12.85	2.60	1.82
16	B	0.15	149.92	69.36	4.62	1.85
16	B	1.50	39.40	19.70		
16	B	0.00	42.77	11.50	1.15	0.46
16	S	0.15			33.78	1.14
16	Z	0.15	15.64	1.68		
17	B	0.15	94.98	15.52	50.71	26.29
17	B	1.50	19.47	4.87		
17	B	0.00	9.83	2.46	4.51	1.80
17	T	0.15	13.75	2.61		
18	B	0.15	111.61	40.75	33.10	13.24
18	T	0.15	2.95	0.44		
19	B	0.15	132.05	59.74		
20	B	0.15	417.19	158.65	62.19	25.53
20	B	1.50	92.49	15.64		
20	B	0.00	54.91	17.01	3.41	2.05
20	S	0.15			67.05	2.49
20	T	0.15	32.12	9.34		
20	T+B	0.15	7.41	2.96		
21	B	0.15	54.24	7.07		
21	B	0.00	5.54	0.55		
21	T+Z	0.15	25.46	5.98		
21	Z	0.15	10.82	0.73		
22	B	0.15	67.03	11.00		
22	B	0.00	1.89	0.19		
22	S	0.15			22.81	1.13
22	T+Z	0.15	29.81	6.71		

(Table A.4. continued).

Zone Number	Material Type	Coating Thickness in mm	Inner-/INTERWALL Area in m**2	Inner-/INTERWALL Volume in m**3	Outer Wall Area in m**2	Outer Wall Volume in m**3
22	Z	0.15	8.34	0.71		
23	B	0.15	236.40	93.82	93.99	67.75
24	B	0.15	100.53	65.61		
24	S+B	0.15	46.12	20.34		
25	B	0.15	95.27	75.52		
25	S+B	0.15	16.07	24.11		
26	B	0.15	125.49	58.08	8.15	5.34
26	B	1.50	33.93	7.26		
26	B	0.00	25.78	15.41	3.42	2.22
26	S	0.15			32.11	1.11
26	Z	0.15	24.98	2.12		
27	B	0.00	7.30			
27	B	0.15	493.41	253.41	297.58	178.55
27	B	0.00	45.12	23.48		
27	B	0.15	15.10	9.06		
27	S	0.15			6.20	0.37
27	S+T	0.15	6.00	2.40		
27	S+T	0.00	8.10	2.32		
27	T	0.15	24.16	8.43		
28	B	0.15	109.40	22.01		
28	P+B	0.00	3.99	0.70		
28	S	0.15			22.38	0.67
28	Z	0.15	25.22	2.14		
29	B	0.15	127.66	49.62	54.37	16.09
29	T	0.15	32.42	5.68		
29	Z+B	0.15	1.60			
30	B	0.15	175.50	63.43		
30	B	0.00	91.67	39.30		
30	S	0.15			57.68	1.73
30	T	0.15	10.14	2.54		
31	B	0.15	253.78	91.69	12.03	7.66
31	B	1.50	42.00	7.18		
31	B	0.00	30.07	18.05		
31	S	0.15			74.31	2.23
31	S+B	0.15	11.34	1.13		

(Table A.4. continued).

Zone Number	Material Type	Coating Thickness in mm	Inner-/INTERWALL Area in m**2	Inner-/INTERWALL Volume in m**3	Outer Wall Area in m**2	Outer Wall Volume in m**3
32	B	0.15	115.73	21.84		
32	B	0.00	10.35	2.38		
32	S	0.15			48.50	1.46
32	T	0.15	17.55	1.76		
33	B	0.15	72.31	35.13		
33	S	0.15			9.05	0.27
33	T	0.15	20.28	7.75		
34	B	0.15	345.18	122.83	4.40	1.76
34	B	1.50	243.36	86.23		
34	B	0.00	26.22	2.62		
34	S	0.15		1.271.46	31.88	
34	S+B	0.15	3.50	3.15		
34	S+B	0.00	513.98	274.96	71.04	74.59
34	T	0.15	5.04	0.50		
Totals			8,397.24	3,071.85	3,234.70	905.84

Abbreviations:

SH	Steel Shell Cont.
B	Concrete
T	Concrete Blocks
S	Steel
Z	Brickework plastered
Sn+B	Concrete with Steelplate Plate thickness: n in mm
P+B	Lead with concrete behind lead thickness: 240 mm

Table A.5 Compilation of metal internals and equipment of HDR-containment

Zone Number	Material Type	Coating Thickness in mm	Material Strength d in mm: Class 1. 0<d<3 Area in m**2	Volume in m**3	Class 2. 23<d<20 Area in m**2	Volume in m**3	Class 3. 20<d<40 Area in m**2	Volume in m**3	Class 4. 40<d<999 Area in m**2	Volume in m**3
01	SA	0.00			0.60	2.40				
01	SS	0.15	0.69	2.00	84.01	505.77				
01	SZ	0.00	26.16	14.64						
01	SZ	0.15			0.24	1.70				
02	AL	0.00	0.09	0.18	0.14	0.58				
02	SA	0.00	1.54	2.75	2.17	10.00	0.10	1.25		
02	SS	0.00	0.99	2.51	0.49	3.66	0.09	2.31		
02	SS	0.15	5.57	9.65	114.86	596.98				
02	SZ	0.00	13.26	7.43						
03	AL	0.00	0.26	0.53	0.72	2.89				
03	CU	0.00	1.39	2.78						
03	SA	0.00	2.38	5.35	3.06	22.28				
03	SS	0.00	0.67	1.32	2.32	9.28				
03	SS	0.15	60.56	90.40	84.37	638.40			0.57	6.41
03	SZ	0.00	212.30	154.81						
04	AL	0.00	0.09	0.18	0.77	4.68				
04	CU	0.00	0.66	0.99						
04	SA	0.00	7.37	18.26	51.00	254.04				
04	SS	0.00			3.90	11.70				
04	SS	0.15	110.02	135.84	53.05	284.25	0.15	0.90		
04	SZ	0.00	100.59	62.97						
05	AL	0.00	3.33	6.01	0.14	0.58				
05	SA	0.00	1.10	2.20	28.21	175.47				
05	SS	0.15	12.39	29.91	27.76	119.98	5.74	162.73		
05	SZ	0.00	71.93	39.27						
06	AL	0.00	6.57	6.01	0.06	0.23				
06	CU	0.00	0.10	0.15						
06	SA	0.00	0.58	1.16	15.10	72.75	0.17	2.79		
06	SS	0.00			29.09	168.36	1.87	32.73	0.28	3.15
06	SS	0.15	9.77	22.77	26.26	153.37	1.19	34.89		
06	SZ	0.00	22.48	15.76						
07	AL	0.00	0.59	0.48	0.06	0.23				
07	CU	0.00	0.60	0.90						
07	SA	0.00	1.64	4.02	16.02	76.95				
07	SS	0.00	0.77	2.00	1.30	4.91	0.10	0.58		
07	SS	0.15	24.22	66.27	20.18	132.40	0.38	11.40	1.40	140.00
07	SZ	0.00	52.92	30.42						

(Table A.5, continued).

Zone Number	Material Type	Coating Thickness in mm	Material Strength d in mm: Class 1. 0<d<3 Area in m**2	Volume in m**3	Class 2. 3<d<20 Area in m**2	Volume in m**3	Class 3. 20<d<40 Area in m**2	Volume in m**3	Class 4. 40<d<999 Area in m**2	Volume in m**3
08	AL	0.00	0.21	0.24	0.14	0.58				
08	GG	0.15			1.06	5.30				
08	SA	0.00	4.73	11.98	1.68	16.69				
08	SS	0.00			0.76	3.04				
08	SS	0.15	10.75	14.65	49.24	283.17				
08	SZ	0.00	60.69	38.36						
09	AL	0.00	4.31	4.27	0.53	2.16				
09	CU	0.00	2.17	3.67						
09	MS	0.00			0.11	0.34				
09	PB	0.00			1.83	21.96			0.07	2.33
09	SA	0.00	9.14	21.18	132.01	962.16	4.65	130.98	0.36	13.15
09	SS	0.00			43.03	337.66	1.50	14.31	0.69	9.59
09	SS	0.15	95.99	196.60	173.22	1.249.14	2.89	64.89		
09	SZ	0.00	536.13	367.03	5.57	16.76				
10	AL	0.00			3.03	12.14				
10	SS	0.00	15.16	17.09	38.09	197.82			0.08	4.00
10	SS	0.10			3.80	19.00				
10	SS	0.15	55.96	50.57	40.70	298.16	0.11	3.30		
10	SZ	0.00	3.58	2.69						
11	AL	0.00	12.81	10.28	0.80	3.51				
11	GG	0.15			1.28	6.40				
11	SA	0.00			0.65	3.25				
11	SS	0.15	93.11	95.29	58.17	183.47				
11	SZ	0.00	308.64	340.65	0.76	1.71	7.17	153.64		
12	AL	0.00	1.07	0.91	0.14	0.58				
12	CU	0.00	0.21	0.33						
12	SA	0.00	1.16	1.32	180.82	1.682.66	0.17	2.83	2.85	101.01
12	SS	0.00			0.68	1.70				
12	SS	0.15	3.71	7.04	45.95	324.87	0.71	6.19		
12	SZ	0.00	52.76	36.17	0.02	0.11				
13	AL	0.00	2.30	1.96						
13	SA	0.00	0.68	0.68	0.68	3.35	0.55	11.79		
13	SS	0.00			2.17	21.70				
13	SS	0.15	3.80	8.88	17.38	62.18			1.60	42.67
13	SZ	0.00	93.24	62.83	5.30	12.86				
14	AL	0.00	0.09	0.18	0.41	2.20				
14	SA	0.00			1.99	16.93				

(Table A.5, continued).

Zone Number	Material Type	Coating Thickness in mm	Material Strength d in mm: Class 1. 0<d<3 Area in m**2	Volume in m**3	Class 2. 3<d<20 Area in m**2	Volume in m**3	Class 3. 20<d<40 Area in m**2	Volume in m**3	Class 4. 40<d<999 Area in m**2	Volume in m**3
14	SS	0.00			0.78	2.99	0.85	7.12	0.14	2.03
14	SS	0.15	2.54	5.69	21.49	143.90	0.05	0.69		
14	SZ	0.00	15.73	9.02	0.08	0.38				
15	AL	0.00	13.02	12.40	1.26	7.24				
15	CU	0.00	2.36	3.18						
15	GG	0.15			0.21	1.03				
15	PB	0.00							0.55	15.13
15	SA	0.00	5.57	14.02	31.12	111.44			0.06	0.95
15	SS	0.00	1.64	2.88	15.41	77.85	1.43	22.98	0.57	7.84
15	SS	0.15	89.97	144.77	215.56	1.233.63	1.02	16.44		
15	SZ	0.00	526.58	431.45	15.84	81.28				
16	AL	0.00	0.69	0.54	8.30	21.88				
16	CU	0.00	1.04	2.08						
16	SA	0.00	4.52	9.94	18.01	69.57				
16	SS	0.00			2.25	7.24				
16	SS	0.15	46.25	89.64	74.08	557.47	2.27	48.26	0.06	0.71
16	SZ	0.00	122.10	104.06	18.57	55.71				
17	AL	0.00	10.41	6.61	0.14	0.58				
17	SA	0.00	0.72	1.80	32.48	232.13				
17	SS	0.15	32.83	74.04	71.11	442.58	4.61	108.72	0.61	7.39
17	SZ	0.00	104.06	18.57	2.29	4.58				
18	AL	0.00	5.83	4.48	0.14	0.58				
18	PB	0.00							1.05	47.25
18	SA	0.00	0.21	0.42	23.46	124.58	1.30	26.70		
18	SS	0.15	14.15	31.70	36.50	159.30	1.56	36.96	0.39	4.71
18	SZ	0.00	106.02	61.57	1.47	3.68				
19	AL	0.00	9.95	10.53	0.94	3.86				
19	SA	0.00	6.17	11.61	53.54	318.60	0.15	2.25		
19	SS	0.00	0.36	0.72	9.67	28.26	0.33	2.30		
19	SS	0.15	3.93	8.01	32.09	287.79	0.56	3.50		
19	SZ	0.00	55.89	39.98						
20	AL	0.00	1.42	1.68	1.73	10.18				
20	AL	0.15	0.44	0.44	2.11	0.55				
20	CU	0.00	1.25	1.49						
20	PB	0.00							1.97	139.20
20	SA	0.00	6.74	11.12	25.53	150.49	3.82	79.84	0.22	7.70
20	SS	0.00	7.44	17.26	125.35	738.92	8.04	71.88	1.45	76.85

(Table A.5, continued).

Zone Number	Material Type	Coating Thickness in mm	Material Strength d in mm: Class 1. 0<d<3 Area in m**2	Volume in m**3	Class 2. 23<d<20 Area in m**2	Volume in m**3	Class 3. 20<d<40 Area in m**2	Volume in m**3	Class 4. 40<d<999 Area in m**2	Volume in m**3
20	SS	0.10			31.53	149.45				
20	SS	0.15	82.59	164.17	176.44	1.411.00	1.82	18.65	5.16	817.39
20	SZ	0.00	478.39	267.39	12.92	82.03				
21	AL	0.00	0.09	0.18	0.06	0.23				
21	SA	0.00	0.66	1.33	5.53	35.52	1.35	33.75		
21	SS	0.00			0.33	2.36				
21	SS	0.15	6.46	13.86	12.87	44.71				
21	SZ	0.00	77.25	58.83						
22	AL	0.00	0.21	0.36	1.36	5.46				
22	SA	0.00	0.83	1.66	0.41	1.31				
22	SS	0.15	18.21	17.36	7.60	34.72				
22	SZ	0.00	42.85	38.88	13.70	34.18				
23	AL	0.00	5.40	4.05	2.70	54.00				
23	CU	0.00	2.14	3.29						
23	MS	0.00			0.73	2.54				
23	PB	0.00			1.36	20.40				
23	SA	0.00	10.62	19.75	67.21	469.08	0.68	15.36	0.37	9.25
23	SS	0.00	4.01	10.76	10.13	56.52				
23	SS	0.15	60.38	125.35	204.88	1.153.44	143.48	3.181.68	1.13	21.19
23	SZ	0.00	114.21	102.62						
24	AL	0.00	0.36	0.72	0.47	2.23				
24	SA	0.00	0.33	0.86	5.91	99.86	3.25	81.25	0.80	33.77
24	SS	0.00	0.90	2.21	15.44	82.00			21.45	3.003.00
24	SS	0.15	39.23	109.69	34.37	216.63	17.65	353.00	6.07	351.70
24	SZ	0.00	52.13	22.69	7.61	29.67				
25	AL	0.00	0.36	0.72	0.56	2.59				
25	SA	0.00	20.11	50.14	31.07	276.59	6.08	171.81		
25	SS	0.00	3.84	5.27	11.07	73.99	0.70	7.00	3.96	316.80
25	SS	0.15	57.54	142.79	27.63	163.86				
25	SZ	0.00	52.42	40.47						
26	AL	0.00	0.19	0.28	0.67	2.70			0.19	2.38
26	CU	0.00	0.29	0.45						
26	MS	0.00	0.06	0.06						
26	SA	0.00	1.74	4.60	15.90	80.80				
26	SS	0.00	0.38	0.53	3.08	26.30	0.04	0.30		
26	SS	0.15	56.20	90.54	63.88	375.46	6.91	164.88		
26	SZ	0.00	231.22	174.98						

(Table A.5, continued).

Zone Number	Material Type	Coating Thickness in mm	Material Strength d in mm: Class 1. 0<d<3 Area in m**2	Volume in m**3	Class 2. 3<d<20 Area in m**2	Volume in m**3	Class 3. 20<d<40 Area in m**2	Volume in m**3	Class 4. 40<d<999 Area in m**2	Volume in m**3
27	AL	0.00	0.18	0.35	17.41	88.09				
27	CU	0.00	1.40	2.01	12.75	110.04				
27	MS	0.00			0.25	0.92				
27	PB	0.00			61.88	33.76				
27	SA	0.00	32.08	69.71	158.26	948.29	2.09	37.12	0.06	0.90
27	SS	0.00	29.12	68.16	74.31	486.01	10.49	217.08	8.35	297.98
27	SS	0.15	102.80	178.96	531.85	2.935.31	9.07	135.13		
27	SZ	0.00	759.82	675.26	0.27	0.68				
28	AL	0.00	0.63	0.72	0.14	0.58				
28	PB	0.00							4.43	354.40
28	SS	0.00	1.12	1.68	0.87	3.05				
28	SS	0.15	11.52	20.33	23.49	111.41				
28	SZ	0.00	183.38	130.28						
29	AL	0.00	1.36	2.04						
29	CU	0.00	2.59	5.18						
29	MS	0.00			0.12	0.37				
29	PB	0.00							1.46	65.70
29	SA	0.00	3.39	6.63	75.46	452.70	4.84	95.07		
29	SS	0.00					0.58	10.63		
29	SS	0.15	28.55	58.21	64.60	389.08	0.73	14.97		
29	SZ	0.00	90.05	75.38	2.69	6.58				
30	AL	0.00	6.89	5.26	3.83	20.53				
30	AL	0.15			0.36	1.26				
30	CU	0.00	0.26	0.26						
30	MS	0.00	0.03	0.06	0.35	1.31				
30	PB	0.00			1.51	9.06				
30	SA	0.00	26.74	14.44	8.43	36.76				
30	SS	0.00	1.17	3.04	4.96	32.29	0.24	9.60		
30	SS	0.15	112.65	176.00	174.89	893.07				
30	SZ	0.00	91.51	87.15	18.76	46.90				
31	AL	0.00	0.46	0.73	5.79	48.19				
31	SA	0.00	9.39	19.59	19.23	143.95				
31	SS	0.00	15.31	31.78	25.73	187.71	0.11	0.91		
31	SS	0.15	77.70	147.24	82.50	427.45	0.59	8.85	0.61	11.53
31	SZ	0.00	256.07	214.26	13.33	33.33				
32	AL	0.00	0.09	0.18	6.04	30.08				
32	SA	0.00	27.92	19.74	17.92	64.62				
32	SS	0.15	16.92	19.39	116.55	526.06	4.03	50.38		

(Table A.5, continued).

Zone Number	Material Type	Coating Thickness in mm	Material Strength d in mm: Class 1. 0<d<3 Area in m**2	Volume in m**3	Class 2. 23<d<20 Area in m**2	Volume in m**3	Class 3. 20<d<40 Area in m**2	Volume in m**3	Class 4. 40<d<999 Area in m**2	Volume in m**3
32	SZ	0.00	135.32	72.37						
33	AL	0.00	0.09	0.18	2.00	9.88				
33	MS	0.00			0.12	0.42				
33	PB	0.00					12.51	225.18		
33	SA	0.00	21.90	42.29	10.51	106.93				
33	SS	0.00			2.49	9.96				
33	SS	0.15	44.25	66.72	70.87	317.28	1.94	38.70		
33	SZ	0.00	67.22	58.06						
34	AL	0.00	30.19	32.54	18.95	89.39				
34	CU	0.00	0.41	0.58						
34	SA	0.00	64.40	54.89	161.51	852.75	134.19	1,649.42	41.95	3,678.89
34	SS	0.00	31.66	46.62	69.21	541.96	38.11	611.67	59.30	2,029.32
34	SS	0.10			78.82	388.17	69.15	927.30	0.84	18.90
34	SS	0.15	262.39	410.67	1,939.61	11,848.52	114.50	1,690.89	72.67	2,683.51
34	SZ	0.00	450.07	371.76	41.29	187.33	0.09	0.56		
Totals:			7,767.32	7,887.15	6,860.73	41,307.13	638.75	10,816.25	243.76	14,328.64

Table A.6 Specification of flow openings in break compartment R 1603

Opening No.	Comp. 1	Comp. 2	Location in R 1603 *	V42	V43	Open Vent Areas for Experiment V44 F_{min}	V21.1 in m^2	V21.2	V21.3
110	1603	1704	O	0.37	0.37	0.37	0.37	0.37	0.37
133	1603	1708	S(O)	0.43	0.43	0.43	0.43	0.43	0.43
140	1603	1704	O	0	0	1.64	0**	0**	0**
143	1603	1701 u	O	3.02	3.02	3.02	3.02	3.02	3.02
145	1603	1701 u	O	0.17	0.17	0.17	0.17	0.17	0.17
150	1502	1603	S	0.28	0.28	0.28	0.28	0.28	0.28
162	1603	1606	S(U)	0.90	0.90	0	5.10**	3.20**	5.10**
163	1603	1606	S	0.1	1.1	1.1	1.1	1.1	1.1
164	1603	1608	S	0	0	0	0	0	0
165	1603	1605	S	0.19	0.19	0.19	0.19	0.19	0.19
166.1	1603	1608	S	0.28	0.28	0	0.28	0.28	0.28
166.2	1603	1608	S	0	0	0	0	0	0
176	1603	1704	O	0.24	0.24	0.24	0.24	0.24	0.24
177	1508	1603	U	0	0	0	1.145	1.145	0
178	1508	1603	U	0	0	0	2.5	2.5	0
179	1508	1603	U	0	0	0	0	0	0
180.1	1603	1704	O	0	0	0	0	0	0
180.2	1603	1704	O	0.15	0.15	0.15	0.15	0.15	0.15
181	1603	Spalt	S	0.51	0.51	0.51	0.51	0.51	0.51
183.1-3	1603	1704	O	0.19	0.19	0.19	0.19	0.19	0.19

* Abbreviations: O ceiling
U floor
S side wall

** Data for V21.1 - 3 only preliminary

NUREG/CR-3262
PNL-5515
Vol. 7
R4

DISTRIBUTION

No. of
Copies

OFFSITE

U. S. Nuclear Regulatory
Commission
Division of Technical
Information and Document
Control
7920 Norfolk Avenue
Bethesda, MD 20014

20 Tim Lee
Analytical Model Branch
Office of Nuclear Regulatory
Research
U. S. Nuclear Regulatory
Commission
7915 Eastern Avenue
MS-1130-SS
Washington, DC 20555

No. of
Copies

ONSITE

50 Pacific Northwest Laboratory

CL Wheeler (43)
Publishing Coordination (2)
Technical Information (5)

NRC FORM 335 (2-84) NRCM 1102, 3201, 3202

U.S. NUCLEAR REGULATORY COMMISSION

BIBLIOGRAPHIC DATA SHEET

SEE INSTRUCTIONS ON THE REVERSE

1. REPORT NUMBER (Assigned by TIDC, add Vol. No., if any)
NUREG/CR-3262
PNL-5515
Vol. 7

2. TITLE AND SUBTITLE
COBRA-NC: A Thermal-Hydraulic Code for Transient Analysis of Nuclear Reactor Component, Volume 7: Assessment Manual for Containment Applications

3. LEAVE BLANK

4. DATE REPORT COMPLETED
MONTH: March YEAR: 1986

5. AUTHOR(S)
C. L. Wheeler, M. J. Thurgood, T. E. Guidotti, D. E. DeBellis

6. DATE REPORT ISSUED
MONTH: April YEAR: 1986

7. PERFORMING ORGANIZATION NAME AND MAILING ADDRESS (Include Zip Code)
Pacific Northwest Laboratory
PO Box 999
Richland, WA 99352

8. PROJECT/TASK/WORK UNIT NUMBER

9. FIN OR GRANT NUMBER
B2466

10. SPONSORING ORGANIZATION NAME AND MAILING ADDRESS (Include Zip Code)
Division of Accident Evaluation
Office of Nuclear Regulatory Research
U. S. Nuclear Regulatory Commission
Washington, D. C. 20555

11a. TYPE OF REPORT
Technical

b. PERIOD COVERED (Inclusive dates)

12. SUPPLEMENTARY NOTES

13. ABSTRACT (200 words or less)
COBRA-NC is a digital computer program written in FORTRAN IV that simulates the response of nuclear reactor components and systems to thermal-hydraulic transients. The code solves multicomponent compressible, three-dimensional, two-fluid, three-field equations for two-phase flow. The three fields are the vapor/gas field, the continuous liquid field, and the liquid drop field. This volume of the manual provides the user with the results of comparisons between COBRA-NC predictions and data obtained from containment systems experiments. These data comparisons provide an indication of the code's ability to predict the response of multicompartment nuclear containment systems to postulated loss-of-coolant accidents that result in the release of steam, water, and/or noncondensable gases into nuclear containments.

14. DOCUMENT ANALYSIS - a. KEYWORDS/DESCRIPTORS
a. Keywords
COBRA-NC, Containment Analysis
3-D, Finite Difference Code
2-Ø, 3-Fields, Compressible Flow
Assessment Manual

b. IDENTIFIERS/OPEN-ENDED TERMS

15. AVAILABILITY STATEMENT
Unlimited

16. SECURITY CLASSIFICATION
(This page) Unclassified
(This report)

17. NUMBER OF PAGES

18. PRICE

UNITED STATES
NUCLEAR REGULATORY COMMISSION
WASHINGTON, D.C. 20555